# Interrelationship of the Fluvial Morphology and the Salinity of the Great Fish River Estuary

by
Enrique Edward Julyan

Thesis presented in partial fulfilment of the requirements for the degree of Master of Science in the Department of Civil Engineering at Stellenbosch University

Supervisor: Prof. Gerrit Basson

March 2015

# DECLARATION

By submitting this thesis electronically, I declare that the entirety of the work contained therein is my own, original work, that I am the sole author thereof (save to the extent explicitly otherwise stated), that reproduction and publication thereof by Stellenbosch University will not infringe any third party rights and that I have not previously in its entirety or in part submitted it for obtaining any qualification.

March 2015

# ABSTRACT

The investigation of the interrelationship of the fluvial morphology and the salinity of the Great Fish River Estuary was performed by the combination of a two-dimensional morphological model and a one dimensional advection dispersion module. Two scenarios were defined for investigation, namely Scenarios A and B. Model bathymetry and grid/network for each model and scenario was compiled from topographical information obtained from aerial photos, SRTM data, LIDAR and 24 measured river cross sections of the area from the river mouth up to 27km upstream of the river mouth. Model boundary conditions were developed from empirical formulas and measured data from the Department of Water and Sanitation (DWS). Both models were calibrated with results obtained during field measurement conducted from 5 – 7 May 2012.

Scenario A consisted of a long term 5 year morphological simulation (1 May 2007 to 30 May 2012) with manual mouth closure events for identified river low flow periods. Water levels upstream of the river mouth were extracted from the two-dimensional morphological module and used as the downstream boundary condition of the one-dimensional advection dispersion (salinity) model. For scenario B floods with return periods between 1:2 and 1:100 years were simulated in the morphological model. The resultant bathymetries were then used to compile the network and bathymetry of the one dimensional advection dispersion (salinity) model. The different flood resultant bathymetries were then used with equal boundary conditions (representative of the average flow in the river) in the one dimensional salinity model. The predicted salinity was compared for each bathymetry used.

From model results distinct trends were observed. During low flow conditions the estuary basin fills with sediments and during floods the sediments are flushed out of the estuary. Large magnitude floods greatly erode the estuary especially in the middle reach, during floods the tidal inlet experiences overtopping and subsequent erosion, the constriction at the tidal inlet is completely destroyed during larger floods. The estuary mouth in its closed state experiences slight overtopping and the mouth is breached during periods of high river flows.

The magnitude of salt intrusion depends mainly on the size (the constriction) of the river mouth (tidal inlet). During periods of mouth closure the average salinity in the estuary decreases, average salinity increases if the tidal inlet area is increased. The extent of salt intrusion is approximately 10 km upstream of the river mouth when the mouth is open and the intrusion length increases during spring tides.

# OPSOMMING

Die verwantskap tussen die Groot Vis Rivier Estuarium morfologie en sout toestand is ondersoek deur die kombinasie van 'n twee dimensionele morfologiese model en 'n een dimensionele sout model. Twee toestande is gedefinieer vir ondersoek naamlik Scenario A en Scenario B. Die area vanaf die rivier mond tot 27 km stroomop van die rivier mond is deur die modelle gesimuleer. Die gemodeleerde area stem ooreen met die area waar gemete rivier-snit diepte metings beskikbaar was, onbrekende data is aangevul met behulp van lugfotos, LIDAR- en SRTM- data. Die model grens toestande is bepaal met empiriese vereglykings asook gemete data vanaf die Departement Waterwese. Beide numeriese modelle was gekalibreer met veld data verkry vanaf 5 tot 7 Mei 2012.

Scenario A het behels 'n langtermyn 5 jaar morfologiese modellering (1 Mei 2007 tot 30 Mei 2012) met toe-mond toestande gedurende gedefinieerde rivier vloei toestande. Die watervlakke van die twee dimensionele morfologiese model stroomop van die mond is gebruik as die stroomaf grenstoestand van die een dimnesionele model om die effek van die morfologiese veranderinge te inkorporeer in die sout model. Scenario B het behels die simulering van rivier vloede met herhaal periodes tussen 1:2 en 1:100 jaar in die morfologiese model. Die rivier-bodem  vlakke verkry van laasgenoemde simulasiesis toe gebruik in die een dimensionele sout model met dieselfde grenstoestande wat ooreenstem met die gemiddelde toestande in die Groot Vis Rivier. Aangesien die grenstoestande dieselfde was en net die rivier-bodem vlakke gevarieer is, kon die effek van vloede op die souttoestand in die estuarium bepaal word.

Uit die model resultate kon duidelike tendense waargeneem word. Gedurende lae rivier vloei toestande is die estuarium gevul met sediment en tydens vloede het die sediment weer ge-erodeer en gedeponeer in die oseaan. Groot vloede veroorsaak baie erosie in die estuarium veral in die middel bereik en by die riviermonding. Indien die vloed groot genoeg is word die riviermond vernouing totaal uitgespoel. Die riviermonding in die geslote staat ondervind effense oorstroming en word oopgespoel indien die rivier vloei groot genoeg is.

Die graad van die sout indringing in die estuarium hang hoofsaaklik af van die grootte (die vernouing) van die rivier mond. Gedurende toe mond toestande is die gemiddelde sout vlakke in die estuarium laer, wanner die rivier monding groter raak, word die gemiddelde sout vlakke in die estuarium meer. Die omvang van die sout indringing  strek tot ongeveer 10 km stroomop van die rivier mond wanneer die mond oop is en die indringing afstand neem toe gedurende spring getye.

## ACKNOWLEDGEMENTS

# TABLE OF CONTENTS

## LIST OF FIGURES

# LIST OF TABLES

# LIST OF SYMBOLS

| | |
|---|---|
| α | helical flow calibration constant |
| $\delta_s$ | the angle between the bed shear stress and the average flow direction |
| $\Delta H_H$ | peak tidal level |
| $\Delta T_H$ | tidal lag |
| θ | Shields parameter |
| $\theta_c$ | critical Shields parameter |
| κ | Von Karman's constant |
| ρ | density |
| τ | flow shear stress |
| ν | kinematic viscosity of water |
| a | bed load slope effect calibration factor |
| A | area |
| $A_e$ | effective area |
| $A_m$ | predicted model accuracy |
| $A_o$ | average tidal height |
| $A_p$ | area proportion |
| AD | advection dispersion |
| ADCP | acoustic Doppler current profiler |
| b | width |
| BF | bed load factor |
| c | suspended sediment concentration |
| $c_e$ | equilibrium sediment concentration |
| C | Chezy roughness coefficient |
| $C_2$ | sink/source term |
| Cr | Courant number |

| CD | Chart datum |
| CPU | central processing unit |
| CSIR | Council for Scientific and Industrial Research |
| d | sediment/grain diameter |
| $d_{50}$ | median sediment diameter |
| D | dispersion coefficient |
| DEM | digital elevation model |
| DHI | Danish Hydraulic Institute |
| DWS | Department of Water and Sanitation |
| $\varepsilon$ | turbulent diffusion coefficient |
| E | eddy/turbulent viscosity |
| EC | electro conductivity |
| EHC | erosion hazard class |
| $EI_w$ | weighted erosion class |
| E(y) | GEV parameter |
| $F_D$ | drag force |
| $F_i$ | nodal amplitude factor |
| $F_L$ | lift force |
| $F_R$ | resistance force |
| g | gravitational acceleration |
| G | bed load slope effect calibration factor |
| GEV | General Extreme Value distribution |
| $G_i$ | local phase lag |
| h | water depth |
| H | surface/water level |
| HAT | highest astronomical tide |

| HD | hydrodynamic |
| $i_s$ | helical flow intensity |
| I | tidal constituent index |
| k | number of tidal constituents |
| $k$ | GEV parameter |
| $k_b$ | bed load calibration factor |
| $k_s$ | suspended load calibration factor |
| $k_s$ | roughness coefficient |
| K | linear decay coefficient |
| LAT | lowest astronomical tide |
| LIDAR | remote sensing technology that measures distance |
| LN | Log Normal distribution |
| LPIII | Log Pearson Type 3 distribution |
| m | metre |
| M | Manning roughness coefficient |
| $M_O$ | overturning moment |
| masl | metres above sea level |
| MHWN | mean high water neap |
| MHWS | mean high water spring |
| ML | mean level |
| MLWN | mean low water neap |
| MLWS | mean low water spring |
| MSL | mean sea level |
| n | curvilinear horizontal component |
| N | Estuary number |
| $N_R$ | Estuarine Richardson number |

| | |
|---|---|
| p | horizontal water flux |
| $P_t$ | tidal prism |
| q | vertical water flux |
| Q | water discharge |
| $Q_f$ | fresh water discharge |
| $Q_s$ | sediment load |
| $Q_P$ | tidal prism discharge |
| R | hydraulics radius |
| $R_n$ | curvilinear n-line radius |
| $R_{nd}$ | river network density |
| $R_s$ | curvilinear s-line radius |
| RHS | right hand side |
| s | curvilinear vertical component |
| $s$ | sediment relative density |
| $S_{bl}$ | sediment bed load |
| $S_s$ | streamwise sediment bed load |
| $S_o$ | river slope |
| $S_{sl}$ | sediment suspended load |
| $S_{tl}$ | sediment total load |
| $S_x$ | sediment transport in x- direction |
| $S_y$ | sediment transport in y- direction |
| SRTM | satellite radar topography mission |
| SRTM-90 | satellite radar topography mission digital elevation with horizontal resolution of 90 metres |
| t | time |
| $t_s$ | time scale |
| T | tidal period |

| | |
|---|---|
| TDS | total dissolved solids |
| $T_c$ | time of concentration |
| u | horizontal Cartesian velocity |
| U | horizontal curvilinear velocity |
| v | vertical Cartesian velocity |
| var(y) | GEV parameter |
| V | vertical curvilinear velocity |
| $V_c$ | inlet flow velocity |
| w | vertical velocity |
| $w_i$ | angular velocity |
| $w_s$ | settling velocity |
| $W_s$ | submerged weight |
| $W_T$ | weight parameter for statistical distributions |
| x | horizontal Cartesian coordinate |
| y | horizontal Cartesian coordinate |
| z | vertical Cartesian coordinate |
| $z_b$ | bed level |

# 1    INTRODUCTION

## 1.1    Estuaries

Estuaries can be defined as the areas of interaction between salt water from the open oceans and fresh water from precipitation on land. The upper limit of the estuary is generally the furthest point upstream where tidal rise and fall can be observed (Open University 1999). An estuary has the characteristics of a river and a sea. The riverine features of an estuary include; parallel banks, water flow (fresh in the upper reaches), sediment transport and floods. Estuaries also have marine characteristics such as tides and the presence of saline water. The transitional area defined as an estuary has an environment different to most water bodies and is a crucial feeding and breeding ground to many life forms. Estuaries have always been important to man, serving as a link of transport between inland areas and the sea and as a source of food. The land bordering estuaries is excellent for agricultural purposes as the land is typically nutrient rich, the land flat and fresh water is available upstream from the river mouth (Savenije 1993).

Understanding the physical phenomenon that determines estuarine processes such as tidal flow, tidal mixing and the subsequent salt intrusion are important in predicting the impacts of upstream interventions in the estuarine environment. Upstream interventions such as river abstraction and dams may cause dramatic and irreversible ecological changes in an estuary. Changes in the salinity distribution in an estuary have direct impact on the water quality, water utilization potential and the estuarine aquatic environment (Savenije 2012). Due to the immense importance of estuaries to nature and mankind the preservation of estuaries is critical.

## 1.2    Study area

This study focusses on the last 30 km of the Great Fish River; the approximate modelled area is indicated by the yellow rectangle on Figure 1-1. The Great Fish River originates east of Graaf Reinet, running a 650 km course to its mouth (33°28'S and 27°10'E) approximately halfway between Port Elizabeth and East London. The river has a catchment area of 30 366 km$^2$, its main tributaries are the Great Brak River, the Tarka River, the Kat River and the Little Fish River.  The river has a mean annual runoff of 525 x 10$^6$m$^3$/yr (NRIO 1987). The Great Fish River catchment is heterogeneous in terms of land use, vegetation and topography. The average rainfall is 430 mm/yr with a coefficient of variation of 30%. Catchment vegetation consists of semi-succulent thorny scrub comprising of succulent bushclump savannah, dwarf shrubland and grassland. The land use of the catchment consist of commercial rangeland, communal rangeland and nature conservation areas (Tanser & Palmer 2000). The Great Fish River is part of the Department of Water and Sanitation (DWS) Fish to Tsitsikama Water Management Area and is impunded by several large dams throughout the catchment.

The Great Fish River was known to have a highly variable flow rate prior to 1975. Periods of zero discharge frequently occurred, resulting in the formation of discrete pools in the river. During prolonged low flow conditions mouth closure ensued (Reddering & Esterhuysen 1982). The completion of the Orange-Fish River tunnel in 1975 stabilized the river flow by provision from the Orange River. The Orange River transfer scheme was implemented by the national Government to augment water supplies to the farming districts of the Eastern Cape. Although flow stabilization occurred the mean annual discharge into the Great Fish River estuary decreased due to increased water abstraction for irrigation (O'Keeffe & De Moor 1988). The estuary is classified by Whitfield (1995) as permanently open and in a good condition. The catchment contains highly erodible Beaufort and Ecca groups resulting in large amounts of salts leached from ancient marine sediments by run-off (O'Keeffe & De Moor 1988).

The spring tidal prism of the estuary is approximately $1.6 \times 10^6$ m$^3$ and the average river flow 12 m$^3$/s (average of daily river flows post 1976 for DWS station Q9H018). This results in a tidal to river ratio of 6:1. This low ratio produces a distinct salt wedge up to a distance of 10 km upstream of the river mouth. The total estuarine extent is approximately 12 km. Large intertidal mudbanks are present throughout the system and the water is highly turbid with minimal aquatic vegetation (Vorwerk 2006). The large mudbanks can be attributed to the large sediment loads from the water transfer scheme and the erodible soil characteristics of the catchment (Ter Morshuizen et al. 1996).



**Figure 1-1: Great Fish River catchment and mouth location (Google 2014)**

## 1.3   Objectives

The main objective of this study was to investigate the relationship between the morphology of the estuarine system on the salinity and tidal influence of the ocean on the estuary. The main objective can be divided into the following sub-objectives:

- To obtain field measurements of sediment transport, flow velocities, channel depth and salinity at defined locations in the estuary.
- The setup and calibration of a two-dimensional hydrodynamic and morphological model.
- The setup and calibration of a one-dimensional hydrodynamic and advection-dispersion (salinity) model.

## 1.4   Available information

The following data was available and used for this study:

- Measured Great Fish River discharges at DWS stations Q9H018 (1977 – 2014), Q9H012 (1954 – 2014) and Q9H010 (1930 – 1955), (Department Water and Sanitation 2014).
- Topographic maps of the study area courtesy of the Chief Surveyor General (Cape Town).
- Digital satellite elevation data courtesy of the Shuttle Radar Topography Mission (SRTM-90), viewed in Google Earth. The SRTM-90 digital elevation model (DEM) has a 90 metre horizontal resolution, (Google 2014).
- Estuary cross-sections done by the CSIR in 1994, 1995 and 1999 in conjunction with surveys done in October 2012 by Amatola Municipality, only the most recent survey was used.
- Conductivity data of the Great Fish River at measurement station Q93_102487 (1977 – 2013) courtesy of the Resource Quality Information Services (Department Water and Sanitation - Resource Quality Information Services 2014).
- Predicted tidal water levels, courtesy of the WXTide 32 open source software.
- Field measurement of river discharge, flow velocity, bed load transport, suspended sediment concentration and salinity obtained during field work done in May 2012.

## 1.5   Methodology

The interrelationship between the fluvial morphology and the salinity of the Great Fish River Estuary was modelled by combining a two-dimensional morphological model created in Mike 21C with a one-dimensional advection dispersion (salinity) model created in the Mike 11 environment; both models were calibrated with data acquired during field work. In this thesis the terms estuary mouth, river mouth and tidal inlet are interchangeable.

Two hydrodynamic scenarios were used to study the effects of estuarine morphological changes on the salinity and salt intrusion.

1. Scenario A - A long term 5 year simulation with artificial mouth closure for defined upstream flow conditions.
2. Scenario B – The routing of different flood intensities down the river i.e. flood intensities with return periods of between 1:2 and 1:100 years (defined by their respective flood hydrographs).

### 1.5.1.1   *Scenario A - Long term simulation*

A 5 year morphological simulation was done in Mike21C. Simulated mouth closures were performed for specified flows. The Mike21C water level just upstream of the river mouth was used as the downstream model boundary condition of the Mike 11 advection dispersion module. Cross-sections used in the Mike 11 model were compiled from the survey data used in this study and not changed over time. The basis of this approach is that the water level (extracted from Mike21C) at the downstream boundary will reflect the morphological changes over the time of the model and specifically the river mouth.

*1.5.1.2     Scenario B - Flood hydrographs*

A set of flood events were simulated in the Mike 21C morphological model. The resulting bathymetry due to the flooding was then used to create cross-sections for the Mike11 advection dispersion (salinity) module. The cross section were used with a 3 month segment (the segment is representative of the average river flow conditions) of the 5 year boundary conditions of Scenario A. The salt intrusion behaviour was then compared for the different bathymetries due to flooding.

## 1.6     Limitations

### 1.6.1     Identified issues with the modelling approach

Ideally the salinity and morphology would be modelled simultaneously by the same model; unfortunately the Mike21C model does not have support for the modelling of salinity. Salinity affects the cohesiveness of sediments and promotes flocculation of fine sediments by increasing the inter particle attraction of particles (Grange et al. 2000). Flocculation in the Great Fish River estuary has been identified by Grange & Allanson (1995), the flocculation occurs predominantly at the river-estuary interface and results in the decrease of suspended particulate material in the middle reaches of the estuary. The separation of the 2 processes does however reduce the total simulation time.

Specific issues of the 2 modelled scenarios are briefly discussed below:

*1.6.1.1     Scenario A - Long term simulation*

River mouth closure is a function of the offshore wave climate, local tidal conditions, longshore sediment transport, local winds, local sediment availability and the river flow (Schumann 2003). Only the effects of the river flow and the tide could be modelled in this exercise. The Great Fish River Estuary is however a river dominated estuary which is permanently open (Reddering & Esterhuysen 1982).

*1.6.1.2     Scenario B - Flood hydrographs*

Mike 21C creates the model bathymetry by combining a grid file with locations of each grid cell with a bathymetry file which specifies the height of each grid cell, whereas Mike 11 accepts cross-section information directly. This causes a loss of accuracy when transferring bathymetry from the one platform to the other. The associated error is debateable.

# 2 LITERATURE REVIEW

## 2.1 Estuary definition

A comprehensive definition as formulated by Dyer (1997) states: "An estuary is a semi-enclosed coastal body of water which has free connection to the open sea, extending into the river as far as the limit of tidal influence, and within which sea water is measurably diluted with fresh water derived from land drainage".

Few South African estuaries comply with the internationally accepted definitions of estuaries, and specifically that of Dyer (1997). Many of our estuaries have intermittently closed river mouths which causes the failure of defined estuarine tidal criteria. Additionally ever present fresh water inflow is not guaranteed at numerous South African estuaries. This leads to an uncertain geomorphic classification of our estuaries (Schumann 2003).

## 2.2 General classification scheme

A scheme of classification of estuaries enables the prediction of the characteristics of estuaries. Different schemes are possible, depending on which criteria are used. River flow, tidal action and topography are factors that influence the mixing processes and extent of estuaries. Wind action may also become significant in certain cases (Dyer 1997).

Savenije (2005) classifies estuaries according to the following characteristics:

- Shape
- Tidal influence
- River influence
- Geology
- Salinity
- Estuarine numbers

### 2.2.1 Classification by shape

The following characteristic estuary shapes can be distinguished (Savenije, 2005):

- Prismatic: These estuaries have parallel banks and are man-made. A constant cross-section is maintained by dredging.
- Delta: A near prismatic estuary where the river overpowers the tidal influence. Deltas occur where the tidal range is small and the river has a high sediment load.
- Trumpet shape: River banks converge upstream of the river mouth. Aluvial estuaries typically have this shape.
- Fjords or drowned river valleys (Ria): Fjords are deep valleys created by glacial erosion and subsequently submerged due to sea level rise.
- Bays: Bays are semi-enclosed bodies which do not have significant river input, bays are similar to fjords.

### 2.2.2 Classification by tidal influence

Estuaries can be described in terms of tidal range, as originally described by Davies (1964):

Microtidal < 2 m range

Mesotidal <4 m, >2m

Macrotidal < 6 m, >4 m

Hypertidal > 6 m

The tidal range determines the volume of water which enters the estuary, *the tidal prism*. A larger tidal range would result in a larger tidal prism and vice versa. The range of the tidal influence and strength of the tidal currents are determined by the interaction between the tidal wave propagation and the morphological characteristic of the estuarine area. If the estuary sides converge the tidal wave will be compressed laterally and in the absence of friction the tidal range shall increase due to the conservation of energy. Friction along shallow water plains has the opposite effect. The relative magnitudes of the channel convergence and channel friction lead to three conditions as identified by Nichols and Biggs (1985):

1. *Hypersynchronous estuaries.* For these estuaries convergence exceeds friction. The tidal range and tidal currents increase toward the upstream end of the estuary until the riverine section is encountered, the convergence diminishes and the friction increases, decreasing the tidal effects. These estuaries tend to have a funnel shape.
2. *Synchronous estuaries.* These estuaries have equal convergence and friction effects; as a result the tidal range is constant along the estuary until the riverine section is reached.
3. *Hyposynchronous estuaries.* Friction exceeds convergence and the tidal effects are diminished throughout the estuary. The estuary mouth is typically restricted and water entering through the mouth is spread out within the estuary. Maximum velocities are encountered at the mouth.

### 2.2.3    Classification by river influence

Estuaries are classified by river influence according to two extreme cases (Dyer, 1997):

- Riverine estuary: Estuary is dominated by river flow for discharge and sediment supply, the water is fresh. This estuary behaves like a river and has parallel banks; tide propagates as a progressive wave. Typically prismatic or delta estuaries.
- Marine estuary: Estuary is dominated by the sea, water is saline and there is no significant fresh water input or sediment input from the land side. Tide propagates as a standing wave. Bays are an example.

### 2.2.4    Classification by geology

The geological history of an estuary determines its shape and characteristics. Depending on the degree of sediment deposition in an estuary the following three estuarine types can be distinguished (Dyer, 1997):

- Fixed bed estuary: These estuaries are remnants from a different geological era. The rate of sediment deposition in the estuary cannot keep up with the rate of sea level rise; these estuaries are drowned river valleys or fjords.
- Short alluvial estuary: These estuaries are situated in submerged valleys (ria's) or fjords, they are alluvial but the rate of sea level rise or tectonic dip is too fast for a morphological equilibrium to form.
- Long alluvial estuary, also known as a coastal plain estuary: These estuaries are fully alluvial and are filled with sediments from the river and the sea. The interaction between the sea and the river has reached a morphological equilibrium. These estuaries typically have a very flat bottom slope.

### 2.2.5    Classification by salinity

An estuary can be classified according to its salinity profile; the salinity profile is related to the estuary shape. Estuaries are defined as either positive or negative estuaries:

- Positive estuary: In these estuaries the salinity gradually decreases upstream. They are generally alluvial with a significant river input. These estuaries occur in temperate and wet tropical climates.
- Negative estuaries: In these estuaries the salinity increases upstream of the river mouth because they are shallow and evaporation exceeds rainfall and fresh water input from rivers. These estuaries occur in arid- and semi-arid climates. Due to the small fresh water input salt flats may result.

### 2.2.6    Classification by estuary number

Tide and river discharge are the dominant factors influencing estuary shape. A simple dimensionless ratio which characterises these factors is the Estuary number N, also known as the Canter-Cremens number. The Estuary number is the ratio between the amount of saline water entering the estuary during a tidal period and fresh water discharge(Savenije 2005). The Estuary number is defined by equation 2-1.

$$N = \frac{Q_f T}{P_t}$$
(2-1)

Where            $Q_f$ = Fresh water discharge [m³/s]

T = tidal period [s]

$P_t$ = Tidal prism [m³]

Estuaries can also be characterised by the ratio of potential energy provided to the estuary by the river due to the buoyancy of fresh water and the kinetic energy supplied to the estuary by the tide. This is referred to as the Estuarine Richardson number. If the Richardson number is high the estuary exhibits a sharp interface between the fresh water and sea water, subsequently stratification occurs. If the Richardson number is low it indicates that enough energy is available to mix the fresh river water with the saline tidal currents the estuary is thus well mixed. The Estuarine Richardson number is defined by equation 2-2.

$$N_R = \frac{\Delta \rho g h Q_f T}{\rho v^2 P_t}$$
(2-2)

### 2.2.7    Characteristics of alluvial estuaries

Typical characteristics of alluvial estuaries are shown in Table 2-1.

**Table 2-1: Characteristics of alluvial estuaries for different estuarine shapes (Savenije 2005)**

| Shape | Tidal wave type | River influence | Geology | Salinity | Estuarine Richardson number |
|---|---|---|---|---|---|
| Bay | Standing wave | No river discharge | - | Sea salinity | Zero |
| Ria | Mixed wave | Small river discharge | Drowned drainage system | High salinity, often hypersaline | Small |
| Fjord | Mixed wave | Modest river discharge | Drowned glacier valley | Partially mixed to stratified | High |
| Funnel | Mixed wave; large tidal range | Seasonal discharge | Alluvial in coastal plain | Well mixed | Low |
| Delta | Mixed wave; small tidal range | Seasonal discharge | Alluvial in coastal plain | Partially mixed | Medium |
| Infinite prismatic channel | Progressive wave | Seasonal discharge | Man-made | Partially mixed to stratified | High |

## 2.3 Classification of southern African estuaries

Due to the wave climate, tidal range and relatively small river flows our southern African estuaries exhibit special features. Reddering and Rust (1990) claim that only 37 of the 289 river mouths in southern Africa have permanent tidal inlets with the sea, additionally they identified the following common characteristics of these estuaries:

- The majority of the estuaries are small with tidal prisms less than $1 \times 10^6 \, \text{m}^3$.
- The majority are drowned river valleys.
- The tidal inlets are periodically obstructed by sand bars.
- The estuaries exhibit well developed flood-tidal deltas and poorly developed ebb-tidal deltas.
- The maximum tidal range of southern Africa is approximately 2 metres and thus defines southern African estuaries as microtidal.

It is important to note that classification of southern African estuaries is subject to the inevitable changes that are experienced by all the estuarine systems. The lifetime of an estuary is short in geological scale and they can be considered ephemeral features of the Coast (Whitfield 1992).

Schumann (2003) classifies a water body as an estuary in the South African context based on the following criteria:

- An estuary should have a predominantly sedimentary basin with seaward barrier present.
- Estuaries should be partially enclosed and experience the subsequent estuary tidal effects, estuaries that are intermittently closed are acceptable.
- Mixing of seawater and fresh water must occur predominantly although constant fresh water inflow is not critical. Tidal bays such as Saldanha Bay fail this requirement.

A typical South African estuary and its geomorphic features are shown in Figure 2-1.
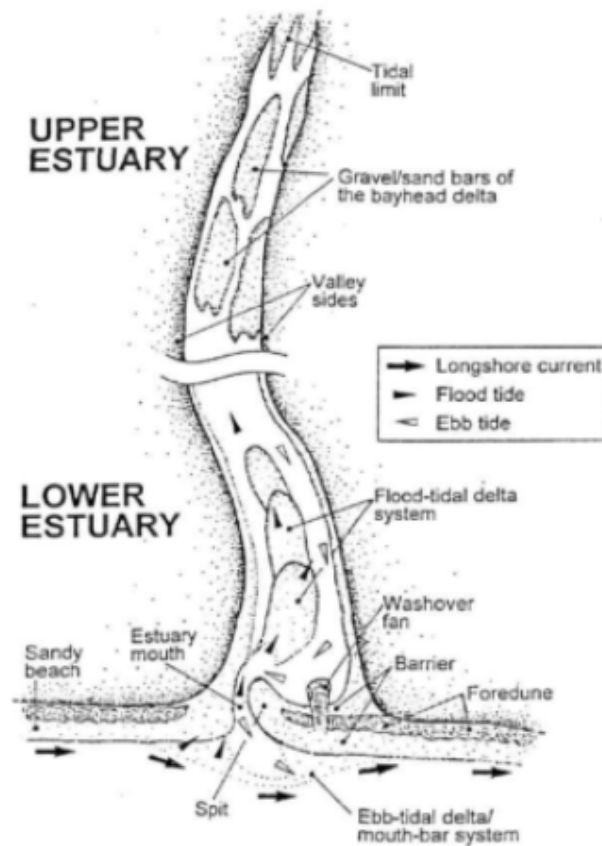
**Figure 2-1: Typical South African Estuary (Schumann 2003)**

## 2.4 Dominant estuarine flows

Estuaries are either; river– or tide– dominated depending in the relative strength of each process (see Section 2.2). South African estuaries such as the Great Fish River, Orange River and Mgeni estuaries are river-dominated, whereas estuaries such as the Berg River and Goukou are tide dominated (Beck 2005). The dominant process influences the composition and the magnitude of the sedimentation in the estuary.

### 2.4.1 Flood tide – dominates estuaries

The main hydrodynamic forcing mechanism in tide dominated estuaries is the tidal flow. Tide–dominated estuaries often experience tidal asymmetry. Tidal asymmetry is caused by the constriction/restriction of tidal flow (Schumann 2003). The degree of restriction is a function of the inlet geometry and the flow resistance due to the bed roughness of the tidal inlet (river mouth). Tidal asymmetry is graphically represented in Figure 2-2. The cross sectional area of the inlet generally varies with the water level, during high water levels (flood tide) the cross sectional area of the inlet is large and the flood flow into the estuary is minimally restricted. The relatively free flowing nature of the tide results in a small tidal lag ($\Delta T_H$) and small variation in peak tidal level ($\Delta H_H$). The reverse is the case during ebb tide when the inlet area is reduced due to the low water level. The tidal lag during ebb tide ($\Delta T_L$) is pronounced as well as the difference in ebb tide water levels ($\Delta H_L$). The lag of the tide in the estuary results in different magnitudes of flood and ebb currents (Beck 2005).

9
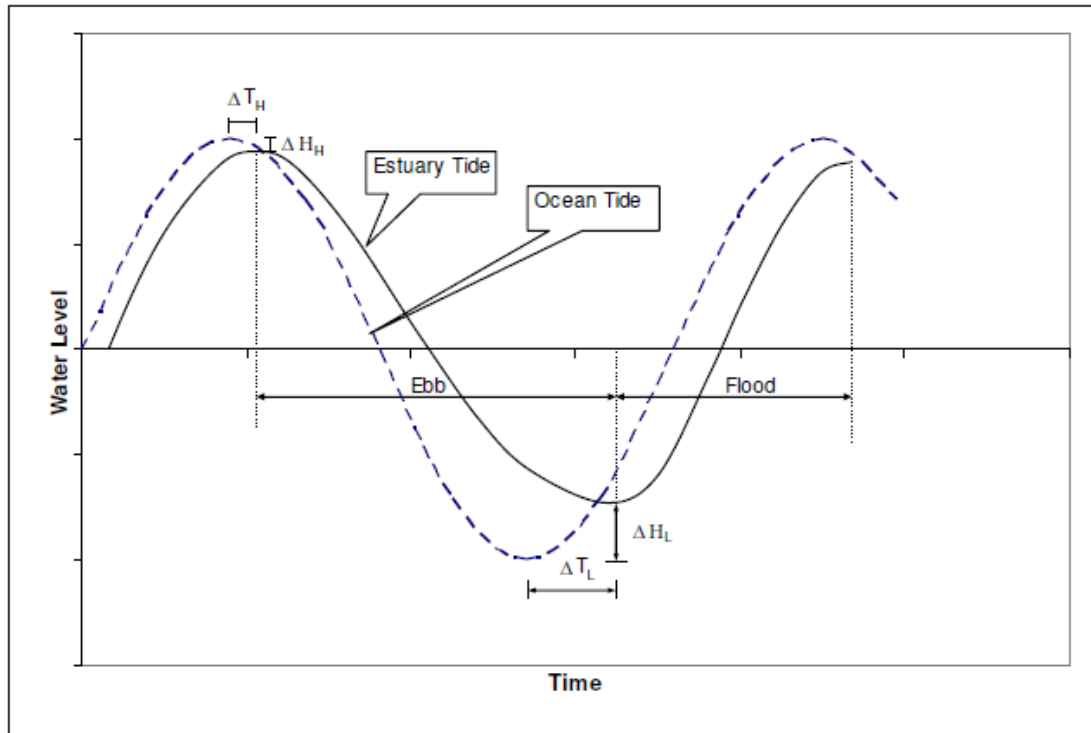
**Figure 2-2: Tidal asymmetry (Schumann, 2003)**

### 2.4.2    Ebb river-Dominated estuaries

In river dominated estuaries the river flows are stronger than the tidal flows. These estuaries have cohesive banks, moderately deep channels and small flood-tidal deltas and no noticeable ebb-tidal deltas. The lack of ebb-tidal delta is due to wave-action. Many KwaZulu-Natal estuaries have high river discharge and high sediment yields. In these estuaries sediments are flushed into the ocean by large floods and the tidal inlet is generally open due to the presence of strong river flows. River dominated estuaries are generally not threatened by marine sediments'.

## 2.5    Estuarine sedimentation

### 2.5.1    Sediment characteristics

The geological setting of South African estuaries determines their sedimentary characteristics. Estuarine sedimentation consists of the deposition of fluvial sediments, the influx of marine sediments and intra-estuarine sediments which are organic and typically a very minor component. Fluvial sediments originate from parent rivers and contain material eroded from the catchment. This sediment consists of clay, silt, fine sand and a sand and granular bed load component. Marine sediments are deposited on beaches and further abraded by the wave action; the resulting finer particles are then carried farther offshore. Beaches are dynamic landscapes which are constantly being reworked by wave action and winds. During low tide dried out sediments on the beach can be transported onshore and into an estuary. Whereas larger waves may again erode the dunes and flush the sediments back to the ocean. Marine sediments are generally composed of quartz or quartzite grains and a biogenetic component of broken up mollusc shells (typically 25 to 50% of beach sediment). These sediments are continually replenished and their composition stays fairly constant. The beach sediments in South Africa can be classified as sand with grain sizes varying between 0.1mm to 2mm. These size particles are generally non-cohesive. Finer sediments like silt and clay have ionic charges on the particles which are much stronger than the force of gravity, thus they are cohesive sediments. The cohesive forces of sediment greatly influence their behaviour (Schumann 2003).

### 2.5.2    Sedimentation-erosion cycles

During the ice–age and other cold-climate periods the sea level was much lower than today, consequently most rivers cut into the landscape to levels well below the current sea level. As the sea level rose these incised valleys were filled with water, this process is similar to the filling of a river valley after the construction of a dam. A sediment trap similar to a dam is created in the process. Estuaries occupying drowned river valleys is the common estuary type in South Africa (Schumann 2003). This sediment trap which is created follows the concept of an erosion base. The erosion base is the theoretical level above which erosion takes place and below which deposition of sediment occurs. The erosion base is generally equal to sea level. During severe floods the erosion base is shifted drastically lower. This eroded area is then filled again up to the erosion base level during typical river flow conditions.

Estuary sediments are from two main sources, namely the river catchment and the sea. Environmental factors influence the magnitude of these sediment components. Highly erodible catchments produce large river sediment yields whereas a highly energetic tidal environment promotes the influx of marine sediments due to processes such as littoral drift. Generally erosion and sedimentation occurs in cycles, these cycles can be classified as long-, medium- and short- term (Schumann 2003) .Long term cycles involve global changes in sea level and change the erosion base level. Some estuaries have not reached equilibrium and consequently experience little erosion during river floods (e.g. Knysna estuary). In the long term estuaries are generally filled by sediments as the sea level is rising. Systems such as the Thukela River which has a high sediment yield and river discharge display distinct offshore sedimentary deposits, indicating that the estuary level is above or equal to the estuary base. Long term is defined as periods of more than 1000 years. Medium term cycles are more noticeable as they are related to the issues with sedimentation experienced in periods of between 10 and 1000 years. Erosion is typically caused by large floods, whereas sedimentation occurs during subdued river flows. Short term cycles are related to tidal and seasonal aspects of the flow and related seasonal accumulation of fluvial and marine sediments.

Cooper (1994) introduced a conceptual model for the cyclic evolution of river dominated estuaries in South Africa. His model is shown in Figure 2-3, the model consists of 4 stages:

> A: Under a stable morphological state a narrow channel is scoured. Wide floodplains consist of cohesive sediments and vegetation.
>
> B: Extreme floods destroy the tidal barrier and cohesive floodplains are washed away, the fluvial catchment and marine sediments from the tidal inlet are deposited as a submerged delta downstream of the system.
>
> C: Post flood the deltas formed by flood events are deposited onshore by wave action and become emergent.
>
> D: During stable hydrodynamic conditions the barriers reform as the floodplains re-vegetate. As the river discharge subsides the wave energy seal the remaining breach at the tidal inlet.
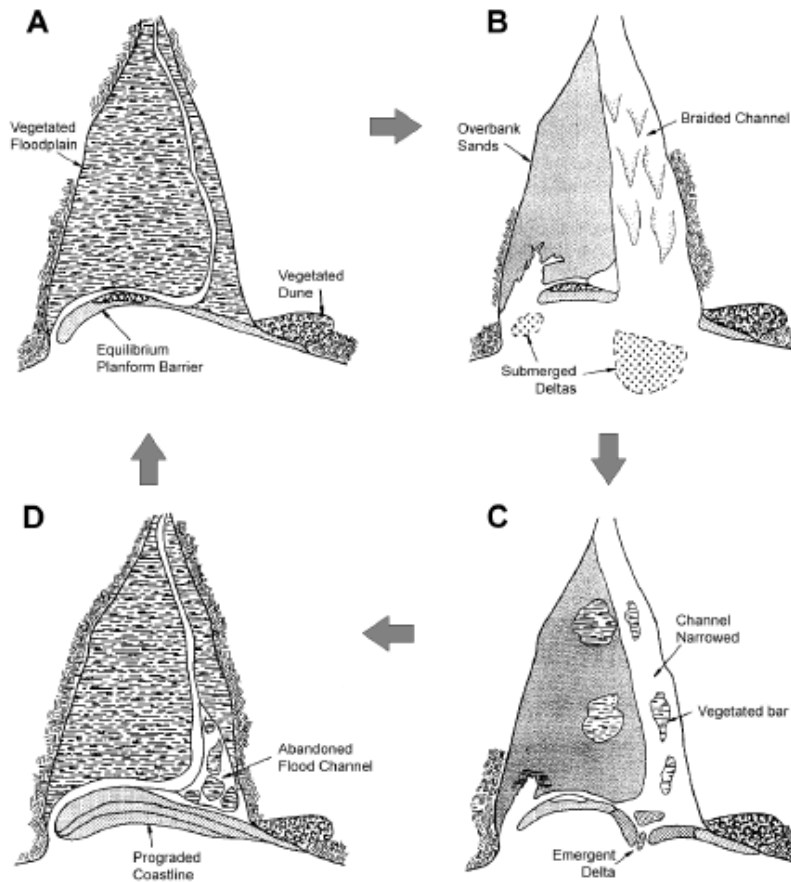
**Figure 2-3: The 4 cyclic stages of a river dominated estuary in South Africa (Cooper 1994)**

### 2.5.3 Sedimentation areas

Estuarine sedimentation is evident in three regions of the estuary (Beck 2005):

1: At the tidal head sediments deposit due to the reduction in bed slope from the steep river reach to the relatively flat estuary reach. Accumulated sediment is mainly fluvial.

2. At the estuary mouth marine sediments from littoral drift accumulates on the tidal delta as tidal currents subside during transition from the narrow inlet to the wide estuary.

3. In the middle estuary the influence of salt water promotes the flocculation of fluvial cohesive sediments which are in suspension.

## 2.6 Tidal inlets

A tidal inlet consist of three distinct morphological elements namely the tidal channel and the ebb and flood delta. (Tran et al. 2012), refer to Figure 2-1. The tidal channel is maintained by the tidal current, the tidal channel can be prone to closure in certain circumstances. The flood delta is a deposition of marine sediments carried inside the estuary by the flood tide, the sudden reduction in flow velocity from the narrow inlet to the wide estuary facilitates the deposition of the marine sediments carried from the tidal inlet. The ebb-tidal delta is similar to the flood-delta but consist of marine and fluvial sediments. Ebb-tidal deltas are generally destroyed by wave action.

Inlet closure occurs when the inlet flow is insufficient to clear the inlet of deposits. Inlet closure is a gradual process or can be caused by an episodic event such as a large storm. Two mechanism (shown in Figure 2-4) are behind the inlet closure of small estuaries situated in wave-dominated micro-tidal coasts with large seasonal variations in river flow, such as those found in South Africa (Ranasinghe et al. 1999):

1. The interaction between inlet current and longshore current

   > Sediment moves along the coast due to the longshore current, if tidal inlet velocities are strong enough the tidal inlet remains open, during periods of low river flows the inlet channel is not maintained and closure ensues.

2. The interaction between the inlet current and onshore sediment transport.

   > During large storm sediment is eroded from the beach and surf zone and deposited in the sea. After the storm has subsided the stored deposited sediments will be transported onshore by the wave action of the sea. If tidal inlet currents are weak mouth closure ensues.
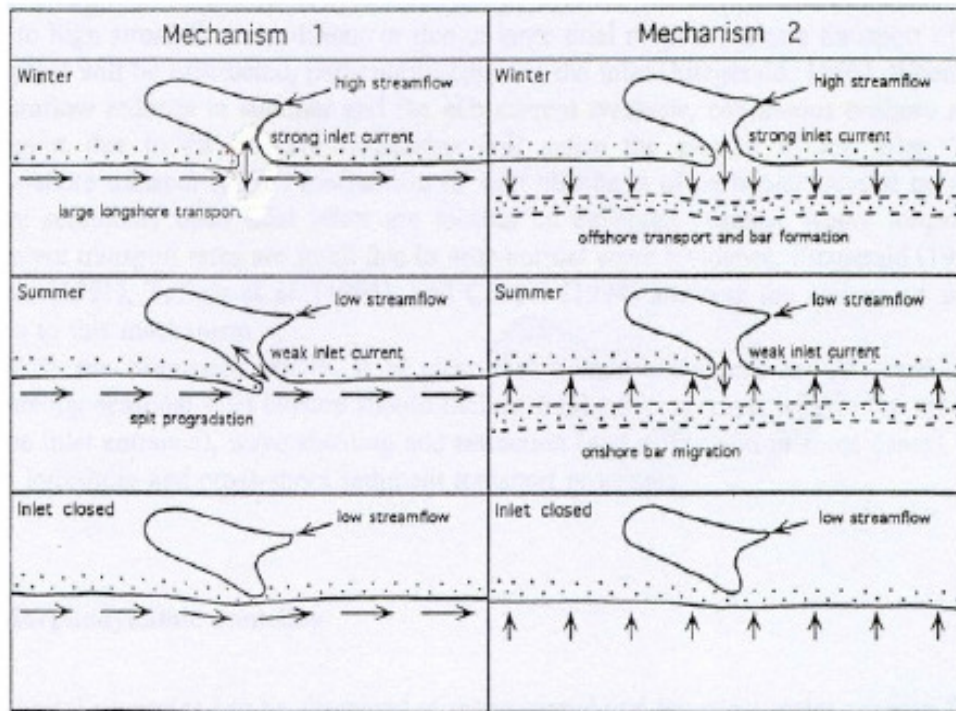


**Figure 2-4: Closure mechanisms (Ranasinghe et al. 1999)**

Authors such as Hayes (1975) and Escoffier (1940) among others have formulated empirical methods of predicting mouth closure based on local conditions. The research of Escoffier culminates in the Escoffier diagram, depicted in Figure 2-5. The stability of the tidal inlet is a function of the flow velocity through the inlet ($V_c$) an the inlet cross- sectional area (A). As the inlet area approaches zero the inlet velocity approaches zero due to the increasing friction forces, friction forces being proportional to the cross-sectional area. Diminished velocities promote the settling the sediment, thereby promoting closure.

13
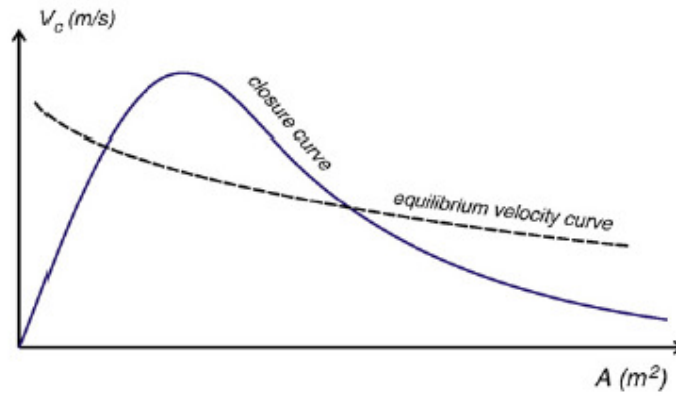
**Figure 2-5: Escoffier diagram (Escoffier 1940).**

Hayes (1975) developed a diagram for inlet closure based on the tidal and wave environment. A weak tidal environment combined with high wave energy results in mouth closure, whereas a large tidal range and weak waves have the opposite effect. Refer to Figure 2-6.
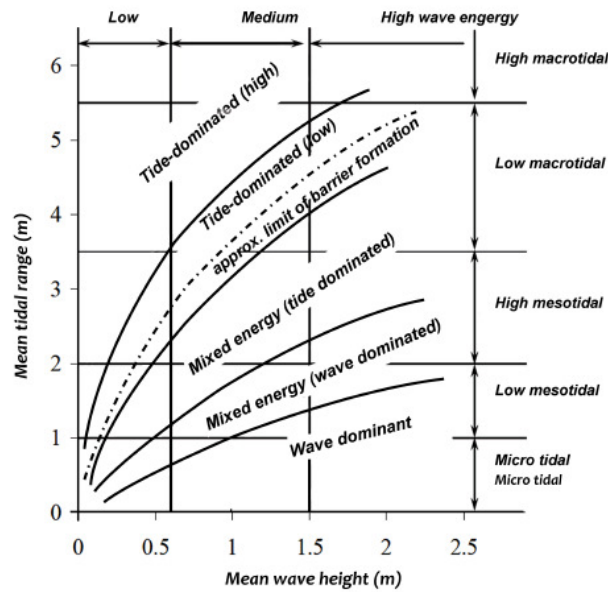


**Figure 2-6: The relationship between the tidal range and wave height at tidal inlets with the predicted limit of barrier formation as defined by Hayes (1975)**

14

## 2.7    Mixing mechanisms

Mixing in estuaries can be attributed to two main drivers: the kinetic and potential energy influx provided by the tide and the potential energy created by the density difference between fresh and salt water. Four mixing mechanisms are attributed to these drivers:

### 2.7.1    Turbulent mixing

Mixing of fresh and salt water occurs due to the flow turbulence produced by the friction from the estuary bottom and banks. Turbulent mixing is considered inferior to other tide generated mixing mechanisms (Fisher et al. 1979).

### 2.7.2    Gravitational mixing

Gravitational mixing is attributed to the density difference and resulting hydrostatic pressure difference between fresh water and sea water, this phenomenon is presented in Figure 2-7. At the interface between the fresh water and seawater the average hydrostatic forces cancels out although the pressures over the water depth is not equal, this phenomenon results in residual currents. At the surface the resultant pressure is directed seawards and the resultant pressure at the estuary bed is upstream. This phenomenon creates a salinity gradient in the water column and is an important cause of estuarine mixing.
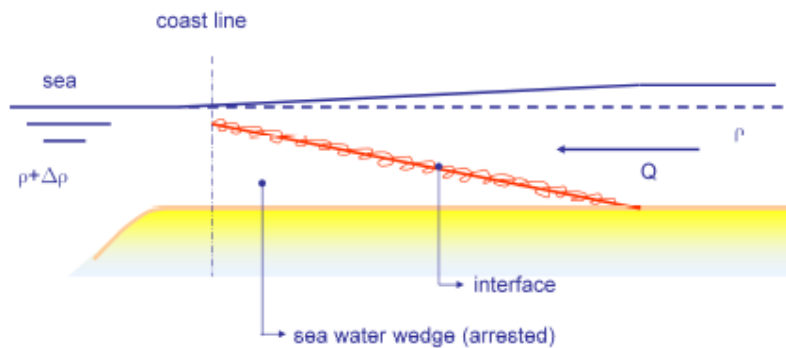


**Figure 2-7: The saline wedge (Savenije 2005)**

### 2.7.3    Trapping

Tidal trapping is caused by the shape and geometric characteristics of an estuary. Water can be trapped if tidal inlets or tidal flats are present. Due to the trapping there is a phase lag between the flow in the tidal flat and the flow in the main channel, resulting in a density difference. Tidal trapping is an important mixing process in estuaries with large tidal flats (Fisher et al. 1979).

### 2.7.4    Tidal pumping

Tidal pumping is the term for the mixing caused by residual currents caused by the occurrence of separate flood and ebb channels of the estuary and not the salinity gradient. This process is dominant at the river mouth rather than in the middle reach where gravitational mixing is dominant (Savenije 2005).

## 2.8   Salt intrusion types

Salt intrusion in estuaries is determined by the balance between the inward dispersive salt transport and the outward advective transport of fresh water (Savenije 1993). Salt intrusion can be predicted by advection dispersion modelling which relies on the concept of conservation of mass (DHI 2011a), as was used in this study, refer to Section 3.2.3 for mathematical background. When advection is dominant the estuary becomes fresher and when dispersion is dominant the estuary becomes more saline. Estuary salt intrusion is influenced by the topography, hydrology and tide of the estuary.

There are generally three types of salt intrusion defined for estuaries, namely:

a)   stratified (saline wedge)
b)   partially mixed
c)   well mixed

The longitudinal salinity distribution for the three types is indicated schematically by Figure 2-8.

The salt intrusion type is related to the estuary number. Stratified estuaries occur when the river discharge is large (large estuary number), such as during flood events. In well mixed estuaries the tidal prism is large compared to the river discharge (small estuary number).
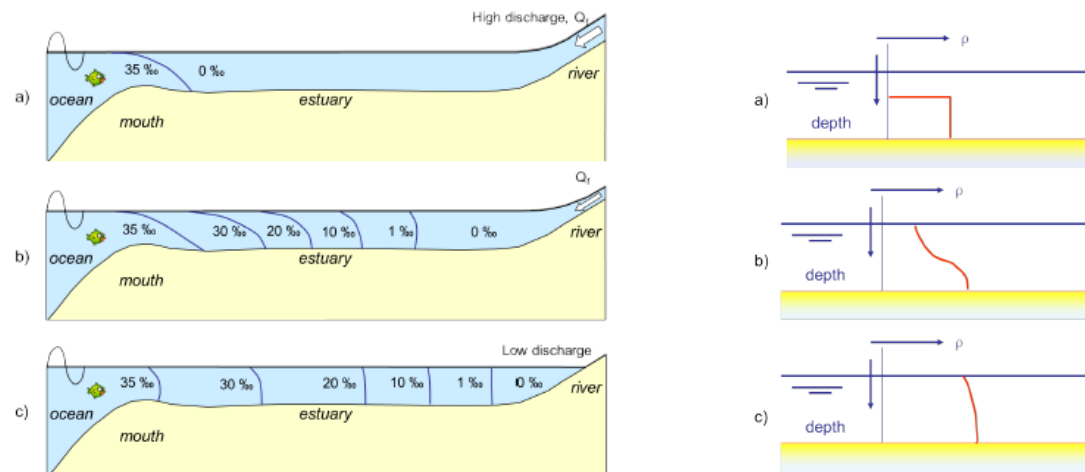


**Figure 2-8: Longitudinal (left) and vertical (right) salinity distribution of (a) stratified, (b) partially mixed and (c) well mixed estuaries (Savenije 2005)**

## 2.9   Literature summary

The classification of estuaries enables the prediction of the characteristics of an estuary. The characteristics of an estuary are determined by the river flow, the tidal environment and the catchment topography. In the South African context a water body is defined as an estuary when it has a predominantly sedimentary basin and seaward barrier which experiences tidal effects and the mixing of fresh and saline water. Southern African estuaries are generally drowned river valleys situated in a micro-tidal environment with distinct sand bars evident at the tidal inlet. Due to the energetic wave climate and microtidal environment tidal inlet closure is common in estuaries where river flow is sporadic and/or small. The flows inside an estuary are either river- or tide- dominated. River dominated estuaries exhibit features similar to rivers whereas tide dominated estuaries resemble bays.

The sedimentation and erosion in estuaries is determined by the geological history of the estuary, the catchment sediment characteristics, the catchment hydrology and the marine environment. Estuarine sediments are of fluvial (river) and marine origin. The estuary has an equilibrium condition (estuary bed level) which is mainly determined by the sea level. Generally the erosion and sedimentation in an estuary occurs in cycles, during low flow periods sedimentation occurs and during floods erosion occurs. The tidal inlet is sensitive to the sedimentary cycle, during low flow conditions the inlet will constrict due to the dominant wave action and the subsequent depositions of marine sediments whereas during flood events the tidal inlet will breach due to the dominant river flow.

The saline environment of an estuary is caused by the mixing of salt water from the ocean and the fresh river water. The mixing is attributed to two main drivers: the kinetic and potential energy influx provided by the tide and the potential energy created by the density difference between fresh and saline water. The salt intrusion of an estuary is determined by the magnitude of the river flow, magnitude of the tidal prism and the tide period. Salt intrusion can be predicted by the estuary number which is a relationship between the previously mentioned parameters. Large river flows result in stratified estuaries whereas small river flows result in well mixed estuaries.

# 3    NUMERICAL MODELLING BACKGROUND

Two numerical models were used in this study, namely Mike11 and Mike21C, both software packages were developed by the Danish Hydraulic Institute (DHI).

## 3.1    Two dimensional hydrodynamic and morphological modelling

### 3.1.1    Numerical model background

Mike 21C is a module of the Mike21 software package which uses a curvilinear (boundary fitted) grid instead of a conventional rectangular grid; the model incorporates an algorithm which simulates the three dimensional helical flow (secondary currents) in river bends. The model supports the simulation of suspended and bed loads of cohesive and non-cohesive sediments. This model is designed with the purpose of predicting the sediment characteristics of rivers and estuaries. The following phenomenon are described by the Mike21C software: (DHI 2011c)

- Flow hydrodynamics (HD) - water levels and flow velocities are computed over the grid (rectangular or curvilinear) by solving the vertically integrated St. Venant equations of continuity and the conservation of momentum.
- Helical flow - secondary currents which develops in channel bends.
- Sediment transport – the morphological changes over time due to the prescribed model boundary conditions which can be described by various sediment transport formulas (e.g Engelund-Hansen, Yang, van Rijn) for cohesive and non-cohesive sediments.

The model consists of 2 modules (parts); namely hydrodynamic and morphological.

### 3.1.2    Hydrodynamic module (HD)

The hydrodynamic (HD) module forms the basis of the Mike21 software package. The HD module simulates water levels and flows throughout the model network due to the specified boundary conditions and model bathymetry. The module solves the vertically integrated Saint Venant equations for continuity and conservation of momentum over a user created grid. The equations include the effects of the following:

- convective and cross momentum
- pressure gradients
- Eddy currents
- sinks and sources

The following approximations apply to the solution process:

***Shallow water approximation***

       The lateral momentum exchange due to fluid friction is omitted.

***Hydrostatic pressure distribution***

       The gradients of the vertical velocity component are neglected.

***Rigid line approximation***

       This approximation implies that the water surface is considered rigid and impermeable. The water surface is shear stress free and only experiences normal forces.

The listed approximations imply that the flow model is valid for shallow, gently varying topography wide river channels with small Froude numbers (DHI 2011c)

Either a Cartesian or curvilinear grid can be used by the solver. The curvilinear grid is created by the solution of elliptic partial differential equations. When a curvilinear grid is used Cartesian coordinates (x, y) are converted to curvilinear orthogonal coordinates (s, n). The curvilinear orthogonal coordinate system (s, n) used by the Mike21C model can be seen in Figure 3-1. The curvilinear grid gives a more accurate description of the flow field at river banks, which is important when computing bank erosion.
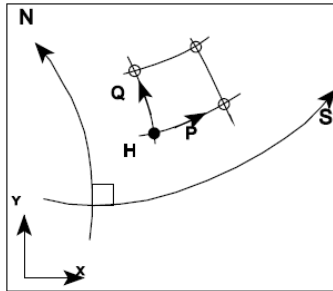


**Figure 3-1: Location of flow parameters: fluxes P and Q, and flow depth H in a curvilinear coordinate system (s, n) (DHI, 2011)**

Transformations between Cartesian and curvilinear coordinate systems are shown below (equations 3-1, 3-2, 3-3):

**Where**          $h$ = Cartesian depth

$H$ = Curvilinear depth

$u, v$ = Cartesian velocity components

$U, V$ = Curvilinear velocity components

$R_s, R_n$ = radius of curvature of s- and n- lines

*For depth:*

$$h = H \ \ and \ \frac{\partial h}{\partial x} = \frac{\partial H}{\partial s} \ and \ \frac{\partial h}{\partial y} = \frac{\partial H}{\partial n} \tag{3-1}$$

*For velocity:*

$$u = U \ and \ v = V$$

$$\frac{\partial u}{\partial x} = \frac{\partial U}{\partial s} - \frac{V}{R_s} \ \ and \ \frac{\partial u}{\partial y} = \frac{\partial U}{\partial n} - \frac{V}{R_n} \tag{3-2}$$

$$\frac{\partial v}{\partial x} = \frac{\partial V}{\partial s} + \frac{U}{R_s} \ \ and \ \frac{\partial v}{\partial y} = \frac{\partial V}{\partial n} - \frac{U}{R_n} \tag{3-3}$$

**The St. Venant equations solved by the hydrodynamic model are:**

*Continuity (eq. 3-4):*

$$\frac{\partial H}{\partial t} + \frac{\partial p}{\partial s} + \frac{\partial q}{\partial n} - \frac{q}{R_s} + \frac{p}{R_n} = 0 \tag{3-4}$$

*Momentum s-direction (eq. 3-5):*

$$\frac{\partial p}{\partial t} + \frac{\partial}{\partial s}\left(\frac{p^2}{h}\right) + \frac{\partial}{\partial n}\left(\frac{pq}{h}\right) - \frac{2pq}{hR_n} + \frac{p^2-q^2}{hR_s} + gh\frac{\partial H}{\partial s} + \frac{g}{C^2}\frac{p\sqrt{p^2+q^2}}{h^2} = RHS \tag{3-5}$$

*Momentum n-direction (eq. 3-6)*

$$\frac{\partial q}{\partial t} + \frac{\partial}{\partial s}\left(\frac{pq}{h}\right) + \frac{\partial}{\partial n}\left(\frac{q^2}{h}\right) + \frac{2pq}{hR_s} - \frac{q^2-p^2}{hR_n} + gh\frac{\partial H}{\partial n} + \frac{g}{C^2}\frac{q\sqrt{p^2+q^2}}{h^2} = RHS \tag{3-6}$$

Where        s, n = Curvilinear coordinates

p,q = Mass fluxes in the s- and n- direction

H = Water level

h = Water depth

g = Gravitational acceleration

C = Chezy coefficient

$R_s$, $R_n$ = radius of curvature of s – and n-lines

RHS = Reynolds stresses, Coriolis force and atmospheric pressure

*RHS s – direction (eq. 3-7):*

$$\frac{\partial}{\partial s}\left(E\frac{\partial p}{\partial s}\right) + \frac{\partial}{\partial n}\left(E\frac{\partial p}{\partial n}\right) - \frac{2E}{R_s}\frac{\partial p}{\partial} - \frac{\partial E}{\partial s}\frac{q}{R_s} - \frac{2E}{R_n}\frac{\partial q}{\partial n} - \frac{\partial E}{\partial n}\frac{q}{R_n} \tag{3-7}$$

*RHS n – direction (eq 3 -8):*

$$\frac{\partial}{\partial s}\left(E\frac{\partial p}{\partial s}\right) + \frac{\partial}{\partial n}\left(E\frac{\partial p}{\partial n}\right) + \frac{2E}{R_s}\frac{\partial p}{\partial} + \frac{\partial E}{\partial s}\frac{q}{R_s} + \frac{2E}{R_n}\frac{\partial q}{\partial n} + \frac{\partial E}{\partial n}\frac{q}{R_n} \tag{3-8}$$

Where        E = eddy viscosity

The equations are solved by an implicit finite difference technique. A space staggered computational grid is used, refer to Figure 3-2.
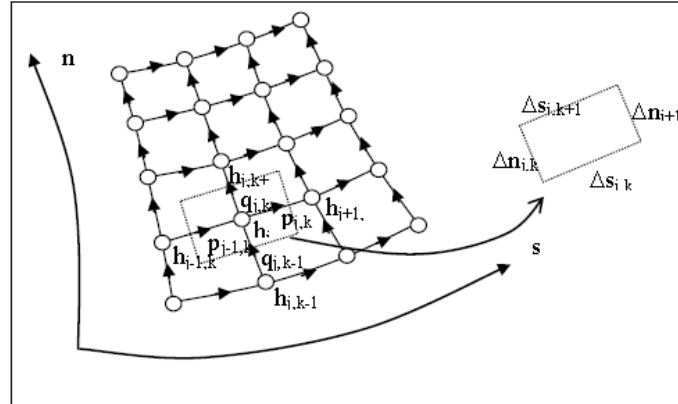
**Figure 3-2: Finite difference grid in space. Water depth denoted by h, p and q are fluxes in their respective directions (s, n).**

### 3.1.3    Helical flow

As water flows around a river bend an imbalance of centripetal force is generated. The flow velocity in the upper part of the flow is higher than the flow velocity near the river bed; therefore the fast water column follows a path with a larger radius of curvature than the slower water column to maintain an approximately constant centripetal force over the flow depth. This phenomenon most apparent in rivers with small width/ depth ratios, helical flow can have a significant influence on sediment transport direction and the subsequent morphological river changes (DHI 2011c). Helical flow is responsible for bend scour.
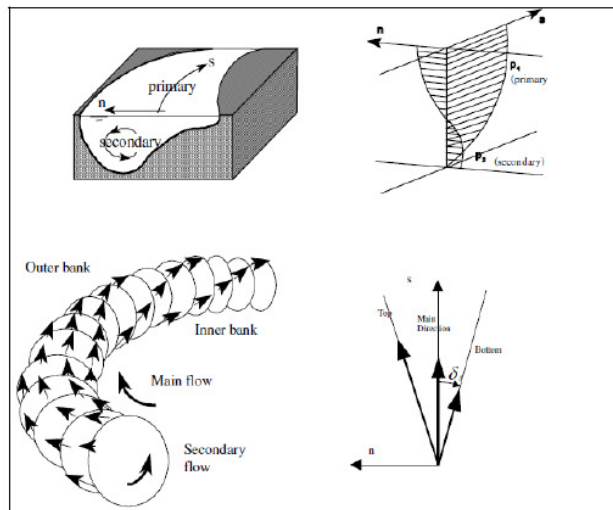


**Figure 3-3: Helical flow phenomenon (DHI 2011c)**

The intensity of the helical flow is related to the transverse velocity component, this is defined by DHI (2011) as (eq. 3-9):

$$i_s = u \frac{h}{R_s}$$
(3-9)

Where            u = Flow velocity

                 $R_s$ = Radius of streamline curvature

                 $i_s$ = Helical flow intensity

21

This gives the following bed shear stress direction (eq. 3-10):

$$\tan \delta_s = \beta \frac{h}{R_s}$$
(3-10)

With

$$\beta = \frac{\alpha 2}{\kappa^2}\left(1 - \frac{\sqrt{g}}{\kappa C}\right)$$
(3-11)

Where           $\delta_s$ = The angle between the bed shear stress and average flow direction

$\kappa$ = von Karman constant, 0.4

C = Chezy number

$\alpha$ = model calibration constant

### 3.1.4    Sediment transport

Estuarine sediment transport is similar to sediment transport in rivers. The four modes of sediment transport in water are sliding, rolling, saltation and suspension, refer to Figure 3-4. Particles that are sliding, rolling and saltating collectively form the bedload. The particles suspended in the water are the suspended load. The suspended load and the bed load combined is the total load. The suspended load also has a wash load component which is defined as the portion of the suspended load which originates upstream and not from the bed material. Suspended load particles seldom come in contact with the bed, they are deposited when the flow velocity diminishes sufficiently. Sliding and rolling are prevalent in slower flows, whereas saltation and suspension occur in faster flows (van Rijn 1984)
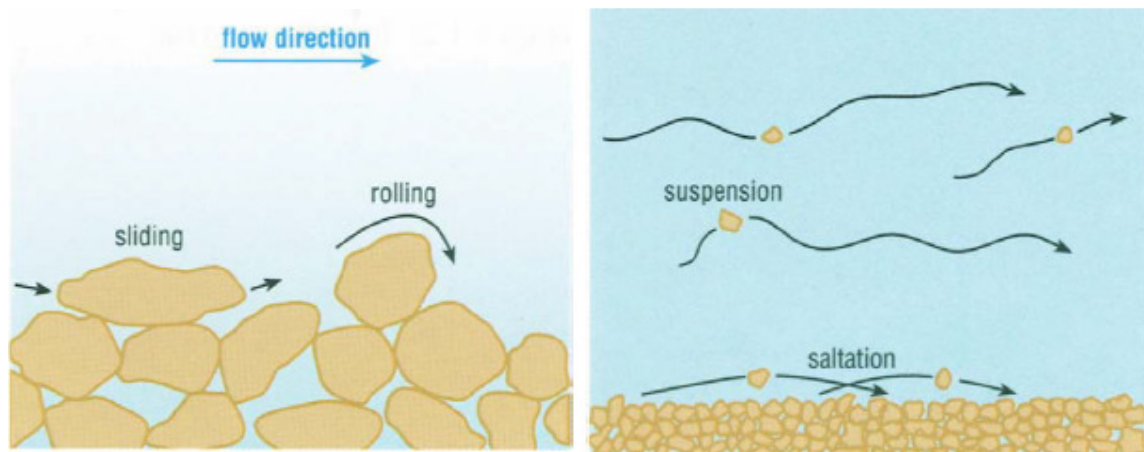


**Figure 3-4: Sediment transport mechanisms (Open University 1999)**

A fundamental concept in sediment transport theory is the threshold condition where the transporting capacity of a flow is sufficiently large to initiate sediment movement. This is referred to as the criteria for incipient motion. Figure 3-5 illustrates the forces acting on a spherical sediment particle at the bottom of a river channel. The channel slope of most rivers is sufficiently small that the component of gravitational force in the flow direction can be ignored. The forces considered are; the drag force $F_D$, the submerged weight $W_s$, the resistance force $F_R$ and the lift force $F_L$.

Incipient motion is achieved when one of the following conditions is satisfied (Engelund & Hansen 1967):

$$F_L = W_s \tag{3-12}$$

$$F_D = F_R \tag{3-13}$$

$$M_O = M_R \tag{3-14}$$

Where $M_O$ = overturning moment due to $F_D$ and $F_L$

$M_R$ = resisting moment due to $F_L$ and $W_S$

Incipient motion criteria are derived from either a velocity (stream power) or shear stress approach.
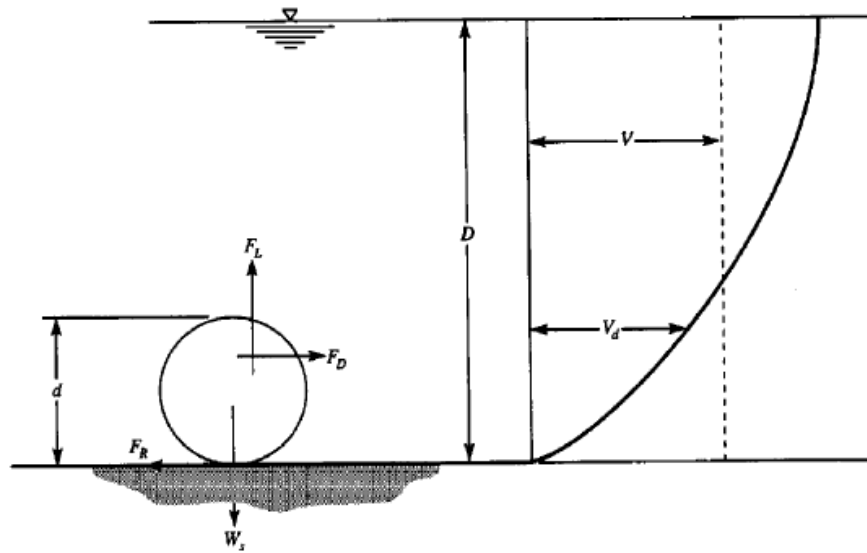


**Figure 3-5: Forces acting on a sediment particle (Yang 1983)**

### 3.1.4.1  *Suspended load transport*

Suspended load is complex due to its three-dimensional nature. The transport of mass has two mechanisms namely; advection and dispersion (AD). Advection and dispersion is also responsible for the intrusion of salt into or out of an estuary. Advection of the sediment mass is linked to the average velocity of the fluid. Dispersion of suspended sediment mass is caused by turbulent mixing and dispersive transport due to concentration gradients. Suspended load modelling differs from bed load modelling as the suspended load is not only dependant on the local hydraulic conditions but also upstream river conditions and previous local hydraulic conditions. A time scale is derived from the settling time of the suspended sediment and a length scale is derived from the distance travelled by the sediment grain during settlement.

The model for suspended sediment transport used by the MIKE 21C package is based on the theory described by Galappatti (1983). The partial differential equation for the transport of suspended sediment by convection and turbulent dispersion is (eq. 3-15):

$$\frac{\partial c}{\partial t} + u \frac{\partial c}{\partial x} + v \frac{\partial c}{\partial y} + w \frac{\partial c}{\partial z} = w_s \frac{\partial c}{\partial z} + \frac{\partial}{\partial x}\left(\epsilon \frac{\partial c}{\partial x}\right) + \frac{\partial}{\partial y}\left(\epsilon \frac{\partial c}{\partial y}\right) + \frac{\partial}{\partial z}\left(\epsilon \frac{\partial c}{\partial z}\right) \tag{3-15}$$

23

Where            c = concentration of suspended sediment

ε = turbulent diffusion coefficient

u, v, w = Flow velocity in the x,y and z directions

$w_s$ = Fall velocity of suspended sediment particle

z = Vertical coordinate

If horizontal diffusion is omitted the equation along a streamline is (eq. 3-16):

$$\frac{\partial c}{\partial t} + u\frac{\partial c}{\partial s} + v\frac{\partial c}{\partial n} + w\frac{\partial c}{\partial z} = w_s\frac{\partial c}{\partial z} + \frac{\partial}{\partial z}\left(\epsilon\frac{\partial c}{\partial z}\right) \qquad (3\text{-}16)$$

Where            n = Transverse coordinate

s = Stream-wise coordinate

u = Stream-wise flow velocity

v = Secondary (transverse) flow velocity

In this study the Engelund Hansen method was used for the estimation of sediment transport, this model is a total load formula which does not directly differentiate between bed load and suspended load. The suspended load component of the total transport is defined by a user specified calibration parameter. When the sediment enters suspension it is incorporated into the sediment budget of the suspended load.

### 3.1.4.2    *Bed load transport*
The morphological behaviour of a river is very dependent on the interaction between the bed load and the alluvial river bed. The bed load reacts immediately to changes in local hydraulic conditions, unlike the suspended load which typically has a sediment component which originated upstream, for this reason there is no need for advection-dispersion modelling when simulating the bed load. When modelling the bed load the following effects are important:

1. The effect of helical flow on the direction of the bed shear stress
2. The effect of a sloping river bed

The bed slope influences the rate of sediment transport and the sediment transport direction, for morphological modelling the change of direction is important (DHI 2011b). There are 2 approaches that have been adopted for modelling. The first approach modifies the critical shear stress for incipient motion (Shields parameter), the following equation (3-17) applies:

$$\theta_c = \theta_{c0}\left(1 + \frac{\partial z_b}{\partial s}\right) \qquad (3\text{-}17)$$

Where            $\theta_c$ = Modified Shields parameter

$\theta_{c0}$ = Critical Shields parameter for uniform shear flow

$z_b$ = Bed level

s = Stream-wise coordinate (horizontal coordinate)

The above equation cannot be used with transport models that assume zero bed load transport at critical shear stress (e.g. Engelund and Hansen formula). The following formula (eq. 3-18) is applied for these transport equations:

$$S_s = \left(1 - \frac{\alpha \partial z^*}{\partial s}\right) S_{bl} \tag{3-18}$$

Where $\qquad$ $\alpha$ = Model calibration parameter

$\qquad\qquad$ $S_{bl}$ = Sediment transport formula bed load

$\qquad\qquad$ $S_s$ = Stream-wise bed load component

The MIKE 21C modelling environment uses the second approach. The parameter $\alpha$ has to be estimated in the calibration process, values are in the range of 0.2 to 1.5.

Several models of transverse bed slope prediction have been proposed. Talmon et al. (1995) carried out extensive experiments on existing mathematical models and suggested the following formula (eq. 3-19):

$$S_n = \left(\tan \delta_s - G \theta^{-a} \frac{\partial z^*}{\partial n}\right) S_{bl} \tag{3-19}$$

Where $\qquad$ G = Transverse bed slope factor

$\qquad\qquad$ a = Transverse bed slope exponent

$\qquad\qquad$ $\tan \delta_s$ = Bed shear direction change due to helical flow strength

G, and a are calibration coefficients. Talmon et al. (1995) recommends values of G = 1.25 and a = 0.5 for natural rivers.

Transport in the x- and y- directions are calculated with the following formulas (eq. 3-20 and 3-21):

$$S_x = S_s \cos \emptyset + S_n \sin \emptyset \tag{3-20}$$

$$S_y = S_n \cos \emptyset - S_s \sin \emptyset \tag{3-21}$$

### 3.1.4.3    *Sediment transport formulae*
The magnitude of sediment brought to suspension is calculated by sediment transport formulas. The MIKE 21C software package uses the following formulas:

***Symbols:***

$c_e$ : Equilibrium mass concentration (g/m$^3$)

C : Chezy number (m$^{0.5}$/s)

$d_{50}$: median particle diameter (mm)

$k_b$ : Bed load calibration factor (-)

$k_s$ : Suspended load calibration factor (-)

s : Sediment relative density (-)

$S_{bl}$ : Bed load (m$^2$/s)

$S_{sl}$ : Suspended load (m$^2$/s)

$t_s$ : Time scale (s)

$S_{tl}$ : Total load (m$^2$/s)

u : Velocity (m/s)

The Shields parameter is defined by equation 3-22:

$$\theta = \frac{\tau}{\rho g(s-1)d_{50}}$$  (3-22)

Where

$\tau$ - Flow shear stress

$\rho$ - Water density

g- Gravitational acceleration

s - Relative sediment density $p/p_s$

Flow shear stress consist of form drag $\tau''$ and skin friction $\tau'$. Total shear stress is estimated from the Chezy number and the flow velocity (eq. 3-23):

$$\tau = \tau' + \tau'' = \rho g \frac{u^2}{C^2}$$  (3-23)

For skin friction the equation below (3-24) developed by Engelund and Hansen (1967) is used unless otherwise calculated for specific transport formulas.

$$\theta' = 0.06 + 0.4\theta^2$$  (3-24)

Non-dimensional sediment transport rate is defined by equation 3-25:

$$\phi = \frac{S}{\sqrt{(s-1)gd^3}}$$  (3-25)

Where:

S - Sediment transport

d – Grain size

$\phi$ - Non-dimensional sediment transport

The basic sediment transport parameters developed in this section can be used with a variety of sediment transport formulas. Transport formulas can be classified by their approach in the determination of the suspended and bed load component of the total sediment transported. Formulas are either for the total load case which does not differentiate between suspended and bed load or formulas that make a clear differentiation between the two transport mechanisms. When total load formulas are used the model differentiates between bed load and suspended load by means of a user defined ratio. The sediment transport formulas available to the user are indicated in Table 3-1.

**Table 3-1: Sediment transport theories available in Mike21C**

| Transport formula | Type | Approach | Notes |
|---|---|---|---|
| Engelund & Hansen (1967) | total load | semi-empirical | Default Mike21C transport formula and widely used. |
| van Rijn (1984) | bed load and suspended load | semi-empirical | The van Rijn model divides suspended sediment and bed load according to the relative magnitudes of the particle fall velocity and the bed shear velocity. Sediment is transported as both suspended load and bed load when bed shear velocity exceeds the particle fall velocity. |
| Engelund Fredsoe & Zyserman (1976) | bed load and suspended load | theoretical, probabilistic ad semi-empirical | This sediment transport model is based on the probability of sediment movement. |
| Meyer-Peter & Muller (1948) | total load | theoretical | Transport formula valid for bed load dominated transport, total load is based on magnitude of shear stress. |
| Smart & Jaeggi (1983) | total load | semi-empirical | Similar to Meyer-Peter & Muller with updated coefficients to enhance the accuracy especially in applications with steep slopes. Best formula for mountainous rivers. |
| Yang – sand (1983) | total load | theoretical | Based on the stream power approach, most accurate formula for 0.063 < d < 2 mm |
| Yang – gravel (1984) | total load | theoretical | Similar to the approach for sand, coefficients adapted for larger particle diameters. |

Only the Engelund & Hansen formula will be discussed as it was the formula used in this study.

***Engelund and Hansen model (1967):***

This model is a total load model and the suspended sediment and bed load components are determined by the following relations:

$$S_{bl} = k_b.S_{tl} \tag{3-26}$$

$$S_{sl} = k_s.S_{tl} \tag{3-27}$$

Total sediment load is determined by equation 3-28:

$$S_{tl} = 0.05 \frac{c^2}{g} \theta^{\frac{5}{2}} \sqrt{(s-1)gd_{50}^3} \tag{3-28}$$

Time scale for the adaptation of the equilibrium profile is given by equation 3-29:

$$t_s = \frac{h}{2w_s} \tag{3-29}$$

Equilibrium concentration $C_e$ is calculated as the suspended load divided by the flux and converted from volume concentration to mass concentration (eq. 3-30):

$$c_e = \frac{S_{sl}}{uh} s \times 10^6 \tag{3-30}$$

**3.1.5     Required model parameter**

The parameters needed by the software to perform simulations can be classified as basic, hydrodynamic and morphological. Each of the parameters used in this study will be discussed briefly.

*3.1.5.1     Basic parameters*

The basic parameters of the model define the study area and the rules for solution. The user selects which modules are used in conjunction with a specified grid and its accompanying bathymetry (grid elevations). The model requires the user to specify the simulation period and what time step is used.  The model also allows the user to specify the points on the grid perimeter which will act as the open boundaries into the model space.

3.1.5.1.1     Modules

The simulation types available are hydrodynamic or hydrodynamic and morphological,

3.1.5.1.2     Grid and Bathymetry

The most critical components of a simulation are the numerical grid and the accompanying bathymetry (grid elevations) which constitute the modelled area. Mike21C grid files and bathymetries are created with the Mike21C Grid Generator.

3.1.5.1.3     Simulation period

The simulation period is required to reference the applicable data from the boundary time series files specified. The simulation is done in discrete time steps (the hydrodynamic time step) which are specified by the user. The hydrodynamic time step ($\Delta t$) is determined by the size and shape of the computational grid and its accompanying grid cell elevations. The correct time step is necessary for the convergence of the numerical solution. For computational stability the time step should be specified that the Courant number (Cr) is $\leq 1$. The Courant number is defined as follows (eq. 3-31):

$$C_r = \frac{u\Delta t}{\Delta s}$$     (3-31)

Where             u = flow velocity

                $\Delta s$ = cell dimension in flow direction

3.1.5.1.4     Boundary

The extents of the computational domain are walled of, thereby containing the flow inside the model space. The user has to define the perimeter grid cells which compromise the open boundaries. The Mike21C package crashes if boundary (open) grid cells dry (depth = 0 m) as the water level and velocity component of the cell is equal to zero and cannot be used by the computational solver.

3.1.5.1.5     Flood and Dry

The software allows the user to specify at which depths to activate (flood) and deactivate (dry) grid cells. Decreasing the respective depths increases total simulation time and vice versa. Small depths for flood and dry are useful to promote numerical stability in cases where significant flooding and drying are expected (DHI 2003).

*3.1.5.2     Hydrodynamic parameters*

The hydrodynamic module calculates the hydrodynamic behaviour of water in response to a variety of forcing conditions; the forcing conditions are collectively referred to as the hydrodynamic parameters.

3.1.5.2.1     Initial Surface Elevation

For the simulation to start the boundary cells have to be assigned initial water depths. The grid cell depth is determined by the difference between the grid cell bed elevations and the initial surface elevation.

3.1.5.2.2     Boundary

The HD module requires water levels or discharges at each open boundary. Boundary values can be specified constant or varied in time by means of a time series boundary file.

3.1.5.2.3    Eddy Viscosity

Model eddy viscosity can be excluded, specified globally by the Smagorinsky formula or velocity or fluxed based in local grid cells or globally. For river models the velocity based approach is recommended by DHI. The velocity based eddy viscosity coefficient seems to have little effect on simulation results in river applications (Dorfmann & Knoblauch 2009). Eddy viscosity can be considered a calibration parameter.

3.1.5.2.4    Resistance

Model bottom friction is the primary model calibration parameter. Bed resistance values can be specified as either Chezy or Manning numbers, globally or grid cell specific.

3.1.5.2.5    HD Integration

Mike21C enables the user to specify the solution scheme used during simulations. The following integration types are available:

*Fully Dynamic:*

This is the default simulation scheme for Mike21C. The model generates results for every time step. The most CPU intensive and accurate solution scheme (Leser et al. 2000).

*Scaled Dynamic:*

The scaled dynamic solution scales the results to perform faster long-term simulations. The scaled dynamic solution cannot be used when the modelled environment is very dynamic, e.g. when tidal water levels are used or floods simulated.

*Quasi-steady & Steady:*

Not applicable for model with variable boundary conditions.

### 3.1.5.3    River Morphology Parameters

The river morphology module has 5 sub modules which can be activated:

1. Helical flow        - The helical flow module simulates secondary currents in river bends, refer to Section 3.1.3
2. Sediment transport        the sediment transport module uses results obtained from the hydrodynamic module and optional helical flow module to predict the sediment transport in the model (Section 3.1.4).
3. Planform        -The planform module is used to simulate bank erosion of a river and has the ability to update the computational grid coordinates.
4. Alluvial resistance        -The alluvial resistance module updates the bed roughness of the model in relation to the changes experienced in the median grain diameter of the river bed due to sediment transport and/or influx at the model boundaries.
5. Morphological update        -The morphological update module changes the grid cell elevations according to the rate of deposition or sedimentation due to prescribed model boundary conditions and local grid conditions.

Modules 1, 2 and 5 were used in this study.

3.1.5.3.1    Starting conditions

The River morphology module can be activated over any interval during a hydrodynamic simulation. The river morphology module utilises a sediment time step which can be specified as a multiple of the hydrodynamic time-step to reduce computation time. All River Morphology simulations were run over the entire hydrodynamic simulation duration with a sediment time step of $20\Delta t$. Sediment time step values in the range of 5 to 30 times the hydrodynamic (general) time step are recommended by DHI (2011). The advection dispersion time step is calculated implicitly by the model.

3.1.5.3.2    Helical flow

Helical flow is included in the River Morphology module by the calibration parameter α. Refer to Section 3.1.3.

3.1.5.3.3    Sediment Transport

Refer to Section 3.1.4. The MIKE 21C software requires the user to specify the number of sediment fractions and their characteristics. Fractions can be either cohesive or non-cohesive; only one cohesive fraction can be specified.

Fractions are defined by their cohesiveness, representative grain size ($d_{50}$), porosity, density and critical Shield Parameter (Section 3.1.4).

The model differentiates between bed load transport and suspended load transport, each transport type has secondary calibration parameters available to the user. The bed- and suspended load components are determined by the sediment transport formula and the accompanying bed load and suspended load factors specified by the user. The sediment transport formula used can be specified for each type (bed or suspended) and for each fraction.

### 3.1.5.3.3.1    Bed Slope Effect

The sediment transport model has the following calibration parameters for the bed load component (DHI 2011c):

- Transverse slope coefficient (G)    - a calibration factor for the prediction of the transverse bed slope, refer to section Bed load transport (default = 1.25)
- Transverse slope power (a)        a calibration factor for the prediction of the transverse bed slope, refer to section Bed load transport (default = 0.5)
- Longitudinal slope coefficient (e)   - a secondary calibration factor, has less effect on the sediment transport compared to a and G (default = 5)

### 3.1.5.3.3.2    Suspended sediment

The suspended load transport model is calibrated by limiting the maximum suspended sediment concentration and by a fall velocity factor which alters the sediment settling velocity. Initial suspended sediment concentration can be specified globally or grid cell specific.

The sediment bed load and suspended load transport calibration parameters listed above were left default in this study as detailed geotechnical and sediment transport information was not available.

### 3.1.5.3.3.3    Morphological Update

For this study 2 fractions were used. When 2 or more fractions are used the software uses a graded sediment transport module. The graded model enables the user to specify riverbed layers, each with their characteristic layer thickness and fraction percentages. The fraction percentages are used to simulate the mean grain diameter of the model, refer to Figure **3**-**6**. The layer thickness enables the user to specify the mass of sediment in the model area. With a graded module component percentages must be specified over the whole model area. When fractions are used the total (combined) sediment transport capacity is reduced on the riverbed by the following factors:

*For bedload (eq. 3-32)*

$$S_{bl,i} = S_{bl}(d_i)\frac{m_i}{\sum_{j=1}^{n} m_j}$$
(3-32)

Where             $S_{bl, I}$ = Reduced bed load capacity for the $i^{th}$ fraction

$S_{bl, i}$ $(d_i)$ = The sediment capacity of the $i^{th}$ fraction

$d_i$ = Grain diameter for the $i^{th}$ fraction

$m_i$ = Mass of the $i^{th}$ fraction

$\sum_{j=1}^{n} m_j$ = Total mass of all fractions

*For suspended load (eq. 3-33)*

$$C_{e,i} = C_e(d_i) \frac{m_i}{\sum_{j=1}^{n} m_j} \tag{3-33}$$

Where $\quad\quad\quad\quad$ $C_{e,I}$ = Reduced suspended load capacity for the $i^{th}$ fraction

$\quad\quad\quad\quad\quad\quad\quad$ $C_e(d_i)$ = The suspended sediment capacity for the $i^{th}$ fraction
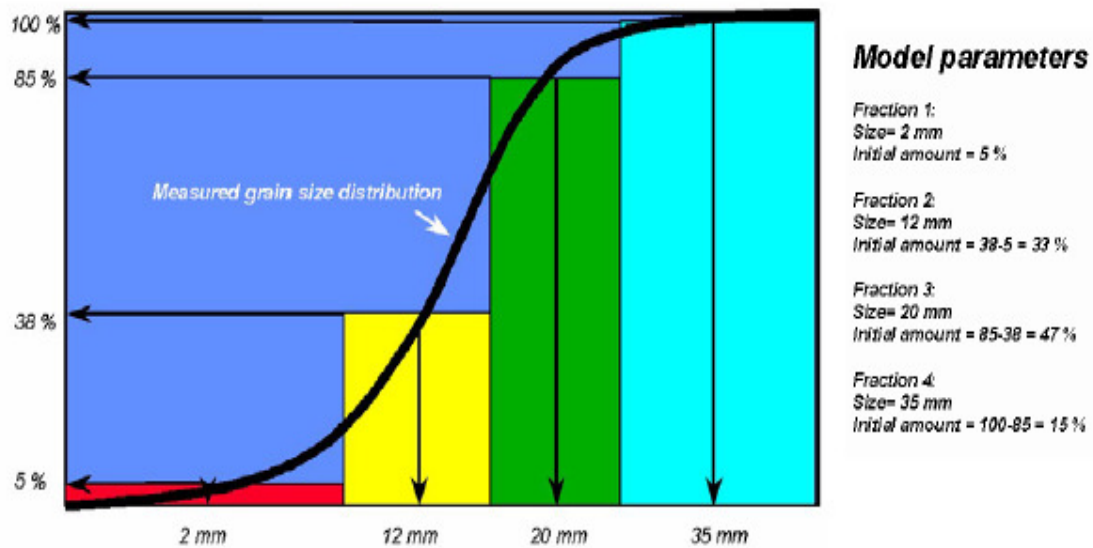


**Figure** 3-6**: Example grain size distribution for a graded model (DHI 2011c).**

*3.1.5.3.3.4      Boundary*
Sediment boundaries can be either constant or time dependant. Values can be specified for each cell on the border.

The boundary types available are:

- Bed level change as a percentage of each sediment component
- Sediment transport in m$^3$/m/s specified for each sediment component
- Sediment concentration in kg/m$^3$ specified for each sediment component

## 3.2    One dimensional hydrodynamic and advection dispersion modelling

### 3.2.1    Mike11 overview

Mike11 is a professional engineering software package developed by DHI for the simulation of flows, water quality and sediment transport in estuaries, rivers, irrigation systems, channels and other water bodies. The basis of the software is the Mike11 hydrodynamic module (HD). Mike11 HD uses an implicit, finite difference scheme for computations. The mathematical background of Mike11 is similar to that of Mike21C. The module can simulate sub- and super-critical flow conditions through a numerical scheme which changes in time and space according to local flow conditions. Modelling over hydraulic structures (static and dynamic) is also supported in additional modules. The computational scheme is applicable for vertically homogenous flow conditions.

### 3.2.2    Hydrodynamic/Saint Venant Equations

The Saint Venant equations are the vertically integrated equations of the conservation of momentum and continuity. Mike11 HD solves the Saint Venant equations based on the following assumptions:

- the water is incompressible and homogenous
- the bottom slope is small, cosine of the angle may be taken as 1
- wave lengths are large compared to water depth, flow is considered parallel to the bottom and vertical acceleration due to wave length is insignificant
- flow is subcritical

The conservation of mass and momentum for a rectangular cross-section with constant width and horizontal bottom can be expressed as follows (friction and lateral inflows ignored):

*Conservation of mass (eq. 3-34):*

$$\frac{\partial(\rho Hb)}{\partial t} = -\frac{\partial(\rho Hb\bar{u})}{\partial x} \tag{3-34}$$

*Conservation of momentum:*

$$\frac{\partial(\rho Hb\bar{u})}{\partial x} = -\frac{\partial(\alpha'\rho Hb\bar{u}^2 + \frac{1}{2}\rho gbH^2)}{\partial x} \tag{3-35}$$

where:   $\rho$ = density

H = depth

b = width

$\bar{u}$ = average velocity along the vertical

$\alpha'$ = vertical velocity distribution coefficient.

*Solution:*

The Saint Venant Equations are transformed to a set of implicit finite difference equations in a computational grid. The grid consists of alternating Q- and h- points which are calculated for each time step. The grid is developed automatically by the model based on user inputs. Q- points are located halfway between h- points, the h- points lie on model cross-sections and are spaced a distance dx from each other. Refer to Figure 3-7.
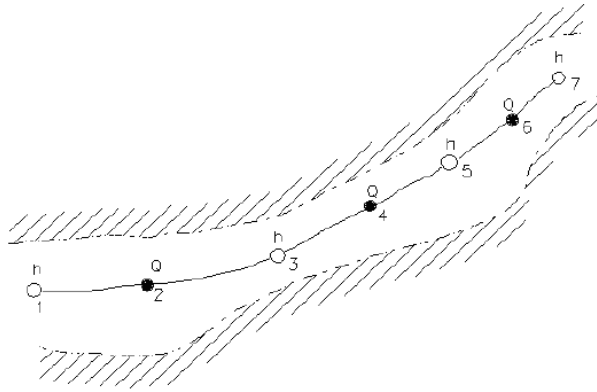
**Figure 3-7: Channel section with computational grid (DHI 2011a)**

### 3.2.3 Advection dispersion (AD)

The Mike11 Advection Dispersion (AD) module was used for the estuary salinity modelling. The AD module can also be used in the modelling of cohesive sediments. The AD module is based on the one-dimensional equation of conservation of mass of dissolved or suspended material. Outputs from the hydrodynamic module are used for the computations. The AD equation is numerically solved using an implicit finite difference scheme.

The advection –dispersion equation in one dimension is given by equation 3-36:

$$\frac{\partial AC}{\partial t} + \frac{\partial QC}{\partial x} - \frac{\partial}{\partial x}\left(AD\frac{\partial C}{\partial x}\right) = -AKC + C_2 q \tag{3-36}$$

Where          C = Concentration

D = Dispersion coefficient

A = cross-sectional area

K = Linear decay coefficient

$C_2$ = Sink/Source coefficient

q = Lateral inflow

x = Space coordinate

t = Time coordinate

The 2 components of the equation are the advective (or convective) transport within the flow, and the dispersive transport due to concentration gradients. The following assumptions apply:

- The source/sink term is considered to mix instantaneously over the cross-section.
- Dispersive transport is proportional to the concentration gradient.
- Linear decay applies

### 3.2.4 Required model parameters

The Mike11 model parameters are similar to the basic and hydrodynamic parameters of the Mike21C model the main difference is that a one dimensional grid (network) is used rather than a 2 dimensional one. The Mike11 model parameters are indicated in Figure 3-8. Each parameter and its function will be briefly discussed:

33
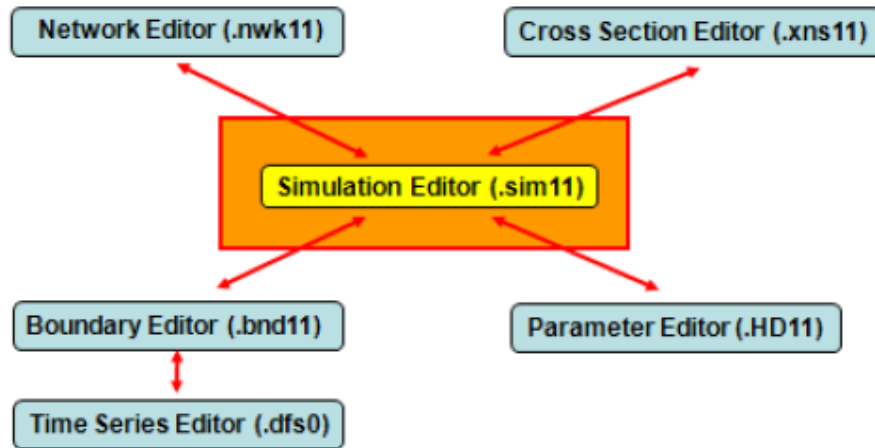
**Figure 3-8: Mike11 model parameters (DHI 2011a)**

### 3.2.4.1    Simulation Editor:

The simulation editor is the Mike11 parameter communication interface. The user uses the simulation editor to specify the Mike 11 models used, the solution scheme, the specific parameters used and the simulation period and time step.

The relevant Mike11 models available are:

1. Hydrodynamic (HD)
2. Advection Dispersion (AD)

### 3.2.4.2    Network Editor:

The Network Editor is used to define the model river network. Each network point corresponds to a user defined cross-section, boundary condition or control structure. The distance between the model generated grid points (dx) is specified in the network editor.

### 3.2.4.3    Cross Section Editor:

The Cross Section Editor is used to define the cross-sections used in the Mike11 Network. Cross sections can be defined into segments of different bed roughness by the use of markers; this functionality is integrated in the Mike11 Cross Section Editor and is used to define floodplains.

### 3.2.4.4    Boundary Editor

The Boundary Editor is used to specify the locations of network boundary points; boundary points are assigned boundary conditions. Boundary conditions can be specified as constant or time varying. Boundary conditions are required for all modules activated during simulations, e.g. HD conditions and AD conditions.

### 3.2.4.5    Parameter Editor

The parameter editor contains information on variables related to the type of computation selected for simulations. HD parameters are similar to the hydrodynamic parameters discussed in Section 3.1.5.2. AD parameters are dependent on the type of AD computations done (salinity, cohesive sediment, pollutants etc.).

# 4   FIELD WORK

## 4.1   Introduction

Field work was carried out at the Great Fish River estuary from 5 to 7 May 2012. This period coincided with a spring tide event. The aim of the investigation was to obtain insight into the sediment and salt dynamics of the Great Fish River Estuary.

The following parameters were investigated:

- Water levels
- Flow velocities and vectors
- Water depths
- Total Dissolved Solids (TDS)
- Electro Conductivity (EC)
- Sediment bedload transport
- Suspended sediment transport
- Water temperature

Salinity and temperature were measured at varying depths along the water column.

## 4.2   Study area

River surveys were carried out at 6 locations on the Great Fish River. Refer to Table 4-1 for coordinates and the river chainage. Chainage is measured from the river mouth. For a plan view refer to Figure 4-1. Site A is near the mouth while site F is 15 km upstream of the mouth.

**Table 4-1: Survey Points**

| Site | Chainage (m) | Latitude | Longitude |
|------|--------------|----------|-----------|
| A | 405 | 33° 29' 37" S | 27° 08' 05" E |
| B | 3023 | 33° 28' 55" S | 27° 06' 38" E |
| C | 5645 | 33° 28' 21" S | 27° 05' 08" E |
| D | 8270 | 33° 27' 17" S | 27° 04' 12" E |
| E | 10888 | 33° 26' 15" S | 27°  03' 22" E |
| F | 14990 | 33° 24' 11" S | 27° 02' 09" E |
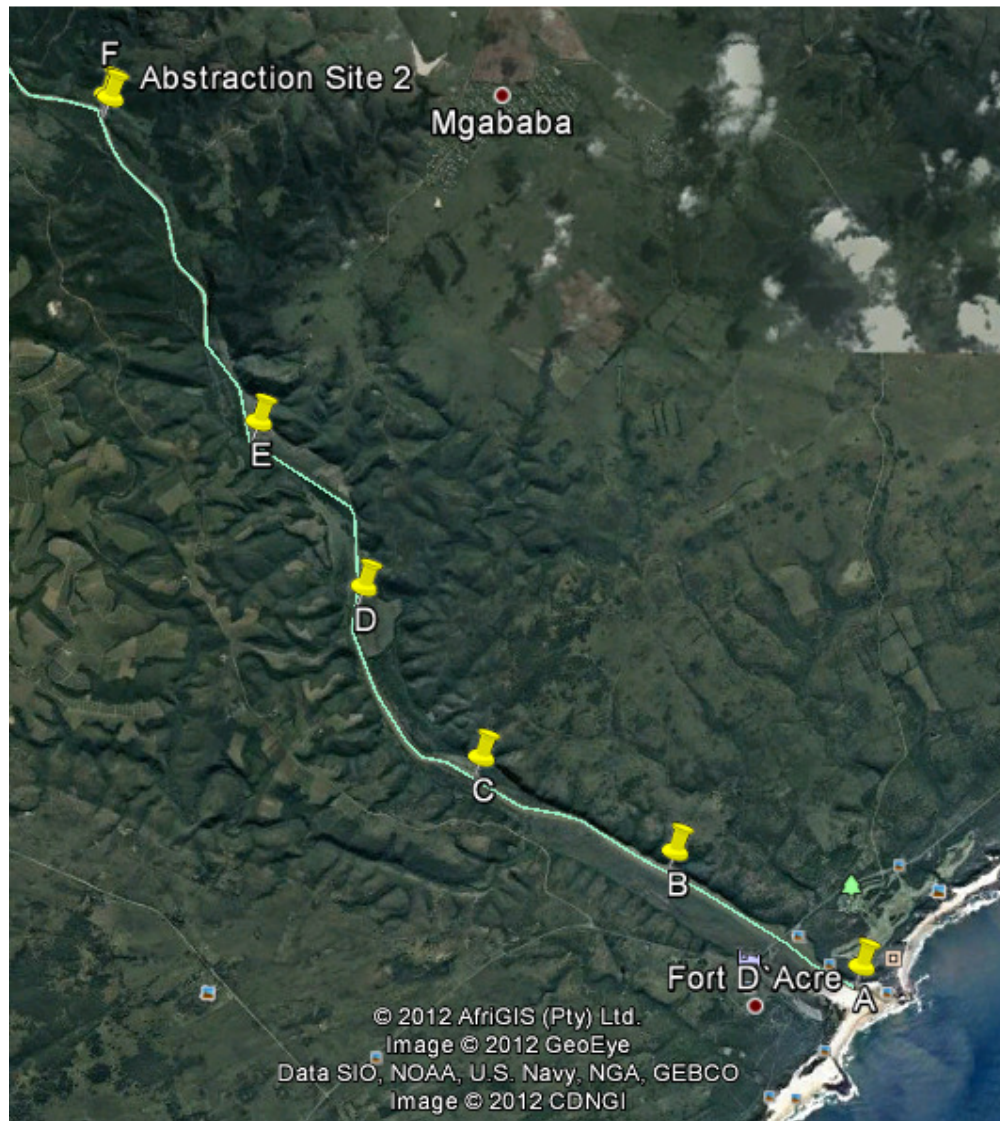
**Figure 4-1: Survey points plan view (Google 2014)**

## 4.3    Field Work Schedule

### 4.3.1    One dimensional (1D) hydrodynamic model

To determine the optimal date and time for measurement of identified parameters a one dimensional (1D) hydrodynamic model was used. The model was set up with generated tides from WXTide 32 (refer to Section 4.3.2), and a constant river flow of 10 m$^3$/s (the estimated river inflow expected during the field work). Bathymetry data was obtained from previous CSIR river surveys.

### 4.3.2    Generated tides

See Appendix D for the complete database.

## Port Alfred generated tides
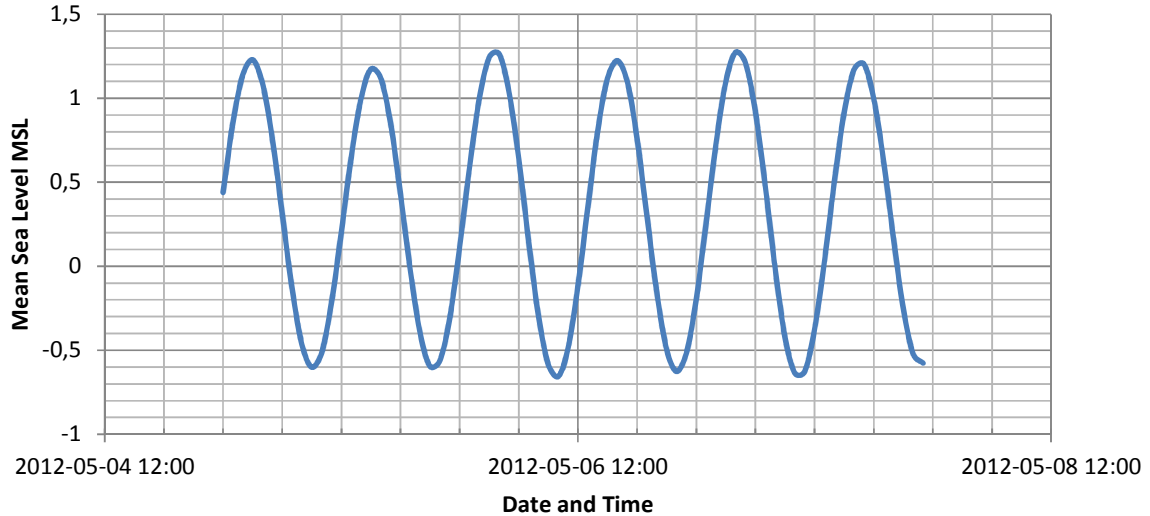


**Figure 4-2: Generated water levels at Port Alfred (masl)**

### 4.3.3    Hydrodynamic model simulation results

Three chainages were identified for analysis:

Chainage 405 m – The first practical measurement location in the estuary.

Chainage 7918 m – The last point in the estuary were simulated salt intrusion is noticeable for a $10m^3/s$ river discharge.

Chainage 4742 m – The midpoint of the above chainages.

The tidal flow patterns upstream are determined by the river, estuary and mouth bathymetry, river discharge, tide levels and hydraulic roughness.

#### 4.3.3.1    *Total Dissolved Solids (TDS)*

Refer to Appendix A for simulation results. Maximum TDS occurs when water level at the site is at its highest (maximum tidal intrusion). Minimum TDS when water level at the site is at its lowest (minimum tidal intrusion). Field work schedule was determined by the time of the peak (min and max) TDS value of the identified chainages. Total travel time, expected measurement duration and the time lag between peaks were then used to determine optimal departure time to ensure that the peaks are not missed. See Figure 4-3.
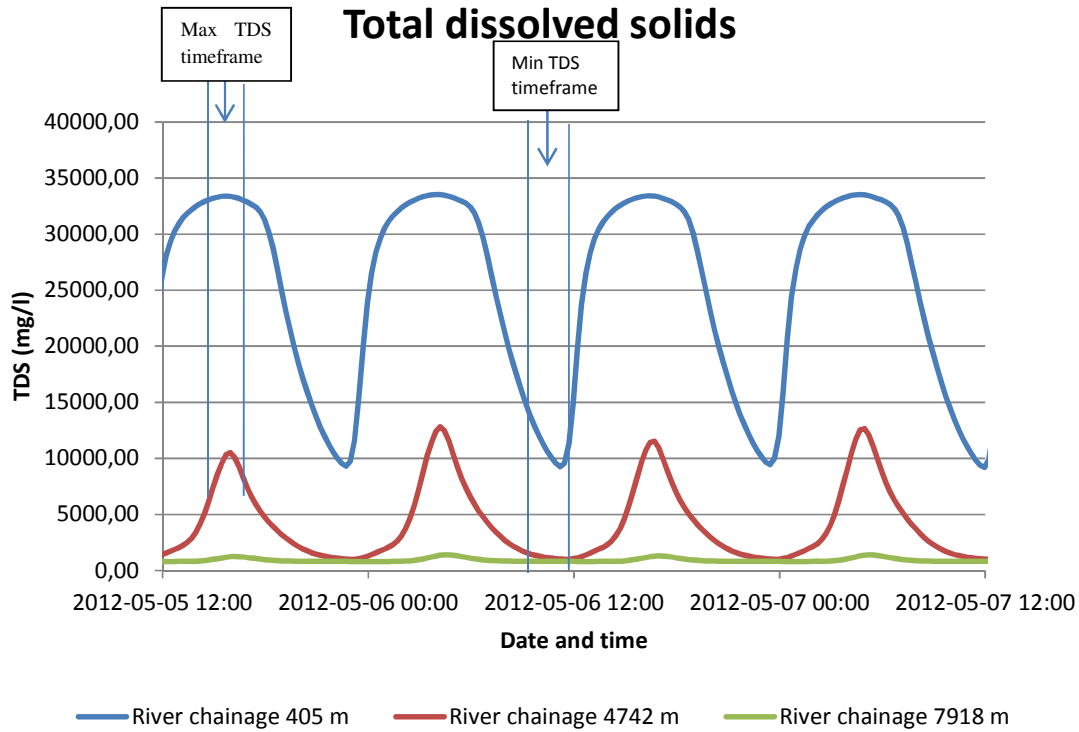
**Figure 4-3: Schedule planning example for TDS measurements from 1D model simulated results**

#### 4.3.3.2    *Flow velocity*

Refer to Appendix A for simulation results. The flow direction of the model is from the mouth upstream. Positive velocities coincide with flood tides in the estuary and negative velocities with ebb tides. To determine sediment transport (suspended and bedload) periods of peak velocity are required for measurement. Peak velocities occur roughly in the middle of either the ebb or flood tide period. Field work schedule was determined by the time of the peak (min and max) flow velocity value of the identified chainages. Travel time between sites, expected measurement duration and the time lag between peaks were then used to determine optimal departure time to ensure that the peaks are not missed. Refer to Figure 4-4.

# Flow velocities
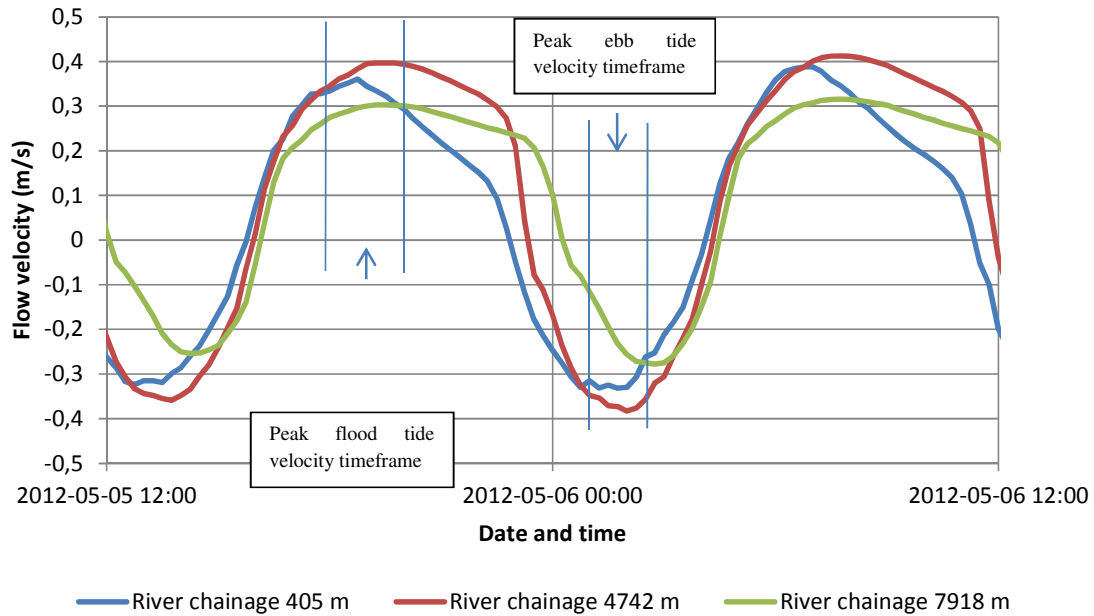


Figure 4-4: Schedule planning example for velocity and sediment transport measurements from 1D model simulated results

### 4.3.4    Schedule

Analyses of hydrodynamic model results were used to determine viable time frames for field test. See Table 4-2 for the complete field work schedule. Test run 5 was omitted due to time constraints and unfavourable tidal conditions. Data presented in this report is labelled by run number and site, 2B represents the results from site B during run 2.

Table 4-2: Field work schedule May 2012

| Run | Date | Test Type | Start time | End Time | Duration |
|---|---|---|---|---|---|
| 1 | 05-May | Minimum Total Dissolved Solids | 10:30 | 12:00 | 01:30 |
| 2 | 05-May | Sediment transport (ebb tide) | 13:00 | 14:30 | 01:30 |
| 3 | 05-May | Maximum Total Dissolved Solids | 15:15 | 17:00 | 01:45 |
| 4 | 06-May | Sediment transport (flood tide) | 07:00 | 08:30 | 01:30 |
| 5 | 06-May | Minimum Total Dissolved Solids | 11:15 | 12:50 | 01:35 |
| 6 | 06-May | Sediment transport (ebb tide) | 13:50 | 15:00 | 01:10 |
| 7 | 06-May | Maximum Total Dissolved Solids | 16:00 | 17:30 | 01:30 |
| 8 | 07-May | Sediment transport (flood tide) | 07:30 | 09:00 | 01:30 |
| 9 | 07-May | Acoustic Doppler Current Profiling (ADCP) | 07:30 | 09:45 | 02:15 |

## 4.4   Methodology

### 4.4.1      River discharge

River discharges as presented in this report are from the Department of Water and Sanitation (DWS) flow measurement station Q9H018 (Figure 4-5) at Matomela as obtained from the DWS website.



**Figure 4-5: Location of DWS flow gauge Q9H018 (Google 2014)**

### 4.4.2      Water levels

Water levels were measured with a borehole depth recorder from the surface of the disused bridge across the Great Fish River. Refer to Figure 4-6 for an aerial view of the bridge and Table 4-3 for coordinates.



**Figure 4-6: Water level measurement location**

**Table 4-3: Measurement location coordinates**

| Latitude | Longitude |
|---|---|
| 33°29'19.73"S | 27° 7'31.93"E |

### 4.4.3    TDS measurements

#### 4.4.3.1    Introduction

Salinity measurements were done at the 6 locations as indicated by Figure 4-1. Two measurement methods were used namely pumping of water into 0.5 liter bottles at different depths for laboratory analysis and salinity measurements with depth by use of the Castaway ® device manufactured by YSI.

#### 4.4.3.2    Abstraction

Water was abstracted at the surface and at 0.5m intervals for the first 2m of water, and deeper samples were taken at 1m increments. Salinity samples were submitted to the CSIR for analysis.

#### 4.4.3.3    Castaway

The Castaway (Figure 4-7) is a hand held hydrographic instrument designed for quick and accurate conductivity, temperature and depth profiles. The device has a six electrode array and a flow through cell. The device is cast into the water and reeled back up at a constant rate. Each cast is referenced with both time and location using it's built in GPS receiver. The output parameters of the Castaway are presented in Table 4-4.



**Figure 4-7: The Castaway**

**Table 4-4: Castaway output parameters**

|  | **Range** | **Resolution** | **Accuracy** | **Measured or Derived** |
|---|---|---|---|---|
| **Conductivity** | 0 to 100,000 µS/cm | 1 µS/cm | ± 0.25% ± 5 µS/cm | Measured |
| **Temperature** | -5° to 45° C | 0.01 ° C | ± 0.05 ° C | Measured |
| **Pressure** | 0 to 100 dBar | 0.01 dBar | ± 0.25%FS | Measured |
| **Salinity** | Up to 42 (PSS-78) | 0.01 (PSS-78) | ± 0.1 (PSS-78) | PSS-78[1] |
| **Sound Speed** | 1400 – 1730 m/s | 0.01 m/s | ± 0.15m/s | Chen-Millero[2] |
| **Density** | 990 to 1035 kg/m$^3$ | 0.004 kg/m$^3$ | ± 0.02 kg/m$^3$ | EOS80[3] |
| **Depth** | 0 to 100 m | 0.01 m | ± 0.25% FS | EOS80[3] |
| **Specific conductivity** | 0 to 250,000 µS/cm | 1 µS/cm | ± 0.25% ± 5 µS/cm | EOS80[3] |
| **GPS** |  |  | 10 m |  |

[1]1978 Practical Salinity Scale

[2]Chen-Millero, 1977. Speed of sound in sea water at high pressures.

[3]International Equation of State for sea water.

### 4.4.4    Velocity vectors

Velocity vectors were obtained by use of the Sontek RiverSurveyor® M9; see Figure 4-8. The RiverSurveyor uses acoustic Doppler current profiling (ADCP) to determine the flow velocity vectors of the river. The RiverSurveyor can be used to determine river cross sections, river discharge and river velocity vectors. For complete specifications see Table 4-5.



**Figure 4-8: Sontek RiverSurveyor M9**

42

**Table 4-5: Specifications for the Sontek RiverSurveyor M9**

| Specifications Sontek River Surveyor M9 | |
|---|---|
| **Velocity Measurements** | |
| Profiling Range (Distance) | 0.06m to 40m |
| Profiling Range (Velocity) | ± 20m/s |
| Accuracy | Up to ± 0.25% of measured |
| Resolution | 0.001 m/s |
| Number of Cells | Up to 128 |
| Cell Size | 0.02m to 4m |
| **Transducer Configuration** | |
| Nine Transducers: Dual 4 Beam 3.0 MHz/ 1.0MHz Janus at 25 °C Slant Angle; 0.5MHz Vertical Beam | |
| **Depth Measurement** | |
| Range | 0.20m to 80m |
| Accuracy | 1% |
| Resolution | 0.001m |
| **Discharge Measurement** | |
| Range with Bottom Track | 0.3m to 40m |
| Range with RTK GPS or DGPS | 0.3m to 80m |
| Computations | Internal |

### 4.4.5  Bedload sediment transport

Bedload sediment transport was determined using a bedload sampler (Figure 4-9). A bedload sampler is lowered to the river bed during periods of peak water velocity. The instrument is weighted to ensure it lays flat on the river surface, the fin ensures that the sampler mouth is directly facing the direction of flow. Bedload sediment is collected in the perforated bag as can be seen in Figure 4-9. Bedload transport is determined by the rate of sediment deposition in the bag.



**Figure 4-9: Bedload sampler (US BL-84)**

#### 4.4.6    Suspended sediment transport

Suspended sediment concentrations were obtained by use of a depth integrating suspended sediment sampler, refer to Figure 4-10. Depth integrating samplers are designed to continuously extract a sample as they are lowered from the water surface to the streambed and returned at a constant rate of travel. The sampler is equipped with a tail vane assembly to orient the intake nozzle into the approaching flow as the sampler enters the water.  As the sample is collected, air in the container is compressed so that the pressure balances the hydrostatic pressure at the air exhaust and the inflow velocity is approximately equal to the stream velocity. After a successful measurement has been completed the fluid (water with suspended material) is removed from the instrument and sent for laboratory testing to determine the concentration of suspended sediment.



**Figure 4-10: Depth integrating suspended sediment sampler (US DH-76)**

#### 4.4.7    Cross-sectional surveys

The RiverSurveyor (ADCP) can be used to measure river cross-sections. Once cross-section is surveyed; the total discharge can also be calculated.

## 4.5    Results

### 4.5.1    River discharge

See Figure 4-11 and Appendix B for river discharges for the Great Fish River during the fieldwork period as obtained from the DWA. The river discharge was similar to the modelled event of 10 m$^3$/s.
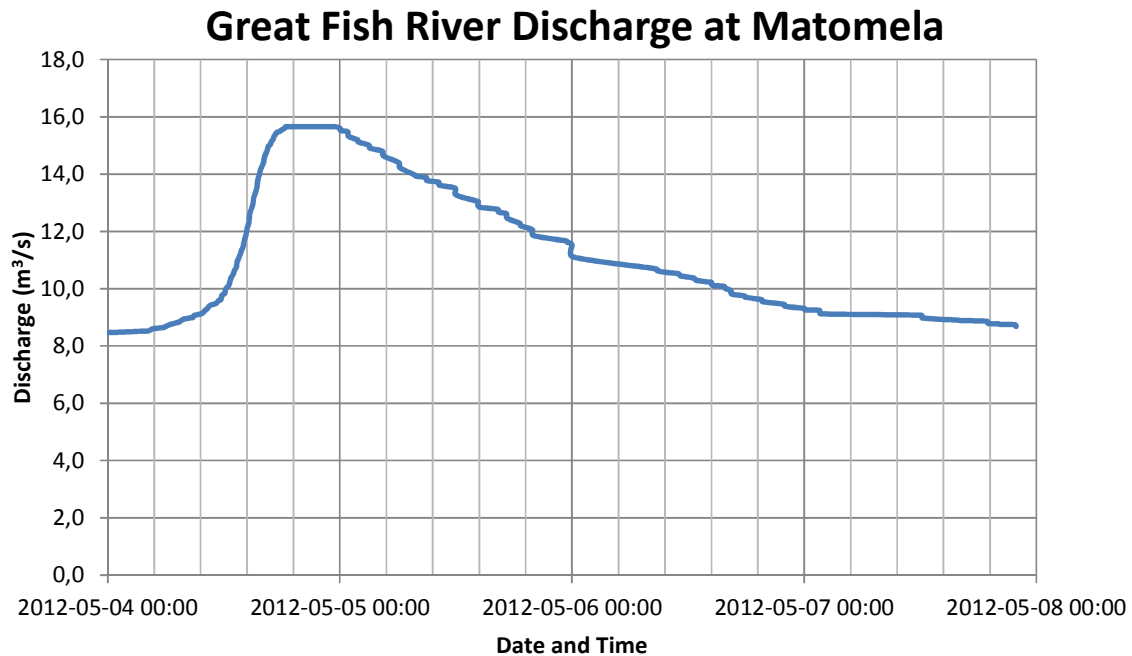


**Figure 4-11: Great Fish River flow recorded at station Q9H018 during the field work**

### 4.5.2    Measured water levels

Observed water levels shown in Figure 4-12. For the complete measurement database refer to Appendix C. The distance indicated in Figure 4-12 is measured from the surface of the bridge to the water surface (see Section 4.2). Water level readings lack accuracy due to very windy conditions for the measurement period, the estimated accuracy is 100mm. In Appendix D it can be seen that the equinox tidal range was greatest on 6 May 2012 and this is also noticeable in the measured levels depicted in Figure 4-12. The reader should note that the 2 data series plotted on Figure 4-11 have different vertical axis.

# Measured and predicted water levels
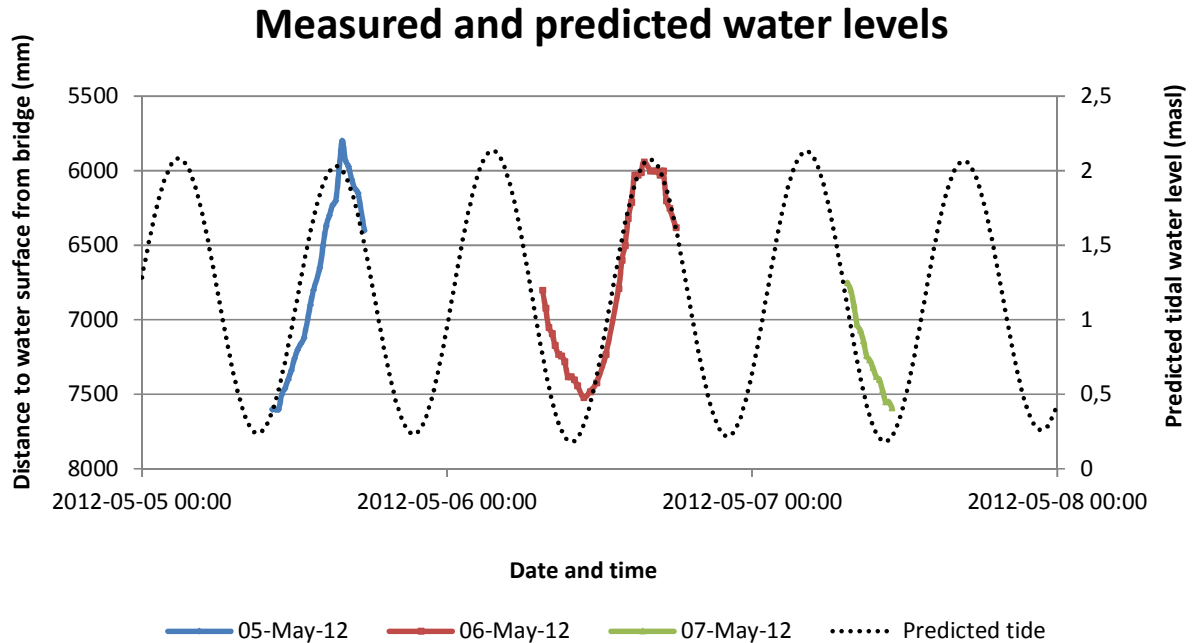


**Figure 4-12: Measured water levels at the N2 bridge and predicted tidal water levels in the ocean**

### 4.5.3    Total dissolved solids and electro conductivity

#### 4.5.3.1    TDS and EC
Refer to Figure 4-13 and Figure 4-14.

For complete TDS (Total dissolved solids, measured in mg/l) and EC (Electro conductivity, measured in milli-Siemens per meter – mS/m) data refer to Appendix E: Observed salinity, electro conductivity and temperature. As the flood tide enters the estuary the salinity level rises to that of the sea. Water was very saline up to site B (during high tide). At low tide the salinity of the estuary is greatly reduced, this is very much dependent on the upstream river flow, drought periods will result in more saline waters. For the river discharge experienced during the field work period the salt intrusion of the tidal waters ends at around 9000m from the river mouth. Maximum TDS measured at the river mouth was 39 475 mg/l (depth averaged), the minimum measured TDS at the river mouth was 3921.2 mg/l (depth averaged). During low tide salt intrusion was only noticeable at sites A and B. The typical river TDS was about 650 mg/l.

TDS values for the castaway device was derived from the observed relationship between EC and TDS values of the laboratory data, see the equation below (eq. 4-1):

$$TDS = 7.52EC - 294.6 \tag{4-1}$$

TDS - Total dissolved solids (mg/l)

EC - Electro conductivity (mS/m)

Site C was the only site were stratification is noticeable (during high tide).

Refer to Figure 4-15 and Figure 4-16

## TDS
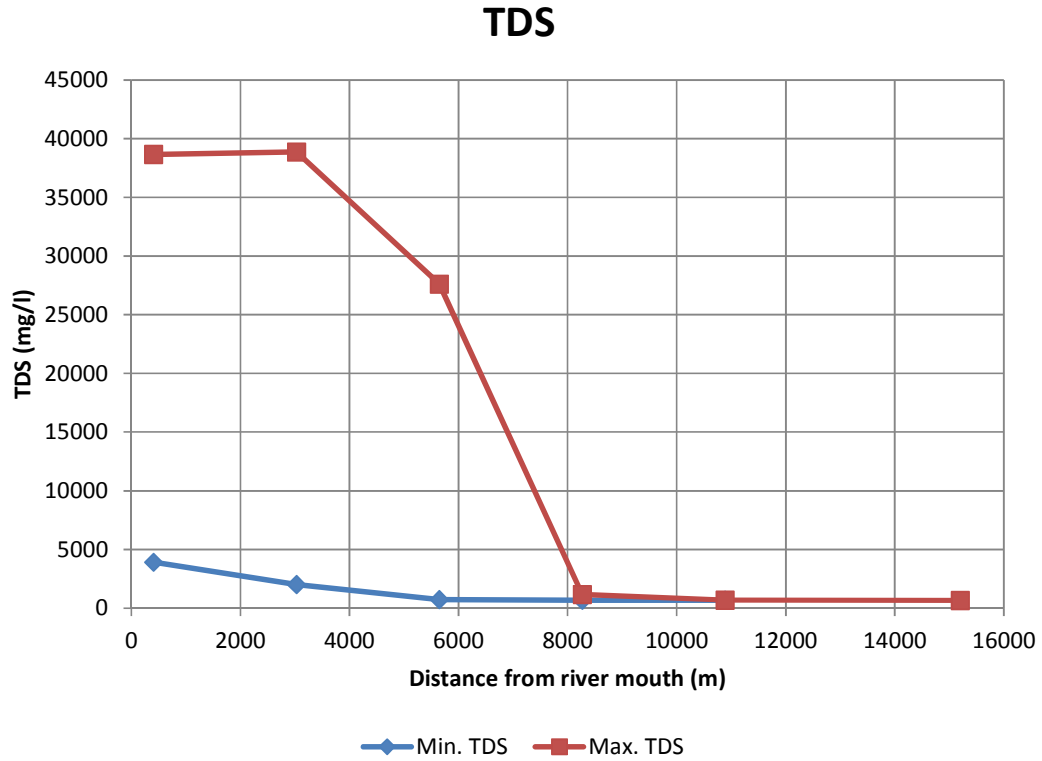


**Figure 4-13: Pumped sample (laboratory) TDS comparison (depth averaged)**

## EC
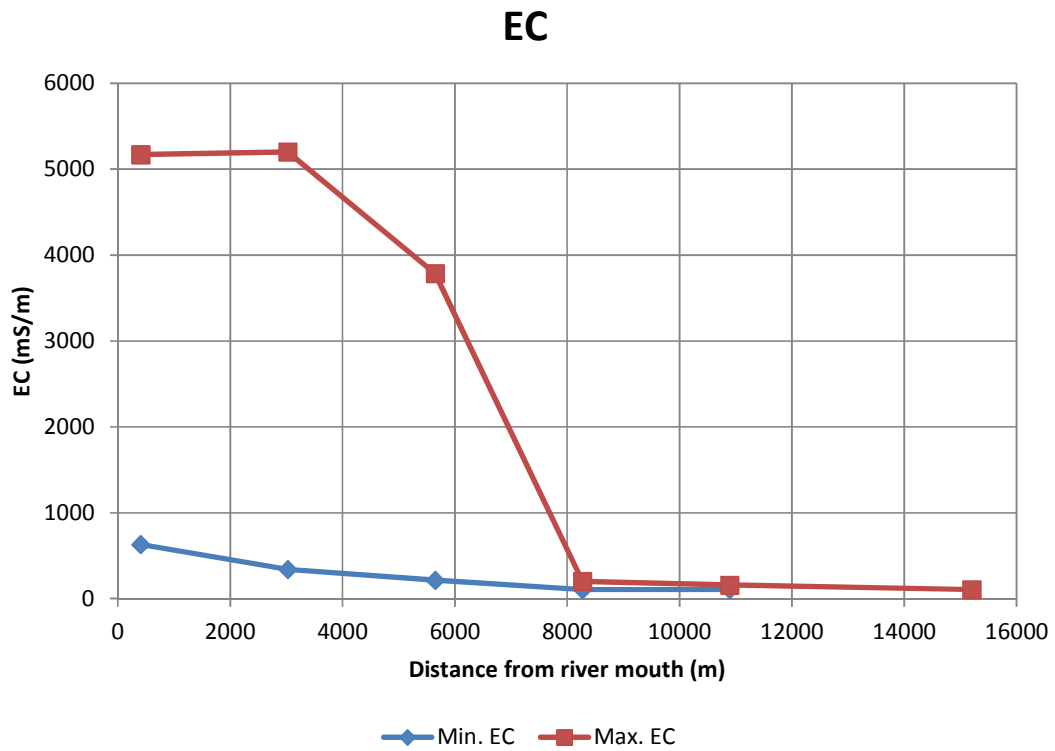


**Figure 4-14: Pumped sample (laboratory) EC comparison (depth averaged)**

## TDS - Site C
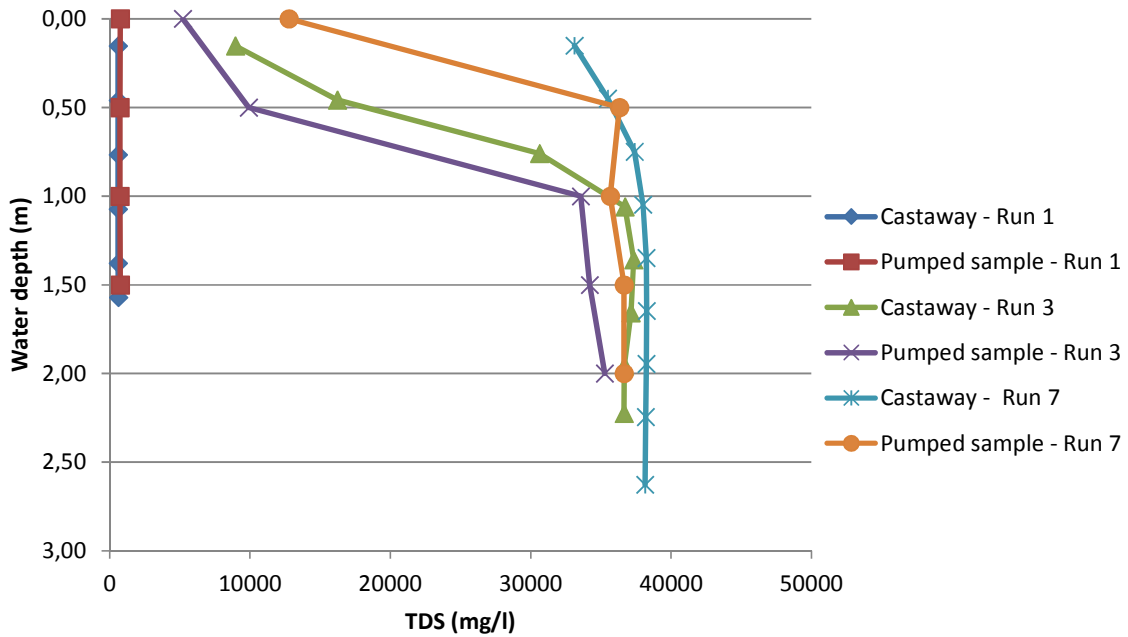


Figure 4-15: Stratification at site C and comparison of pumped samples (laboratory) and Castaway results

## EC - Site C
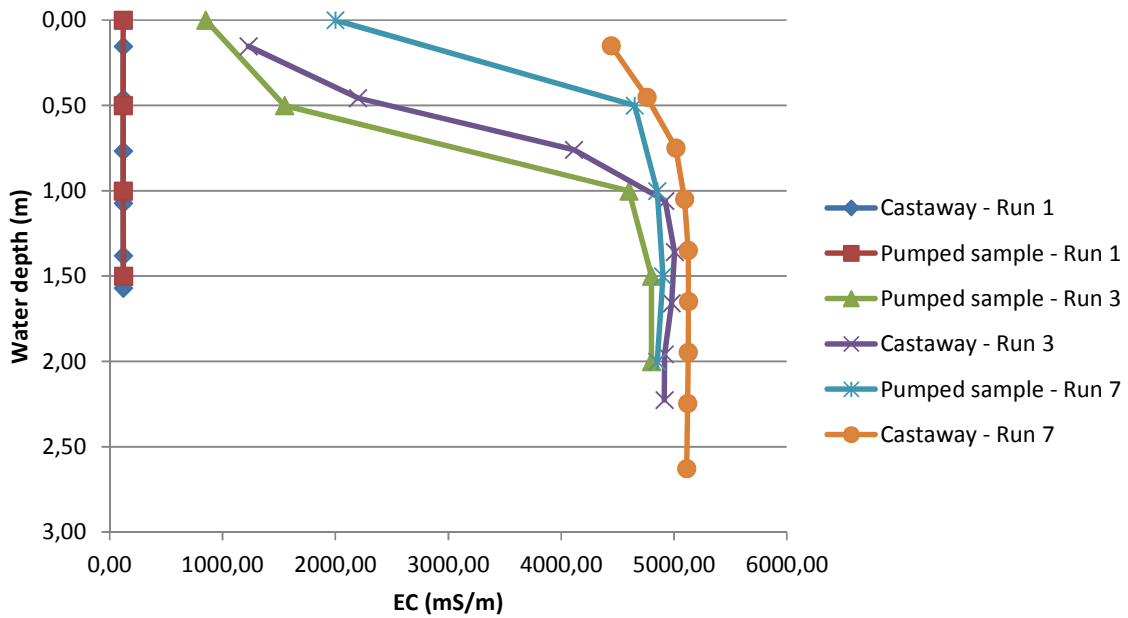


Figure 4-16: Stratification at site C and comparison of pumped samples (laboratory) and Castaway results

48

### 4.5.4    Flow velocities

Minimum and maximum flow velocities are indicated in Figure 4-17. See Appendix F: The maximum flow velocities were observed at the river mouth, values were between 0.9 m/s (flood tide) and 1.2 m/s (ebb tide). The flow velocities gradually decrease upstream of the river mouth up to site E, at site F flow velocity is slightly higher (only ebb tide measurement done). Flow velocity upstream of site B varied between 0.39 m/s and 0.5 m/s.

## Water Speed
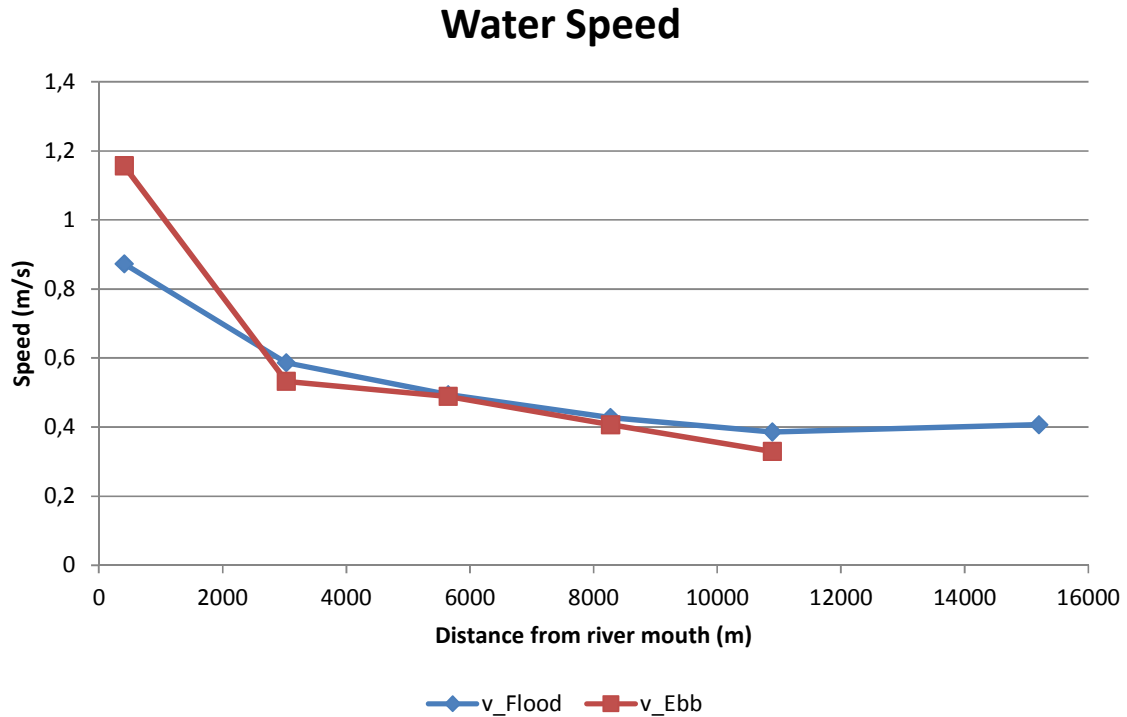


**Figure 4-17: Observed flow speed during Ebb and Flood tides**

### 4.5.5    Bedload sediment transport

For complete grading of samples see Appendix G. Figure 4-18 depicts the sediment composition along the estuary. Coarser sediments are encountered at the river mouth (sea sand) and further upstream in the estuary, silt and clay are present at sites B, C and D. Figure 4-19 represent the median bedload particle sizes along the estuary for ebb tides. Figure 4-20 represent the median bedload particle sizes along the estuary for flood tides

49

## Sediment composition
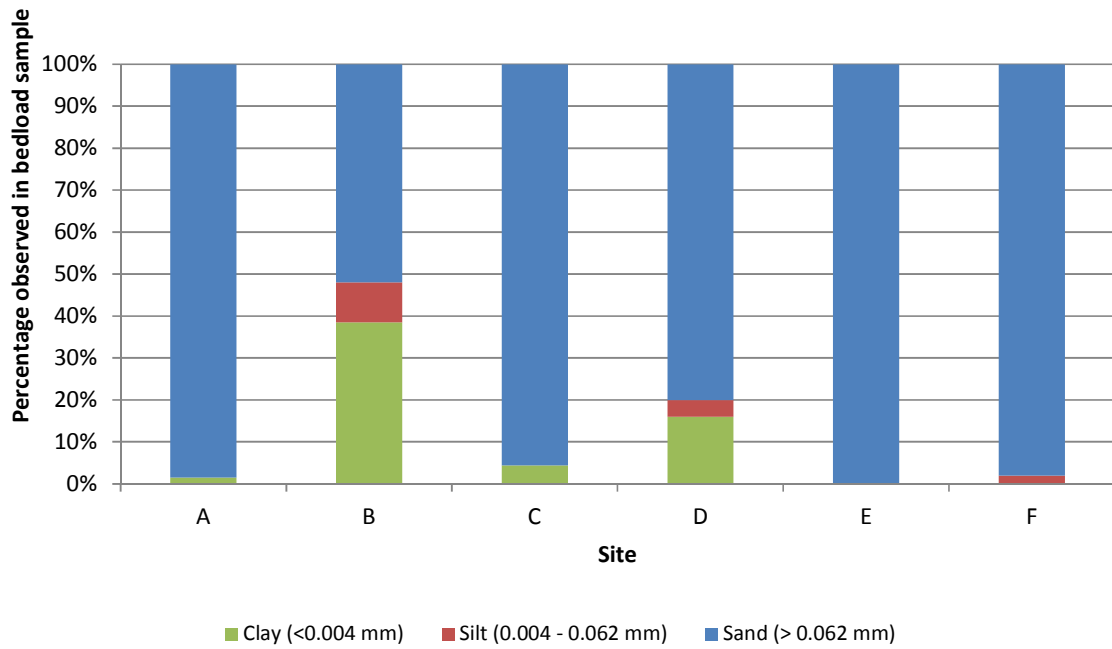


**Figure 4-18: Observed sediment composition along the Great Fish River estuary**

## Ebb Tide Bedload sample grading d50
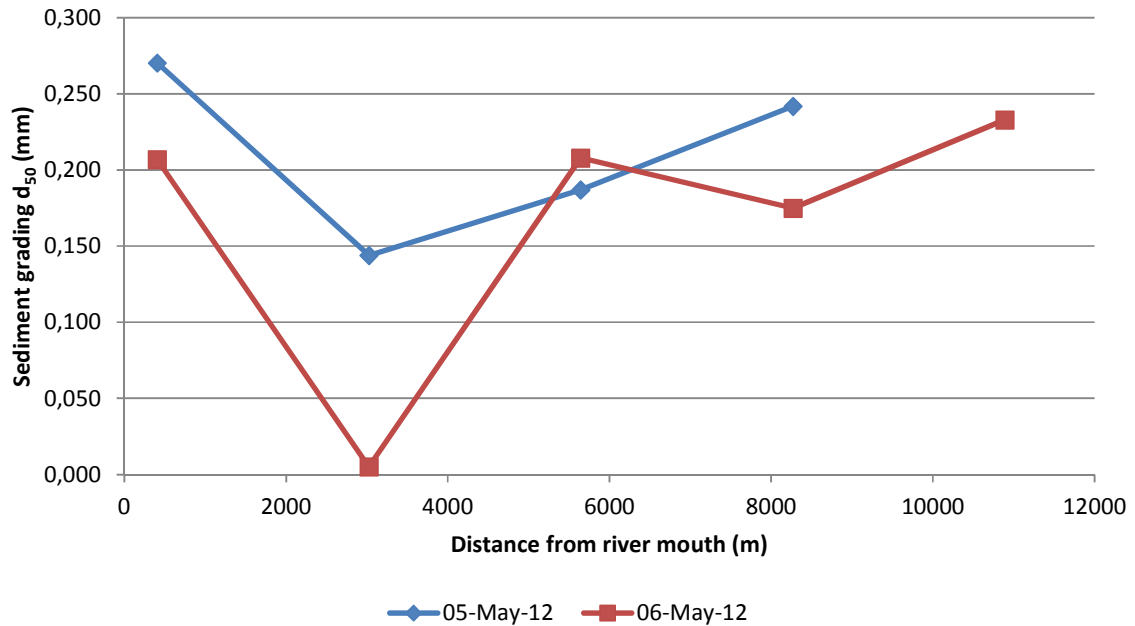


**Figure 4-19: Observed ebb tide median sediment size**

## Flood Tide Bedload sample grading d50
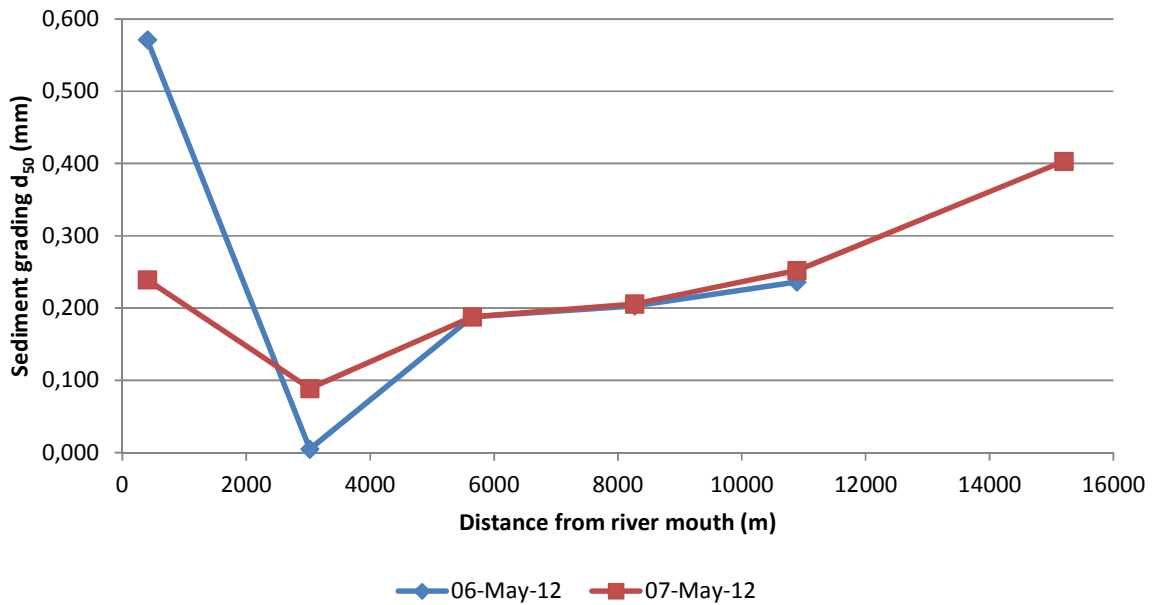


**Figure 4-20: Observed flood tide median sediment size**

### 4.5.6    Suspended sediment concentrations

The CSIR laboratory conducted the sample analysis. Refer to Figure 4-21 and Figure 4-22. For complete results refer to Appendix H: Observed suspended sediment. The data at site D in Figure 4-22 is probably an outlier.

## Suspended sediment concentration - Ebb tide
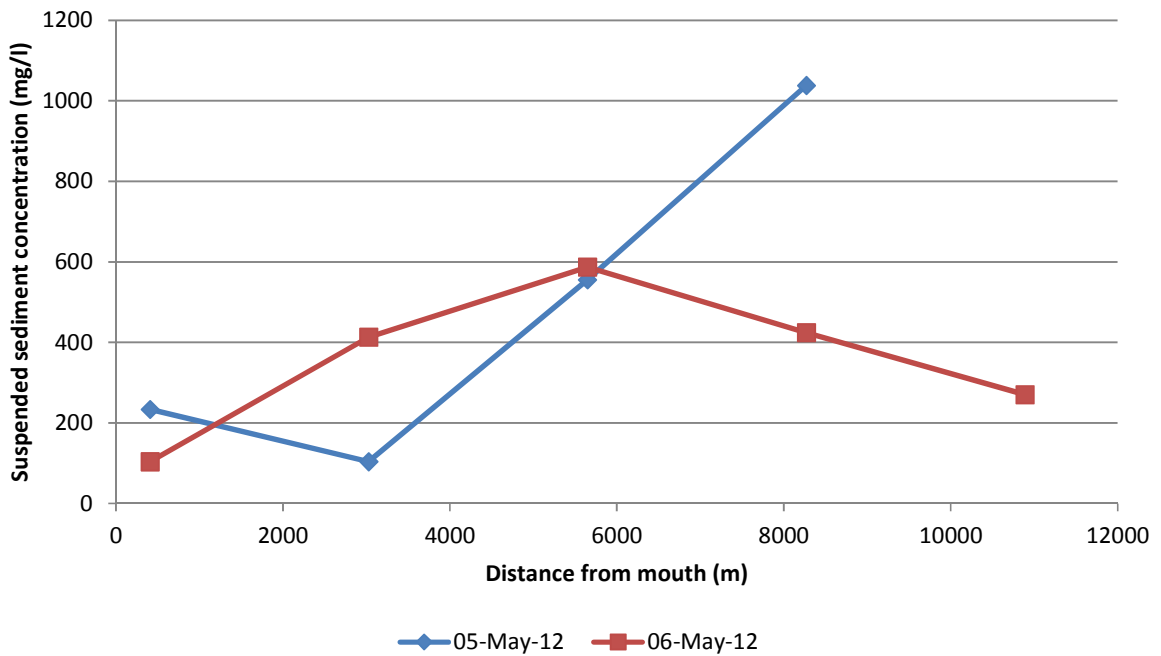


**Figure 4-21: Observed suspended sediment concentration during ebb tide**

# Suspended sediment concentration - Flood tide
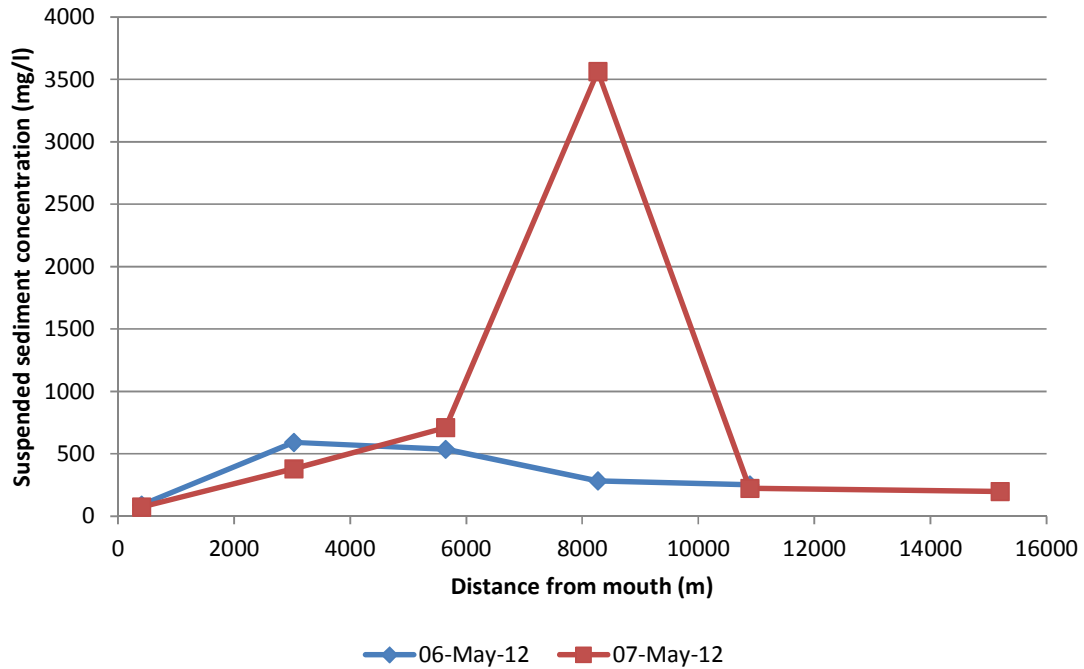


**Figure 4-22: Observed suspended sediment concentration during flood tide**

### 4.5.7 ADCP cross sectional velocity surveys

Refer to Appendix I for results. Two discharges were determined, see Table 4-6. The much larger discharge at B is due to the tidal effects of the estuary.

**Table 4-6: Observed ADCP river discharge**

| Site | E | B |
|---|---|---|
| Date | 6 May 2012 | 7 May 2012 |
| Time | 09:07 | 07:27 |
| Discharge (m³/s) | 18.5* | 79 |

*There is a discrepancy between the measured discharge (18.5 m³/s) and the gauge reported discharge (11 m³/s, Figure 4-11), this might be due to the small increase in river catchment, tidal flow at the measurement location or instrument (ADCP of DWS gauge) error.

## 4.6   Survey

A survey of the Great Fish River was done approximately 6 months after the data collecting field trip. The survey was done in the form of cross-sections at 24 locations, the survey locations and the river chainage extents (405 & 26742) are shown in Figure 4-25. The survey data consist of land based data which is extended by LIDAR data. The extent of the land based survey is shown in Figure 4-23. All cross-sections extended with LIDAR data can be seen in Figure 4-24.

**Great Fish River Survey 2012-11-21**
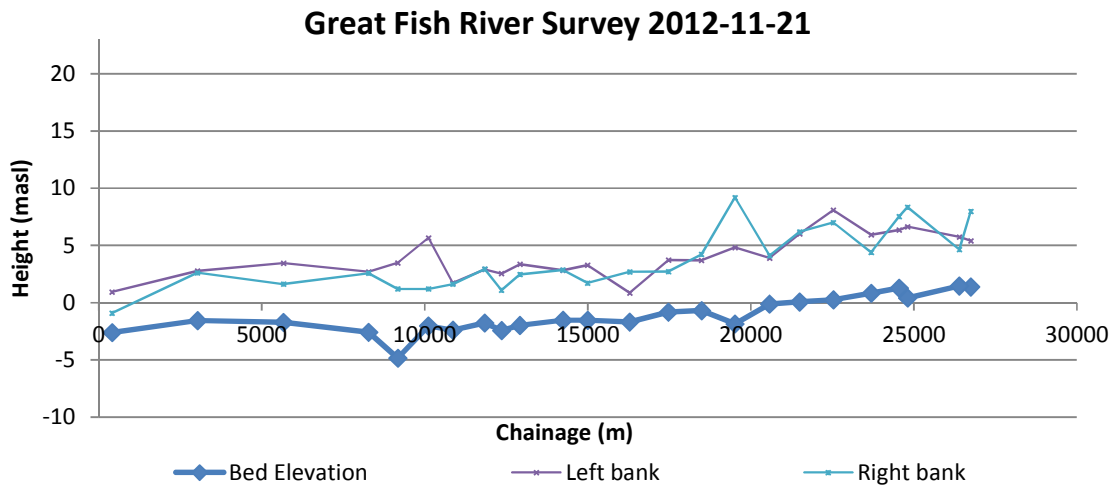
**Figure 4-23: Great Fish River land based survey.**
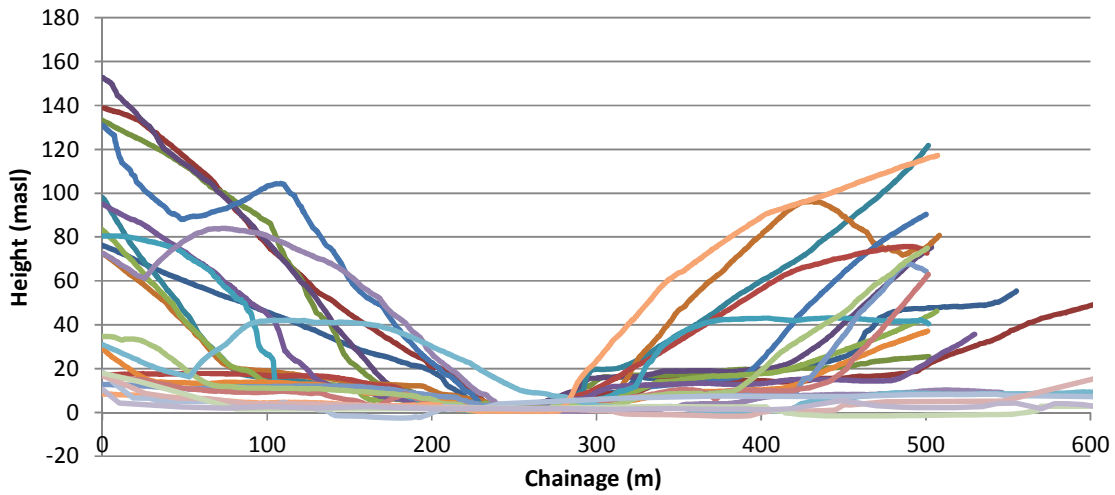
**Figure 4-24: Compilation of survey cross sections, each colour represents one of the 24 river cross-sections.**

53
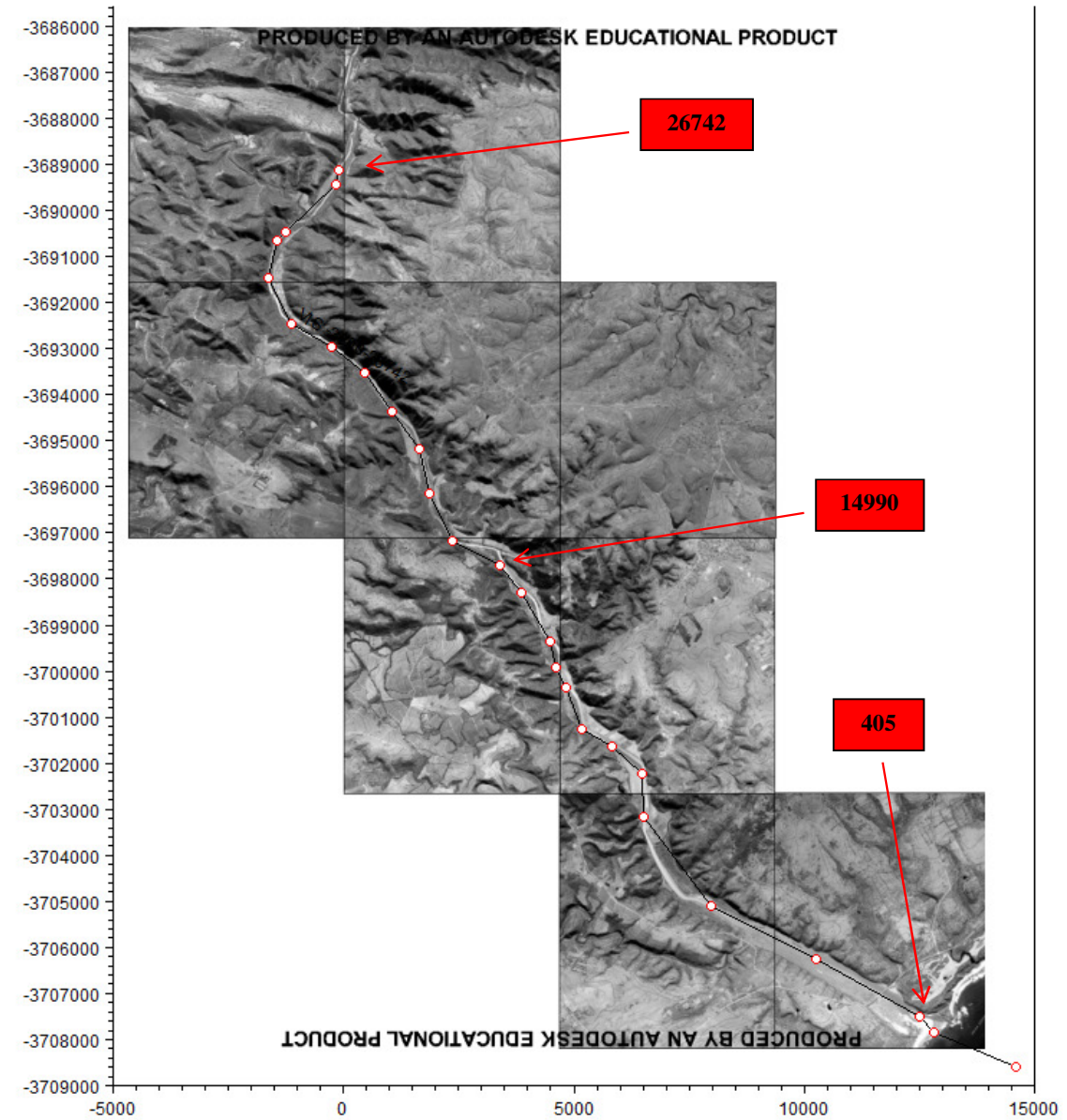
**Figure 4-25: Locations of survey cross-sections**

# 5    TWO-DIMENSIONAL MODEL SETUP

A background of the model parameters is given in Section 3.1.5. Boundary conditions for Scenario A and Scenario B differ and are discussed separately.

## 5.1    Simulation period

The simulation commenced 1 May 2007 and ended 30 May 2012. The general time step used was 5 seconds; time step was adjusted during flood events to ensure numerical stability. The effect of mouth closure on the estuarine salinity was simulated by manual mouth closures in the morphological model for identified flow conditions. The mouth closure is discussed in Section 5.3.1. The flow condition for mouth closure was a 30 day period which has an average flow of 3 m$^3$/s or less. Two events were identified for mouth closure namely 30 November 2009 and 10 September 2010.

## 5.2    Grid generation

The grid of a numerical model is one of the most important components to ensure model accuracy and stability. The size of the grid is directly related to the computation time for a simulation and the accuracy of the results. Data can only be extracted from the model at defined grid points. The user defines the borders of the area of interest (grid) and defines grid points within the model boundaries. The difference between a rectangular and curvilinear grid is shown in Figure 5-1. The following considerations for curvilinear grid generation apply (DHI, 2011):

- Grid quality affects model quality
- Grid cells should be orthogonal, especially in the inner model area
- Model accuracy is reduced when grid cells are too coarse and do not align to bed contours sufficiently
- Grid cells are typically elongated in the flow direction, the cell length in the j-direction should be between 1 to 8 times the cell width in the k-direction (Aspect ratio 1 – 8).
- Expected flow velocities determine grid size as model instability occurs if water is allowed to flow through a grid cell in one time step or less (Courant number).

The generation of the grid is an iterative process. Finer grids tend to be more stable as the variation in grid size and cell height is typically smaller. Finer grids are however extremely taxing on a computer. In an ideal grid setup the flow around bends would not jump between cells in the vertical axis. When the vertical velocity component within a cell is high strong eddy currents are formed which may cause model instability or unrealistic morphological changes in the model area in question. It is however close to impossible to create the perfect grid for all hydrodynamic conditions and the best compromise should be sought. .The grid extents were specified to allow capacity for up to the 100 year flood event, and to the limit of the surveyed area. The 100 year flood water levels were determined by the uncalibrated one dimensional model used in the field work planning process.

The grid is enclosed by a boundary. Refer to Figure 5-1. The user specifies the boundary and then fills the enclosed area with grid cells as deemed relevant. The boundary lines for this study were the 40 m contour lines traced from aerial photographs (boundary lines J and J'), a line perpendicular to the river flow line a distance 2000 m into the sea (boundary line K') and a line perpendicular to the river flow a distance 30000m upstream of the river mouth (boundary line K). The foot of the wave breaker zone is used as the reference location in the model. The resolution of the grid was varied to increase the accuracy in the main river channel. Figure 5-2 shows a grid segment and the relative orthogonality of this segment, blue areas are ideal, red areas not. Orthoganality is easily remedied by increasing the grid size but this is detrimental to model performance. A segment of the final grid used in this study is shown in Figure 5-3, note the increased resolution in the main channel.
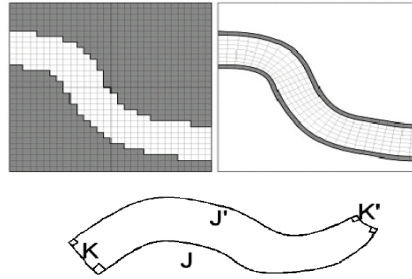
**Figure 5-1: Rectangular (left) and curvilinear (right) typical grid shape with boundary notations (bottom).**
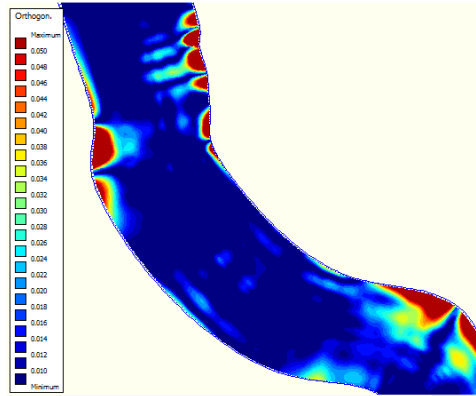


**Figure 5-2: Curvilinear grid orthogonality represented by a colour map for a segment of the computational grid.**
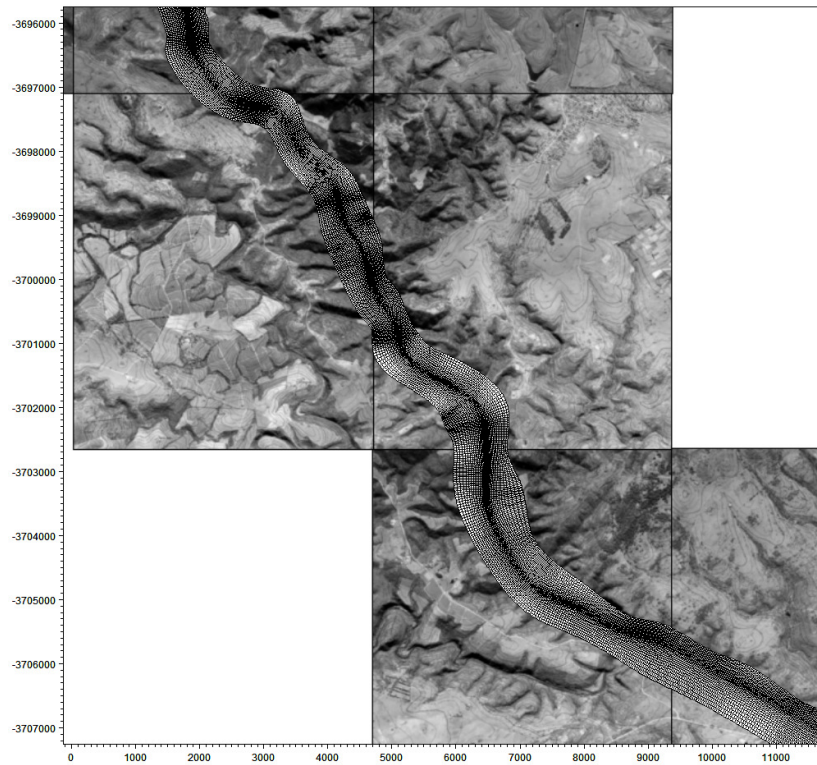


**Figure 5-3: Curvilinear grid segment indicating the increased cell resolution in the river channel.**

56

## 5.3 Bathymetry

After a suitable grid has been created the grid cells need to be specified elevation values. A field survey with 24 river cross-sections was available; the cross-sections were at average 1097 m apart, refer to Section 4.6 and Figure 5-5 (left). To compensate for the limited field measurements aerial topographic photos with contour lines obtained from the Survey department (NGI) were used in conjunction with Google Earth SRTM data to estimate elevation points for the missing areas (no topographic contour lines) above the river and at the river mouth. Contours were hand drawn to facilitate the desired bed level (bathymetric) interpolation between grid cells. Topographical photographs used were taken in 2004; the compiled aerial photographs and hand drawn contour lines are shown in Figure 5-4. Figure 5-5 (right) shows all the elevation points used for bathymetry generation.
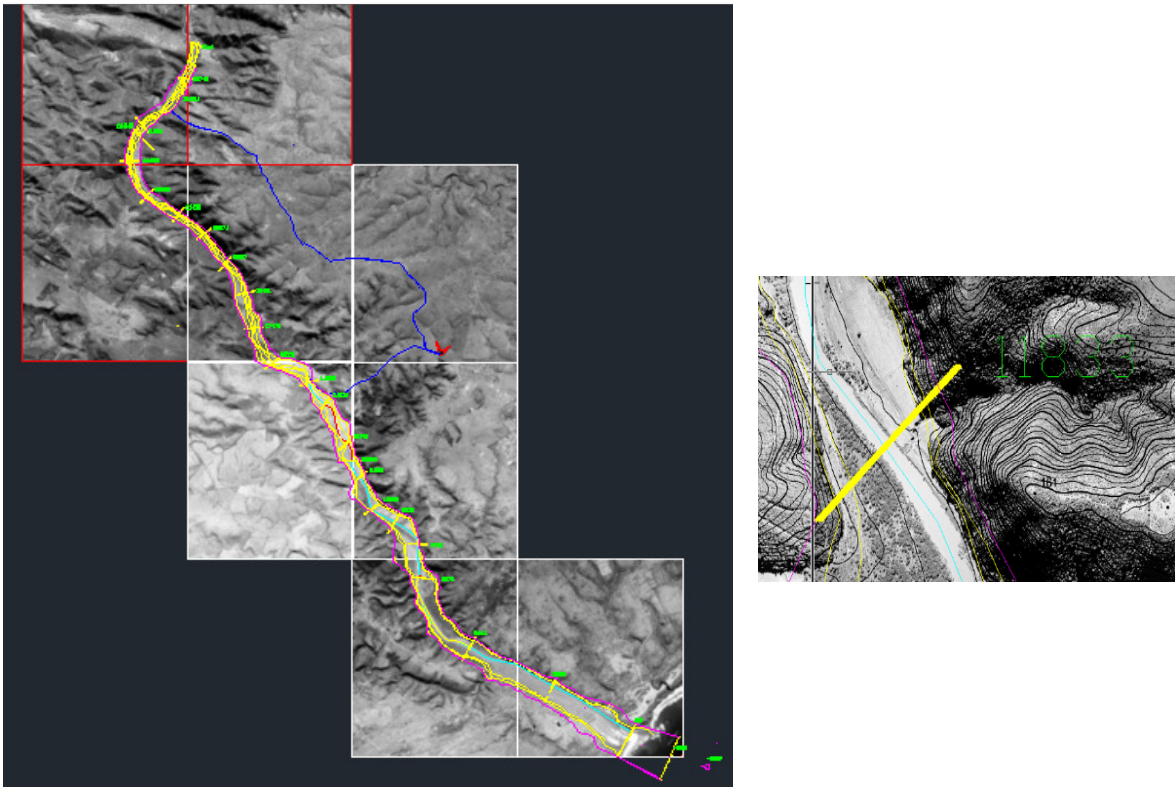


**Figure 5-4: Grid of aerial photographs used for contour estimation. Figure on the right shown a typical river cross section.**
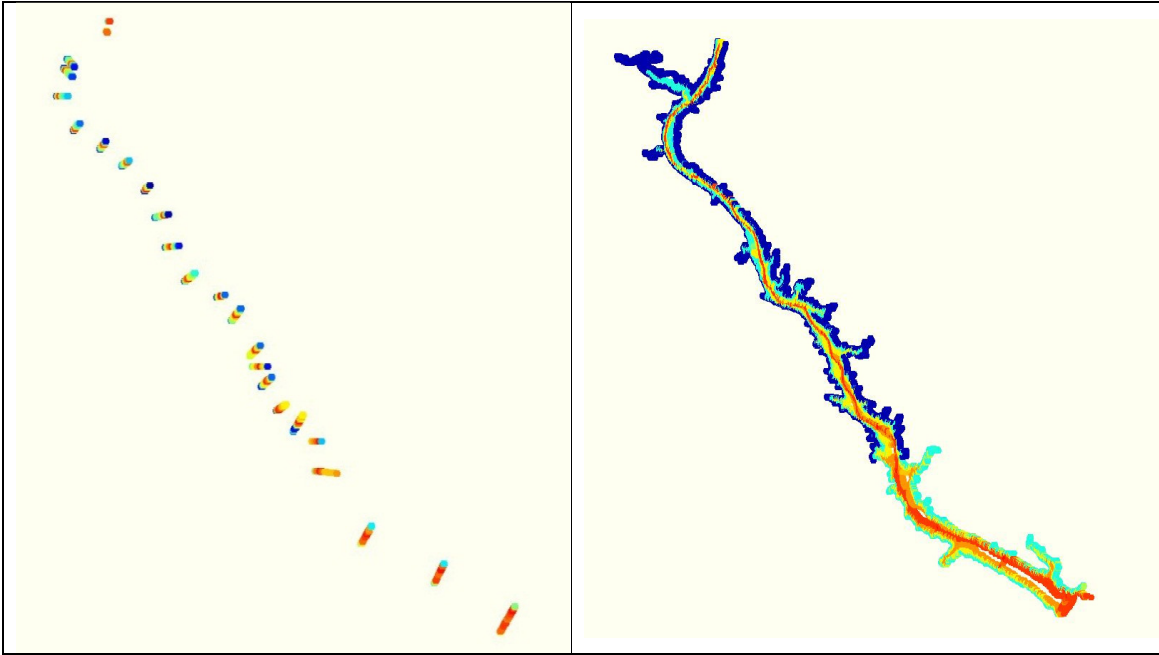
**Figure 5-5: Elevation points used for model bathymetry generation. Left is the elevation points supplied by the survey, right is survey elevation points and hand generated contour lines from aerial photographs and Google earth SRTM data.**

After an adequate number of elevation points were defined the grid cells were filled by means of 2 stages of interpolation. The first stage consisted of interpolating the available cross-sectional surveys for the river bed and the second stage the interpolation of the points along the river banks. The software averages all the points in a grid cell and then fills blank grid cells between defined grid cells by means of triangular interpolation. Due to the distance between sections the river bed elevation is a rough estimation. A quality grid increases the accuracy of the interpolation. The grid and bathymetry is shown for all the interpolation stages in Figure 5-6. A 3D view of the whole model area is shown in Figure 5-7. The final bathymetry used for the two-dimensional model is shown in Appendix K.
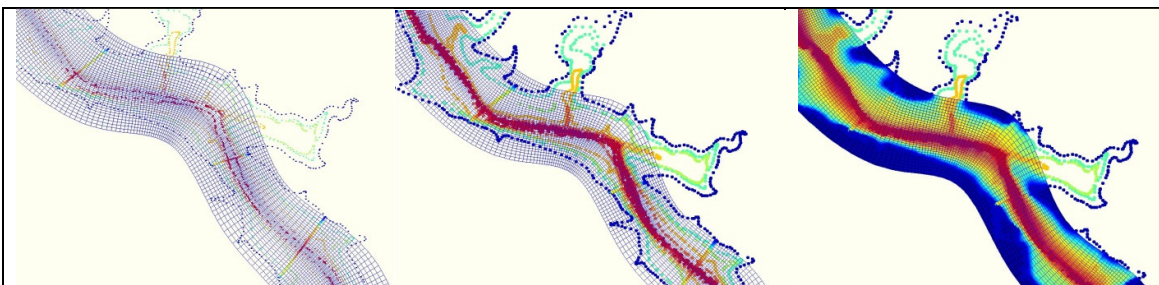


**Figure 5-6: Left- model grid and bathymetry before interpolation. Middle – model grid and bathymetry after stage one of interpolation. Right – model grid and bathymetry after stage 2 of interpolation.**
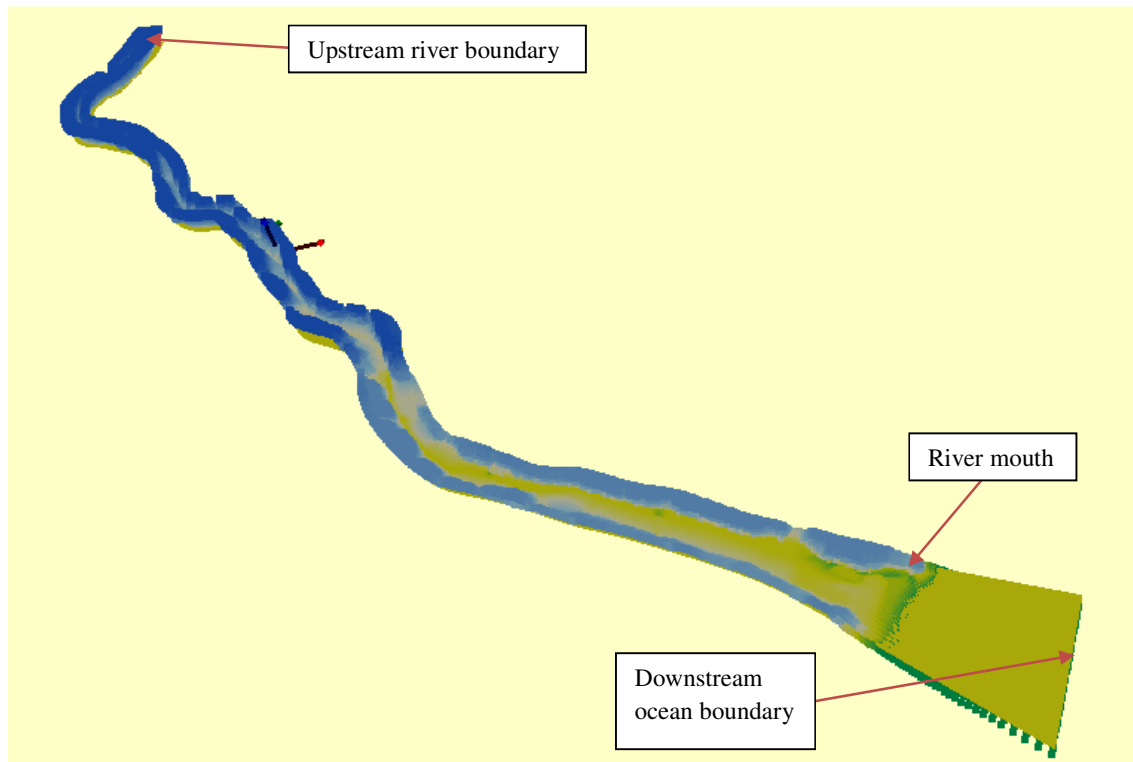
**Figure 5-7: 3D view of the model bathymetry.**

### 5.3.1    Mouth closure

#### 5.3.1.1    *Background*

After initial model setup it was attempted to close the river mouth by specifying an indefinite constant low river discharge of 1 $m^3$/s. The time scale required for mouth closure was unrealistic and this method of mouth closure not deemed feasible for this study. The approach was unsuccessful due to the lack of a longshore (wave) boundary in the model setup and the relatively small sediment influx due to the low flow condition. As the effect of mouth closure and the hypothetical mouth breaching was desired manual mouth closure was done when specified river flow conditions were observed.

### 5.3.1.2    Method

No surveys were available for the river mouth in a closed state. Historical aerial photos of the river mouth were obtained from the Surveyor General to investigate the mouth shape and possible closed mouth events. Aerial photos for 1955, 1956, 1965, 1976, 1998 and 2004 (used in the generation of model bathymetry) are available, refer to Figure 5-9. No discernible closed mouth states could be identified from the historical aerial photos, it is possible that the mouth was closed in 1956 and/or 1965 but due to the glare from the sand no definite conclusion can be made. A sediment plume is visible in the aerial photo for 1998 which indicates a recent flood event. The mouth is clearly unobstructed in the photos for 1973 and 2004.

As no closed mouth states could be found the mouth was closed by extending the height of the dune across the channel. The dune height was derived from the survey done at the river mouth and interpreted topographic information from the aerial photographs of 2004. A small notch was created on the hypothetical dune berm to promote breaching in the main river channel area. The estuary mouth state before closure (left) and after closure (right) can be seen in Figure 5-8 below.
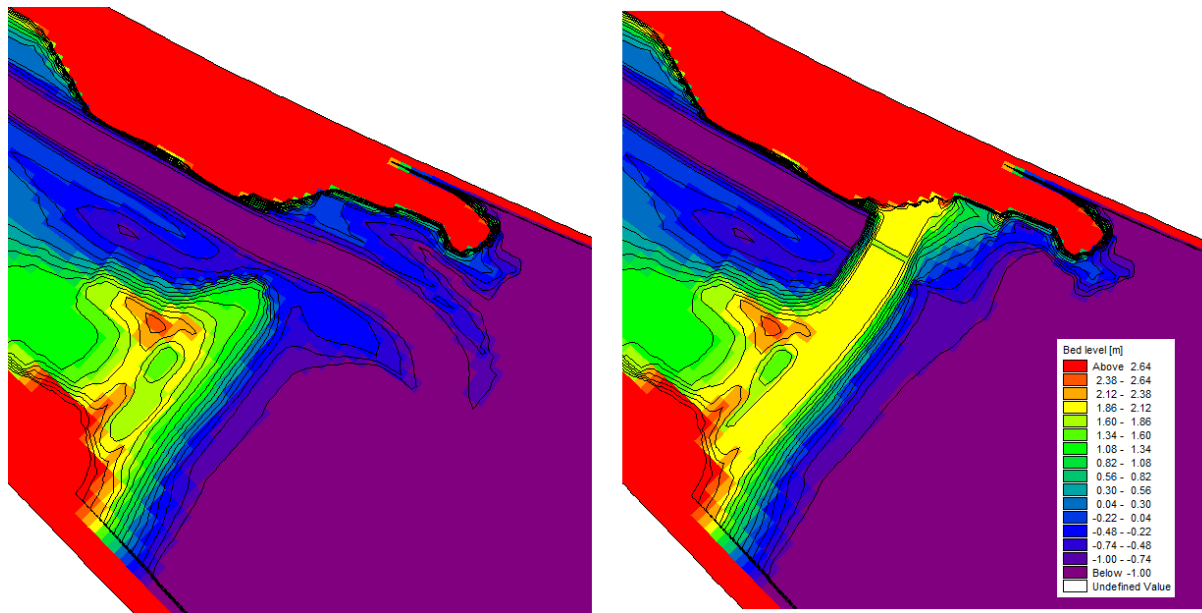


**Figure 5-8: Estuary mouth before (left) and after (right) artificial closure.**

60

**1955**

**1956**

**1965**

**1973**
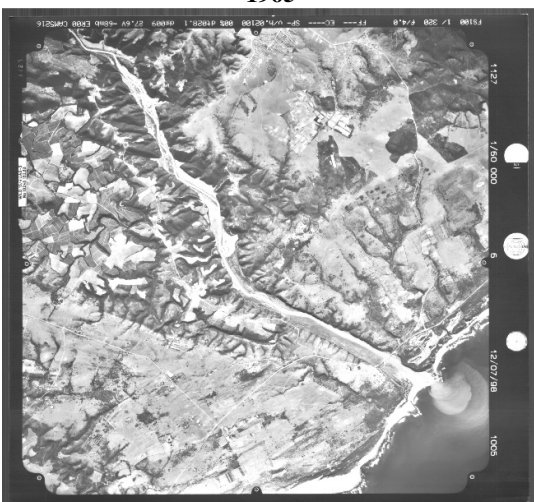
**1998**

**2004**

**Figure 5-9: Historical aerial photographs of the lower Great Fish River.**

## 5.4    Model boundary conditions

The model has 2 open boundaries namely; the upstream river boundary and downstream sea boundary. Each boundary has a hydrodynamic and sediment component. The following boundary conditions can be specified:

Hydrodynamic boundary:

- Water level
- Flux (discharge)

Sediment boundary:

- Bed level
- Sediment transport
- Sediment concentration

All boundary conditions can be static or varied over time.

### 5.4.1    Downstream sea boundary

The downstream boundary of the model was a tidal water level. Tidal levels were obtained in 6 minute intervals from the WXTide32 freeware software application. WXTide32 is an astronomical tide prediction application. WXTide32 provides tidal information relative to Chart Datum (CD). The model environment was referenced to sea level, the downstream tidal boundary was thus converted to masl.

Gravitational forces acting between the sun, moon and earth are directly or indirectly responsible for the observed tides in our oceans and seas. Tidal motion can be described by a series of simple harmonic constituent motions, each with a characteristic angular velocity (frequency). Constituent amplitudes and phases vary with the positions of where measurements were taken.

The general form of the tide prediction formula used by WXTide32 as developed by Doodson (1921) is given by equation 5-1:

$$H(t) = A_0 + \sum_{i=1}^{k} A_i F_i \cos(w_i t + (V_0 + u)_i - G_i) \tag{5-1}$$

where:

| | |
|---|---|
| H(t) | = height of tide at time t |
| $A_0$ | = average tidal height over a certain period |
| k | = number of tidal constituents |
| I | = index of tidal constituent |
| $A_i$ | = local constituent amplitude |
| $F_i$ | = nodal amplitude factor |
| $w_i$ | = angular velocity |
| $(V_0+u)_i$ | = astronomical argument |
| $G_i$ | = local phase lag |

The input variables $A_0$, $A_i$, $G_i$ are dependent on the tidal station location. Constituent values can be obtained from Admiralty Tables. The system calculates F and ($V_0$ +u) for selected tidal constituent over the prediction period specified. Water levels are generated as a time series.

Tidal heights were available at Port Elizabeth and East London. The level at the Great Fish River mouth was determined by distance interpolation between these two stations. The estuary is classified as micro-tidal by the tidal estuary classification scheme of Davies (1964), most south African estuaries are micro-tidal (Cooper 2002; 2001). Characteristic tidal levels for the Great Fish River mouth are shown in Table 5-1 and  Figure 5-10.

**Table 5-1: Tidal characteristics for Port Elizabeth, East London and The Great Fish River mouth** (SANHO 2012)

| Place | LAT* | MLWS | MLWN | ML | MHWN | MHWS | HAT | Distance from PE (km) |
|---|---|---|---|---|---|---|---|---|
| | meters above Chart Datum  (CD) | | | | | | | |
| Port Elizabeth | 0 | 0.21 | 0.79 | 1.04 | 1.29 | 1.86 | 2.12 | - |
| East London | 0 | 0.23 | 0.78 | 1.02 | 1.25 | 1.82 | 2.08 | 240 |
| Great Fish River mouth* | 0 | 0.22 | 0.78 | 1.03 | 1.27 | 1.84 | 2.10 | 145 |

*Refer to List Of Symbols for abbreviations.
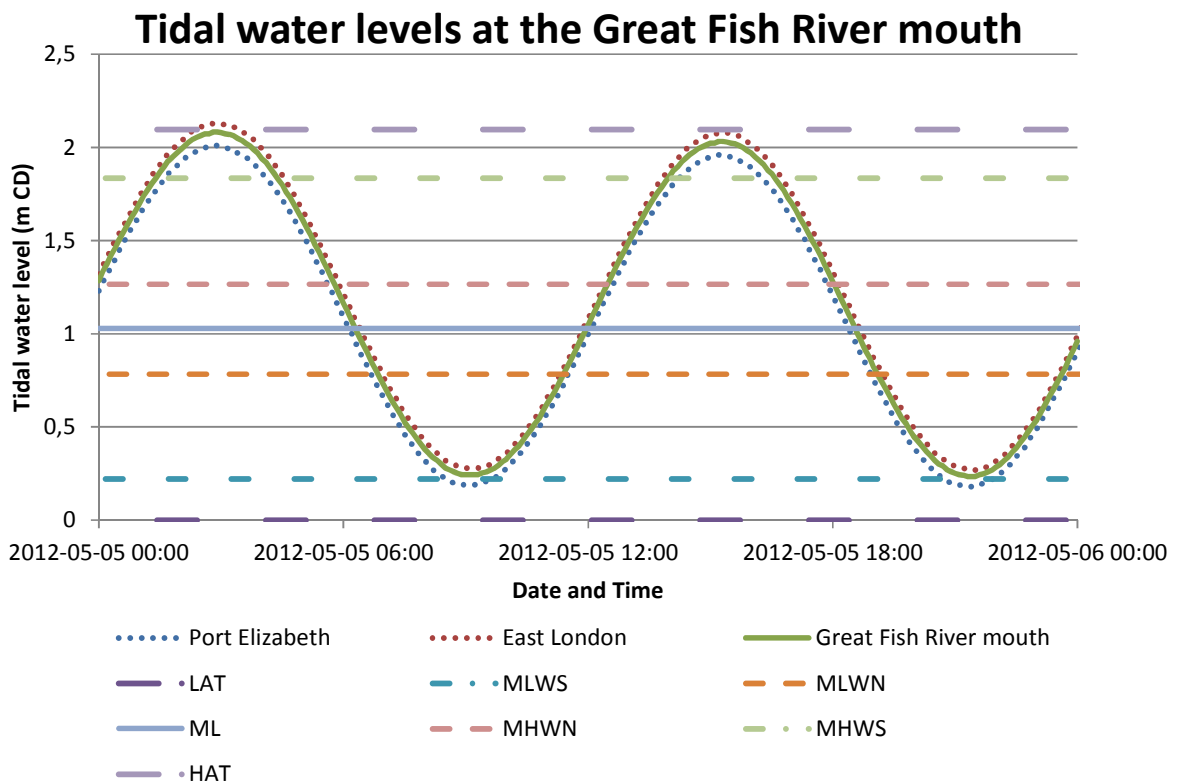


**Figure 5-10: Characteristic tidal water levels at the Great Fish River mouth.**

### 5.4.2      Upstream river boundary

#### 5.4.2.1      *Scenario A - Long term simulation*

The river discharge (flux boundary) for DWS station Q9H018 was used, data was extracted a daily timestep. The software uses linear interpolation between specified input values (which are daily average river flows) to calculate instantaneous flow into the model area. Due to the interpolation of daily average values to instantaneous data the actual flow crest and troughs (when flow is likened to a wave) of the daily period might be missed. The river discharge during scenario A is shown in Figure 5-12. River discharge statistics are shown in Figure 5-11 and Figure 5-13.

63

## Flow exceedance probability during the 5 year simulation period for DWS station Q9H018
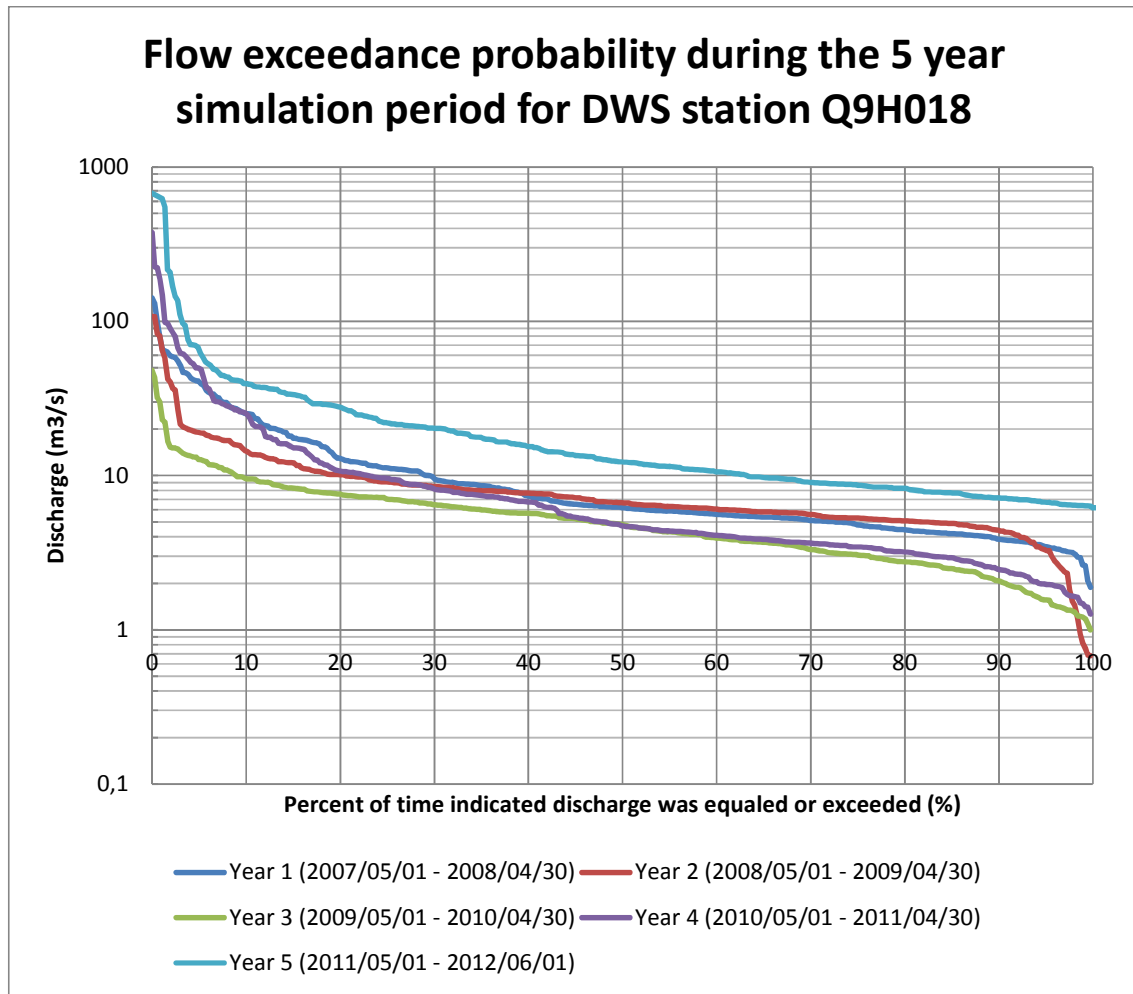


**Figure 5-11: Flow exceedance probability**

## River discharge for scenario A, DWS station Q9H018
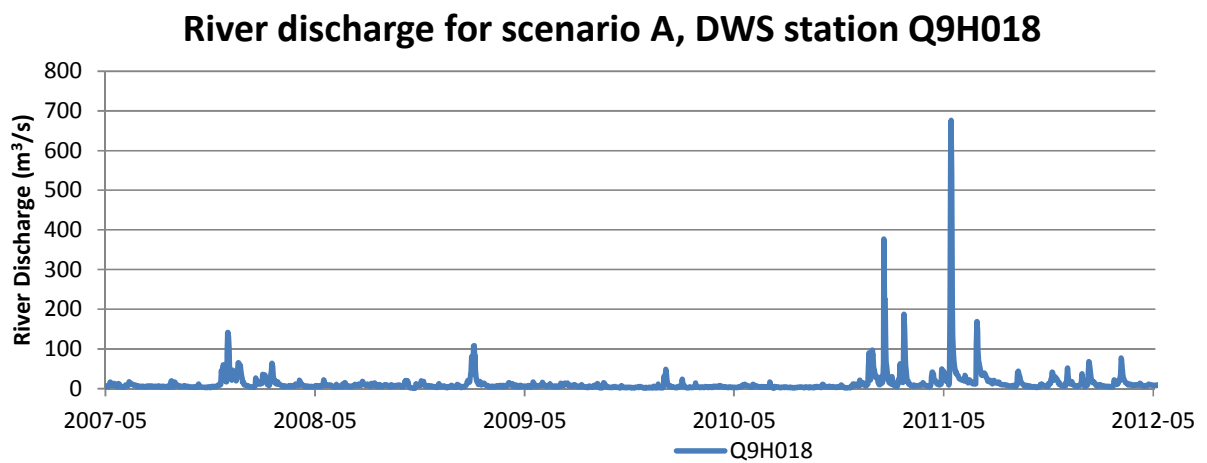


**Figure 5-12: River discharge of station Q9H018 during the simulation period of Scenario A.**

64

## River discharge for simulation period, DWS station Q9H018



| | 2007 | 2008 | 2009 | 2010 | 2011 | 2012 |
|---|---|---|---|---|---|---|
| ■ Min | 1,89 | 0,68 | 1,10 | 1,00 | 2,83 | 4,39 |
| ■ Average | 11 | 11 | 8 | 5 | 29 | 17 |
| ■ Max | 255 | 65 | 108 | 48 | 676 | 127 |
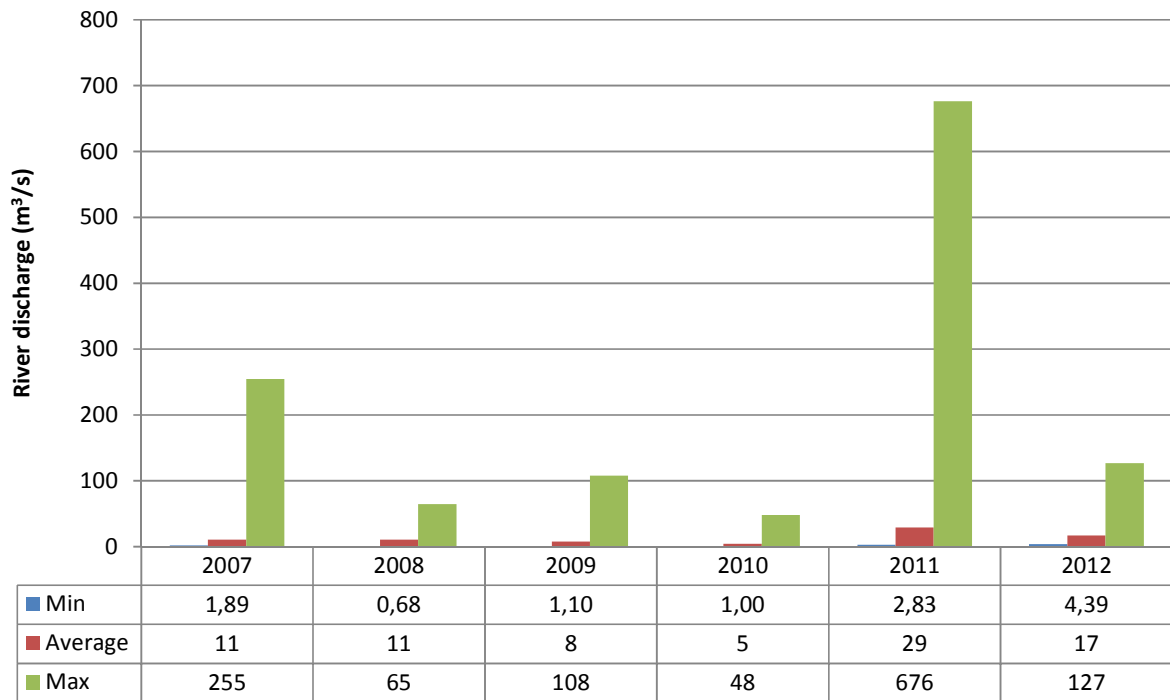
**Figure 5-13: River discharge statistics for station Q9H018 during the simulation period of Scenario A.**

### *5.4.2.2    Scenario B - Flood hydrographs*

5.4.2.2.1    Flood hydrology

Statistical analysis was done on the observed flood peaks of DWA gauging stations Q9H010 and Q9H018 (station information shown in Table 5-2), flood peaks were scaled up with the square root of the areas to obtain flood peaks at the river mouth. The total catchment area of the Great Fish River is 30192 km². Yearly flood peaks can be seen in Figure 5-14, from Figure 5-14 it is evident that the flow record from gauging station Q9H018 is not reliable as the developments and dams in the catchment area could not have reduced flood peaks to such an extent. As flow records from 1969 were deemed unreliable for flood calculation the flood peaks for station Q9H010 were used instead. Refer to Table 5-3 for results of the statistical analysis.

**Table 5-2: Flow gauge stations used for determination of flood peaks.**

| DWA Station | Record length | Latitide | Longitude | Catchment area |
|---|---|---|---|---|
| Q9H010 | 1930/07/13 – 1956/03/31 | 33.20876 | 26.86575 | 29328 km² |
| Q9H018 | 1969/07/30 – 2013-09-04 | 33.23781 | 26.99486 | 29745km² |

# Great Fish River historical yearly flood peaks
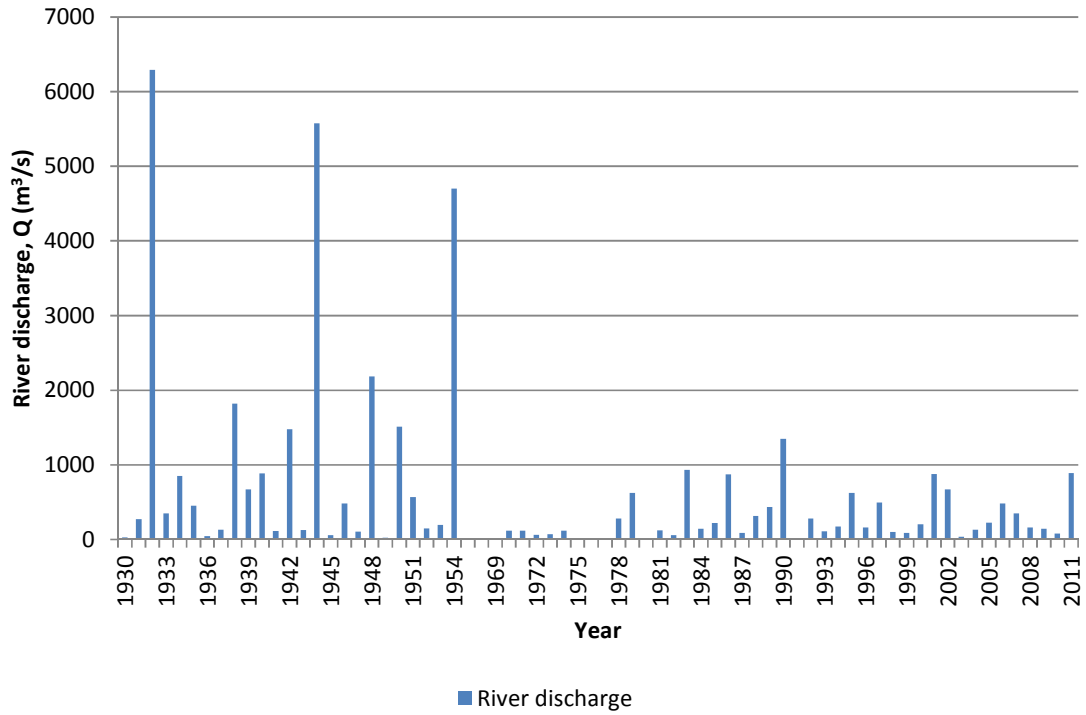


**Figure 5-14: Historical yearly flood peaks for gauging station Q9H010 and Q9H018**

**Table 5-3: Statistical flood peaks for the Great Fish River**

| Return period | LN | | LPIII | | GEV$_{PARAM}$ | | GEV$_{MM}$ | GEV$_{PWM}$ | Proposed |
|---|---|---|---|---|---|---|---|---|---|
| Years | W$_T$ | Q (m³/s) | W$_T$ | Q (m³/s) | W$_T$ | Par. | Q (m³/s) | Q (m³/s) | Q (m³/s) |
| 2 | 0.000 | 352 | 0.006 | 356 | 0.375 | k | 863 | 643 | **356** |
| 5 | 0.842 | 1673 | 0.843 | 1678 | 1.655 | -0.129 | 2691 | 1848 | **1678** |
| 10 | 1.282 | 3776 | 1.278 | 3748 | 2.610 | E(y) | 4057 | 3091 | **3748** |
| 20 | 1.645 | 7396 | 1.634 | 7255 | 3.618 | 1.093 | 5497 | 4785 | **7255** |
| 50 | 2.054 | 15762 | 2.034 | 15202 | 5.069 | var(y) | 7570 | 8053 | **15202** |
| 100 | 2.326 | 26104 | 2.300 | 24841 | 6.276 | 0.041 | 9295 | 11657 | **24841** |

GEV: General Extreme Value

LN: Log Normal

LPIII: Log Pearson III

W$_T$: Weight applied to function/data

5.4.2.2.2    Flood hydrographs

Flow records for station Q9H010 were used to determine the typical flood hydrograph shape for the Great Fish River catchment. Floods of magnitude 344 m³/s, 1783 m³/s, 4603 m³/s and 6156 m³/s were identified.  Identified hydrographs were scaled in time and flood magnitude to simulate predicted flood events. The largest observed flood had a magnitude of 6156 m³/s and occurred on the third of January 1932. From historical floods the time of concentration (T$_c$) of the catchment is approximately 66 hours; as such larger floods were not scaled in time but merely in magnitude. Refer to Table 5-4 for a summary of the flood events and the historical peak used.

All flood hydrographs were plotted with primary (highest resolution) data obtained from the DWS.

**Table 5-4: Measured and predicted flood events for various return periods**

| Flood event | Peak discharge (m³/s) | Historical flood used(m³/s) | Flood volume (m³)* | Date of historical flood peak | Observed time of concentration (hours) | Figure |
|---|---|---|---|---|---|---|
| Q$_2$ | 356 | 344 | 58x10⁶ | 1933/04/06 | 33 | Figure 5-15 |
| Q$_5$ | 1678 | 1783 | 80x10⁶ | 1937/12/19 | 41 | Figure 5-16 |
| Q$_{10}$ | 3748 | 4603 | 564x10⁶ | 1953/10/22 | 64 | Figure 5-17 |
| Q$_{20}$ | 7255 | 6156 | 916x10⁶ | 1932/01/03 | 66 | Figure 5-18 |
| Q$_{50}$ | 15202 | 6156 | 1920x10⁶ | 1932/01/03 | 66 | |
| Q$_{100}$ | 24841 | 6156 | 3138x10⁶ | 1932/01/03 | 66 | |

*Flood volume is calculated for the total observed flood duration.

## 2 Year flood hydrograph
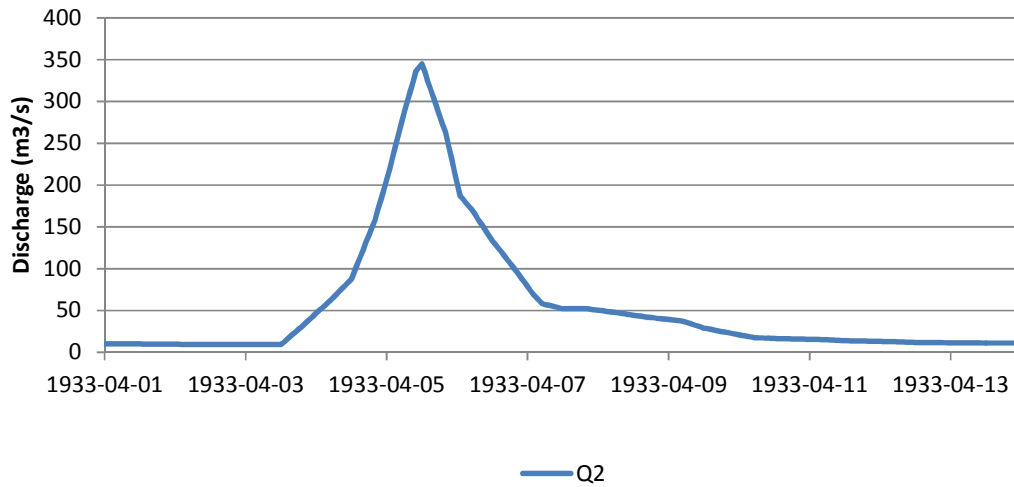


**Figure 5-15: Hydrograph of flood event with a return period of 5 years.**

## 5 Year flood hydrograph
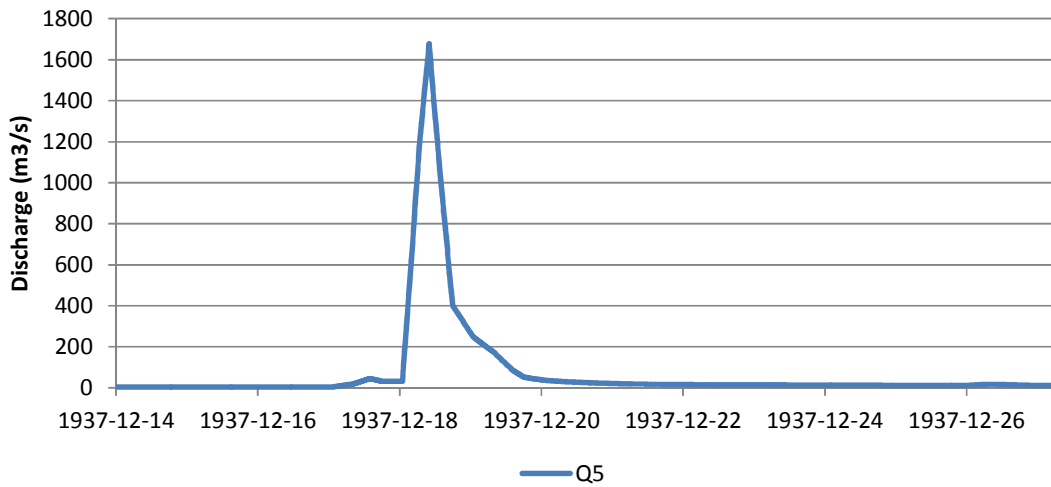


**Figure 5-16 Hydrograph of flood event with a return period of 2 years.**

## 10 Year flood hydrograph
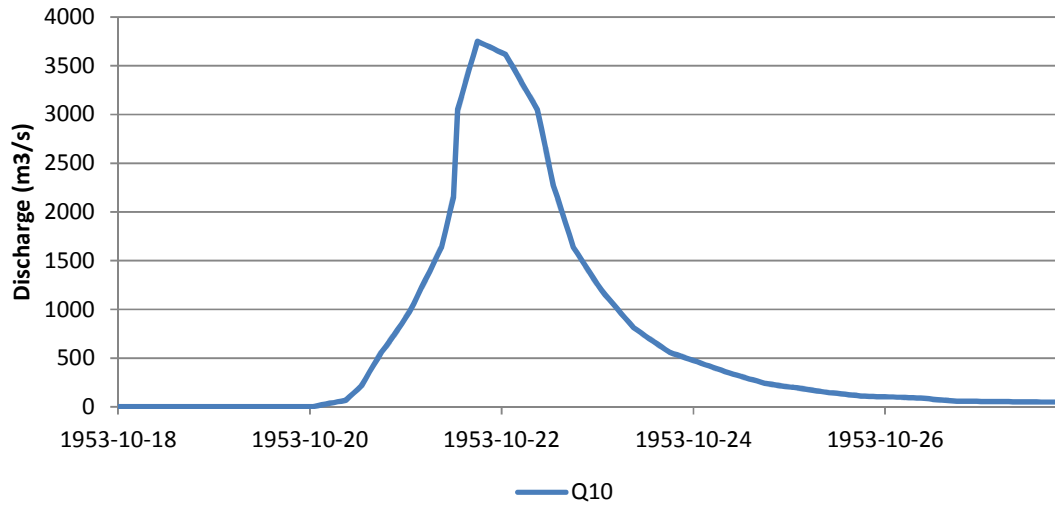


**Figure 5-17: Hydrograph for flood event with a return period of 10 years.**

## 20, 50 and 100 year flood hydrographs
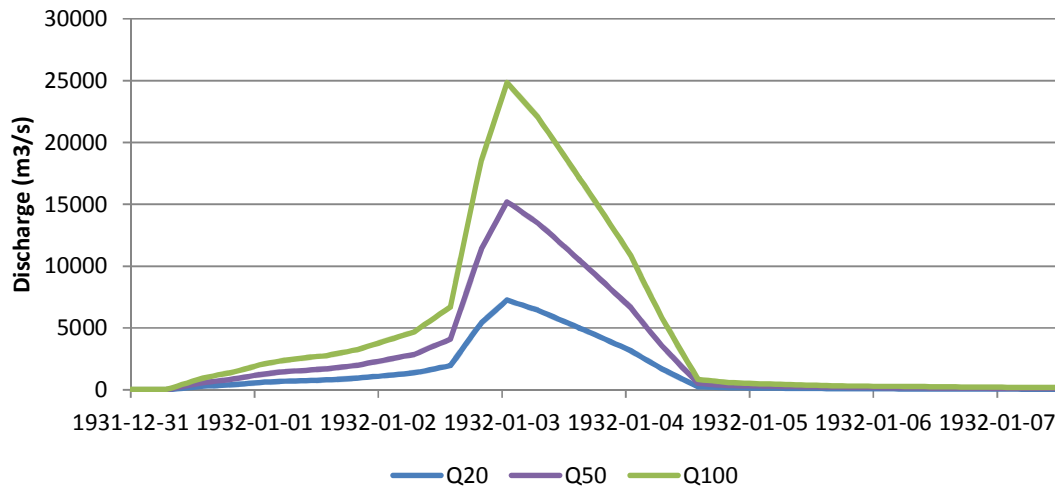


**Figure 5-18: Hydrogrpahs for floods of return periods 20, 50 and 100 years.**

## 5.5    Bed sediment fractions

Two sediment fractions were used in the model setup, namely cohesive (silt and clay) and non-cohesive (sand). Bed sediment fractions characteristics were derived from bed load samples collected during field work. A total of 31 bed load samples were collected at 5 sites, samples were analysed to determine suitable fraction sizes. The methodology used to obtain bed samples is covered in Section 4. Refer to Appendix G for all bed load samples. Figure 5-19 is a compilation of the sediment grain distributions of all the bed load samples taken.

Fraction 1 is the non-cohesive component and Fraction 2 the cohesive component. In this study sediment can be considered as sand (non – cohesive) when d > 0.0625 mm and as silt (cohesive) when d < 0.0625 mm.

The methodology used in determining the representative bed sediment fraction sizes is discussed in the following sections.
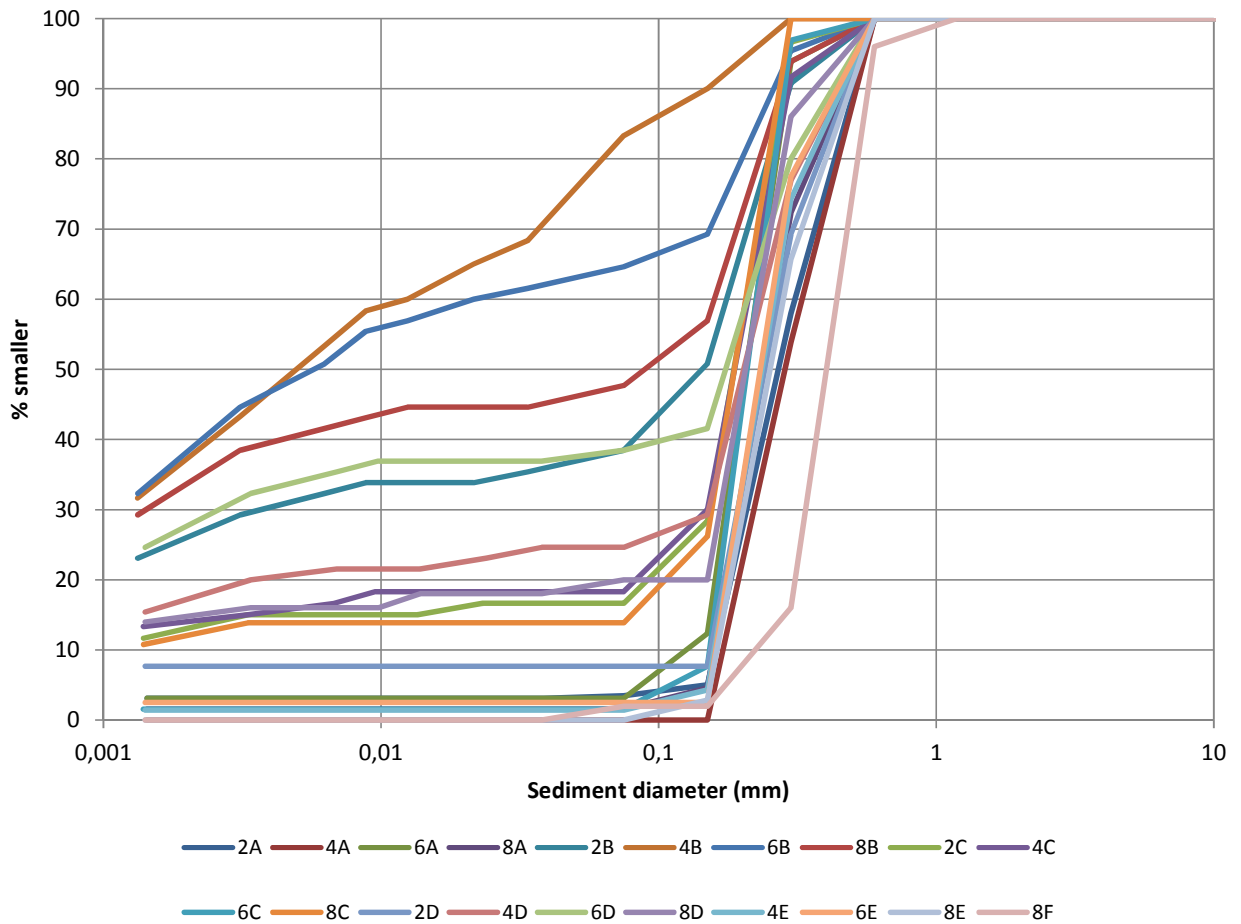


**Figure 5-19: Bed grading plot of all bedload sediment samples collected during field work.**

### 5.5.1.1    *Fraction 1 – non cohesive*

A weighted average of the sand particles (d>0.0625) was determined and used for the sand fraction. The representative particle diameter selected was 0.3 mm.

70

### 5.5.1.2    Fraction 2 - cohesive

A representative particle diameter was estimated by determining the average weighted sediment settling velocity for all cohesive samples, cohesive samples defined as particles of d < 0.0625mm, sediment grain diameter was then determined for this velocity. The sediment settling velocity as defined by Stoke was used.

Stokes sediment settling velocity (eq. 5-2):

$$w = \frac{(\rho_s - \rho_w)d^2 g}{18\nu}$$
(5-2)

With:    w = settling velocity

$\rho_s$ = particle density = 2650 kg/m³

$\rho_w$ = density of water

$\nu$ = kinematic viscosity = 1 x 10⁻³ m²/s

d = particle diameter

The representative particle diameter for Fraction 2 was d = 0.0252 mm.

### 5.5.1.3    Layer composition

The mean grain size over the model area is defined by the layer fraction percentage (Refer to Section 3.1.5.3.3.3). The component of Fraction 1 and Fraction 2 should sum to 100%, i.e. 85% sand implies 15% silt giving a representative diameter of 0.26 mm. As bed information was only available between Sites A (405m) and F (15000m) the upper and lower reach was extended with the bed grading of these sites. Bed grading was interpolated between measured sites. The floodplains were assumed 90% silt. Refer to Figure 5-20 for the component percentage of Fraction 1.
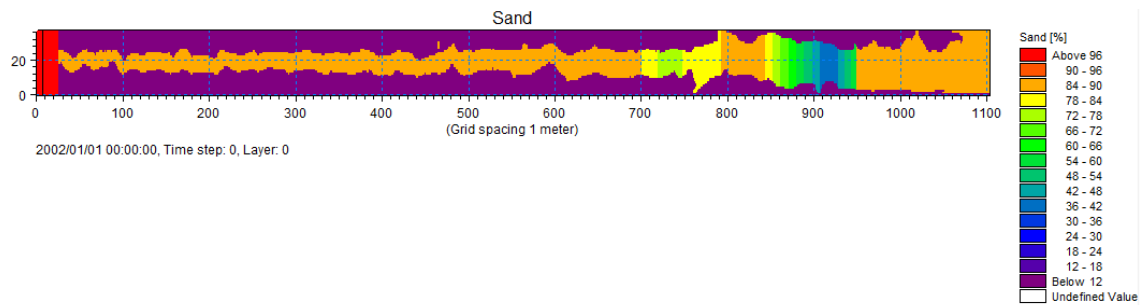


**Figure 5-20: Fraction 1 component percentage over the model area in the form of a rectangular grid.**

## 5.6    Fluvial Sediment yield prediction

The fluvial sediment yield is needed to predict the sediment influx into the model (sediment boundary condition). The fluvial sediment yield was determined using the methods derived in the WRC report; Sediment Yield Prediction for South Africa 2010. The Great Fish River catchment is situated in sediment yield region 7, refer to Figure 5-21.
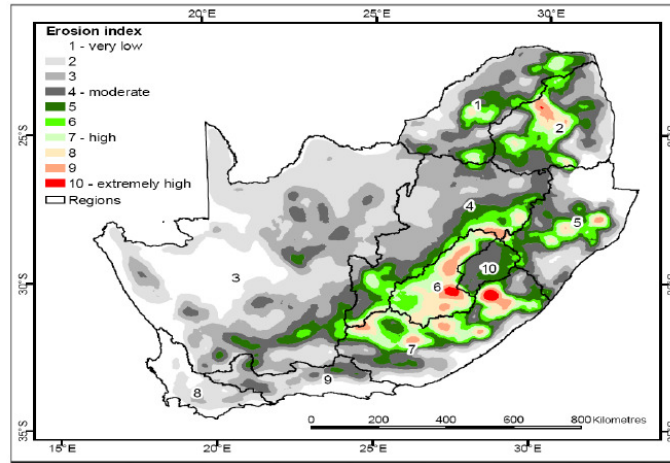
**Figure 5-21: Sediment yield regions (Msadala et al. 2010)**

There are two methods of calculating the estimated sediment yield namely; empirical and probabilistic methods. The probabilistic method is not accurate for erosion region 7 (Msadala et al. 2010) and thus the empirical method was used to estimate sediment yield. The report Sediment Yield Prediction South Africa 2010 includes interactive PDF maps for each erosion area which are used to determine the characteristic parameters for sediment yield prediction. Refer to Figure 5-22 for the PDF map used for region 7.
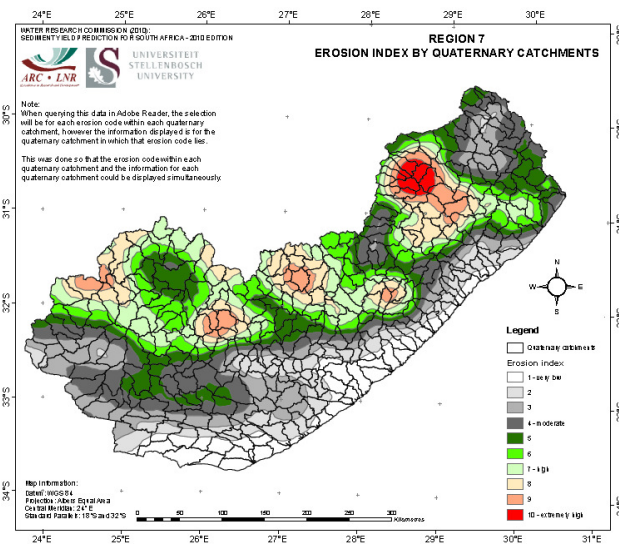


**Figure 5-22: Erosion index by quaternary catchment (Msadala et al. 2010)**

The empirical sediment yield prediction formula was determined through the unit stream power concept and regression analysis (Msadala et al. 2010). Location data for the sediment yield prediction is shown in Table 5-5.

**Table 5-5: Location data for sediment yield prediction.**

| Location data | | |
|---|---|---|
| Department of Water and Sanitation drainage region | Q (Great Fish River) | |
| Total catchment area (A) | 30189 | km$^2$ |
| Effective catchment area (A$_e$): | 13989 | km$^2$ |
| Sediment yield region | 7 | |

The sediment load ($Q_s$) for region 7 is calculated by equation 5-3:

$$Q_s = 30Q_{10}^{0.36}S_0^{0.33}R_{nd}^{0.29}A_e^{0.61}EI_W^{0.58} \hspace{3cm} (5\text{-}3)$$

Where:   $Q_s$ = sediment load (t/a)

$Q_{10}$ = 10 year return period flood of the catchment ($m^3$/s)

$S_0$ = average river slope (m/m)

$R_{nd}$ = river network density (m/$km^2$)

$A_e$ = effective catchment area ($km^2$)

$EI_w$ = weighted erosion class

The weighted erosion class parameter is a quantitive parameter of the following catchment characteristics: soil profile, relief, climate, land use and land management practices. The weighted erosion class is calculated by equation 5-4:

$$EI_w = \sum A_p EHC \hspace{3cm} (5\text{-}4)$$

Where:   $A_p$ = proportion of the catchment area

EHC = Erosion Hazard Class

The area of the catchment in the erosion hazard class is measured from the PDF maps. The area of the catchment in each hazard class and the weighted erosion class is shown in Table 5-6. The weighted erosion class for this catchment was calculated as equal to 4.21.

**Table 5-6: Characteristics areas for the determination of the weighted erosion class (EI$^w$)**

| Erosion Hazard Class | Area ($km^2$) | Area proportion ($A_P$) | Weighted Erosion Class ($EI_w$) |
|---|---|---|---|
| 1 | 68 | 0.005 | 0.005 |
| 2 | 1939 | 0.139 | 0.277 |
| 3 | 2313 | 0.165 | 0.496 |
| 4 | 4348 | 0.311 | 1.243 |
| 5 | 2931 | 0.21 | 1.048 |
| 6 | 1128 | 0.08 | 0.483 |
| 7 | 989 | 0.071 | 0.495 |
| 8 | 189 | 0.014 | 0.108 |
| 9 | 87 | 0.006 | 0.056 |
| 10 | 0 | 0 | 0 |
| **Total** | **13989** | **1** | **4.21** |

The dependant and independent variables used for the calculation of the sediment yield is summarised in Table 5-7. The total catchment sediment yield/load is predicted as 3345831 tons per year (t/a).

**Table 5-7: Catchment sediment load and associated variables.**

| Dependant and independent variables | | |
|---|---|---|
| Recurrence interval flood ($Q_{10}$) | 3570 | m$^3$/s |
| Average river slope ($S_0$) | 0.00407 | m/m |
| River network density ($R_{nd}$): | 202 | m/km$^2$ |
| Effective area ($A_e$): | 13989 | km$^2$ |
| Weighted Erosion Class ($EI_w$) | 4.21 | |
| Sediment load  ($Q_s$) | 3345831 | t/a |
| Sediment load per unit area ($Q_{sa}$) | 239 | t/km$^2$/a |

## 5.7   Fraction – sediment yield relationship

In the model space two sediment fractions were defined, the fractions and their characteristics are shown in Table 5-8. The total sediment load (yield) was divided between each fraction. The methodology used was to determine the transport capacity of the river for the large fraction and subtract this component from the total sediment load. The remaining load was then assigned to the smaller fraction. As the transport of sediment is dependent on the river flow/discharge, discharge-sediment load relationships were derived for each fraction.

**Table 5-8: Fractions used in the model setup.**

| Fraction | $d_{50}$ (mm) | Critical Shield's number, $\theta$ | Density (kg/m$^3$) |
|---|---|---|---|
| 1: Non-cohesive sand | 0.3 | 0.056 | 2650 |
| 2: Cohesive silt and clay | 0.0252 | 0.054 | 2650 |

### 5.7.1    Non-cohesive sediment component – Fraction 1

The load component of fraction 1 was determined by calculating the total load capacity of the river cross-sections at the upstream river boundary. The purpose of the model boundary total load capacity calculation was to ensure that larger diameter sediment load (fraction 1) specified at the model boundary do not deposit at the upstream model boundary. The river total load capacity was calculated by means of the Engelund Hansen formula for total load. The sediment capacity of the upstream river boundary is a function of the river slope, particle diameter, critical shields parameter, and the bed roughness. The formulas used for the determination of the cross section transport capacity are discussed in Section 3.4.

Cross section parameters for the first six upstream river cross sections were obtained from the Mike11 Cross Section Editor. The Cross Section Editor specifies the hydraulic radius, area and width of the cross section at varying water levels. The total sediment load for the first 6 upstream cross sections is shown in Figure 5-23. The flow rate for each water level was calculated using the Chezy formula with the assumption that the representative bed roughness ($k_s$) is equal to 2.5$d_{50}$, $d_{50}$ being equal to the representative grain diameter of fraction 1 which is 0.3 mm. The river slope was taken as the bed slope of the upper reach of the estuary from the survey bed levels.

The Chezy formula is defined by equation 5-5  (Rooseboom 2007):

$$v = 18\log(\tfrac{12R}{k_s})\sqrt{RS_o} \tag{5-5}$$

Where:          v = velocity

                    R = hydraulic radius

74

$k_s$ = roughness coefficient, assumed equal to $2.5d_{50}$

$S_o$ = river slope

The predicted sediment load was averaged across the 6 river sections. The relationship between the river discharge and the sediment load for the first 6 river cross sections is shown in Figure 5-24. A trend line was determined for this data set and the following relationship was obtained:

$$Q_s = 4.73E^{-5}Q^{1.55} \tag{5-6}$$

Where    $Q_s = S_{TL}$ = sediment total load, as defined in Section 3.4 [m³/s]

$Q$ = river discharge [m³/s]
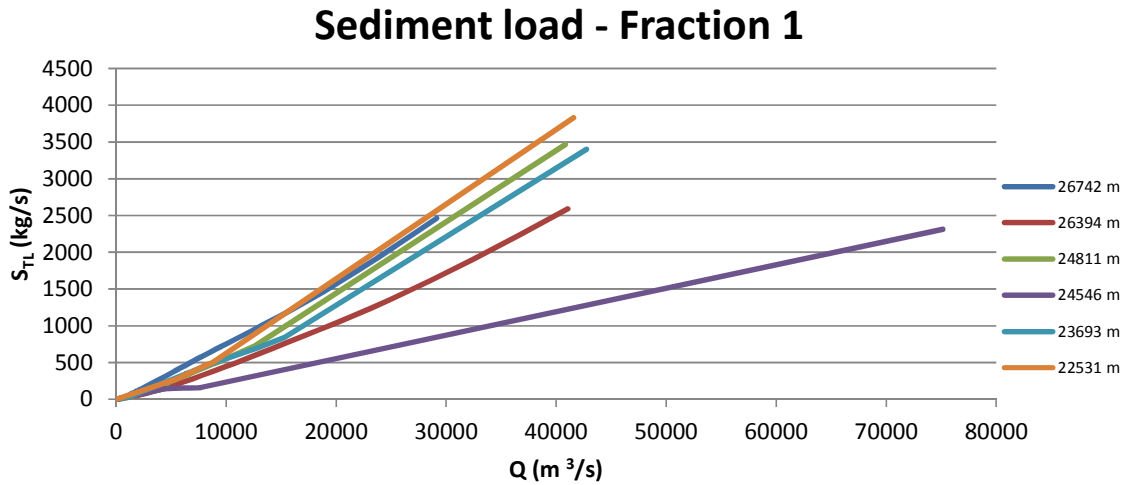


**Figure 5-23: Total predicted sediment load of Fraction 1 at various upstream cross-sections for variable river discharge (water level).**
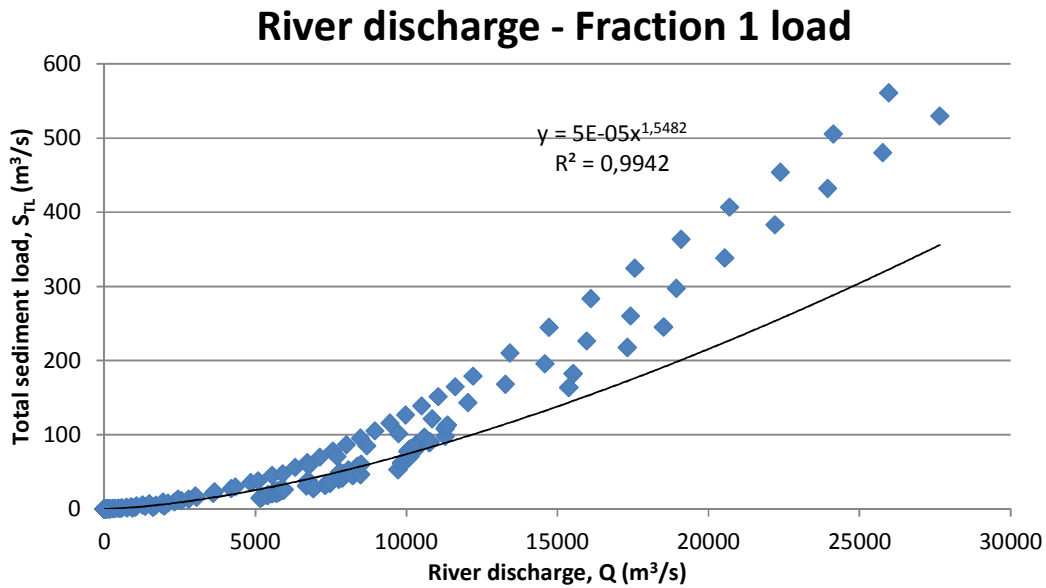


**Figure 5-24:Relationship between sediment load and river discharge for Fraction 1**

### 5.7.2     Cohesive sediment component - Fraction 2

The suspended sediment load is typically specified by sediment load - water discharge relationship derived from local field measurements. The form of the equation (5-7) is:

$$Q_s = aQ_w^b \tag{5-7}$$

Where    $Q_s$ = sediment load [kg/s]

$Q_w$ = water discharge [m³/s]

a,b = coefficients

A 20 year flow period was used with the load equations of each fraction. The average annual computed sediment load for both fractions should be equal to the predicted total average annual sediment load which was calculated as 3.34 Mt/a (Section 5.6). The coefficient a and b were adjusted until the needed total sediment load was achieved.

Through inspection the sediment load relationship for Fraction 2 was determined as (eq. 5-8):

$$Q_s = 0.021Q_w^{1.92} \tag{5-8}$$

Refer to Figure 5-25 for the relationship between sediment concentration of each fraction and river discharge. The sediment influx composition on average is 87 % Fraction 2 (silt) and 13 % Fraction 1(sand). The majority of the load attributed to Fraction 2 occurs during floods.
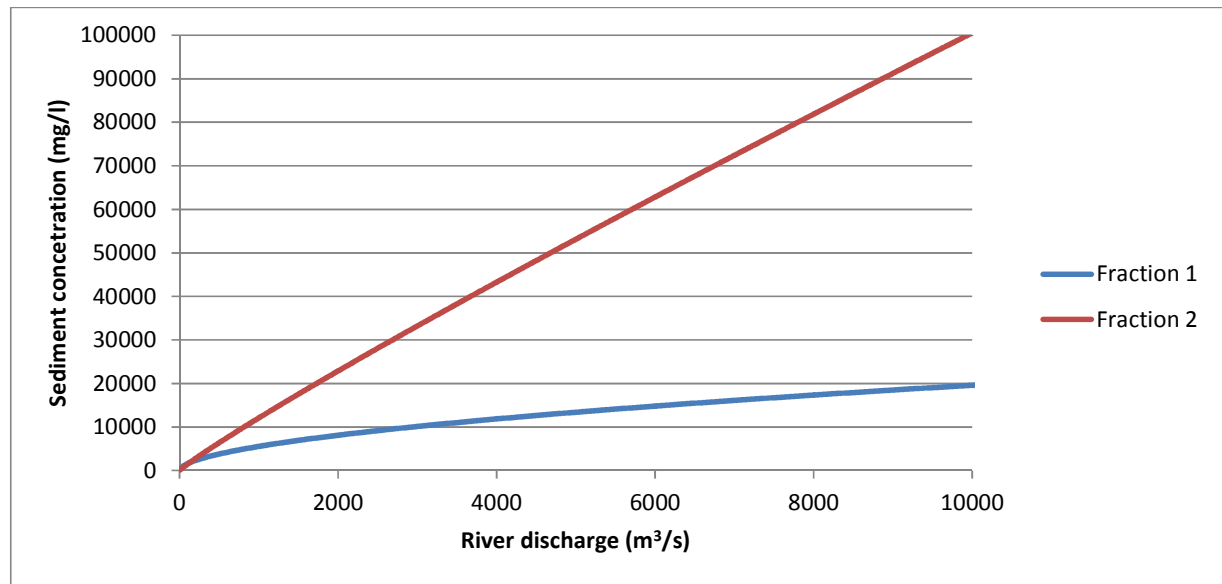


**Figure 5-25: Relationship between suspended sediment concentrations of model fractions and river discharge for scenario A.**

### 5.7.3     Sediment influx boundary

The sediment load relationship of each fraction was used to determine the concentration of sediment into the model space for a flow. If the sediment density is assumed 2650 kg/m³ the sediment discharge ($Q_S$) in m³/s can be related to river discharge (Q) with the following equation (eq. 5-9):

$$Q_S = \frac{CQ}{2.65 \times 10^6} \tag{5-9}$$

With                    C = sediment concentration [mg/l]

76

The sediment influx concentration was predicted for all hydrodynamic boundary conditions as develop in Section 5.4.

## 5.8   Model calibration

The MIKE 21C model was calibrated with data obtained during field work done in May 2012 (Section 4). Calibration is done in 2 stages, namely Hydrodynamic and Morphological.  Refer to Section 4 for the field work schedule and data obtained.

The "result accuracy" for this study is given by equation 5-10:

$$A_m = \frac{x_m}{x_f} * 100 \qquad\qquad (5\text{-}10)$$

Where:   $A_m$ = Model accuracy (%)

$x_m$ = Predicted model parameter

$x_f$ = Measured field parameter

### 5.8.1   Calibration limitations

Model calibration is challenging, especially when field data is limited. Due to the nature of the modelled environment one can expect field measurement and model prediction errors. The following should be kept in mind when assessing the model calibration:

- The ADCP was dragged across the river by a boat during cross-sectional velocity measurements and thus a perfect perpendicular cross-section measurement was hard to achieve.
- The ADCP has a "dead spot" close to the river bed.
- The ADCP is unable to be used in very low water depths (<0.4 m), thus the velocity in shallow river areas cannot be measured.
- Only 24 cross-sections were available on the 30 km estuary modelled, missing areas were filled by means of interpolation.
- Field measurements were done approximately 5 months prior to the survey; during this period 3 high river flow events took place (80, 94 and 126 $m^3$/s respectively) which may have altered the river bed. Refer to Appendix J.
- Sediment bed load samples are representative of the location of the bed load sampler and not the entire river cross-section.
- The river mouth was surveyed by means of one cross-section.
- The downstream ocean boundary uses predicted and not measured data.
- No reliable time series of water levels were available for calibration.
- The upstream sediment concentration boundary values were determined by empirical formulas and not measured.
- Grid resolution and layout influences model accuracy, refer to Section 5.2.

The data used for model calibration was collected during runs. The runs are discussed in Section 4. Refer to Table 5-9.

**Table 5-9: Field work run description**

| Run | Description |
|---|---|
| 2 | Flood-tide |
| 4 | Ebb-tide |
| 6 | Flood-tide |
| 8 | Ebb-tide |

### 5.8.2    Hydrodynamic model calibration parameters

The HD module calibration is achieved by modifying the following model parameters:

- Boundary lag(s) – The measurement position of the tidal level and river discharge do not coincide with the boundary locations on the model area, to compensate the boundaries can be lagged until favourable results are obtained. During the calibration period the river discharge was low and fairly uniform, the estuary hydrodynamics were thus tide dependant. Due to unfavourable conditions during the field work accurate tidal levels could not be obtained upstream of the river mouth, complicating tidal lag estimation. The tidal lag was determined by trial and error.
- River bed resistance – The river bed resistance influences the velocity and depth of the flow, suitable values were determined by trial and error. Flood plain bed resistance was estimated with values from literature.
- Eddy Viscosity – In river models the Eddy viscosity is not of much relevance, a default value was used for simulation (DHI, 2011).

Refer to Table 5-10 for final calibrated model parameters and Table 5-11 for the measured and predicted hydrodynamic parameters.

**Table 5-10: Hydrodynamic model calibration parameters**

| Parameter | Value | Unit |
|---|---|---|
| Boundary lag (tide level) | 1 | hour |
| Boundary lag (river) | unchanged | - |
| River bed resistance | 50 | Manning M |
| River floodplain resistance | 20 | Manning M |

The model generally under-predicted both depth and velocity. This could not be remedied by the uniform variation of the bed resistance or the alteration of the boundary lag(s). Higher bed resistance would cause greater depths but decrease the flow velocity and vice versa. The most likely cause of the dual underestimation is a too small tidal prism or inaccurate model bathymetry. The tidal prism is influenced by the mouth geometry, offshore (boundary) tidal level and the estuarine convergence; refer to Section 2.2.2. The model results and field measurements varied the most at the river mouth; this is likely a combination of low quality ADCP measurements due to the unfavourable conditions at the mouth and the mouth geometry estimations from satellite data and surveys which do not correspond in time with the measurements, or each other. The measured and predicted flow velocities are shown in Figure 5-26 and the measured and predicted flow depth in Figure 5-27.

**Table 5-11: Comparison of measured field data and model predicted results for the hydrodynamic case**

| Site | | Run id | Date & Time | Velocity (m/s) | | | Depth (m) | | |
|---|---|---|---|---|---|---|---|---|---|
| | | | | Field | Model | Accuracy (%) | Field | Model | Accuracy (%) |
| 405 | A | 2 | 2012-05-05 13:38 | 1.18 | 0.58 | 49 | 3.68 | 3.16 | 86 |
| | | 4 | 2012-05-06 07:28 | 0.87 | 1.02 | 117 | 3.14 | 1.99 | 63 |
| | | 6 | 2012-05-06 13:40 | 1.14 | 0.70 | 62 | 3.27 | 2.96 | 91 |
| | | 8 | 2012-05-07 07:27 | 1.31 | 1.12 | 86 | 3.03 | 2.30 | 76 |
| | | | | | | | | | |
| 3023 | B | 2 | 2012-05-05 14:21 | 0.43 | 0.37 | 86 | 1.81 | 2.28 | 126 |
| | | 4 | 2012-05-06 07:46 | 0.59 | 0.50 | 86 | 1.32 | 1.53 | 116 |
| | | 6 | 2012-05-06 13:55 | 0.64 | 0.39 | 62 | 1.64 | 1.96 | 119 |
| | | 8 | 2012-05-07 08:05 | 0.52 | 0.50 | 96 | 1.35 | 1.62 | 120 |
| | | | | | | | | | |
| 5645 | C | 2 | 2012-05-05 14:34 | 0.49 | 0.36 | 74 | 2.37 | 1.91 | 81 |
| | | 4 | 2012-05-06 08:01 | 0.49 | 0.38 | 76 | 1.18 | 1.43 | 121 |
| | | 6 | 2012-05-06 14:20 | 0.49 | 0.39 | 81 | 2.22 | 1.63 | 73 |
| | | 8 | 2012-05-07 08:20 | 0.64 | 0.39 | 61 | 1.8 | 1.50 | 83 |
| | | | | | | | | | |
| 8270 | D | 2 | 2012-05-05 14:55 | 0.34 | 0.34 | 101 | 3.1 | 2.18 | 70 |
| | | 4 | 2012-05-06 08:17 | 0.43 | 0.36 | 83 | 2.09 | 1.78 | 85 |
| | | 6 | 2012-05-06 14:44 | 0.48 | 0.37 | 78 | 2.82 | 1.90 | 67 |
| | | 8 | 2012-05-07 08:36 | 0.40 | 0.34 | 87 | 2.35 | 1.81 | 77 |
| | | | | | | | | | |
| 10888 | E | 4 | 2012-05-06 08:29 | 0.39 | 0.28 | 73 | 2.46 | 1.52 | 62 |
| | | 6 | 2012-05-06 15:10 | 0.33 | 0.29 | 89 | 3.12 | 1.64 | 53 |
| | | 8 | 2012-05-07 08:52 | 0.36 | 0.28 | 77 | 2.41 | 1.55 | 64 |
| | | | | | | | | | |
| 15200 | F | 4 | 2012-05-06 09:18 | 0.41 | 0.21 | 51 | 1.76 | 1.78 | 101 |
| | | 8 | 2012-05-07 09:14 | 0.32 | 0.20 | 63 | 4.07 | 1.86 | 46 |
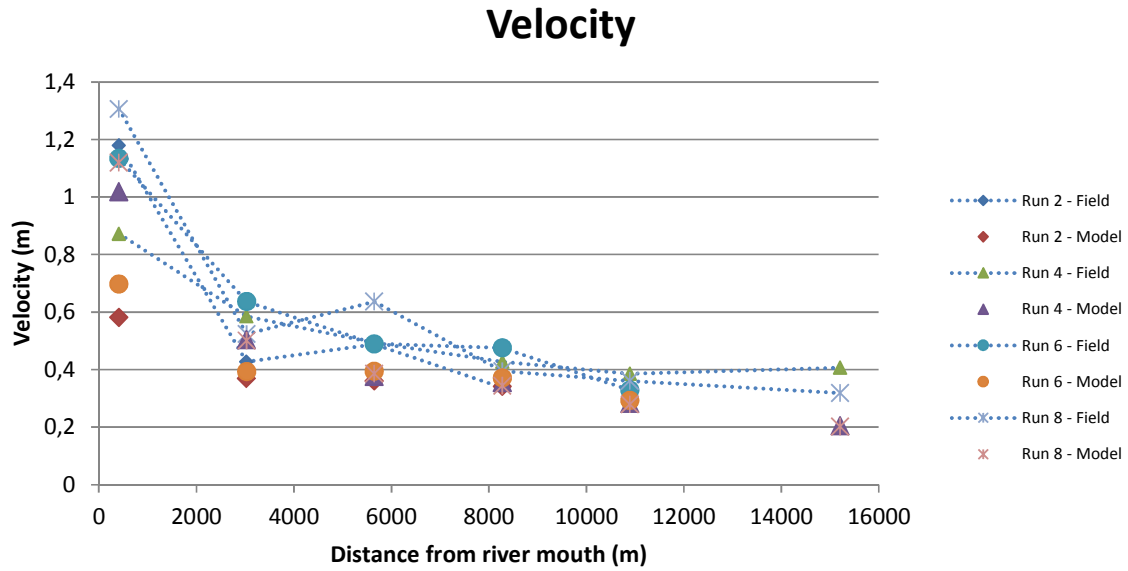
## Velocity



**Figure 5-26 Current velocity during field measurement period and model calibration run.**
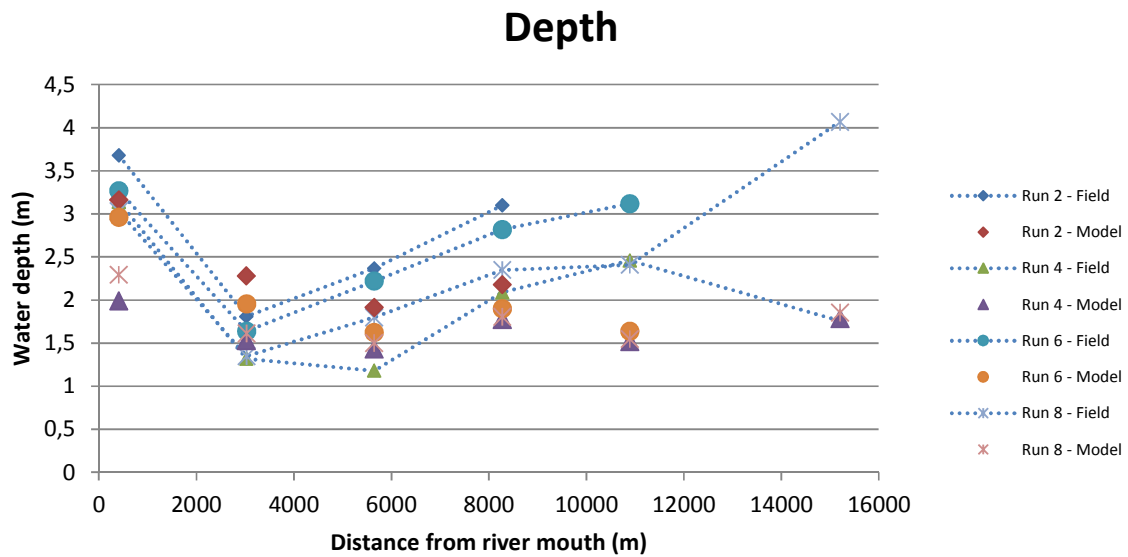
## Depth



**Figure 5-27: Water depth during field measurement period and model calibration run.**

### 5.8.3    Morphological model calibration

Morphological calibration was done with the calibrated hydrodynamic model, as discussed in the previous section. The Morphological model can be calibrated by a variety of parameters. Morphological calibration is challenging due to the dynamic environment modelled. There are various sediment transport equations available, refer to Section 3.4. The Engelund Hansen Total Load formula was used for this model study as the river transport capacity was calculated using this method. The Engelund Hansen formula is widely used for sediment transport calculations (USBR 2006). The morphological model was calibrated using the field data acquired and the accompanying hydrodynamic boundary conditions refer to the section Field Work and Appendix F.

80

Model calibration can be achieved by the adjusting following parameters (Section 3.1.5):

- Helical flow constant
- Transverse slope coefficient
- Transverse slope power
- Longitudinal slope coefficient
- Factor on fall velocity for suspended sediment
- Dispersion coefficients in x and y directions (relevant for the advection dispersion of suspended sediment)
- Bed load and Suspended load factors for each defined fraction

Due to the limited sediment samples only the bed load and suspended load factors were varied during the calibration process, other calibration parameters were set to defaults and kept constant. Final calibration parameters were determined by inspection and trial and error. The morphological calibration did not include any modifications to the defined fraction diameters or layer compositions and it was assumed that the upstream sediment flux is correct.

Refer to Table 5-12 and Figure 5-28 for measured and predicted results. The sediment transport magnitude varied the most at the river mouth, during Run 4 (Ebb tide) the model over-predicted the total sediment transport by about 13 times, from Table 5-12 it is clear that the field results indicate the lowest total load measurement at the site, this is most likely a measurement error as one would expect a greater total load transport during ebb tides. The sediment load was generally overestimated. The accuracies varied wildly over the model area.

**Table 5-12: Measured and predicted sediment transport results.**

| Site | | Run id | Date & Time | Field | Model | |
|---|---|---|---|---|---|---|
| | | | | Total Load (kg/s/m) | Total Load (kg/s/m) | Accuracy (%) |
| 405 | A | 2 | 2012-05-05 13:38 | 1.03 | 0.18 | 18 |
| | | 4 | 2012-05-06 07:28 | 0.28 | 3.72 | 1339 |
| | | 6 | 2012-05-06 13:55 | 0.44 | 0.15 | 34 |
| | | 8 | 2012-05-07 07:27 | 0.93 | 2.16 | 231 |
| | | | | | | |
| 3023 | B | 2 | 2012-05-05 14:21 | 0.09 | 0.11 | 120 |
| | | 4 | 2012-05-06 07:46 | 0.49 | 0.44 | 91 |
| | | 6 | 2012-05-06 14:20 | 0.65 | 0.42 | 64 |
| | | 8 | 2012-05-07 08:05 | 0.30 | 0.46 | 152 |
| | | | | | | |
| 5645 | C | 2 | 2012-05-05 14:34 | 0.66 | 0.43 | 66 |
| | | 4 | 2012-05-06 08:01 | 0.36 | 0.17 | 48 |
| | | 6 | 2012-05-06 14:44 | 0.57 | 0.19 | 33 |
| | | 8 | 2012-05-07 08:20 | 0.87 | 0.17 | 19 |
| | | | | | | |
| 8270 | D | 2 | 2012-05-05 14:55 | 1.09 | 0.10 | 9 |
| | | 4 | 2012-05-06 08:17 | 0.28 | 0.11 | 40 |
| | | 6 | 2012-05-06 15:10 | 0.28 | 0.32 | 115 |
| | | 8 | 2012-05-07 08:36 | 3.30 | 0.11 | 3 |
| | | | | | | |
| 10888 | E | 4 | 2012-05-06 08:29 | 0.25 | 0.16 | 64 |
| | | 8 | 2012-05-07 08:52 | 0.20 | 0.12 | 59 |
| | | | | | | |
| 15200 | F | 8 | 2012-05-07 09:14 | 0.26 | 0.11 | 42 |
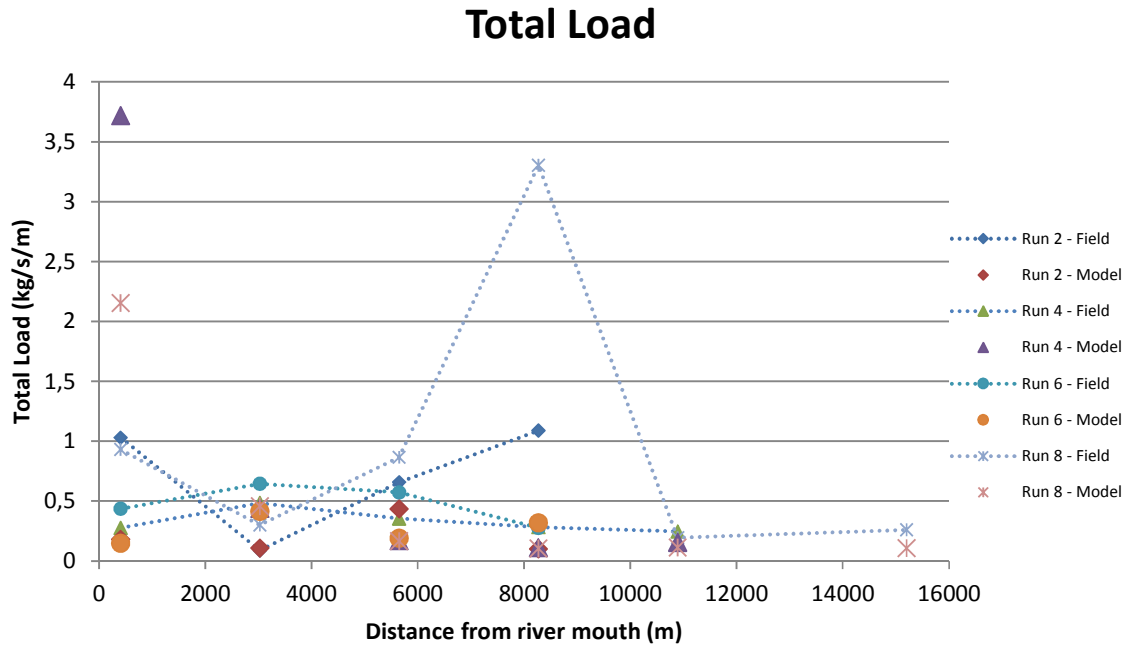
**Figure 5-28: Sediment total load during field measurement period and model calibration run.**

## 5.9 Final model inputs

The final model inputs used for Scenario A is shown in Table 5-13 and the final model inputs used for Scenario B shown in Table 5-14. The difference between the two model scenarios is the boundary conditions used, for Scenario A a 5 year simulation was performed with measured river flows, predicted sediment loads and predicted downstream water levels for this period. For Scenario B the boundary conditions used correspond to simulated flood hydrographs and their accompanying sediment loads and downstream water levels (predicted based on the date of the flood event). The parameters listed can be divided into basic parameters (Section 3.1.5.1), hydrodynamic parameters (Section 3.1.5.2) and morphological parameters (3.1.5.3).

The hydrodynamic module was calibrated by varying the model bed roughness and adjusting the hydrodynamic boundary lags, additional calibration parameters were kept default.

Due to the limited field sediment information the morphological module was calibrated only by adjustment of the bed load and suspended load factors, other calibration parameters were set to defaults and kept constant. Final calibration parameters were determined by inspection and trial and error. The morphological calibration did not include any modifications to the defined fraction diameters or layer compositions and it was assumed that the upstream sediment flux is correct.

### 5.9.1    Scenario A model inputs
**Table 5-13: Scenario A morphological model imputs**

| Basic Parameters | | | | |
|---|---|---|---|---|
| Modules | Hydrodynamic and Morphological | | | |
| Grid and Bathymetry | 1103x38 curvilinear grid | | | |
| | Increased resolution in main river channel | | | |
| | Model grid extents at 40 masl, 30 000m upstream of mouth and 2000m downstream (to sea) | | | |
| Simulation Period | 1 May 2007 - 1 June 2012 | | | |
| Source and Sink | none | | | |
| Flood and Dry | Flood | 0.3 | metres | |
| | Dry | 0.2 | metres | |
| *Hydrodynamic parameters* | | | | |
| Initial surface elevation | Sufficient to activate boundary grid cell | | | |
| Boundaries | Upstream | Discharge boundary, flow rates from DWS station Q9H018 | | |
| | Downstream | Water level boundary, predicted by WXTide32 software | | |
| Eddy viscosity | | 0.5 | Default | |
| Resistance | Main channel | 50 | Manning M | |
| | Flood plains | 20 | Manning M | |
| HD Integration | Fully hydrodynamic | | | |
| | HD time step | 5 | seconds | |
| *Morphological parameters* | | | | |
| Simulation period | 1 May 2007 - 1 June 2012 | | | |
| Sediment time step | 100 | seconds | | |
| Modules | Helical flow | | | |
| | Sediment transport | | | |
| | Morphological update | | | |
| | Advection Dispersion - QUICKEST scheme | | | |
| Helical flow constant | | 1 | Default | |
| Sediment transport theory | Engelund Hansen | | | |
| | Fractions | 2 | | |
| | Bed load factor | 1 | | |
| | Suspended load factor | 3 | | |
| Sediment fractions | | d50 (mm) | θ | |
| 1 | Non-cohesive | 0.3 | 0.056 | |
| 2 | Cohesive | 0.0252 | 0.054 | |
| Layer | Thickness | 0-15 metres main channel, 2 metres flood plains | | |
| | Fraction percentage | Location specific | | |
| AD coefficients | X-direction | 1 | $m^2/s$ | Default |
| | Y-direction | 1 | $m^2/s$ | Default |
| Boundaries | Upstream | Sediment concentration boundary | | |
| | Downstream | Fixed bed level boundary | | |

### 5.9.2    Scenario B model inputs
**Table 5-14: Scenario B morphological model inputs**

| Basic Paramters | | | | |
|---|---|---|---|---|
| **Modules** | Hydrodynamic and Morphological | | | |
| **Grid and Bathymetry** | 1103x38 curvilinear grid | | | |
| | Increased resolution in main river channel | | | |
| | Model grid extents at 40 masl, 30 000m upstream of mouth and 2000m downstream (to sea) | | | |
| **Simulation Period** | Flood hydrograph dependant | | | |
| **Source and Sink** | none | | | |
| **Flood and Dry** | Flood | 0.03 | meters | |
| | Dry | 0.02 | meters | |
| ***Hydrodynamic parameters*** | | | | |
| **Initial surface elevation** | Sufficient to activate boundary grid cell | | | |
| **Boundaries** | Upstream | Discharge boundary, flow hydrographs derived from historical flow of Q9H010 | | |
| | Downstream | Water level boundary, predicted by WXTide32 software | | |
| **Eddy viscosity** | | 0.5 | Default | |
| **Resistance** | Main channel | 50 | Manning M | |
| | Flood plains | 20 | Manning M | |
| **HD Integration** | Fully hydrodynamic | | | |
| | HD time step | 0.1 - 5 | seconds | |
| ***Morphological parameters*** | | | | |
| **Simulation period** | 1 May 2007 - 1 June 2012 | | | |
| **Sediment time step** | 10xHD time step | seconds | | |
| **Modules** | Helical flow | | | |
| | Sediment transport | | | |
| | Morphological update | | | |
| | Advection Dispersion - QUICKEST scheme | | | |
| **Helical flow** | | 1 | Default | |
| **Sediment transport theory** | Engelund Hansen | | | |
| | Fractions | 2 | | |
| | Bed load factor | 1 | | |
| | Suspended load factor | 3 | | |
| **Sediment fractions** | | d50 (mm) | θ | |
| 1 | Non-cohesive | 0.3 | 0.056 | |
| 2 | Cohesive | 0.0252 | 0.054 | |
| **Layer** | Thickness | 10 metres main channel, 5 metres flood plains | | |
| | Fraction | Location specific | | |
| **AD coefficeints** | X-direction | 1 | m²/s | Default |
| | Y-direction | 1 | m²/s | Default |
| **Boundaries** | Upstream | Sediment concentration boundary | | |
| | Downstream | Fixed bed level boundary | | |

# 6   RESULTS – SCENARIO A

## 6.1   Modelling comments

Due to the significant computation time of large numerical models the simulation is stopped periodically and restarted with a program generated hotstart file. The hotstart file contains all the computational hydrodynamic parameters and the model grid elevations (bathymetry) of the last time step. The hotstart file does however not contain information regarding to the model layer thickness or component percentage, subsequently when the model restarts the model bed grading and layer thickness is reset to the initial conditions as defined in Section 5.9.

This is not the case for the flood hydrograph simulations as they were uninterrupted. The loss of layer composition and thickness is not detrimental to results as the alluvial resistance module was not used.

Due to the geometry of the model space map results are difficult to present, data extracted from map results will be used predominantly in this section. The site designations used correspond to the site defined in Section 4.2; additional upstream sites are defined in the following sections. For the purpose of the result discussion the model areas defined by "lower reach" refers to a distance up to 10km from the river mouth (chainage), "middle reach" to the area between chainages 10km and 20km and "upper reach" the rest of the modelled area.

The respective dates of the mouth closure events are: 30 November 2009 and 10 September 2010. River discharge statistics are shown in Figure 6-1, Table 6-1 and Appendix J.
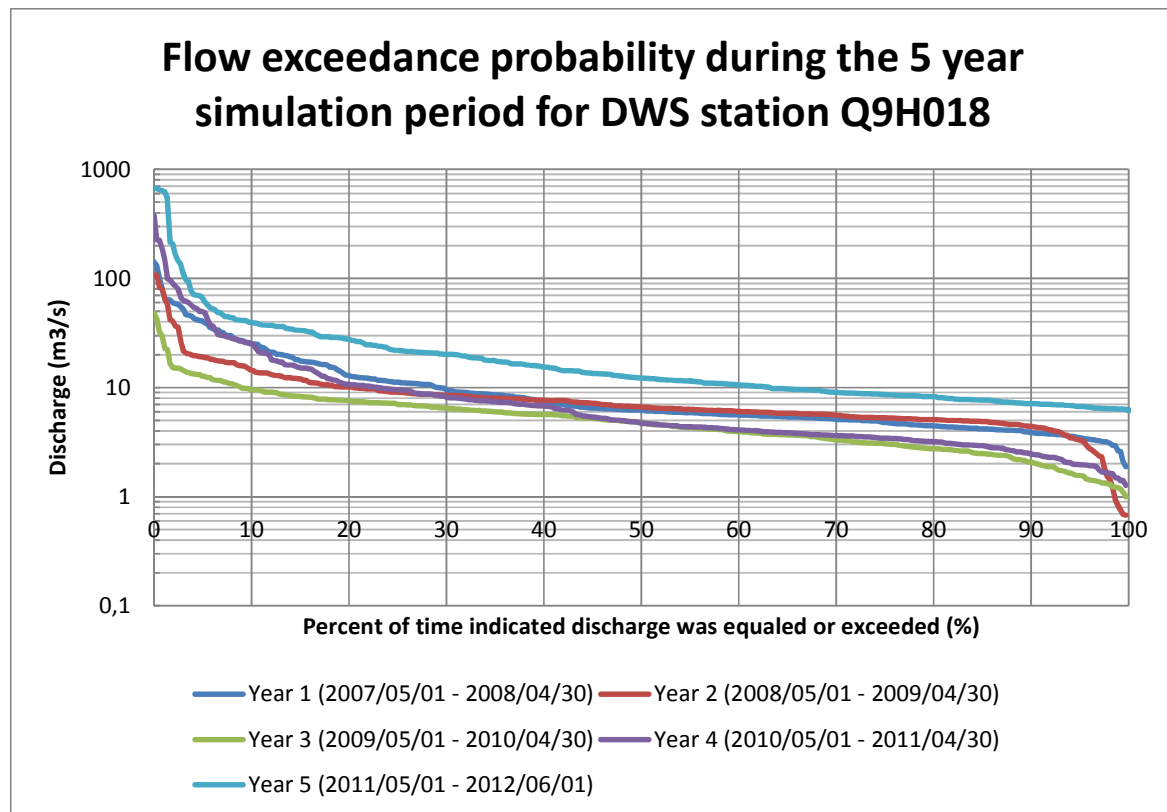


**Figure 6-1: Flow exceedance probability during the 5 year simulation period for DWS station Q9H018**

85

**Table 6-1: River discharge statistics during Scenario A**

| Period | River discharge (m³/s) | | |
|--------|-----|---------|-----|
|        | Min | Average | Max |
| Year 1 | 2 | 12 | 142 |
| Year 2 | 1 | 9 | 108 |
| Year 3 | 1 | 6 | 48 |
| Year 4 | 1 | 13 | 377 |
| Year 5 | 3 | 23 | 676 |

## 6.2    Bed level changes

### 6.2.1    River long section

The minimum bed level at each surveyed cross-section location (defined by grid cells in model space) was extracted from the model results after yearly periods of simulation. Refer to Figure 6-2.

#### 6.2.1.1    Initial – 12 months

The initial bed level (red line) differs significantly from the bed levels after 12 months (green line). The main observation is the scouring of the upper reach of the river, the deposition of sediments in the middle reach and the relatively constant bed level in the lower reach. The lower reach remains fairly flat as the tidal influence is dominant and the bed slope fairly flat. The bed level perch at Site B (chainage 3023) is eroded and the eroded sediment deposited downstream, this is also a model bed smoothing effect as the approximate slope between Site A (chainage 405) and Site B remains constant up to the end of the simulation. The scour is due to bed smoothing and river channel definition in the flat upper reach which is a remnant of the bathymetric interpolation process.

#### 6.2.1.2    12 – 24 months

The bed elevations after 24 months (purple line) remain fairly stable; there is sediment deposition in the middle reach and some erosion at the upper limit of the model. The sediment eroded from the upper reach follows the trend observed in the first year of simulation.

#### 6.2.1.3    24 – 36 months

The large bed level discrepancy at Site A for the 36 month (blue line) bed level profile is due to the manual mouth closure of the tidal inlet in November 2009 of the simulation period.  Due to the closure of the mouth the middle reach of the estuary acts as a sediment sink with the bed elevations peaking during this period\

#### 6.2.1.4    36 – 48 months

From the series 48 months (orange line) it is clear the tidal inlet has breached completely and resumed a minimum bed level similar to pre-closure. The lower reach of the estuary remains fairly constant except for a perch developed at Site D (chainage 8273) which is a likely sedimentary deposit from the flood events just preceding the data extraction time (peak river discharge for January 2011, February 2011 and March 2011 are 97 m³/s, 377 m³/s and 187 m³/s respectively, refer to Figure 5-12 or Appendix J). The sediment basin created in the middle reach after 36 months is eroded away.

#### 6.2.1.5    48- 60 months

The bed elevations after 60 months (light purple) exhibit the largest changes during the simulation barring the initial remodelling of the model area. The whole model has scoured and the modelled area is the deepest of any of the modelled durations. This large erosion volume is due to the large flood events of year five (Table 6-1).
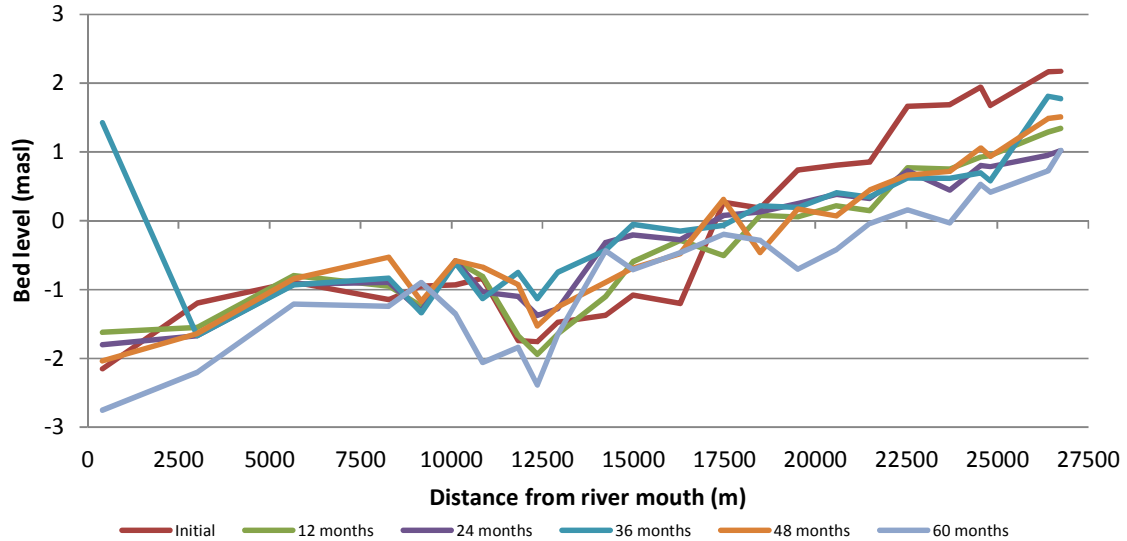
**Figure 6-2: Great Fish River minimum bed elevations during Scenario A.**

### 6.2.2 River cross-sections

The river cross section bed elevations were extracted at the sites defined during field work after defined periods of simulation. Section A denotes the cross section at Site A etc. The bed levels are extracted from grid elevation files and are plotted in Figure 6-3. Sites A to E lie in the estuarine area as defined by Vorwerk (2006), whereas Site F lies in the river reach.

Section A is a cross-section over the tidal inlet, the inlet is initially very slotted (dark blue line) and is abraded by tidal action to a more rounded shape after 12 months (red line). The closed tidal inlet at 36 months (purple line) is completely washed away after 48 months (light blue line) and the tidal inlet resumes a familiar shape. The inlet area remains relatively constant but seems to decrease during low flow conditions and increase during floods. The flood events re-create a notched profile as is evident by the cross section of 60 months (orange line). The upstream river sections B – F all retain their shape except for the period 60 months where channel migration (evident in Section C), channel scour (evident in Section E) and sediment deposition on the river bank (Section F) were noticed. The sediment deposited in the middle reach of the estuary during mouth closure was transferred to site D after 48 months (light blue line), creating a perch.
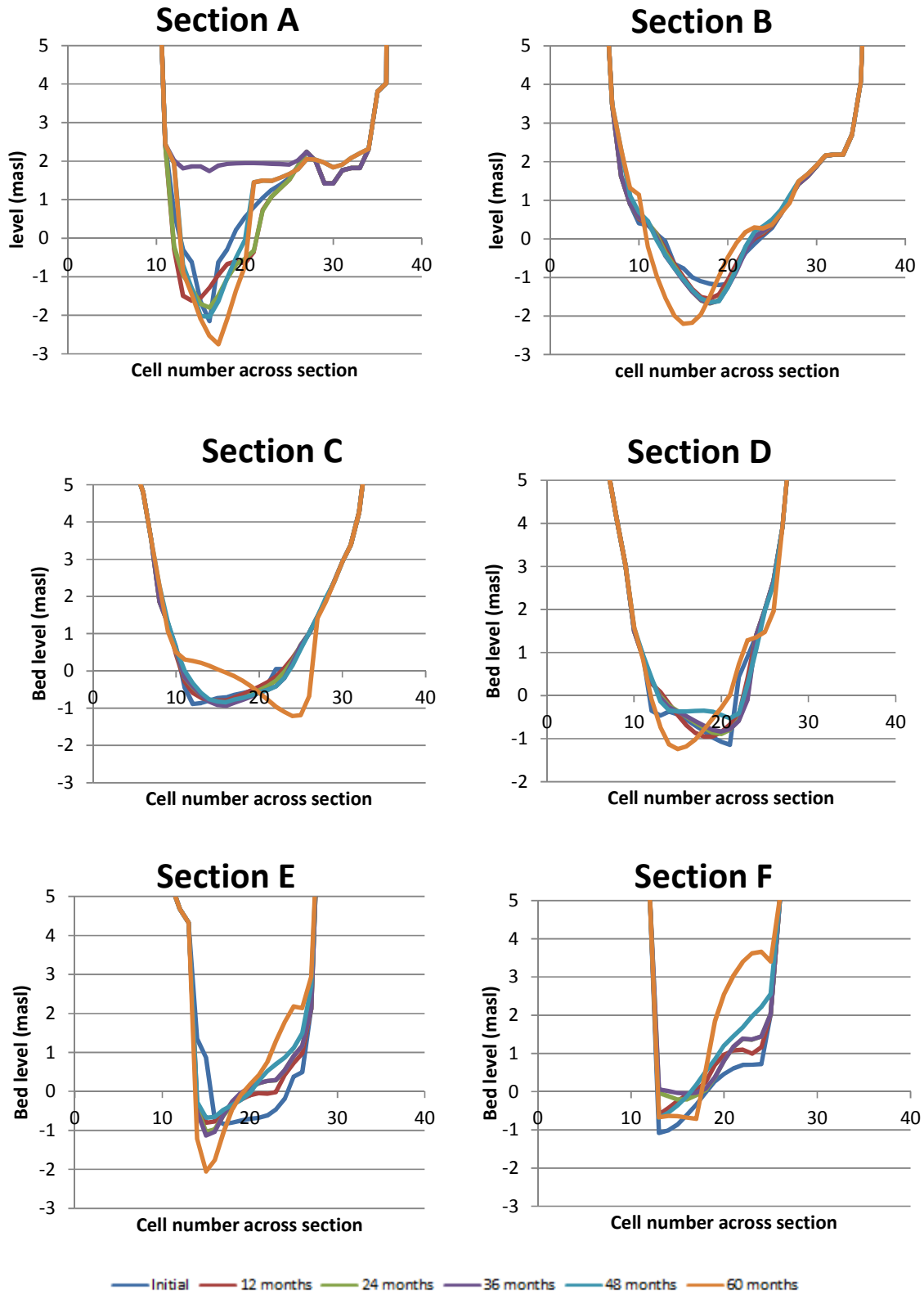
**Figure 6-3: Cross sections at selected sites during Scenario A**

## 6.3   Tidal inlet discharge

The discharge through the tidal inlet gives an indication of the state of the tidal inlet.  The tidal prism is a function of the tidal water level and the geometry of the estuary, specifically the tidal inlet. The impact of the hydrodynamic and sedimentary boundary conditions should have a direct effect on the discharge through the tidal inlet. The tidal inlet discharge will be briefly discussed. Refer to Figure 6-4. Please note that the tidal prism is evaluated by inspection of the tidal inlet discharge, and not the actual tidal prism which is a volume.

The tidal prism is negated by flood events. Mouth closure completely restricts the tidal prism for about a month (mouth is completely closed from 30 November 2009 to 29 December 2009). The small breach of the river mouth reinstates a subdued tidal environment upstream of the mouth. The subdued tidal environment stays relatively constant up to the second manual mouth closure (10 September 2010).
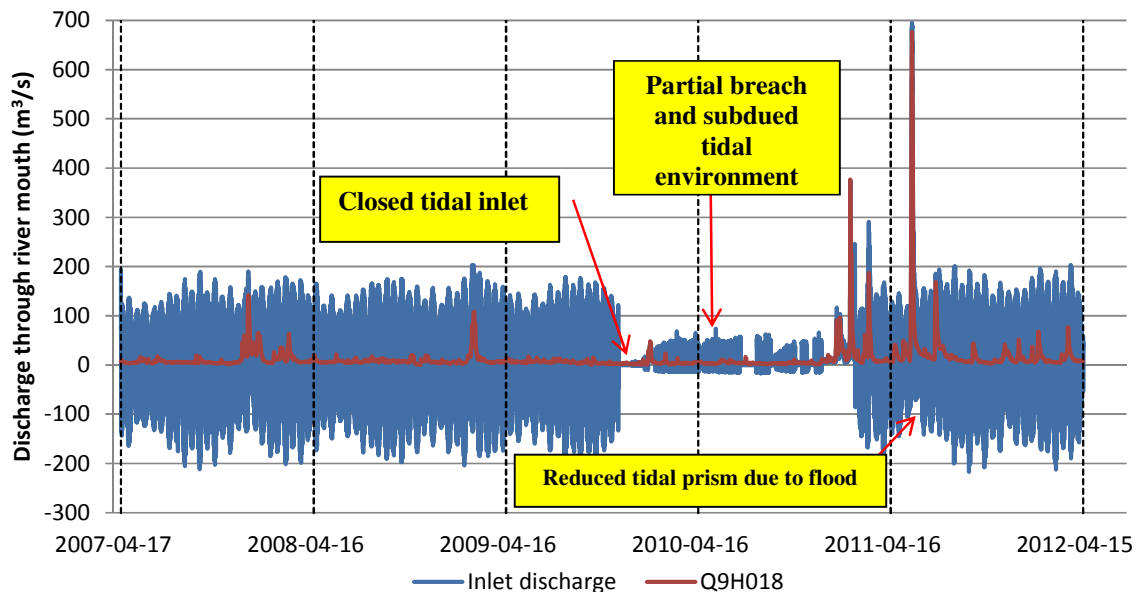


**Figure 6-4: Discharge through river mouth during Scenario A. Positive discharge denotes flow out of the estuary and vice versa. Dotted lines denoted yearly intervals**

The minimum, average and maximum inlet discharge for the simulation period can be seen in Table 6-2. The minimum inlet discharge is an indication of the yearly state of the tidal inlet. There is a steady reduction in the tidal prism for the first 4 years of the simulation. The reduction corresponds to the reduction in cross sectional area at the tidal inlet for this period as shown in Figure 6-3. This trend is reversed in the fifth year; the reverse is due to the mouth flushing due to the large floods during this period (shown in Figure 6-4). The average discharge through the tidal inlet is approximately equal to the river discharge for this period and the maximum discharge is the sum of the maximum river discharge and the tidal flow. The relative parity between the average river and inlet discharge implies that the estuary does not dam the river flow. From Table 6-1 and Table 6-2 it is clear that the maximum river discharge into the sea can be subdued by the backwater profile of the tidal water level as is the case for "Year 4" of the simulation.

89

**Table 6-2: Discharge statistics during yearly periods through river mouth during Scenario A. Positive discharge denotes flow out of the estuary and vice versa.**

| Period | Inlet discharge (m³/s) | | |
|--------|------|---------|-----|
| | Min | Average | Max |
| Year 1 | -212 | 11 | 190 |
| Year 2 | -204 | 9 | 203 |
| Year 3 | -196 | 6 | 179 |
| Year 4 | -181 | 13 | 374 |
| Year 5 | -217 | 23 | 695 |

The relationship between the tidal water level and the inlet discharge is shown Figure 6-5. From Figure 6-5 it is evident that there is a linear relationship between tidal water level and the inlet discharge, baring the flooding events.
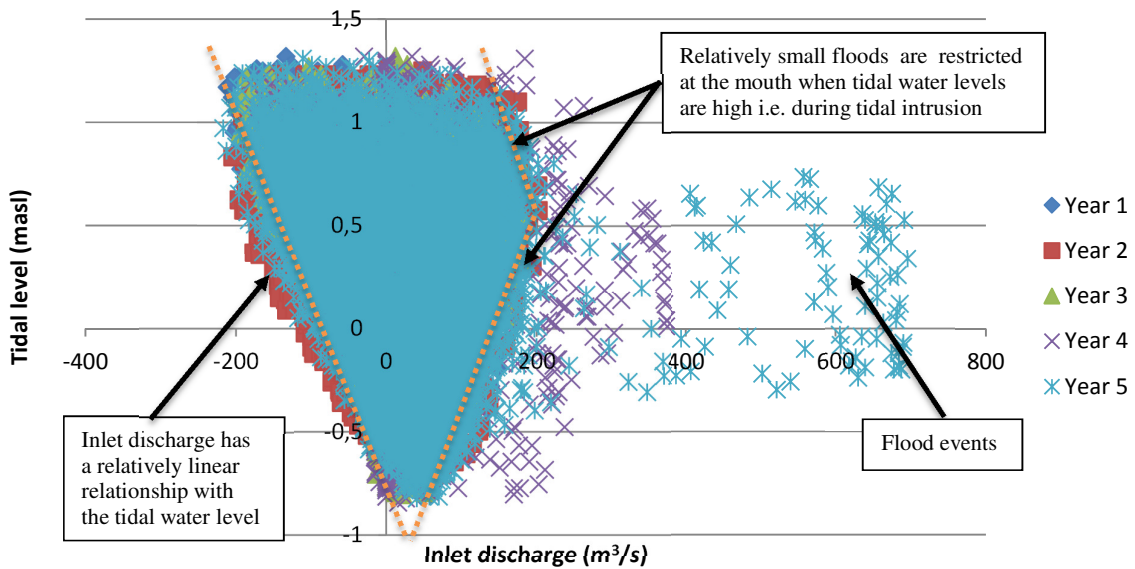


**Figure 6-5: Mouth discharge and tidal level relationship during Scenario A. Positive discharge denotes flow out of the estuary and vice versa.**

## 6.4    Tidal inlet evolution

The evolution of the tidal inlet is depicted Figure 6-6.

### 6.4.1.1    *0 – 12 months*

The mouth geometry determined by interpolation is unrecognisable after a year of simulation, the width at the river mouth increases and sediment is deposited in the deep patches of the initial bathymetry and on the right bank directly downstream of the mouth creating a mouth spit. An ebb-tidal delta develops directly downstream of the mouth. These ebb-tidal deltas are typical features when wave activity is relatively subdued (Schumann 2003), which is of course the case as no waves were simulated. The river channel just upstream of the river mouth is more linear after the first 12 month period; this is probably caused by the tidal prism, as the river discharge is small compared to the tidal prism during normal river discharges.

### 6.4.1.2    *12 – 24 months*

No large changes to the river mouth can be observed. The ebb-tidal delta is slightly larger which indicates the deposition of riverine sediments as there is no sediment influx from the downstream boundary.

### 6.4.1.3    *24 – 30 months (mouth closure)*

The mouth was manually edited and the ebb-tidal delta removed, refer to Section 5.3.1.

### 6.4.1.4    *30 months – 36 months*

As can be seen in Section 6.3, the mouth has not breached completely. The water level inside the estuary remains fairly constant as the river mouth acts as a dam wall. The flow creates a small pit at the foot of the mouth. The water capacity of the estuary is large and results in small water level changes inside the estuary due to attenuation effects. The surface elevation of the river mouth is at the upper limit of the tidal reach and therefore there is no tidal intrusion. The mouth can be considered open as there is an influx of water from the downstream side (Figure 6-4).

### 6.4.1.5    *36 – 44 months (mouth breach)*

The estuary was exposed to very subdued tidal effects for a period of approximately 14 months, this period coincides with the relatively dry year of 2010 (average river flow = 4.82 $m^3$/s).  A flood event with a peak discharge of 377 $m^3$/s took place in February 2011; the flood resulted in the opening of the river mouth. The cross section post breach can be seen in Figure 6-3.

### 6.4.1.6    *44 - 48 months*

The mouth has reclaimed its familiar linear shape similar to what was observed at 12 months, the channel is however deeper with steeper side slopes at the mouth. This is likely remnant sediment of the artificial mouth closure.

### 6.4.1.7    *48 – 60 months*

The main river channel has been deepened significantly; the river channel is at its deepest at the river mouth due to the flow constriction. This scour was caused by the numerous flood events during this period, refer to Figure 6-4.

**Initial bed level – 01/05/2007**

**12 months – 01/05/2008**

**24 months – 01/05/2009**

**mouth closure – 30 November 2009**

**36 months – 01/05/2010**

**Mouth breach  22 Feb 2011**

**48 months – 01/05/2011**

**60 months – 01/05/2012**

Bed level [m]

| | | |
|---|---|---|
| Above | 8.7 | |
| 7.3 - | 8.7 | |
| 6.0 - | 7.3 | |
| 4.7 - | 6.0 | |
| 3.3 - | 4.7 | |
| 2.0 - | 3.3 | |
| 0.7 - | 2.0 | |
| -0.7 - | 0.7 | |
| -2.0 - | -0.7 | |
| -3.3 - | -2.0 | |
| -4.7 - | -3.3 | |
| -6.0 - | -4.7 | |
| -7.3 - | -6.0 | |
| -8.7 - | -7.3 | |
| -10.0 - | -8.7 | |
| Below | -10.0 | |
| Undefined Value | | |
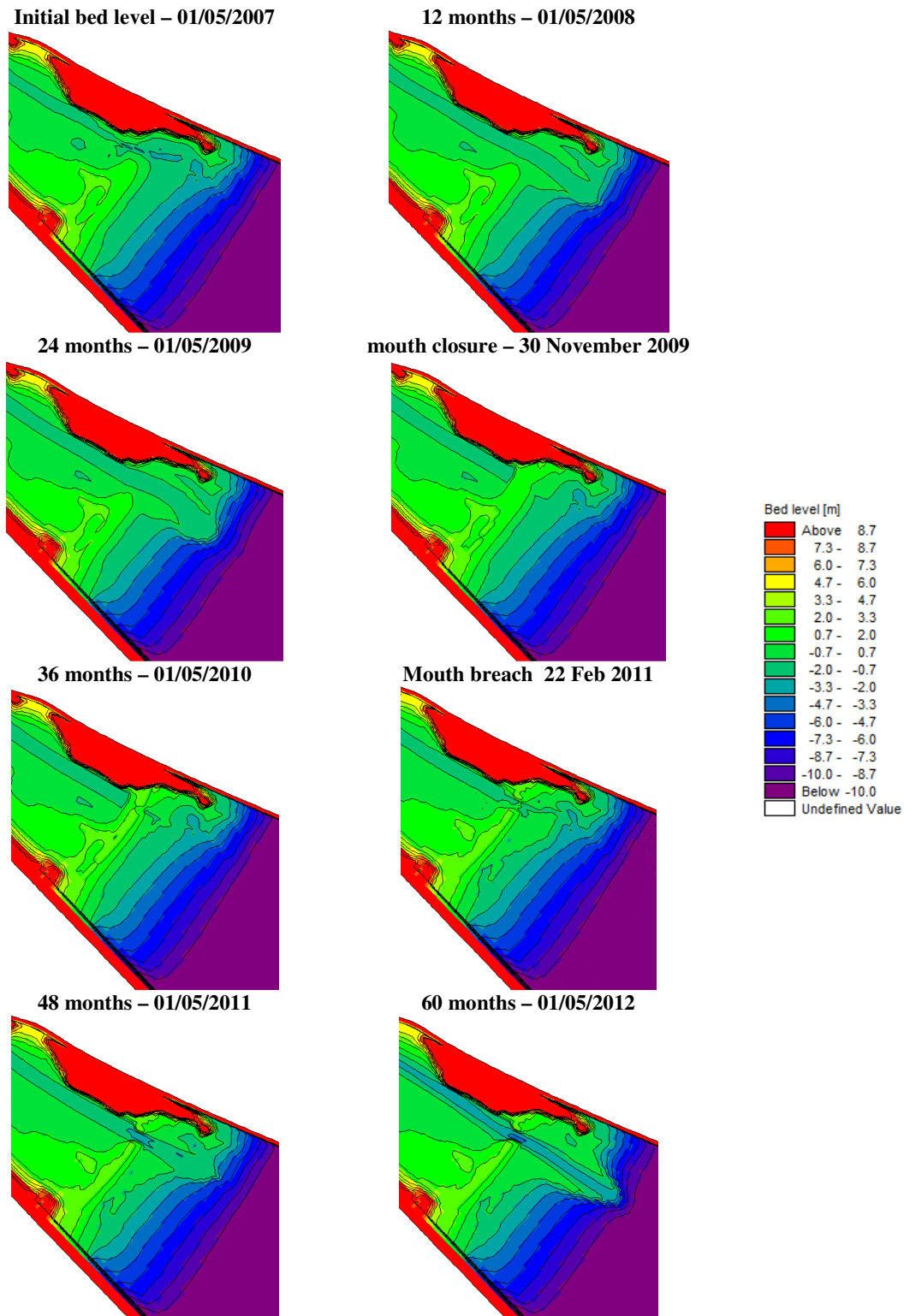
**Figure 6-6: The geometric state of the estuary tidal inlet during Scenario A extracted in periods of one year and during noteworthy inlet states.**

## 6.5   Estuary tide

Water levels were extracted at specified cross-sections to evaluate the tidal characteristics of the estuary over time. It should be noted that the surface elevations were extracted at a single grid point on the cross-section in the model space. The tidal levels were analysed in intervals of 12 months. The tidal levels are influenced by the downstream tidal water level boundary, the upstream river discharge and the shape of the estuary and specifically the tidal inlet. The cross-section at which data was extracted corresponds with the cross-sections investigated during field work, and two extra upstream cross-section denoted by G and H. The upstream river discharge (DWS station Q9H018) is indicated by the dashed light purple line and the tidal water level is indicated by the black dotted line. The value after the cross-section identifier is the distance upstream (chainage) of the reference location which is situated in the wave breaker zone.

### 6.5.1.1   Initial bed level

Refer to Figure 6-8 for the water levels at defined river sites. The most striking observation is the depression of the tidal water level at the river mouth, which is denoted by A – 405 m. The phenomenon is represented graphically in Figure 6-7. The variation in surface elevation is most likely caused by the constricted river mouth and the subsequent turbulence (due to increased flow velocity) caused by the tidal flow contraction (Özsoy & Ünlüata 1982). The estuary tidal reach is evident up to site F. Sites G and H are in the upstream river reach of the estuary but they experience a slight water level rise a few hours after the peak tidal level. No tidal amplification is apparent but damming of tidal water can be observed in all estuarine sites upstream of the river mouth. The damming is likely caused by the constricted river mouth and local river pools. Tidal lag is apparent between all estuarine sites. The upstream river discharge has little effect on the investigated sites and their water levels.
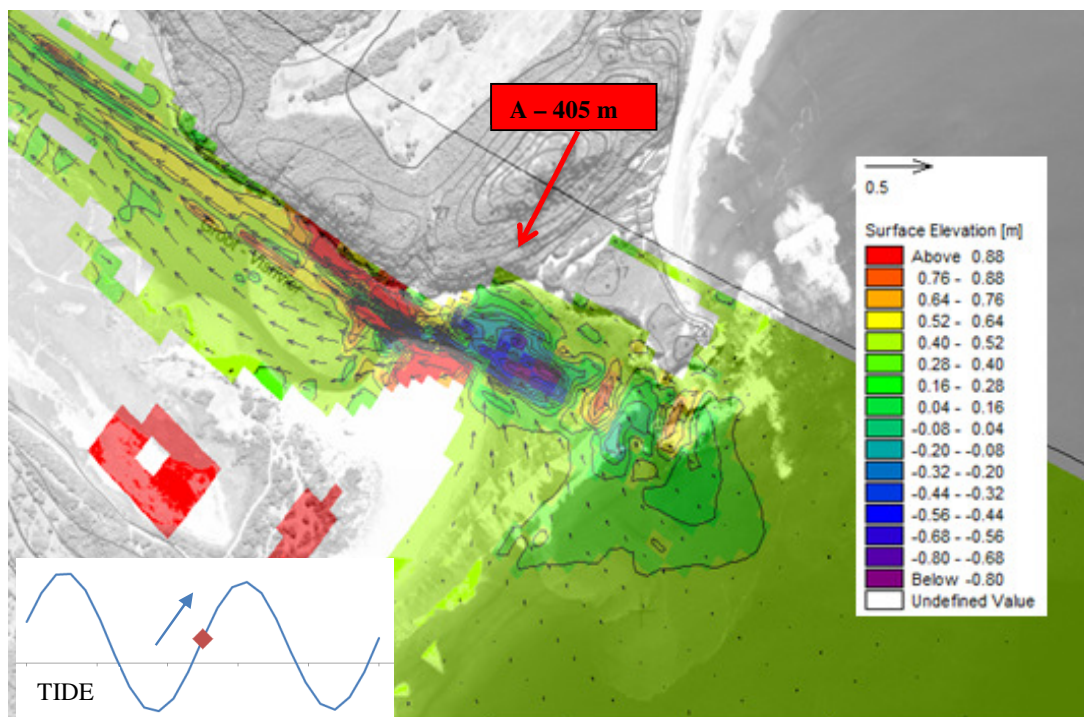


**Figure 6-7: Surface water levels at the river mouth at the start of the long term morphological simulation. Large variations in surface water level can be observed at the river mouth. The red cells are cells that were flooded during the initiation of the simulation.**

### 6.5.1.2      12 months

Refer to Figure 6-9. After 12 months of simulation the patterns observed at the start of the simulation are still present. The tidal depression at the site A is still present but less pronounced (≈0.25 m), this is likely due to the decreased tidal amplitude at this time and the enlarged tidal inlet cross-section. Tidal amplification and damming of tidal water is still detected in all estuarine sites upstream of the river mouth. Tidal lag is apparent between all estuarine sites. Upstream river sites G and H are still outside the tidal reach and are clearly affected by the incease in river discharge from 2 May 2008. The tidal amplification is not caused by the upstream river discharge as the relative amplification stays constant during the period shown on Figure 6-9. The gradual increase in water levels inside the model are attributed to the interpolation of the upstream boundary condition (river flow) which is not indicated on the figure.

### 6.5.1.3      24 months

Refer to Figure 6-10. No tidal amplification is apparent; this is likely due to the relatively small tidal amplitude and subsequently small tidal prism which is less constricted by the river mouth which has not changed noticeably over the 12 month period in question. Site F is at the edge of the tidal reach. The tidal prism is still large compared to the river discharge as the increase in river discharge does not noticeably affect the water level at all the estuarine sites.

### 6.5.1.4      36 months

Refer to Figure 6-11. The estuary mouth was closed during this period. All sites upstream of the river mouth have river characteristics and are only a function of the upstream river discharge and the local conditions such as bed elevation and roughness. The closed mouth does experience some overtopping; this is reflected by the water level at site A and the mouth discharge, refer to Figure 6-4. The decreased tidal range at site A is due to the closed mouth and the slight overtopping.

### 6.5.1.5      48 months

Refer to Figure 6-12. The tidal lag is the least significant of any of the analysed tidal relationships. The diminished tidal lag is likely due to the breaching of the closed tidal inlet and the related inlet flushing due to the dammed up water behind the tidal inlet and the large flood just prior to the date of data extraction, refer to Figure 6-5. Tidal influence is noticeable up to Site F.

### 6.5.1.6      60 months

Refer to Figure 6-13. The flooding prior to the 60 month period created significant bed scour in the model and reduced the bed elevation in the whole model area. The reduced bed levels increases the tidal reach up to Site G, which is more than 20 km upstream of the river mouth. The tidal reach does not guarantee salt intrusion up to Site G as the salt intrusion is linked to the tidal excursion which is a function of tide period.
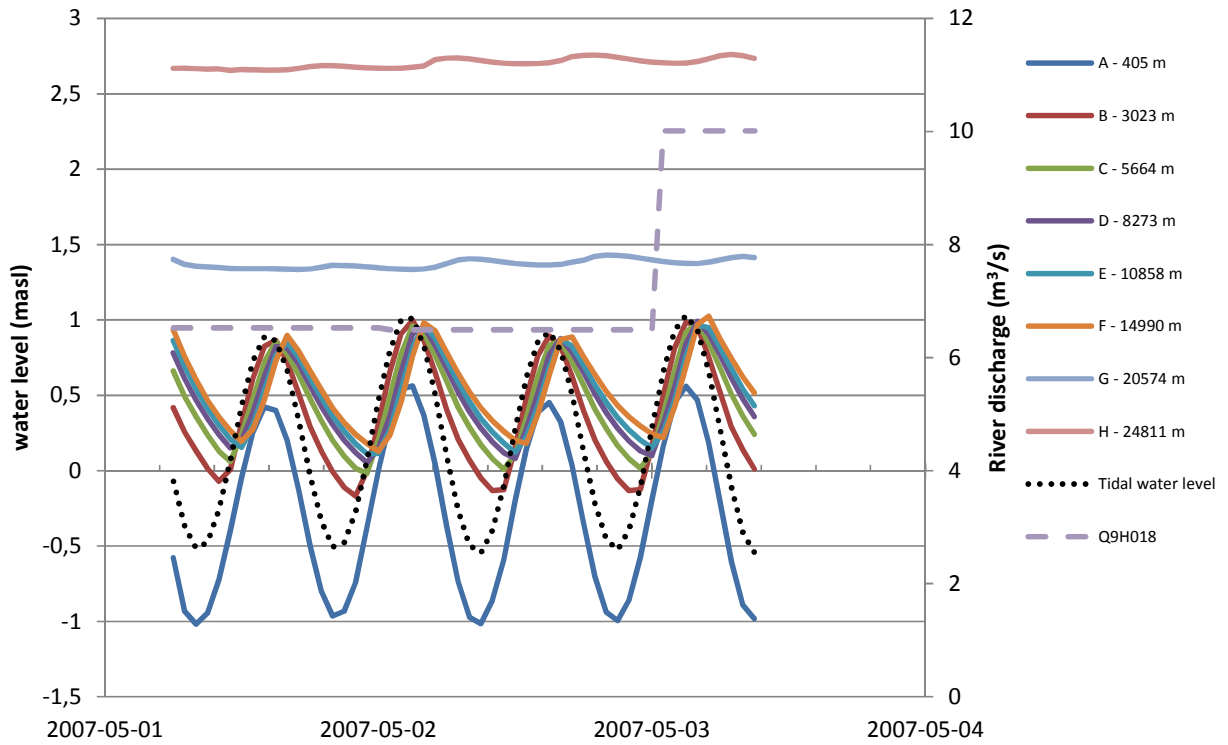
**Figure 6-8: River discharge and water levels at defined river cross-sections at the start of the simulation period**
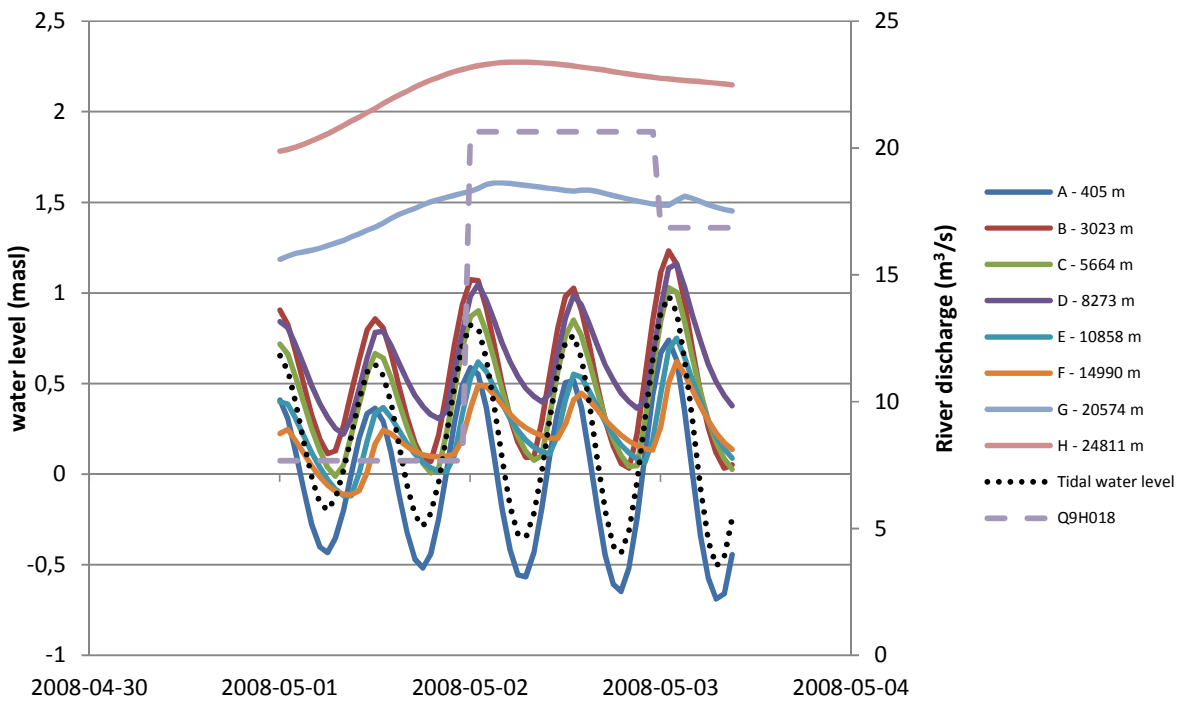


**Figure 6-9: Water levels at defined locations and river discharge for 1 May 2008 – 3 May 2008**

95
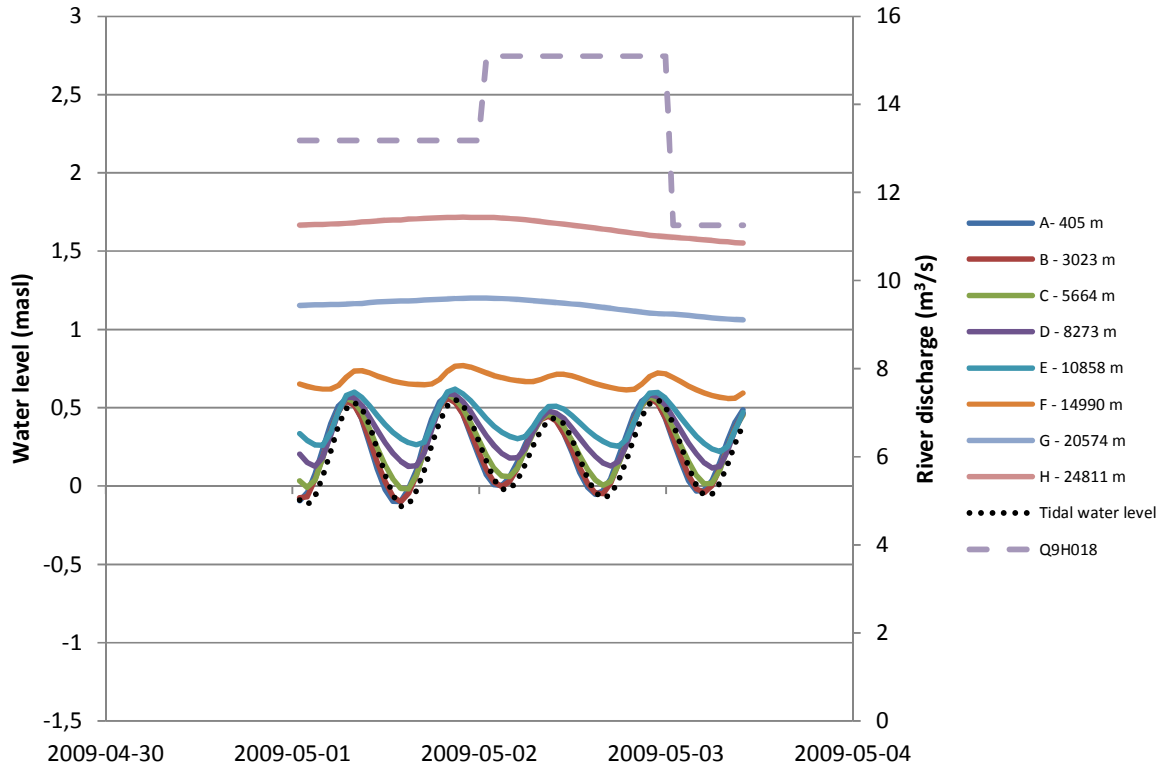
**Figure 6-10: Water levels at defined locations and river discharge for 1 May 2009 – 3 May 2009.**
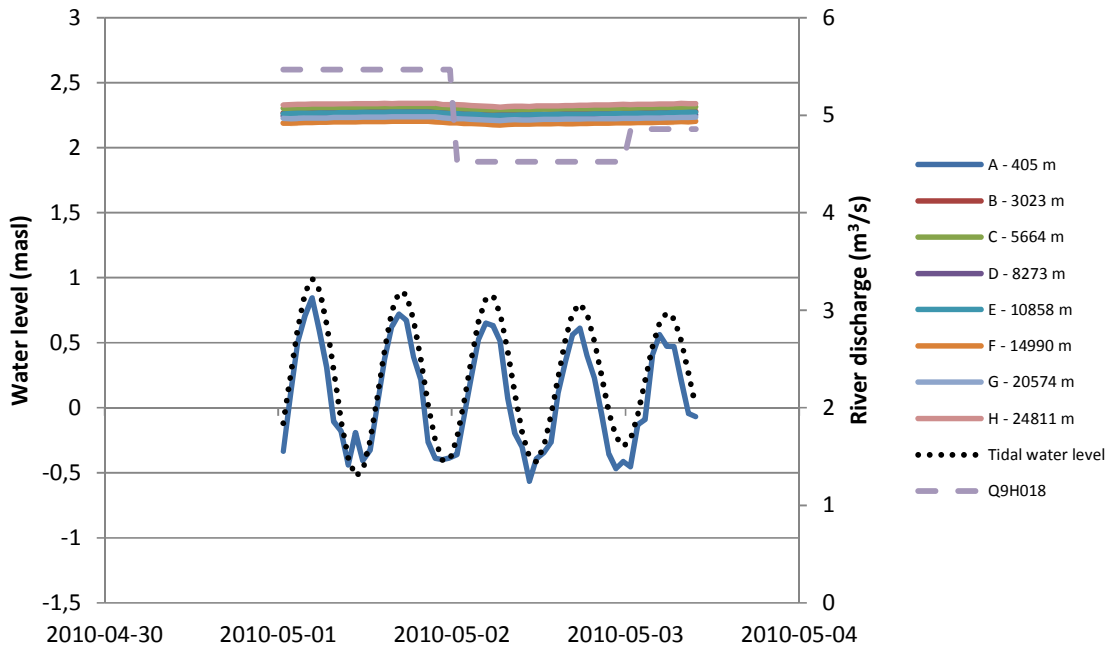


**Figure 6-11: Water levels at defined locations and river discharge for 1 May 2010 – 3 May 2010. The estuary is temporarily closed.**

96
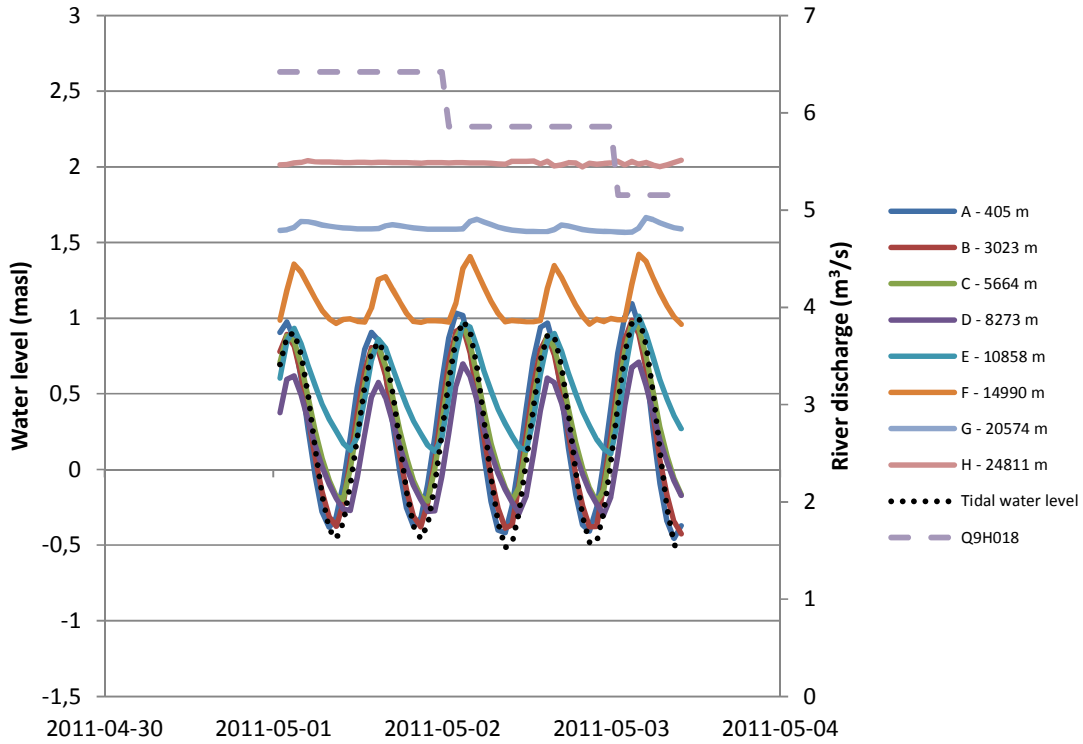
**Figure 6-12: Water levels at defined locations and river discharge for 1 May 2011- 3 May 2011. The estuary has re-opened.**
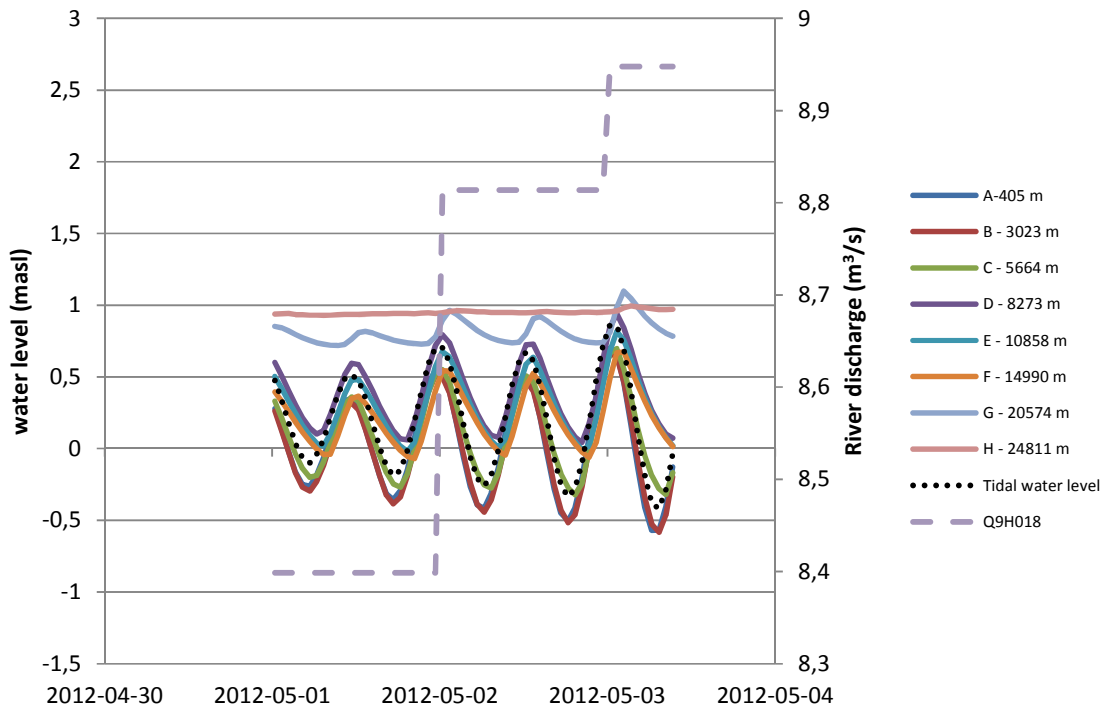


**Figure 6-13 Water levels at defined locations and river discharge for 1 May 2012- 3 May 2012.**

97

## 6.6   Summary of results for Scenario A

The upper reach of the estuary erodes throughout the simulation. The slope is possibly incorrect or interpolation was inaccurate. The bed grading might be coarser as steeper rivers exhibit larger bed sediments which are more resistant to erosion. Generally the model scours when the mouth is open and fills with sediment if the mouth is closed. Flood events erode the middle reach of the river significantly and the deepest areas occur in the middle reach. After mouth closure the mouth experiences slight overtopping but remain constricted until a flood occurs, a flood breaches the mouth to a condition similar to pre-closure. In the absence of waves the cross-sectional area of the mouth (tidal prism) decreases slightly. Due to the absence of waves an ebb-tidal delta/shelf forms downstream of the mouth and the mouth forms spits. The tidal characteristics of the river are closely related to the mouth condition but localised bed elevation can trap or limit tidal flow.

# 7 RESULTS – SCENARIO B

The reader should keep in mind that the sediment bed thickness (model layer thickness) was not based on any field data; consequently bed level changes might be exaggerated or limited. Model bed grading was based on samples collected at the field work sites (Section 4) and are predominantly in the lower reach of the model area, the bed grading of the upper reach was merely an extension of the bed grading observed at Site F. As the river is steeper in the upper reach the median bed diameter is possibly larger. As the bed sampler only collects sediment at river bed level no data was available for the underlying (bellow river bed) and probably coarser sediments. If flood events are investigated specifically the model should include an additional large fraction.

The identifier $Q_n$ refer to a flood event of return period n years.

## 7.1 Flood water levels

The flood peak water levels are shown in Figure 7-1 and Table 7-1. The upper reach of the model experiences flood peak water levels of up to 32 masl. Peak water levels decrease gradually towards the tidal inlet. The maximum water level at the tidal inlet is approximately 8 metres which is quite significant considering the width of the tidal inlet and adjacent sand bar. There are localised dips in the water levels at deep areas; this phenomenon is most noticeable at 19000 metres. The maximum water level variation (between $Q_2$ and $Q_{100}$) at the upstream Site H is 26.8 m whereas the maximum variation at the mouth is 4.3 metres, this shows that the river and tidal inlet areas are approximately equal at low water levels but the discharge through the inlet increases significantly with higher water levels. This is due to the rate that the cross-sectional areas increase with increased water levels at these sites; Site H has steep river banks whereas Site A has flat river banks (above the peak tidal level).

**Table 7-1: Flood peak water levels at selected sites.**

| Flood event | Peak water levels at defined Sites (masl) | | | | | | | |
|---|---|---|---|---|---|---|---|---|
| | A | B | C | D | E | F | G | H |
| | 405m | 3012m | 5664m | 8273m | 10858m | 14990m | 20574m | 24811m |
| $Q_2$ - wl | 3.8 | 3.0 | 2.9 | 3.4 | 3.4 | 4.1 | 3.3 | 4.8 |
| $Q_5$ - wl | 3.7 | 3.6 | 4.6 | 4.3 | 5.7 | 7.6 | 7.8 | 9.4 |
| $Q_{10}$ - wl | 4.5 | 6.3 | 5.7 | 7.4 | 9.7 | 13.3 | 13.0 | 15.0 |
| $Q_{20}$ - wl | 5.9 | 8.0 | 7.5 | 9.2 | 12.7 | 18.9 | 18.7 | 22.5 |
| $Q_{50}$ - wl | 6.3 | 9.9 | 9.2 | 13.5 | 16.9 | 23.5 | 25.8 | 28.1 |
| $Q_{100}$ - wl | 8.1 | 12.1 | 13.1 | 17.1 | 20.9 | 29.5 | 31.7 | 31.6 |
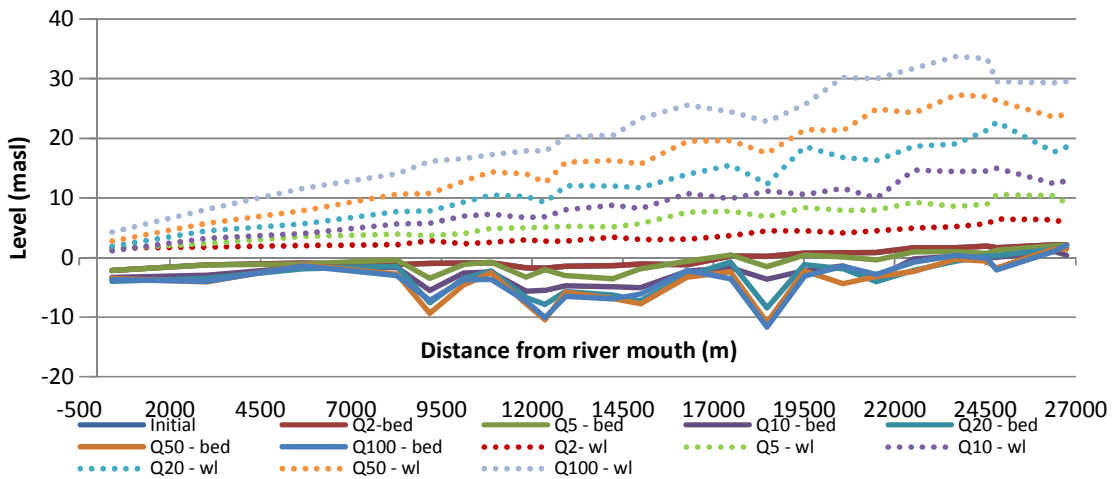


**Figure 7-1: Flood peak water levels ( -wl) for various flood hydrographs and resulting bed (-bed) elevation**

## 7.2    Bed level changes

### 7.2.1    River long section

Refer to Figure 7-2. The simulated flood events reduce the bed levels significantly. The large reduction in bed levels for the 2 year return period flood is exaggerated as the rough interpolated model bathymetry is smoothed; this smoothing is also observed in Scenario A. The erosion pattern is similar for all the flood events, the magnitude of erosion the only difference. The whole river/estuary is eroded significantly except at Site C (5664m). The hump is likely caused by the deposition of upstream sediments where the flow energy (velocity) drops due to the backwater pressure from the ocean and the associated flatter bed slope.
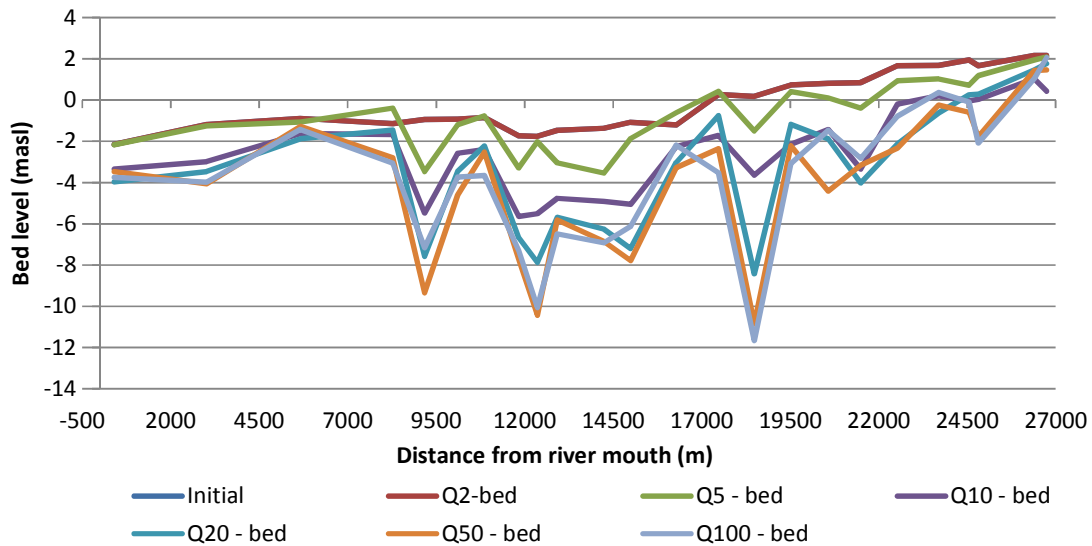


**Figure 7-2: River bed elevations after various flood events.**

### 7.2.2    River cross-sections

Refer to Figure 7-3. Generally the simulated floods scour the channels and increase the channel depth and area. The erosion pattern for all flood events is similar; the magnitude of erosion is linked to the magnitude of the flood.

- Significant bed scour and bed level change is apparent for flood events with a return period of 10 years or more (purple, light blue, orange and violet lines).
- Site A denoted by Section A experiences the largest bed level change of all the investigated sites.
- From the results it is clear that there is overtopping of the sand bar at Section A on the right bank (looking downstream, cell area 28 – 33).
- An interesting observation is the deposition in the sandbar for the 5 year return period flood (green line).
- Channel migration is noticed at Site C for larger floods.
- There is significant bend scour and related sediment deposition at Section F.
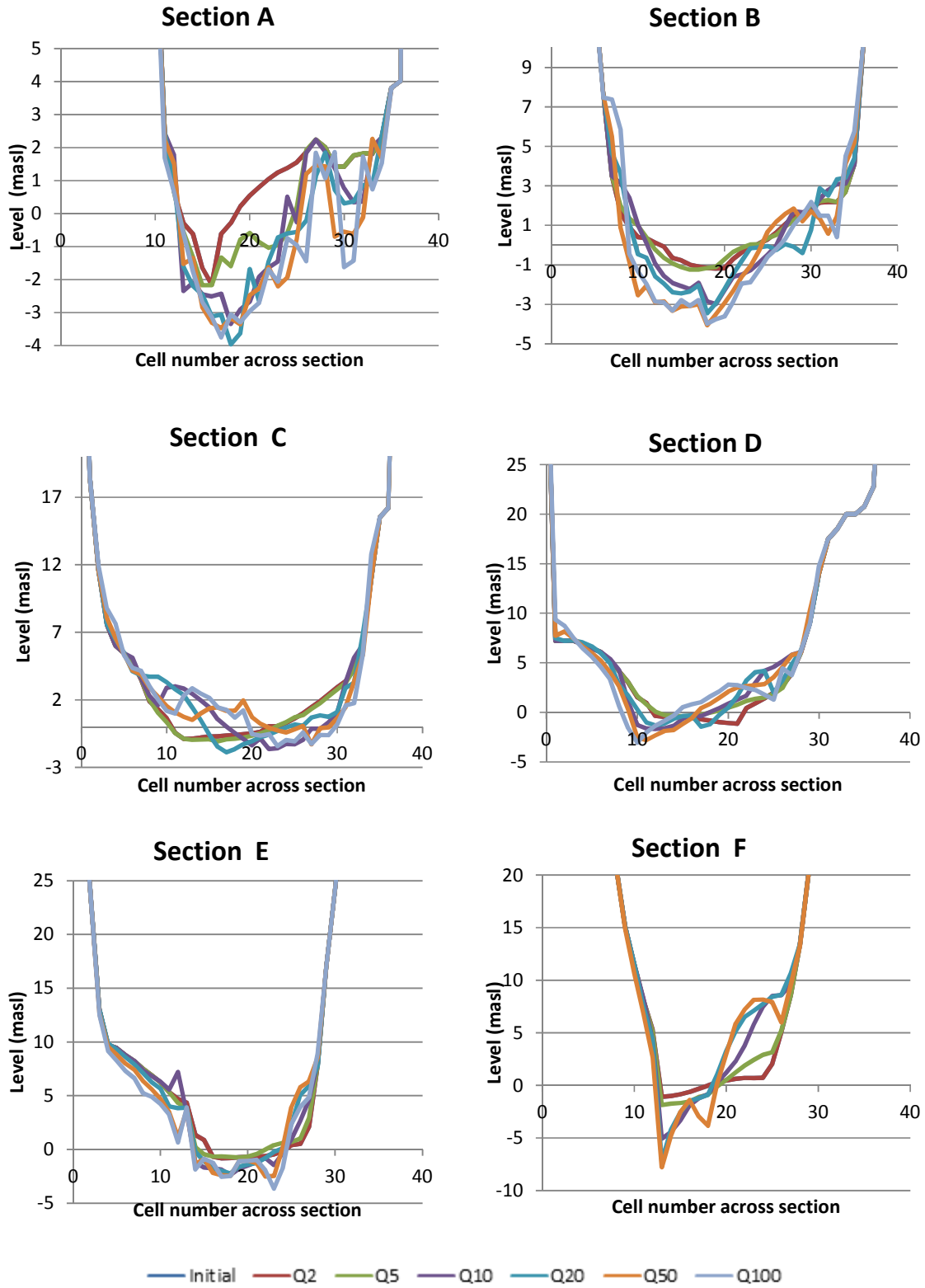
**Figure 7-3 Cross sections at selected sites during Scenario B**

## 7.3    Tidal inlet discharge

The impact of the flood bed level changes on the tidal inlet discharge was investigated. The tidal inlet discharge was evaluated with a constant upstream river discharge of 10 $m^3$/s in conjunction with the predicted tidal water levels of 1 – 6 May 2012. Positive discharge indicates downstream flow; negative discharge values indicate upstream (tidal) flow. Tidal inlet discharge is depicted over time in Figure 7-4. The basic tidal discharge statistics are shown in Table 7-2. The relationship between tidal level and tidal inlet discharge is shown in Figure 7-5.

The peak inlet discharge is accompanied by the 100 year flood bathymetry. This can be expected as the tidal inlet area for this bathymetry is the largest (Figure 7-3). An interesting trend is that the inlet discharge decreases from the initial bathymetry to the 5 year return period flood. Peak discharge then increases by almost 66% when the 10 year flood bathymetry is used. The peak discharge then decreases again for the run with the 50 year bathymetry and jumps again to a global maximum with the 100 year bathymetry run.

Figure 7-5 shows that the linear relationship between tidal water level and inlet discharge remains after flood events.
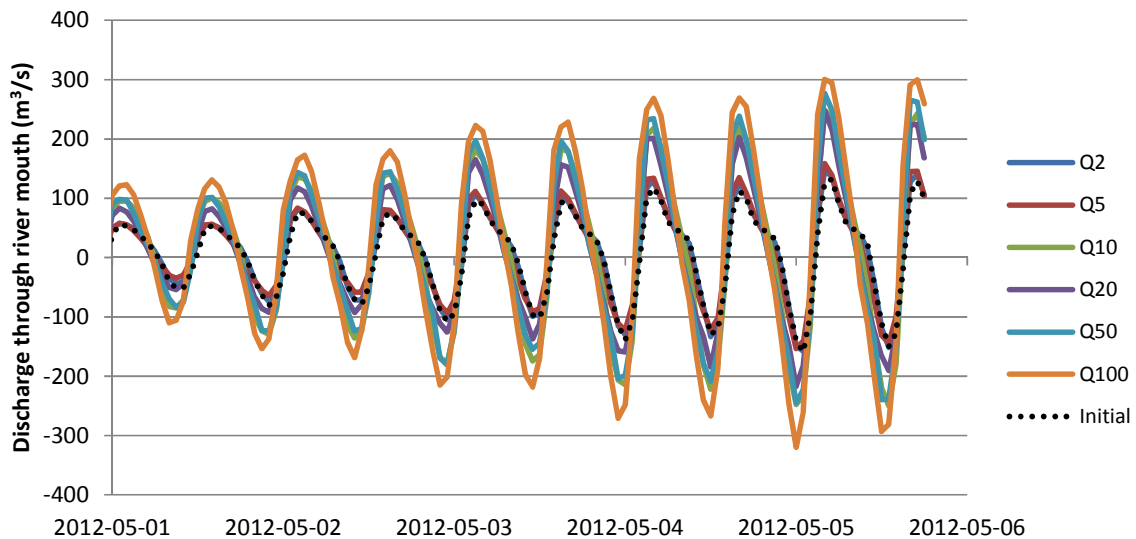


**Figure 7-4: Tidal inlet discharge with bathymetries from flood simulation events for Q = 10 $m^3$/s**

**Table 7-2: Tidal inlet discharge statistics for constant upstream river discharge of 10 $m^3$/s and predicted tidal water levels.**

| Scenario | Inlet discharge $m^3$/s) | | |
|---|---|---|---|
| | Min | Average | Max |
| Initial bathymetry | -159 | 9 | 223 |
| Q2 | -158 | 14 | 209 |
| Q5 | -153 | 13 | 195 |
| Q10 | -250 | 13 | 249 |
| Q20 | -217 | 11 | 247 |
| Q50 | -245 | 11 | 277 |
| Q100 | -320 | 18 | 300 |
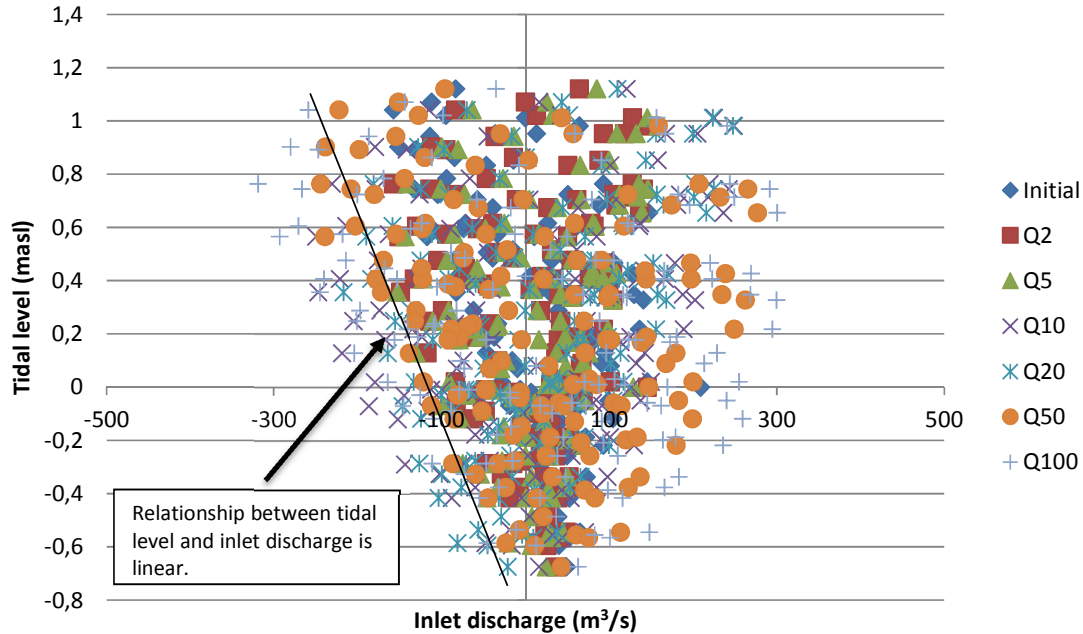
**Figure 7-5: relationship between the tidal inlet discharge and the tidal water level for various model post-flood bathymetries used. The same patter**

## 7.4 Tidal inlet morphology

The state of the tidal inlet pre- and post-flood events can be seen in Figure 7-6. The "sandbar" is the shelf on the left hand side of the tidal inlet, looking upstream.

### 7.4.1.1 $Q_2$

The tidal inlet does not change significantly due to the 2 year return period flood, there is noticeable bed smoothing. The shape of the tidal inlet is similar to the tidal inlet of Scenario A after 12 months, the ebb-tidal delta is however not evident. The missing delta is due to the less significant influx of sediment during the 2 year flood event than would be the case for a year of sediment influx. There is no change to the sandbar.

### 7.4.1.2 $Q_5$

The main channel tidal inlet is noticeably broadened for floods with return periods of 5 or more year.  The inlet retains the characteristics of the initial and 2 year return period flood case. A slight ebb-tidal delta has formed. The sandbar remains unchanged.

### 7.4.1.3 $Q_{10}$

The main channel has deepened, a mouth spit has formed and the sandbar has been transformed. The bed level changes at the sandbar imply that overtopping has occurred in this area. The tidal inlet begins to resemble phase B of the conceptual model of the evolution cycle of river-dominated estuaries as defined by Cooper (2002).

### 7.4.1.4 $Q_{20}$

The trends of $Q_{10}$ are apparent but the sandbar has experienced greater change and the beach profile has steepened. The beach profile steepening might be the cause of the increased (tidal inlet discharge increases and decreases due to floods, see Table 7-2) tidal inlet discharge for flood events > $Q_{10}$ (Section 7.3).

### 7.4.1.5 $Q_{50}$

The tidal inlet has been demolished and the areas of erosion and deposition are erratic, indicated highly turbulent flow events at the tidal inlet.

### 7.4.1.6    $Q_{100}$

The erosion and deposition patterns are even more erratic than for the 50 year flood event simulation. The estuary is starting to resemble the trumpet shape of tide dominated estuaries.

**Initial bed level ($Q_0$)**    **$Q_2$**

**$Q_5$**    **$Q_{10}$**

**$Q_{20}$**    **$Q_{50}$**

Bed level [m]

| | | |
|---|---|---|
| Above | 8.7 | |
| 7.3 - | 8.7 | |
| 6.0 - | 7.3 | |
| 4.7 - | 6.0 | |
| 3.3 - | 4.7 | |
| 2.0 - | 3.3 | |
| 0.7 - | 2.0 | |
| -0.7 - | 0.7 | |
| -2.0 - | -0.7 | |
| -3.3 - | -2.0 | |
| -4.7 - | -3.3 | |
| -6.0 - | -4.7 | |
| -7.3 - | -6.0 | |
| -8.7 - | -7.3 | |
| -10.0 - | -8.7 | |
| Below | -10.0 | |
| Undefined Value | | |

**$Q_{100}$**
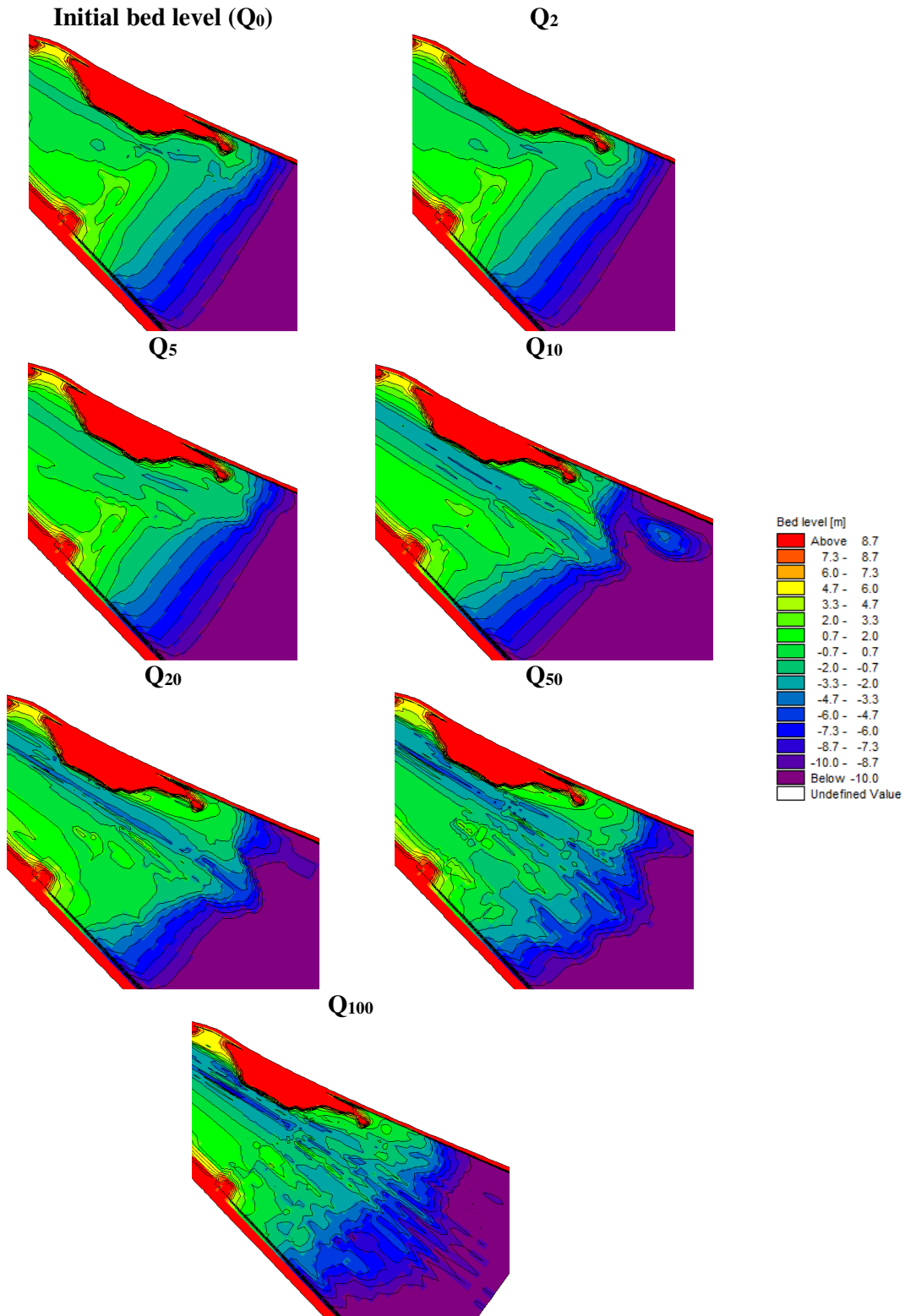
**Figure 7-6: Morphological state of the tidal inlet after simulated flood events**

104

## 7.5   Estuary tide

The estuary tidal levels were compared for pre- and post-flood events. A constant upstream river discharge of 10 $m^3$/s was used in conjunction with the predicted tidal levels for 1 – 6 May 2012. As tidal lag is due to the constriction of tidal flow specifically at the inlet it is expected that the tidal lag will be reduced after flood events. The estuary water levels obtained using the initial interpolated bathymetry is indicated in Figure 7-7. It should be noted that the predicted tidal water levels used correspond with a spring tide.

### 7.5.1.1   $Q_2$

Refer to Figure 7-8. The tidal influence in the upstream reaches is reduced compared to the case with the initial bathymetry. This is caused by the increased capacity of the estuary due to the bed scour from the 2 year return period flood.

### 7.5.1.2   $Q_5$

Refer to Figure 7-9. The estuary water levels at Site G and H have dropped significantly; this is a consequence of the increased cross-sectional area at these sites due to the 5 year return period flood. Tidal action is apparent at all the Sites except Site H; the tidal influence at Site G is extremely small and only noticeable during peak spring tidal levels. Tidal trapping can be observed for sites upstream of Site C. The tidal trapping is due to the deep pool created by the flood at and around Site D and the perch at Site C which creates a negative bed slope (positive bed slope refers to a bed slope with higher elevation on the upstream end and vice versa), refer to Figure 7-2.

### 7.5.1.3   $Q_{10}$

Refer to Figure 7-10. The perch at Site C is eroded by the 10 year flood event and the tidal water level trapping is consequently reduced. Tidal amplification is noticeable at Sites upstream of B and downstream of Site H where there is no noticeable tidal influence.

### 7.5.1.4   $Q_{20}$

Refer to Figure 7-11. The estuary water levels are exactly the same at Sites A to E, this implies that the tidal inlet does not constrict the flow of water into or out of the estuary. Tidal trapping occurs at sites upstream Site E, which can be expected to the due to the deep pools created in the middle reaches of the estuary for large floods (Figure 7-2.). All estuary sites experience tidal water level variations.

### 7.5.1.5   $Q_{50}$

Refer to Figure 7-12. All investigated site experience tidal water levels. Site upstream of B are slightly lagged and tidal trapping occurs upstream of Site B.

### 7.5.1.6   $Q_{100}$

Refer to Figure 7-13. The estuary water levels and trends are similar to that of the simulation with the 50 year flood bathymetry, the main difference being that the tidal influence at Site H has reduced significantly. The before mentioned occurrence is due to sediment deposition at the upper limit of the model.
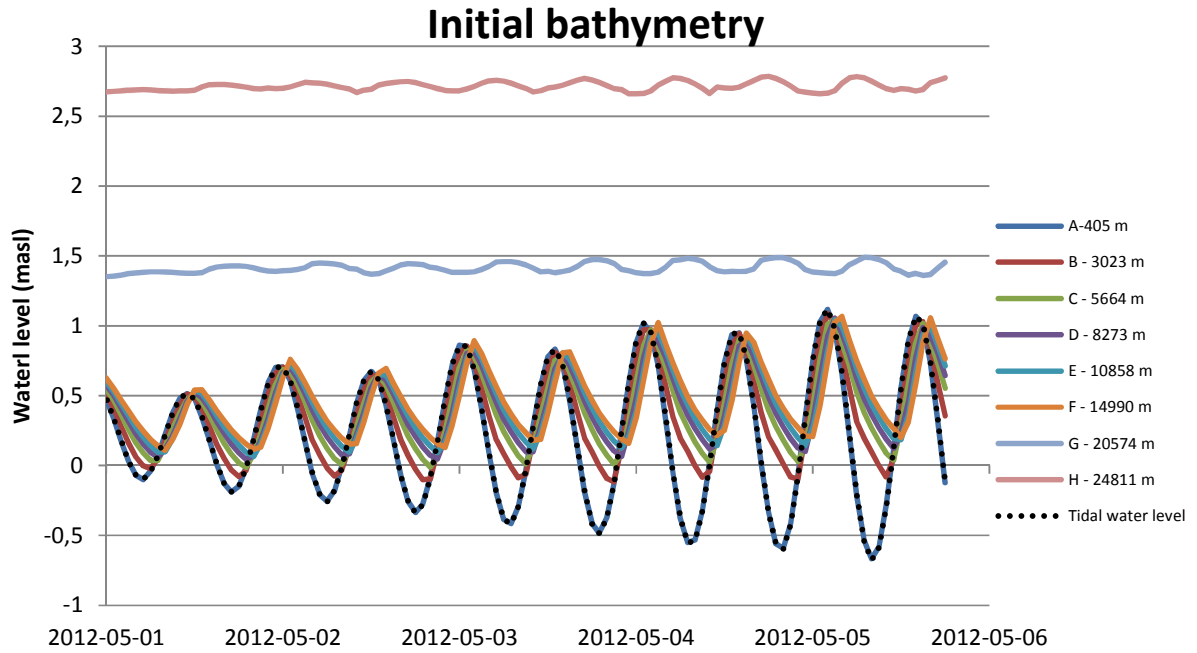
**Figure 7-7: Estuary tidal water levels at various cross sections with the initial model bathymetry**
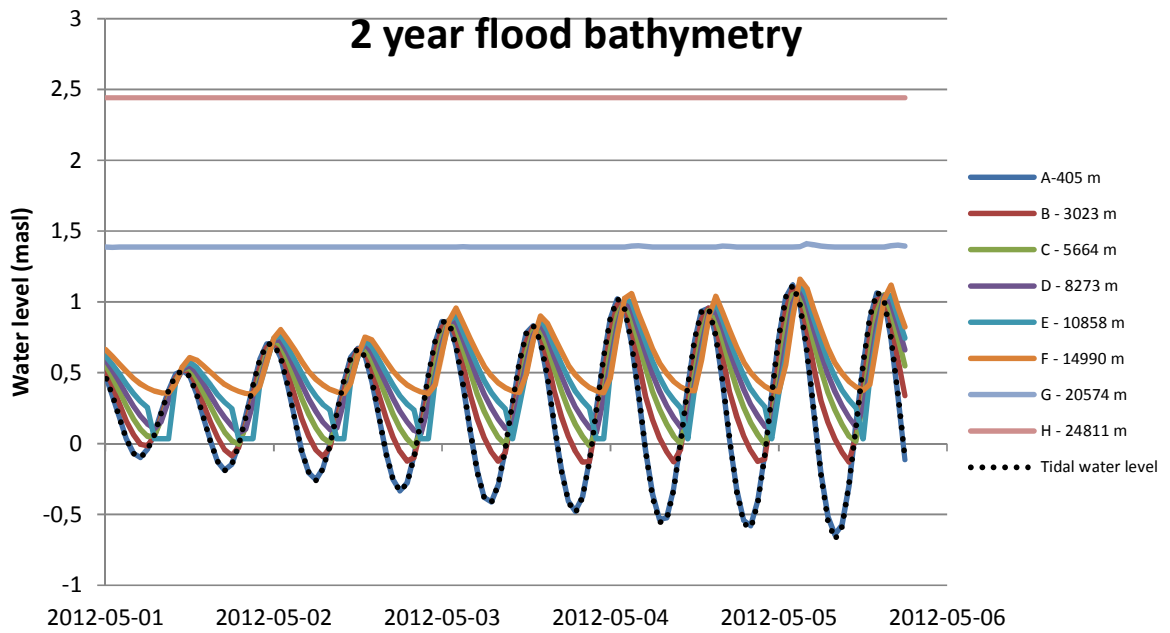


**Figure 7-8: Estuary tidal water levels at various cross sections with 2**

106
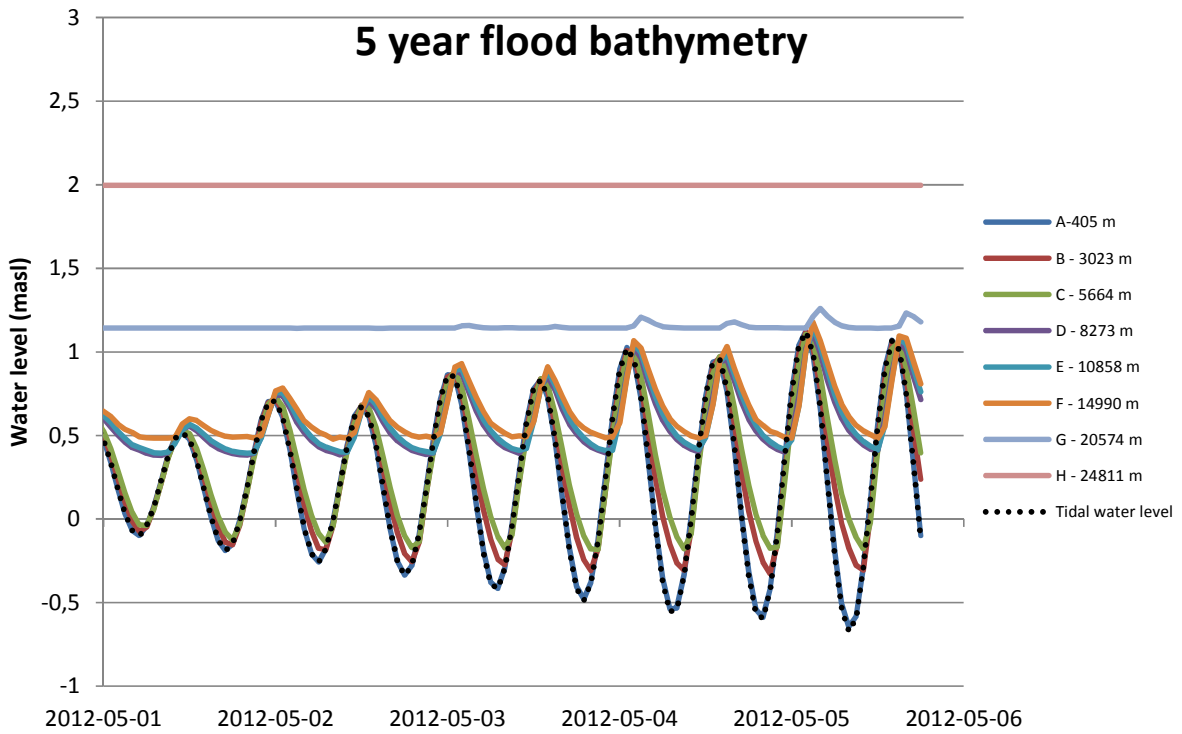
**Figure 7-9: Estuary tidal water levels at various cross sections with 5 year flood bathymetry**
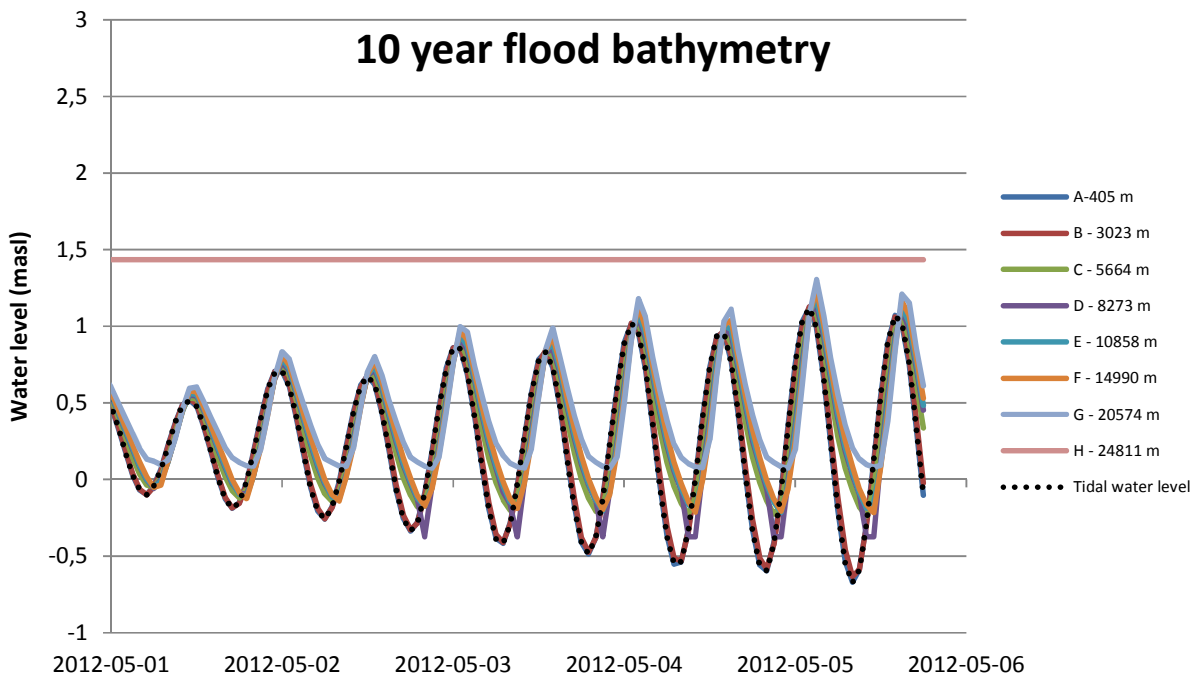


**Figure 7-10: Estuary tidal water levels at various cross sections with 10 year flood bathymetry**

107
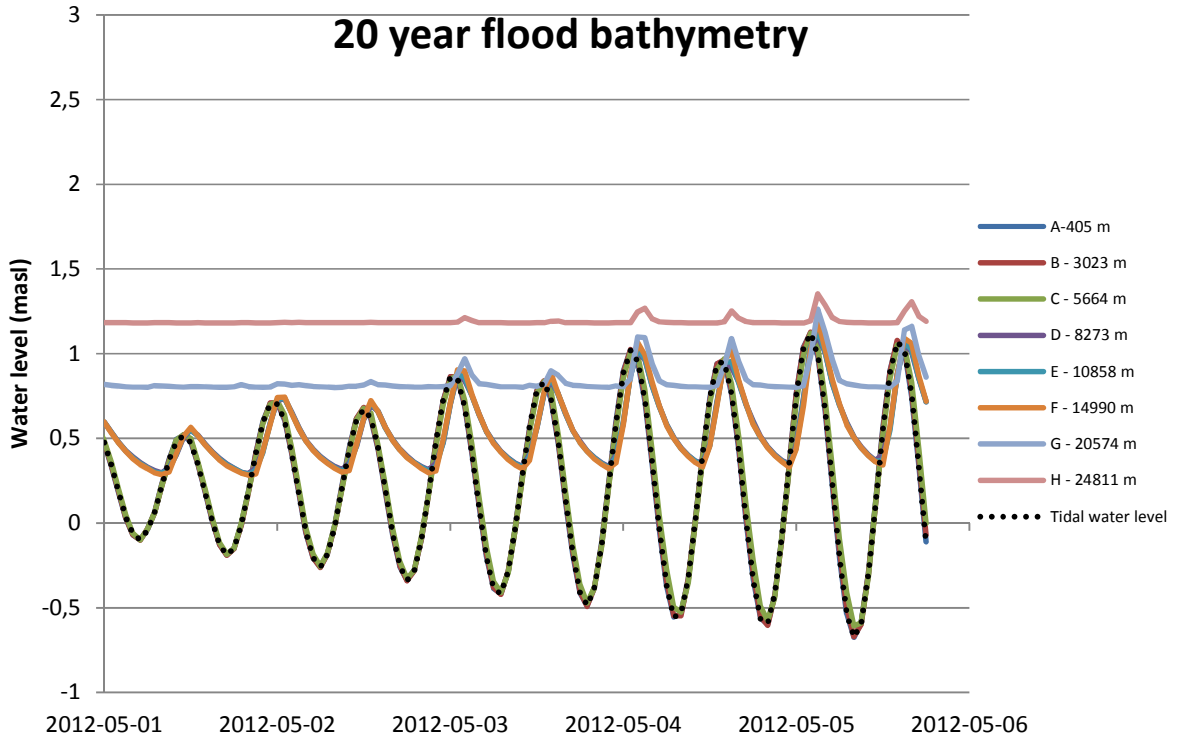
**Figure 7-11: Estuary tidal water levels at various cross sections with 20 year flood bathymetry**
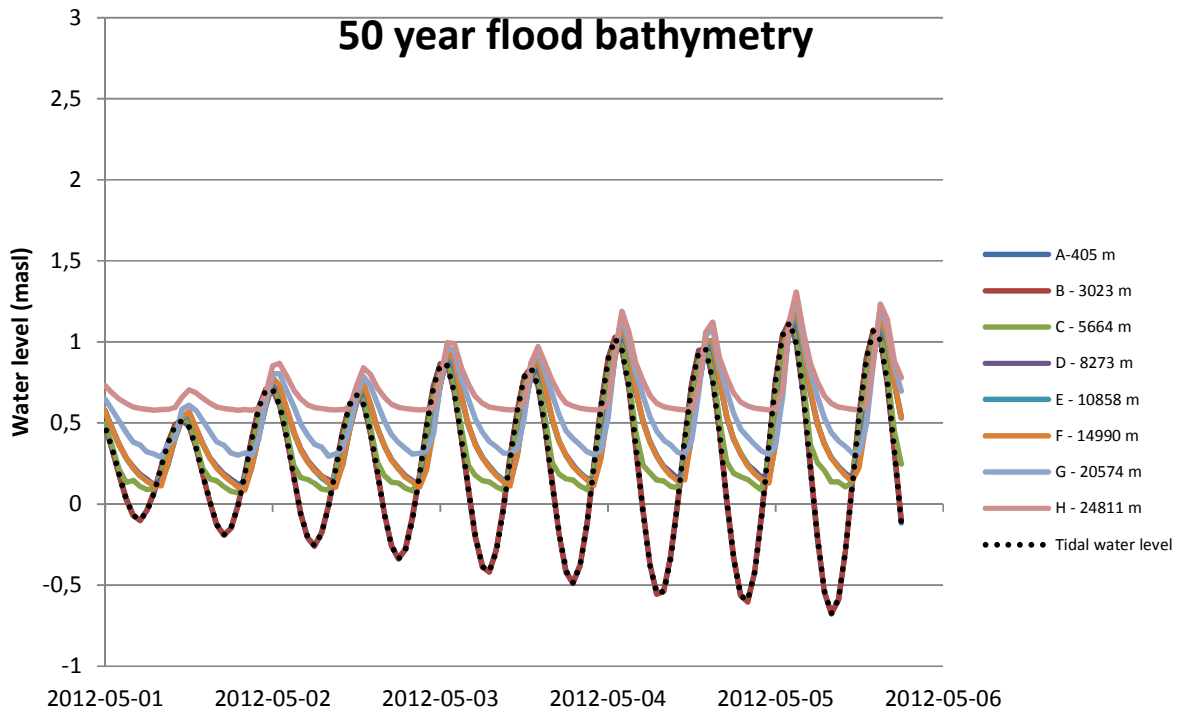


**Figure 7-12: Estuary tidal water levels at various cross sections with 50 year flood bathymetry**

108
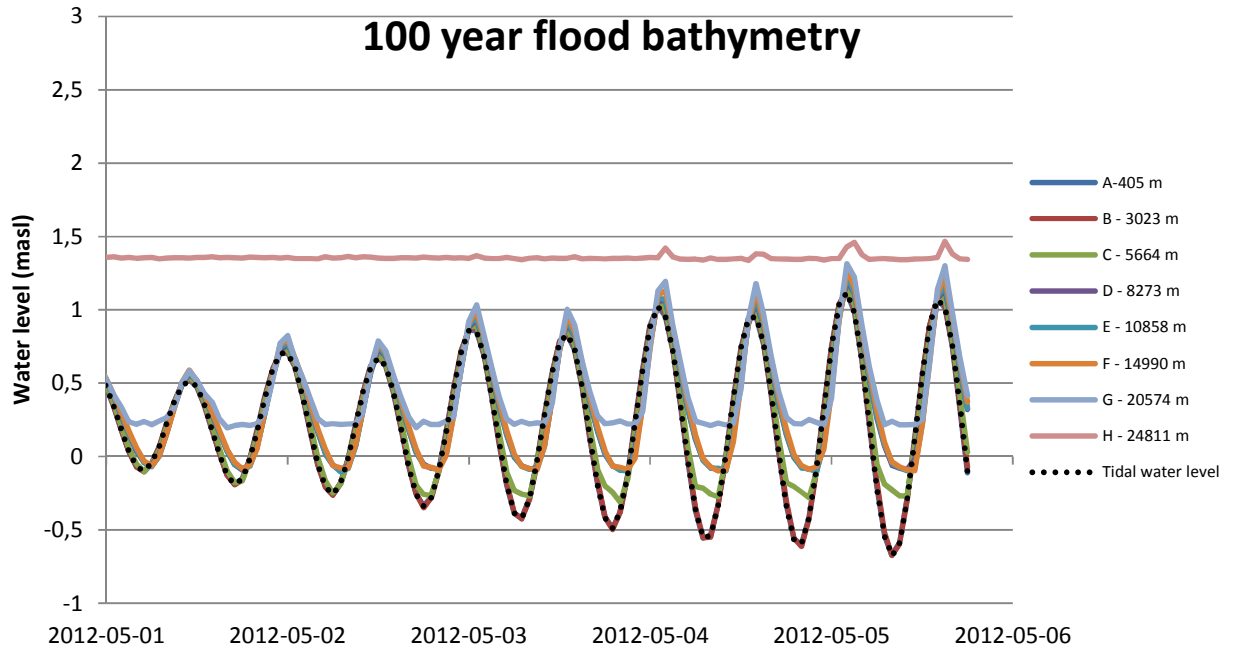
**Figure 7-13: Estuary tidal water levels at various cross sections with 100 year flood bathymetry**

## 7.6   Summary of results for Scenario B

- Peak flood levels at the upper and downstream reaches are similar for small floods, during large floods there is a major difference in water levels at the upstream and downstream end. This shows that the upstream river valley is steep and the cross sectional area does not increase as dramatically as the downstream side which is relatively flat and has large floodplains.
- Local dips in peak water levels are experienced at areas with deep pools.
- The erosion patterns for all floods are similar but the magnitude of scour and deposition differs, floods with return periods greater than 10 years significantly alter the estuary.
- The only site with visible bend scour and river bank deposition is the riverine Site F.
- Site C is the most protected against scour and creates a perch behind which tidal flows are trapped. This is due to the drop in flow velocity due to the backwater pressure of the ocean.
- Large floods especially with return periods larger than 20 years completely remove the sandbar in the mouth over the full river width (approximately 700 m) and consequently greatly diminish the tidal lag.

# 8    ONE-DIMENSIONAL MODEL SETUP

## 8.1    Modelling approach

As indicated earlier, the main purpose of the one-dimensional (1D) model study (compiled in Mike11) was to investigate the salinity regime in the estuary and river due to morphological changes in the estuary (modelled area) as predicted by the two dimensional model (Mike21C). The background of the one dimensional numerical model (Mike11) and the model parameters required are discussed in Section 3.2. Results obtained from the morphological model were used in the setup of the one dimensional Mike11 model. The approach for each modelled scenario is discussed below. The term "chainage" refers to the distance in meters upstream of the reference point "0 meters" which is located in the wave breaker zone offshore of the river mouth. The reader should note that not all the hydrodynamic boundary conditions of Scenario A&B correspond between the one- and two- dimensional models.

### 8.1.1    Scenario A - Long term 5 year model

To simulate the effect of the long term morphological changes in the estuary the downstream water level boundary of the Mike11 model was defined by the water levels obtained from the Mike21C model just upstream of the river mouth rather than the predicted tidal levels at the ocean, as used in the two dimensional morphological model. The upstream hydrodynamic river boundary is identical for the one- and two – dimensional models (Section 5.4). As the one dimensional model is used to predict the estuarine salinity characteristics the upstream advection dispersion (salinity) boundary condition was developed, refer to Section 8.4.2. The simulation period coincides with the morphological simulation (1 May 2007 – 30 May 2012). The downstream water level boundary was closed (deactivated) for the periods of mouth closure in the Mike21C model. The mouth closure was manually implemented during identified low river flow conditions (Section 5.3.1). The validity of this method will be investigated in the results obtained. All cross-sections upstream of the water level boundary were kept constant.

### 8.1.2    Scenario B - Effect of flood hydrographs/events

The estuary bed levels after the simulated flood events were extracted from the two dimensional morphological model and used to create cross sections in Mike11. A 3 month simulation (1 March 2012 – 1 June 2012) was performed with the hydrodynamic boundary conditions developed in Section 5.4 for Scenario A (3 month segment of the 5 year period used in Scenario A), rather than the flood hydrographs of Scenario B (which were used in the two dimensional model of Scenario B), as during flood events no salt intrusion from the ocean would occur. The accompanying advection dispersion boundary was developed as discussed in Section 8.4.2. As the model boundary conditions were equal and the bathymetries varied, the effect of the morphological changes due to floods on the estuarine salinity regime could be inspected.

## 8.2    River network

The river network specifies the locations of the cross sections the user uses for the model bathymetry. The river network points (grid/node points) used corresponds to the points where cross sectional surveys were performed, refer to Section 4.6. The river network coordinates and plan view can be seen in Figure 8-1. Coordinates for each river node (cross-section) correspond to the lowest point in the river for that sectional survey. The river network used in Scenario A and B differ. To simulate the morphological changes to the estuary and river mouth due to Scenario A, a cross section, chainage 1714 m (yellow cells in Figure 8-1, upstream of the river mouth), was created with bed and water levels obtained from the morphological model. The point at chainage 1714 was used as the downstream boundary of the one dimensional model of Scenario A. River cross-sections at chainages -2000 m, 0 m and 405 m were thus omitted for the long term salinity simulation. All cross sections (network points) were used during model calibraton and the salinity modelling of Scenario B.

| Distance from river mouth (m) | Clarke 1880 Gauss Conform Lo27 | |
|---|---|---|
| | X | Y |
| -2000 | -14900 | 3707850 |
| 0 | -12910 | 3707636 |
| 405 | -12509 | 3707491 |
| **1714** | **-11172** | **3706854** |
| 3023 | -10255 | 3706262 |
| 5664 | -7968 | 3705103 |
| 8273 | -6501 | 3703180 |
| 9172 | -6489 | 3702244 |
| 10110 | -5833 | 3701624 |
| 10858 | -5180 | 3701255 |
| 11833 | -4840 | 3700360 |
| 12356 | -4600 | 3699909 |
| 12921 | -4497 | 3699371 |
| 14236 | -3867 | 3698289 |
| 14990 | -3400 | 3697707 |
| 16281 | -2361 | 3697167 |
| 17474 | -1874 | 3696160 |
| 18491 | -1647 | 3695174 |
| 19517 | -1051 | 3694378 |
| 20574 | -461 | 3693521 |
| 21493 | 268 | 3692974 |
| 22531 | 1137 | 3692450 |
| 23694 | 1640 | 3691464 |
| 24547 | 1450 | 3690644 |
| 24811 | 1250 | 3690474 |
| 26394 | 165 | 3689452 |
| 26742 | 102 | 3689124 |



**Figure 8-1: Plan view of the one dimensional model grid point coordinates. Point coordinates correspond to the centre of the river cross sections determined during the topographic survey (Section 4.6).**

## 8.3   River cross-sections

### 8.3.1     Scenario A

River cross-sections were created from the survey information (Section 4.6); refer to Figure 8-2 for a typical cross-section. The cross-section at chainage 1714 m was created and bathymetric data obtained by means of interpolation in the Mike21C Grid Generator software. The Mike11 model requires the user to specify the main flow channel and the floodplains of each cross-section; this is done by the use of markers which are manually defined in the cross-section editor. The user can specify Manning values or relative resistance values for each cross-sectional floodplain and main channel. Manning values were determined through calibration with field results obtained during May 2012 field work (Section 4.5 and Appendix F); refer to Section 8.5 for validation of values used. Manning resistance values used are shown in Table 8-1.

**Table 8-1: Manning n values used for model cross sections of Scenario A.**

| Chainage | Manning n | |
|---|---|---|
| | Main channel | Flood plain |
| 1714 - 12000 | 0.02 | 0.06 |
| 12000 - 26742 | 0.025 | 0.06 |
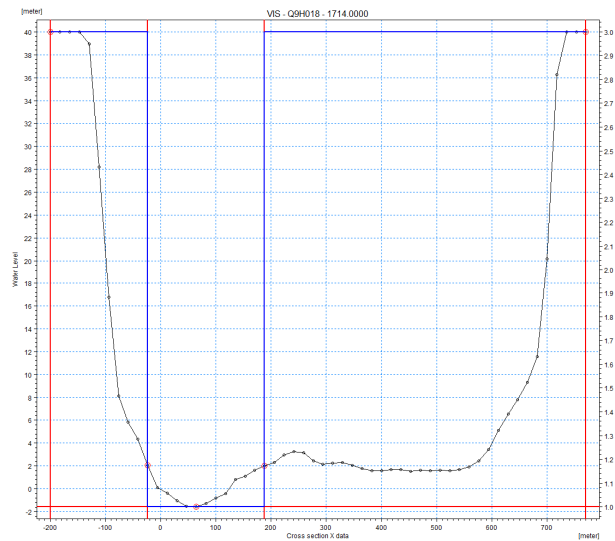


**Figure 8-2: Cross-section at chainage 1714**

### 8.3.2     Scenario B

River cross sections were compiled with data from the Mike21C grid elevation (bathymetry) results for Scenario B. A set of cross sections were created for each (post) flood event, the shape of the cross sections are discussed in Section 7.2.2 and shown in Figure 7-3. Cross sections were extracted at all the network points shown in Figure 8-1. As the bathymetry is gridded the data is presented in the form of a cell coordinate and with the accompanying elevation as a result some bathymetric resolution is lost during cross section definition. All cross section sets were divided into river channels and floodplains as was the case for Scenario A (Section 8.3.1), the Manning resistance values used over the model area can be seen in Table 8-2. The model was not calibrated for each bathymetry as no relevant calibration information was available for these altered bed level states.

112

**Table 8-2: Manning n values used for model cross sections of Scenario B.**

| Chainage | Manning n | |
|---|---|---|
| | Main channel | Flood plain |
| -2000 - 12000 | 0.02 | 0.06 |
| 12000 - 26742 | 0.025 | 0.06 |

## 8.4 Boundaries

Boundary conditions are required at all model boundaries. The hydrodynamic boundary conditions can be used with an advection dispersion (AD) component; the AD component can be used to model the transport of cohesive sediments, the dispersion of pollutants or to predict the salinity of a water system such as an estuary. The AD component is modelled as total dissolved solids (TDS) by the software.  Refer to Section 3.2.3 for the mathematical background of the Mike11 AD model. The total dissolved solids are generally presented in the form of a concentration (mg/l). In this report the terms TDS and salinity are interchangeable. Numerous salinity samples were acquired during the field work done; refer to the Section 4.4.3 and Appendix E.

### 8.4.1 River hydrodynamic boundaries

#### 8.4.1.1 Scenario A - Long term 5 year simulation

8.4.1.1.1 Upstream

For Scenario A the upstream hydrodynamic river boundary used in Mike11 is identical to the boundary condition used in the Mike21C model, refer to Section 5.4.2.1.

8.4.1.1.2 Downstream

Water levels were extracted from the results of the long term Mike21C morphological simulation at the river chainage 1714 m. This site is approximately halfway between Site A and Site B which are defined in Section 4. The tidal water level (black line), water level at chainage 1714 m (redline) and the river discharge (dark blue line) can be seen in Figure 8-3. The dramatic rise in water level is due to the manual mouth closure in the morphological model. The water level is maintained by the damming of the tidal inlet up to the total mouth breach caused by the flooding of early 2011 (refer to Appendix J for river discharge statistics). The downstream boundary was opened during periods were tidal flow into the estuary was observed, refer to Section 6.3.
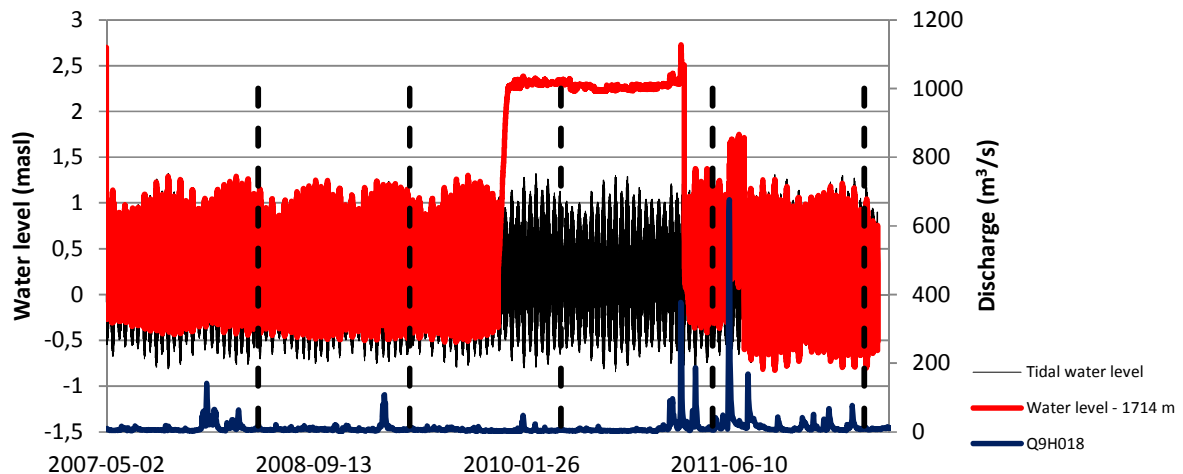


**Figure 8-3: Hydrodynamic boundary conditions for Scenario A TDS simulations**

113

### 8.4.1.2    Scenario B - Flood hydrograph simulations

8.4.1.2.1    Upstream

A 3 month simulation (1 March 2012 – 1 June 2012) was performed with the upstream and downstream hydrodynamic boundary conditions developed in Section 5.4.2.1.

8.4.1.2.2    Downstream

The downstream boundary is at location chainage -2000 m rather than at chainage 1714 m as used for the one dimensional case of Scenario A. Chainage -2000 m is used as the ocean tidal water level point. Refer to Section 5.4.1 for the downstream (tidal) water level background and values used.

The model hydrodynamic boundaries for Scenario B is shown in Figure 8-4.
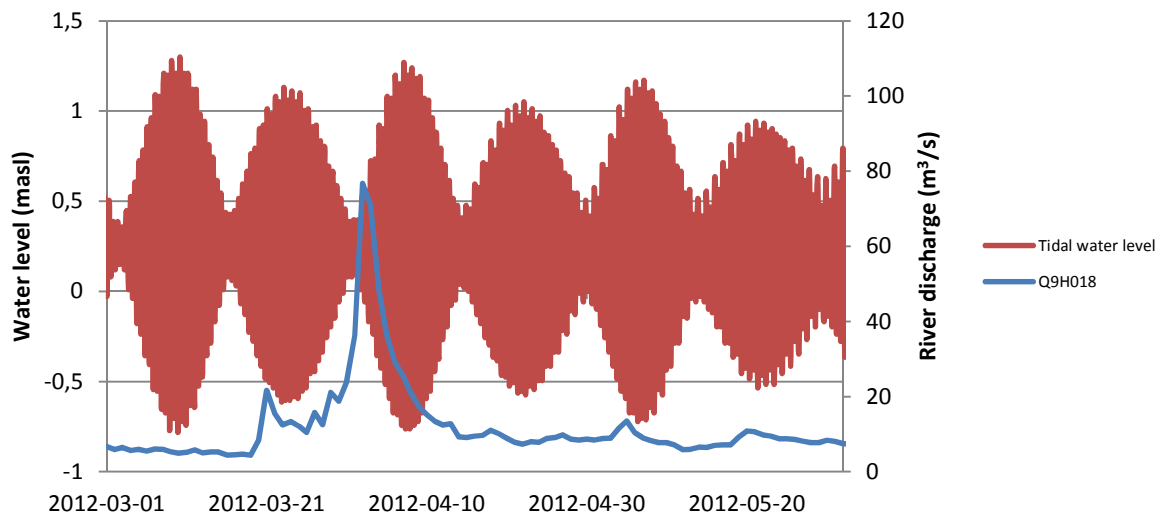


**Figure 8-4: Hydrodynamic boundary conditions for Scenario B TDS simulations**

### 8.4.2    River AD/salinity boundary

The river TDS was predicted by the analysis of the conductivity data from the Great Fish River measurement station Q93_102487 courtesy of the Department of Water and Sanitation Resource Quality Information Services (DWS - RQIS). Station Q93_102487 is located at the same position as DWS flow gauge Q9H018, for station coordinates refer to Table 5-2, the locations of the stations are shown in Figure 8-5. Conductivity data is available for the period 1977 to 2013. A plot of the river discharge and corresponding total dissolved solids (TDS) can be seen in Figure 8-6.

114
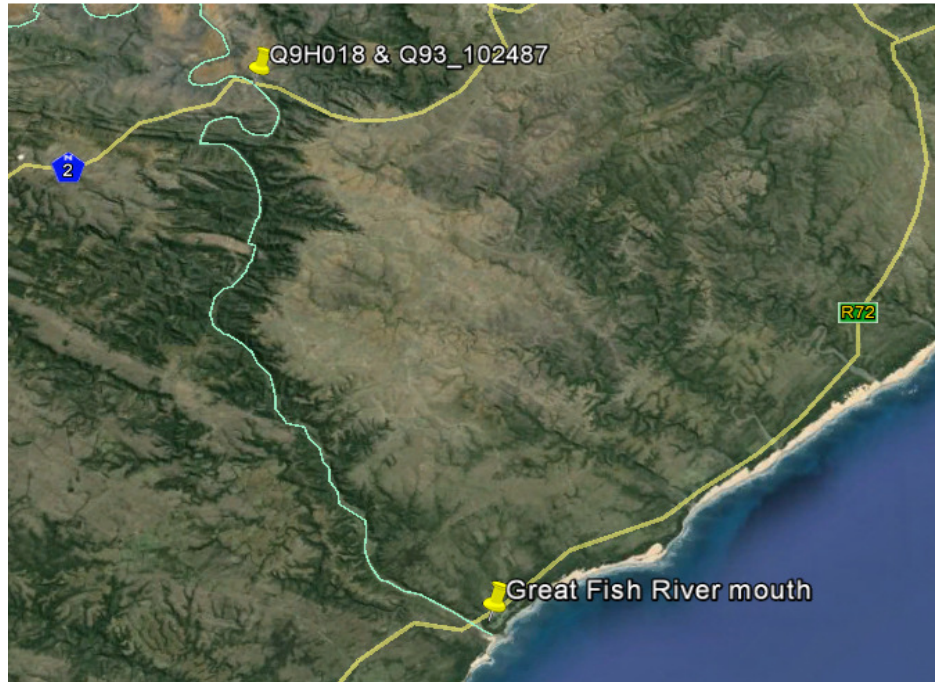
**Figure 8-5: Location of water quality (Q93_102487) and river flow (Q9H018) gauge stations (Google 2014).**
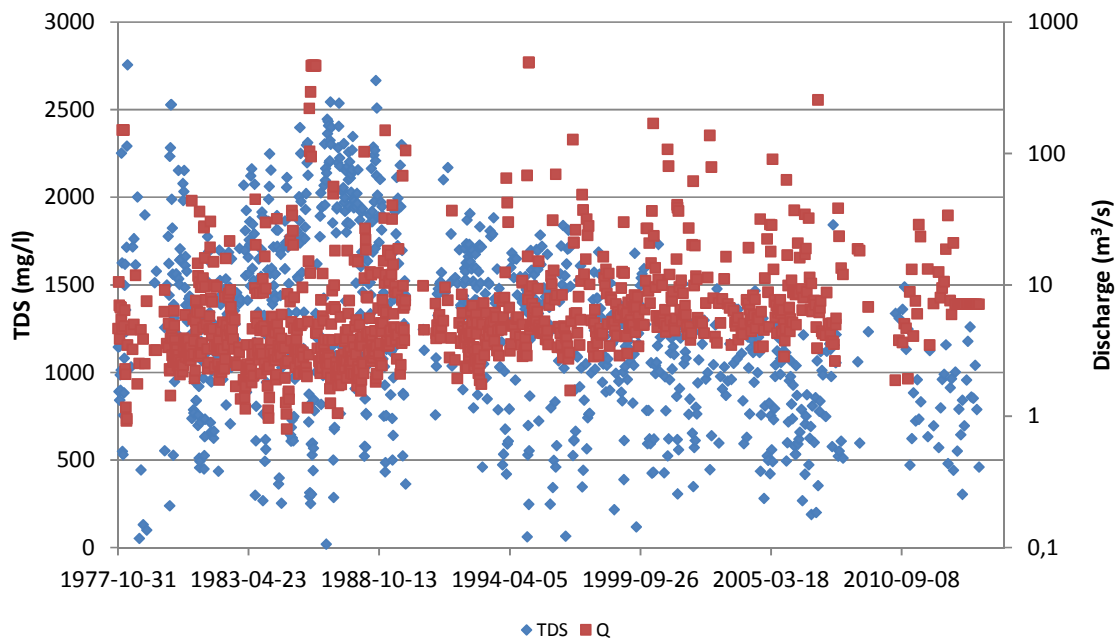


**Figure 8-6: Total dissolved solids (TDS) and river discharge (Q) for the Great Fish River.**

### 8.4.2.1    *TDS prediction*

As can be seen in Figure 8-6 there is no discernible relationship between the river discharge and the river TDS. Regression analysis was attempted but a favourable correlation could not be determined ($R^2 = 0.026$). For TDS prediction the river flow was divided into discharge bins, for each bin the corresponding TDS values were averaged, the bins, data point count and average TDS per discharge bin is shown in Table 8-3.

**Table 8-3: TDS values for different river discharges.**

| | Discharge bin (m³/s) | | | | | | |
|---|---|---|---|---|---|---|---|
| | 0-2.5 | 2.5-7.5 | 7.5-15 | 15-25 | 25-50 | 50-100 | 100+ |
| Data points | 125 | 600 | 148 | 46 | 42 | 11 | 27 |
| Average TDS (mg/l) | 1768 | 1341 | 1035 | 882 | 615 | 449 | 590 |
| Combined average (mg/l) | 1176 | | | | | | |

The Mike11 AD boundary time series file was created by assigning TDS values to flows that fall into the bins defined in Table 8-3. The relationship between TDS and river discharge can be seen in Figure 8-7.
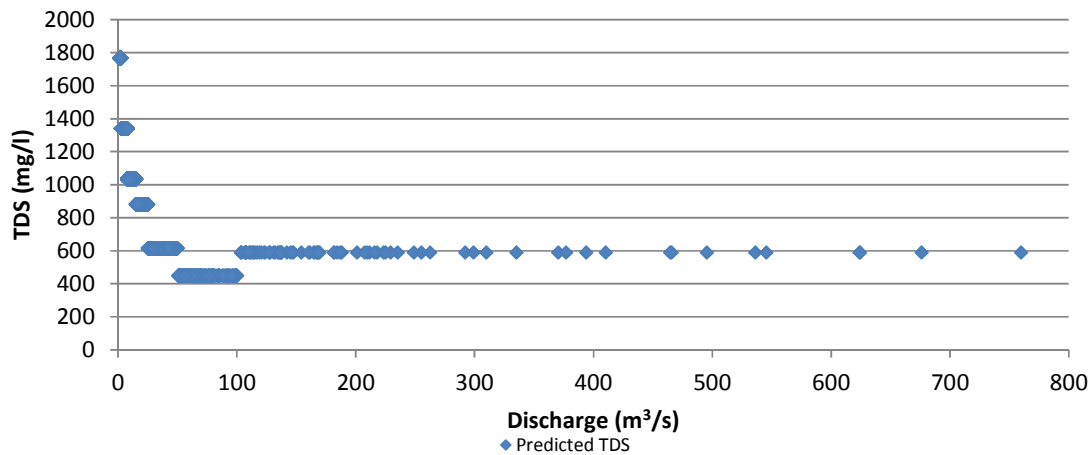


**Figure 8-7: TDS – river discharge relationship**

### 8.4.2.2 *Downstream*

The typical salinity of the sea is about 35000 mg/l (Open University 1999), however as can be seen in the results from the Field Work (Appendix E) maximum salinities of up to 40000 mg/l were observed. Through calibration a downstream sea boundary TDS value of 36000 mg/l was decided upon. All simulations with open downstream mouth boundaries had a salinity value of 36000 mg/l.

## 8.5   Model calibration/parameters

Model calibration is achieved by the altering the calibration coefficients available to the user. The calibration coefficients are similar to those of the two dimensional model and are discussed in Sections 3.2.4 and 3.1.5. The Mike11 model was calibrated with data obtained during field work done in May 2012 (Section 4). Refer to Section 4.3.4 for the field work schedule and data obtained. For the calibration of the one dimensional model only the model bed roughness and boundary lag was varied. A trial and error approach was used to determine the most favourable calibration parameters.

### 8.5.1   Hydrodynamic model calibration

The "result accuracy" for this study is given by equation 8-1(equal to eq. 5-10):

$$A_m = \frac{x_m}{x_f} * 100$$

(8-21/ 5-10)

Where:   $A_m$ = Model accuracy (%)

$x_m$ = Predicted model parameter

$x_f$ = Measured field parameter

116

The hydrodynamic model was calibrated successfully. Calibration was achieved by a tidal lag of one hour and Manning roughness coefficients listed in Table 8-2 (the one dimensional model was not calibrated for the altered bed level states used in Scenario B). The tidal lag and roughness values correspond well to the values used in the calibration of the two dimensional model (Refer to Section 5.8). The measured and predicted hydrodynamic model characteristics are shown in Table 8-4, Figure 8-8 and Figure 8-9.

**Table 8-4: Summary of measured and predicted flow hydrodynamics**

| Hydrodynamic | | | | Velocity | | | Depth | | |
|---|---|---|---|---|---|---|---|---|---|
| | | | | ADCP | MIKE 11 | Accuracy | ADCP | MIKE 11 | Accuracy |
| Chainage | Date | Time | Run id. | v (m/s) | v (m/s) | -(%) | (m) | (m) | -(%) |
| 405 | 2012/05/05 | 13:38 | 2 | 1.18 | 0.90 | 76 | 3.68 | 3.48 | 95 |
| 3023 | 2012/05/05 | 14:21 | | 0.43 | 0.39 | 91 | 1.81 | 2.41 | 145 |
| 5664 | 2012/05/05 | 14:34 | | 0.49 | 0.42 | 86 | 2.37 | 2.81 | 119 |
| 8270 | 2012/05/05 | 14:55 | | 0.34 | 0.31 | 92 | 3.10 | 3.76 | 121 |
| | | | | | | | | | |
| 405 | 2012/05/06 | 07:28 | 4 | 0.87 | 1.04 | 119 | 3.14 | 2.58 | 82 |
| 3023 | 2012/05/06 | 07:46 | | 0.59 | 0.55 | 94 | 1.32 | 1.67 | 126 |
| 5664 | 2012/05/06 | 08:01 | | 0.49 | 0.61 | 123 | 1.18 | 1.50 | 162 |
| 8270 | 2012/05/06 | 08:17 | | 0.43 | 0.41 | 96 | 2.09 | 2.79 | 133 |
| 10888 | 2012/05/06 | 08:29 | | 0.39 | 0.43 | 110 | 2.46 | 2.69 | 109 |
| 15200 | 2012/05/06 | 09:18 | | 0.41 | 0.33 | 80 | 1.76 | 1.68 | 96 |
| | | | | | | | | | |
| 405 | 2012/05/06 | 13:40 | 6 | 1.13 | 0.76 | 67 | 3.27 | 3.24 | 99 |
| 3023 | 2012/05/06 | 13:55 | | 0.64 | 0.52 | 81 | 1.64 | 2.19 | 134 |
| 5664 | 2012/05/06 | 14:20 | | 0.49 | 0.62 | 126 | 2.22 | 2.47 | 112 |
| 8270 | 2012/05/06 | 14:44 | | 0.48 | 0.46 | 97 | 2.82 | 3.46 | 123 |
| 10888 | 2012/05/06 | 15:10 | | 0.33 | 0.44 | 135 | 3.12 | 3.53 | 113 |
| | | | | | | | | | |
| 405 | 2012/05/07 | 07:27 | 8 | 1.31 | 0.86 | 70 | 3.03 | 2.93 | 97 |
| 3023 | 2012/05/07 | 08:05 | | 0.52 | 0.55 | 105 | 1.35 | 1.75 | 132 |
| 5664 | 2012/05/07 | 08:20 | | 0.64 | 0.61 | 95 | 1.80 | 2.00 | 111 |
| 8270 | 2012/05/07 | 08:36 | | 0.40 | 0.42 | 106 | 2.35 | 2.88 | 123 |
| 10888 | 2012/05/07 | 08:52 | | 0.36 | 0.43 | 119 | 2.41 | 2.77 | 115 |
| 15200 | 2012/05/07 | 09:14 | | 0.32 | 0.34 | 105 | 4.07 | 2.00 | 45 |

# Comparison of measured and predicted flow velocity
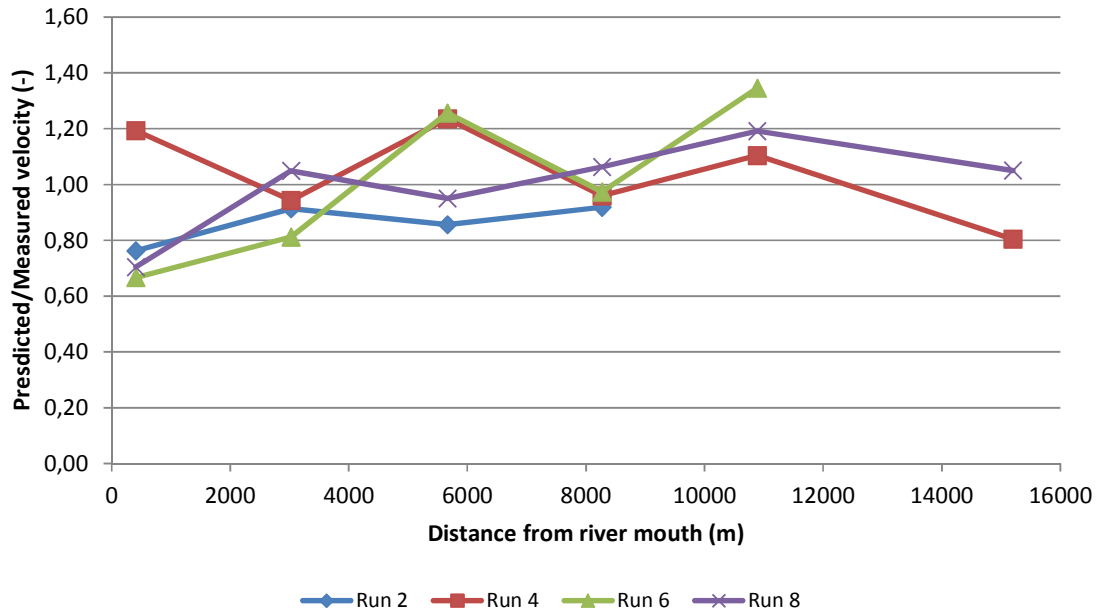


**Figure 8-8: Comparison of measured and predicted flow velocities**

# Comparison of measured and predicted flow depth
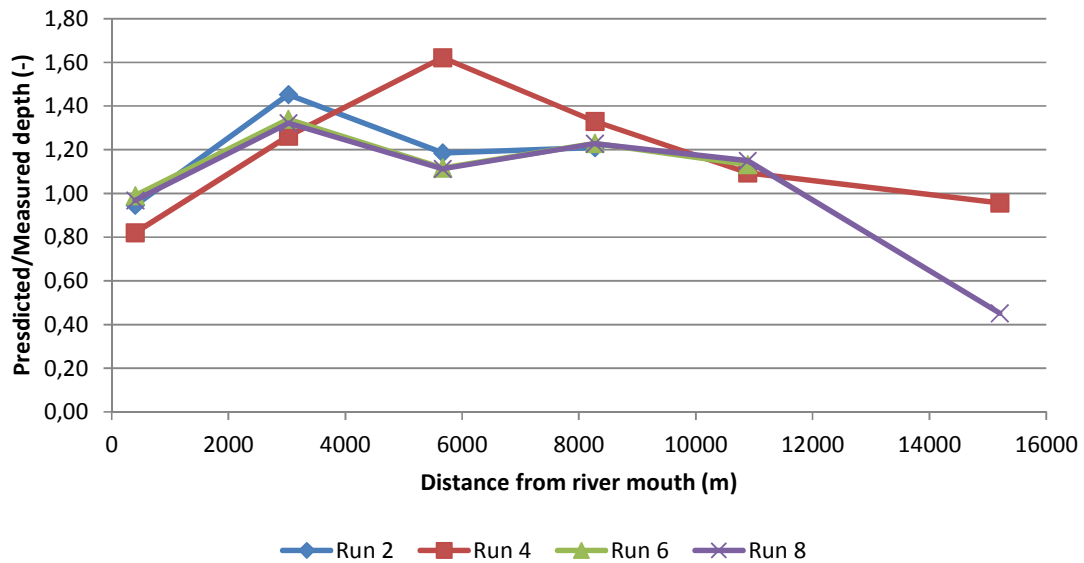


**Figure 8-9: Comparison of measured and predicted flow depths**

**8.5.2    Advection dispersion (AD) model calibration**

The advection dispersion (AD) module uses output from the hydrodynamic module to compute results, a properly calibrated HD module is thus essential for AD calibration. There are however additional AD calibration factors which can be used to increase model accuracy. The following calibration constant is available to the user:

The dispersion coefficient, D [m$^2$/s] is given by equation 8-2:

$$D = aV^b \qquad\qquad\qquad\qquad (8\text{-}2)$$

Where

        a = dispersion factor [-]

        b = dispersion exponent [-]

        V = mean flow velocity [m/s]

The dispersion coefficient is a function of the velocity in the computational point and the user defined calibration factors a and b. Values for a (dispersion factor) and b (dispersion exponent) can be specified at individual locations or globally in the model. Typical values of D (dispersion coefficient) for small streams typically range between 1 and 5 m$^2$/s and between 5 and 20 m$^2$/s for rivers (DHI 2011a). Limits for the minimum and maximum value of D can also be specified.

The AD calibration was performed by only altering the dispersion factor (a). The calibration parameter value was determined by trial and error. The most favourable results were obtained with a global constant value for a equal to 22, for results refer to Table 8-5 and Figure 8-10. The model generally overestimates the salinity.

**Table 8-5: Measured and predicted salinities used for calibration.**

| Advection dispersion | | | | Field | MIKE 11 | Accuracy |
|---|---|---|---|---|---|---|
| Chainage | Date | Time | Run id. | mg/l | mg/l | (%) |
| 405 | 2012/05/05 | 10:48 | | 3921 | 4024 | 97 |
| 3023 | 2012/05/05 | 11:24 | | 2030 | 1100 | 185 |
| 5664 | 2012/05/05 | 11:45 | 1 | 746 | 700 | 107 |
| 8270 | 2012/05/05 | 12:04 | | 682 | 700 | 97 |
| 10888 | 2012/05/05 | 12:19 | | 681 | 700 | 97 |
| | | | | | | |
| 405 | 2012/05/05 | 15:40 | | 39476 | 34519 | 114 |
| 3023 | 2012/05/05 | 16:00 | | 38630 | 30959 | 125 |
| 5664 | 2012/05/05 | 16:14 | 3 | 23632 | 23396 | 101 |
| 8270 | 2012/05/05 | 16:31 | | 1128 | 2288 | 49 |
| 10888 | 2012/05/05 | 16:48 | | 664 | 700 | 95 |
| | | | | | | |
| 15200 | 2012/05/06 | 09:18 | 4 | 574 | 700 | 82 |
| | | | | | | |
| 405 | 2012/05/06 | 15:53 | | 37868 | 34796 | 109 |
| 3023 | 2012/05/06 | 16:11 | | 39089 | 32071 | 122 |
| 5664 | 2012/05/06 | 16:23 | 7 | 31615 | 27027 | 117 |
| 8270 | 2012/05/06 | 16:35 | | 1225 | 1034 | 118 |
| 10888 | 2012/05/06 | 16:49 | | 707 | 705 | 100 |
| 15200 | 2012/05/06 | 17:04 | | 654 | 700 | 93 |
| | | | | | | |
| 15200 | 2012/05/07 | 09:44 | 8 | 726 | 700 | 104 |

# Comparison of measured and predicted salinity
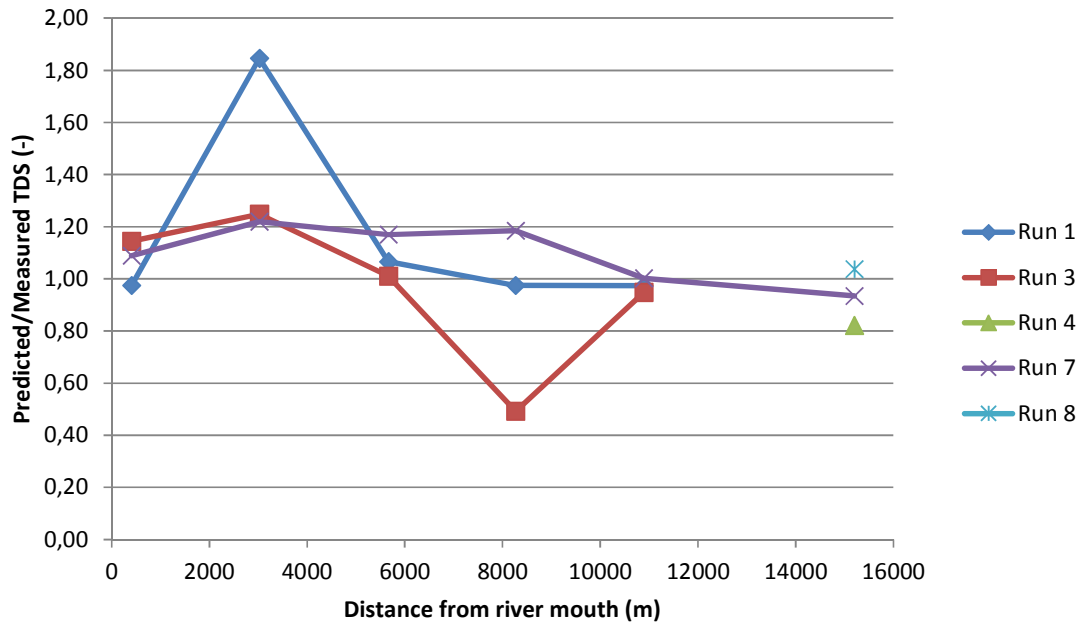


**Figure 8-10: Plot of the salinity model accuracy**

### 8.5.3    Calibration overview

The hydrodynamic and advection dispersion model was successfully calibrated. The hydrodynamic model was calibrated by altering the (local) model bed roughness (values used for Scenario A are shown in Table 8-1, and for Scenario B in Table 8-2) and by altering the downstream boundary (tidal water level) lag. The model underestimates the velocity slightly and marginally overestimates the depth, refer to Table 8-4.

The advection dispersion model was calibrated by altering the dispersion factor, the best correlation between field and model results were obtained with dispersion factor, a, equal to 22. The model overestimates the salinity slightly; refer to Table 8-5 for the predicted and measured salinity parameters.

# 9   SALINITY MODELLING RESULTS

## 9.1   Scenario A - Long term simulation

The modelling of Scenario A consisted of 5 model simulations (runs), the runs are described in Table 9-1. Simulation results are presented by their run number and in periods of 1 year. Predicted salinity over time is shown in Figure 9-1 for the total simulation period. The predicted salinity over time during the closed mouth period (estuary does not experience tidal water levels) is shown in Figure 9-2. Maximum, average and minimum predicted salinity is shown per run in Figure 9-3 and Table 9-2 and per year in Figure 9-3 and Table 9-3. The terms "salinity" and "TDS" are used interchangeably in the interpretation of results.

**Table 9-1: TDS simulation run description and downstream boundary state for Scenario A.**

| Run | Run start date | Event | Mouth/boundary state |
|---|---|---|---|
| 1 | 2007/05/01 | Start of simulation | open |
| 2 | 2009/11/30 | First manual mouth closure | closed |
| 3 | 2009/12/29 | First signs of tidal influence | open |
| 4 | 2010/09/10 | Second manual mouth closure | closed |
| 5 | 2010/10/15 | First signs of tidal influence | open |
| end | 2012/05/30 | End of the simulation | end |

During open mouth states the salt intrusion occurs in the form of a saline wedge, during closed mouth conditions the salt intrusion is of the well mixed type. The salt generally intrudes up to Site E, which is about 11 km upstream of the river mouth, however salinity values slightly larger than that of the river boundary occur at Site F during spring tides. This correlates to the findings of previous studies (Vorwerk, Grange & Allanson among others) that the salt intrusion is typically 10 km into the estuary, and with the statement of Savenije (2005) that the intrusion length is related to the tidal excursion and is typically 10 km in regions with diurnal tides.

The maximum TDS in the model always occurs at the downstream ocean boundary, this is due to the presence of the AD boundary condition (36000 mg/l). When the tidal inlet was closed the average salinity inside the estuary started to drop. This is due to the damming of water behind the blocked inlet. As the mass of salt inside the estuary is not being supplemented by the extremely saline sea the salinity veers to that of the river. The estuary water body is less saline than the river inflow in the later stages of the closed mouth condition; this is due to low river flows having a higher salinity than flood flows which are fresher and constitute a higher volume of the total water in storage (stored in the closed estuary). Even though the downstream boundary was opened in the model at the end of run 2 there was no noticeable effect on the salinity inside the estuary. This leads the modeller to believe that it is unnecessary to close the downstream boundary (HD and AD) condition when this modelling approach is used.

 Generally the average TDS of the river varies with the tide, as can be seen when comparing the profile of the average TDS time series (red line) in Figure 9-1 and the downstream water level boundary in Section 8.4.1. The correlation is however weak due to the influence of the upstream river discharge and associated salinity and the effect of the tidal inlet on the estuary tide. On average the water is very saline at Site B when the river mouth is open (≥17000 mg/l). Although the estuary experiences tidal water levels at Site G and H during year 5 of the simulation (Section 6.5 Estuary tide) no salt intrusion is detected at these sites. This might be due to the different models used which have different bathymetries or the fact that the water level is influenced by the backwater level of the downstream boundary. As is seen in Section 6.5 the tidal reach is enhanced when the upstream bed levels are reduced (erosion). The reduction in upstream bed levels is due to flooding events which would also

have breached the river mouth, further promoting the maximum possible tidal reach. The scoured bed levels would also enhance the storage capacity of the estuary.

As flood events generally contain less salts in concentration than low flows the deepened estuary is filled with comparatively fresh water and residual salts from dry periods are flushed out of the system. From observations the most saline estuary would occur if fresh water storage is minimal, the tidal inlet completely unrestricted and low river flows with high salt concentrations occur for extended periods.
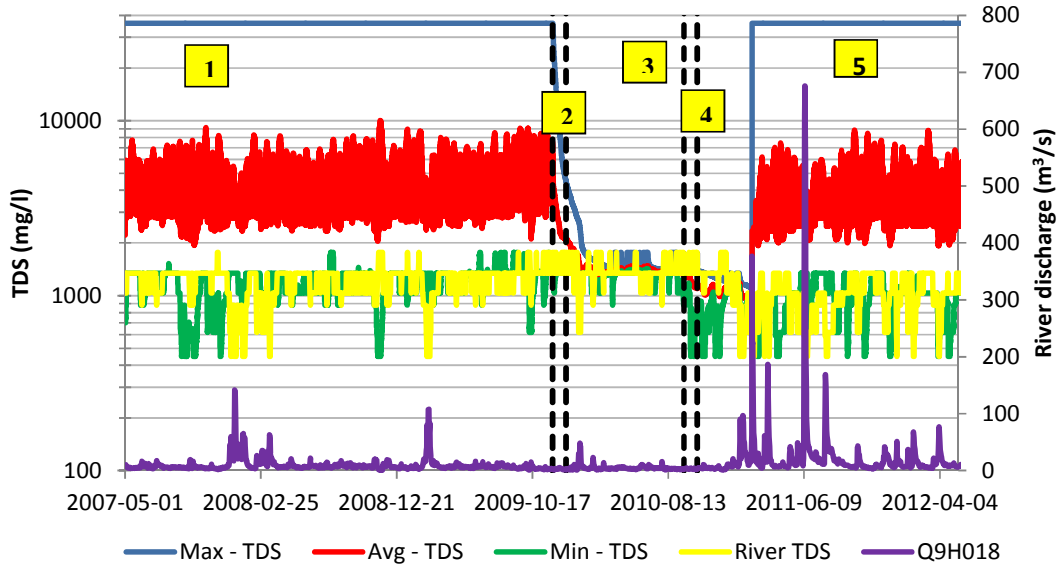


**Figure 9-1: Predicted maximum, average and minimum estuary salinity during simulation of Scenario A. Salinity statistics are for the whole model area. Black dotted lines indicate the end/start of a run, run number shown in yellow box (Table 9-1). Series Q9H018 (purple) denotes river discharge.**
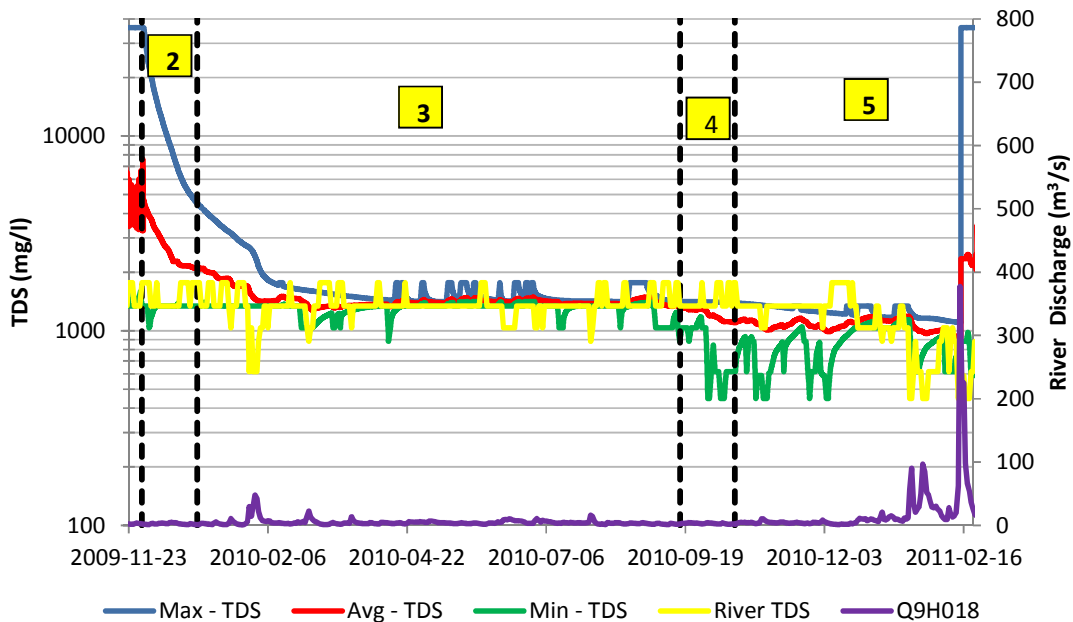


**Figure 9-2: Predicted maximum, average and minimum estuary salinity during the closed mouth period of Scenario A. Salinity statistics are for the whole model area. Black dotted lines indicate the end/start of a run, run number shown in yellow box (Table 9-1). Series Q9H018 (purple) denoted river discharge.**

123
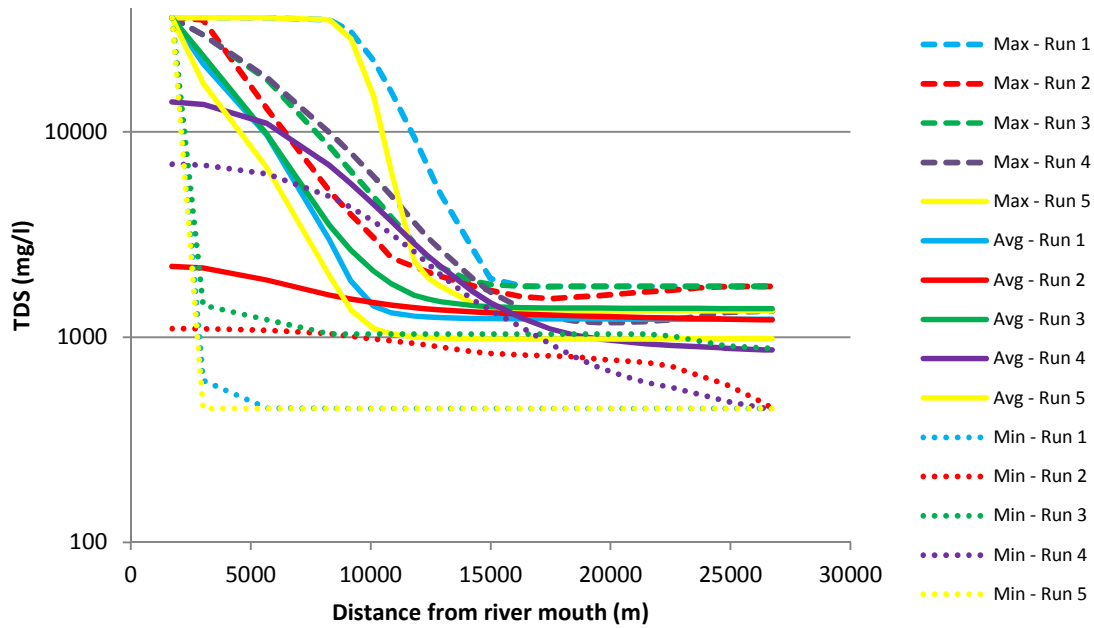
**Figure 9-3: Predicted TDS as a function of river chainage. Maximum, average and minimum TDS values indicated per run during simulation of Scenario A.**
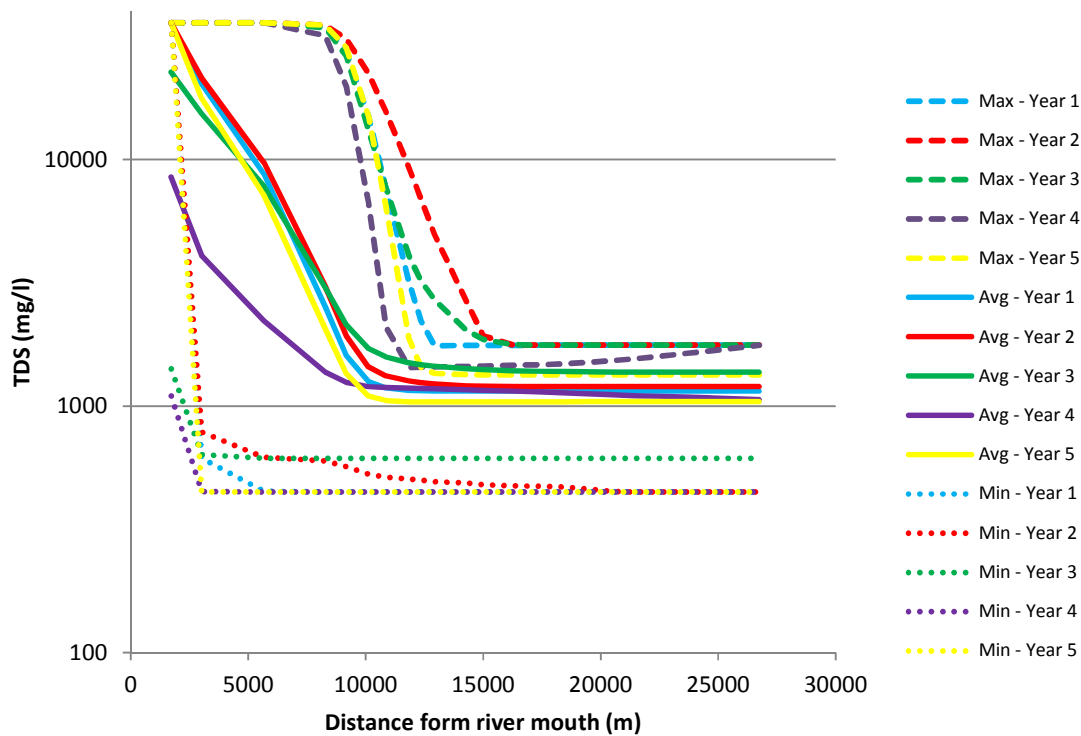


**Figure 9-4: Predicted TDS as a function of river chainage. Maximum, average and minimum TDS values indicated per year of Scenario A simulation.**

124

**Table 9-2: TDS statistics per run for selected river sites.**

| | Run | Distance from river mouth (m) | | | | | | | |
|---|---|---|---|---|---|---|---|---|---|
| | | A1 | B | C | D | E | F | G | H |
| | | 1714 | 3012 | 5664 | 8273 | 10858 | 14990 | 20574 | 24811 |
| Max TDS (mg/l) | 1 | 36000 | 36000 | 36000 | 35223 | 15628 | 1933 | 1768 | 1768 |
| | 2 | 36000 | 35201 | 12991 | 5162 | 2440 | 1689 | 1629 | 1765 |
| | 3 | 36000 | 29726 | 17948 | 8496 | 3845 | 1803 | 1767 | 1768 |
| | 4 | 36000 | 29691 | 18404 | 9939 | 4890 | 1659 | 1181 | 1319 |
| | 5 | 36000 | 36000 | 36000 | 35214 | 6433 | 1341 | 1341 | 1341 |
| Avg TDS | 1 | 36000 | 21456 | 9689 | 2987 | 1314 | 1229 | 1224 | 1224 |
| | 2 | 2203 | 2168 | 1893 | 1599 | 1433 | 1314 | 1251 | 1224 |
| | 3 | 36000 | 23490 | 9763 | 3511 | 1820 | 1405 | 1383 | 1377 |
| | 4 | 13981 | 13620 | 11015 | 6880 | 3677 | 1469 | 948 | 883 |
| | 5 | 36000 | 17212 | 6729 | 1998 | 1036 | 978 | 979 | 982 |
| Min TDS (mg/l) | 1 | 36000 | 616 | 451 | 449 | 449 | 449 | 449 | 449 |
| | 2 | 1101 | 1099 | 1082 | 1041 | 960 | 833 | 766 | 588 |
| | 3 | 36000 | 1428 | 1215 | 1037 | 1035 | 1035 | 1035 | 906 |
| | 4 | 6965 | 6892 | 6251 | 4857 | 3179 | 1354 | 645 | 488 |
| | 5 | 36000 | 449 | 449 | 449 | 449 | 449 | 449 | 449 |

**Table 9-3: TDS statistics per year for selected river sites.**

| | Year | Distance from river mouth (m) | | | | | | | |
|---|---|---|---|---|---|---|---|---|---|
| | | A1 | B | C | D | E | F | G | H |
| | | 1714 | 3012 | 5664 | 8273 | 10858 | 14990 | 20574 | 24811 |
| Max TDS (mg/l) | 1 | 36000 | 36000 | 36000 | 34770 | 7627 | 1766 | 1768 | 1768 |
| | 2 | 36000 | 36000 | 36000 | 35223 | 15628 | 1933 | 1768 | 1768 |
| | 3 | 36000 | 36000 | 36000 | 34357 | 7692 | 1865 | 1768 | 1768 |
| | 4 | 36000 | 36000 | 35997 | 31913 | 2095 | 1455 | 1534 | 1682 |
| | 5 | 36000 | 36000 | 36000 | 35214 | 6433 | 1341 | 1341 | 1341 |
| Avg TDS (mg/l) | 1 | 36000 | 20263 | 8758 | 2528 | 1186 | 1150 | 1151 | 1151 |
| | 2 | 36000 | 21430 | 9740 | 3054 | 1326 | 1204 | 1198 | 1199 |
| | 3 | 22702 | 15345 | 7789 | 3021 | 1582 | 1406 | 1372 | 1371 |
| | 4 | 8507 | 4077 | 2218 | 1373 | 1190 | 1159 | 1111 | 1078 |
| | 5 | 36000 | 17708 | 7190 | 2055 | 1052 | 1039 | 1041 | 1041 |
| Min TDS (mg/l) | 1 | 36000 | 616 | 451 | 449 | 449 | 449 | 449 | 449 |
| | 2 | 36000 | 786 | 620 | 600 | 515 | 480 | 450 | 449 |
| | 3 | 1416 | 636 | 615 | 615 | 615 | 615 | 615 | 615 |
| | 4 | 1101 | 450 | 449 | 449 | 449 | 449 | 449 | 449 |
| | 5 | 36000 | 449 | 449 | 449 | 449 | 449 | 449 | 449 |

## 9.2  Scenario B - Flood hydrograph bathymetries

Refer to Figure 9-5 and Table 9-4 for the predicted TDS over the estuary (model) area for different bathymetries (one dimensional network and accompanying cross sections) used. The bathymetry used is indicated by the series legend, "Q2 – Max" refers to the maximum salinity at a location in the model when the resultant bed levels of a flood of return period 1:2 years is used. As the hydrodynamic boundary conditions used for the one dimensional simulation of Scenario B are equal (Section 8.4.1.2) the variation in predicted salinity is purely related to the model bathymetry due to the morphological results of the two dimensional simulation of Scenario B. The tidal boundary is at a location of -2000 m from the reference point; this is why the maximum salinity at site A is less than 36000 mg/l. Salt intrusion is in the form of a saline wedge. The saline intrusion is again only noticeable up to Site E, validating the observations by previous studies and Savenije (2005). There is no influence of the ocean on Site F, unlike what was noticed in Scenario A, The greatest average salinity is associated with the cross section derived from the 100 year flood event and the minimum with the cross sections associated with the 2 year return period flood. This is purely related to the fact that the tidal inlet constriction is reduced for larger floods. Site E is significantly more saline after the $Q_{100}$.
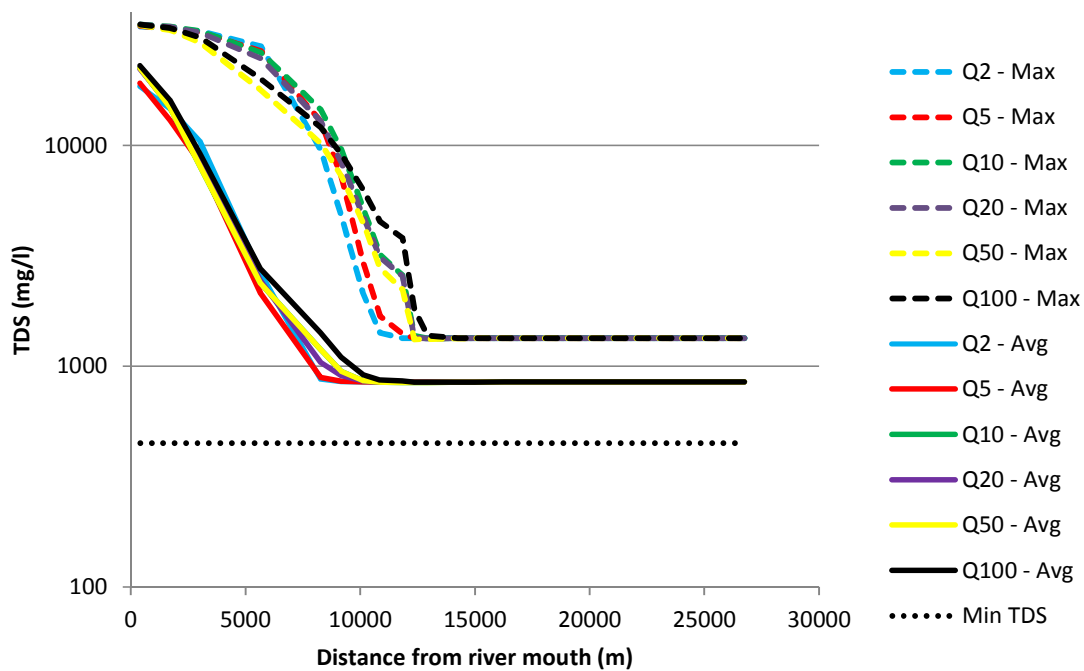


**Figure 9-5: Predicted TDS along the river for various flood bathymetries used.**

**Table 9-4: TDS statistics for flood cross-section scenarios. Red cells indicate high TDS, green indicates low TDS (the colour scale in the table relates to different TDS values for the maximum and average cases).**

| | Cross Sections | Site | | | | | | | |
|---|---|---|---|---|---|---|---|---|---|
| | | A | B | C | D | E | F | G | H |
| | | 405 | 3012 | 5664 | 8273 | 10858 | 14990 | 20574 | 24811 |
| Max TDS (mg/l) | Q2 | 34610 | 32957 | 28188 | 9572 | 1419 | 1341 | 1341 | 1341 |
| | Q5 | 34798 | 32574 | 26852 | 12897 | 1691 | 1341 | 1341 | 1341 |
| | Q10 | 35363 | 33009 | 26408 | 14543 | 3207 | 1341 | 1341 | 1341 |
| | Q20 | 35388 | 32484 | 24818 | 12859 | 3119 | 1341 | 1341 | 1341 |
| | Q50 | 34994 | 29289 | 17861 | 10232 | 2789 | 1340 | 1341 | 1341 |
| | Q100 | 35344 | 30897 | 20016 | 12100 | 4535 | 1341 | 1341 | 1341 |
| | | | | | | | | | |
| Avg TDS (mg/l) | Q2 | 18505 | 10451 | 2626 | 873 | 850 | 850 | 850 | 850 |
| | Q5 | 19156 | 8362 | 2139 | 892 | 849 | 850 | 850 | 850 |
| | Q10 | 21804 | 9110 | 2580 | 1080 | 849 | 849 | 850 | 850 |
| | Q20 | 22160 | 8815 | 2439 | 1043 | 848 | 849 | 850 | 850 |
| | Q50 | 22417 | 8093 | 2374 | 1193 | 847 | 848 | 850 | 850 |
| | Q100 | 23009 | 9208 | 2755 | 1416 | 867 | 848 | 850 | 850 |
| | | | | | | | | | |
| Min TDS (mg/l) | Q2 | 449 | 449 | 449 | 449 | 449 | 449 | 449 | 449 |
| | Q5 | 454 | 449 | 449 | 449 | 449 | 449 | 449 | 449 |
| | Q10 | 461 | 449 | 449 | 449 | 449 | 449 | 449 | 449 |
| | Q20 | 448 | 449 | 449 | 449 | 449 | 449 | 449 | 449 |
| | Q50 | 570 | 449 | 449 | 449 | 449 | 449 | 449 | 449 |
| | Q100 | 552 | 449 | 449 | 449 | 449 | 449 | 449 | 449 |

## 9.3   Summary of results of Scenarios A and B salinity simulations

The estuary salinity is determined by the tide. The salt intrusion length is directly related to the intrusion of the tide which is a function of the state of the tidal inlet. Salts generally intrude up to Site E (10 km), where after the estuarine salinity drops rapidly during open mouth states. The salt intrusion in the estuary is of the well mixed type during closed mouth conditions. During closed mouth conditions the estuary is generally fresher than during open mouth states.

# 10  CONCLUSIONS AND RECOMMENDATIONS

The two scenarios (Scenario A and B) of this study were successfully modelled by the combination of two numerical models (i.e. a two dimensional model, Mike21C and a one dimensional model, Mike11). Mike21C was used to obtain insight into the morphodynamics of the estuary and its output was used as input into the Mike11 model to investigate the salinity in the estuary. Both models were successfully calibrated with data acquired during field work conducted 5-7 May 2012.

The morphodynamic environment clearly reflects on the saline characteristics of the Great Fish River Estuary, especially when mouth closure is simulated. Accuracy is probably reduced when working across model interfaces. However in view of other error inducing phenomena such as poor boundary conditions, inadequate survey information and field measurements the error caused by the interface of the 1D and 2D models is considered insignificant. From the results of the 2D and 1D simulations the following trends were observed:

- During open mouth conditions the estuary is filled with fluvial sediments and the mouth inlet area reduces, the sedimentation process is however extremely slow. Inlet sedimentation would occur at a higher rate with the presence of an offshore wave climate and associated marine sediments – which was not modelled in this study.
- After manual mouth closure the estuary fills up behind the mouth and starts to experience overtopping. The overtopping is sufficient to re-establish a subdued tidal environment. The subdued tidal environment is maintained up to the occurrence of a flood which completely breaches the mouth, the mouth after the breach resembles the pre-closure state.
- During floods the estuary is flushed of sediments and overtopping occurs at the estuary sandbar.
- The upstream reach of the model was under constant erosion, this is possibly due to the incorrect bed grading specified in the model, as the upper reach has a steeper river slope. It can be expected that larger diameter sediments are prevalent which are less prone to erosion.
- The middle reach experiences the greatest erosion during floods; this area coincides with the end of the relatively steep upstream river bed slope and the start of the relatively flat estuarine bed slope. Additionally the areas that experience pronounced erosion are located in river bends and areas with steep river banks, both factors contributing to large flow velocities and consequently high erosion rates.
- Salt intrusion is typically noticeable up to 10 km upstream of the mouth and drops rapidly further upstream. This is mainly related to the tidal period (diurnal tide) of the South African coastline.
- Tidal effects were noticeable up to 15 km upstream of the river mouth, as salt intrusion was only noticeable up to 10 km it is evident that the water level variations more than 10 km upstream can be attributed to back water pressure from the tidal flows.
- The estuary is less saline when the mouth is closed.
- The larger the tidal inlet the greater the salt intrusion, as the tidal inlet area is enlarged after floods - larger floods promotes increased salt intrusion.

Salt intrusion is predominantly driven by the tide; consequently the salinity inside the estuary is, for all intents and purposes, dependent on the state of the estuary mouth and the tidal channels.

This study omits three aspects that influence the morphodynamic and saline environment of the estuary:

- As salts and sediment transport is not modelled simultaneously the flocculation of cohesive sediments due to the interaction of cohesive suspended sediments and salt water is not investigated.
- No wave boundary conditions were included in the model. Mouth closure and the related influx of marine sediments are mostly attributed to the offshore wave environment.
- Evaporation and rainfall was not included during salinity modelling. The effect of these aspects on the estuary salinity is debatable as the mouth does not remain closed for extended periods of time.

As the saline characteristics of the estuary are dependent on the sea it is recommended that a numerical model is used which has wave modelling capabilities and support for advection dispersion modelling of salts and cohesive sediments. If future studies are done it is recommended that the model area is limited to the estuarine area which experiences tidal effects, in this exercise tidal effects were generally noticeable up to 15 km upstream of the river mouth. Computational speed is directly related to grid size and as such a grid of half the size will compute two times faster. The two-dimensional model study is immensely computer taxing and time consuming, especially to the inexperienced modeller. Long term morphological simulations can take weeks at a time. As such it is the view of the author that models should be optimized for speed either by obtaining more powerful computers and the needed licensing or by limiting the scope of the models. When complex scenarios are modelled it is difficult to differentiate between the driving factors behind the phenomenon observed.

# REFERENCES

Beck, J.S., 2005. *Sediment Transport Dynamics in South African Estuaries*. Stellenbosch University.

Cooper, J.A.G., 2001. Geomorphological variability among microtidal estuaries from the wave-dominated South African coast.

Cooper, J.A.G., 1994. Sedimentary processes in the river-dominated Mvoti estuary, South Africa. , 9, pp.271–300.

Cooper, J.A.G., 2002. The role of extreme floods in estuary-coastal behaviour: contrasts between river- and tide-dominated microtidal estuaries. *Sedimentary Geology*, 150, pp.123–137.

Davies, J., 1964. A morphogenic approach to the world's shorelines. *Geomorphology*, 8, pp.127–142.

Department Water and Sanitation, 2014. DWS. *Verified data from the Hydrological Information System and Peak Flows (monthly and hydrological year)*. Available at: www.dwaf.gov.sa/Hydrology/.

Department Water and Sanitation - Resource Quality Information Services, 2014. DWS-RQIS. Available at: www.dwaf.gov.sa/iwqs/.

DHI, 2011a. *Mike 11 - a Modelling Sytem for Rivers and Channels* DHI, ed., Horsholm, Denmark.

DHI, 2003. *Mike 21 flow model - Hints and recommendations in applications with significant flooding and drying* Mike by DHI, ed., Horsholm, Denmark.

DHI, 2011b. *Mike 21C curvilinear model for river morphology user guide* Mike by DHI, ed., Horsholm, Denmark: Mike by DHI.

DHI, 2011c. *Mike 21C curvilinear model scientific documentation*, Horsholm, Denmark: Mike by DHI.

Doodson, A.T., 1921. The Harmonic Development of the Tide-Generating Potential. *Proceedings of the Royal Society A: Mathematical, Physical and Engineering Sciences*, 100(704), pp.305–329. Available at: http://rspa.royalsocietypublishing.org/cgi/doi/10.1098/rspa.1921.0088 [Accessed October 6, 2014].

Dorfmann, C. & Knoblauch, H., 2009. ADCP measurements in a reservoir of a run-of-river hydro power plant. *6th International Symposium on Ultrasonic Doppler Methods for Fluid Mechanics and Fluid Engineering*, pp.45–48.

Dyer, K.R., 1997. *Estuaries: a physical introduction*, Chichester: John Wiley & Sons Ltd.

Engelund, F. & Hansen, E., 1967. *A monograph on sediment transport in alluvial channels*, Copenhagen, Denmark: Danish Technological University.

Escoffier, F.F., 1940. The stability of tidal inlets. *Shore and Beach*, 8, pp.111–114.

Fisher, H. et al., 1979. *Mixing in inland and coastal waters*, New York: Academic Press.

Galappatti, R., 1983. *A depth-integrated model for suspended transport*,

Google, 2014. Google Earth Pro 7.1. Available at: www.google.com/earth.

Grange, N. et al., 2000. The response of two South African east coast estuaries to altered river flow regimes. , 177(January), pp.155–177.

Grange, N. & Allanson, B.R., 1995. The influence of freshwater inflow on the nature, amount and distribution of seston in estuaries of the Eastern Cape, South Africa. *Estuarine, Coastal and Shelf Science*, 40, pp.403–420.

Hayes, M.O., 1975. *Morphology of sand accumulation in estuaries* Estuarine ., New York: Academic Press.

Leser, G., van Kester, J. & Roelvink, J.A., 2000. *On-line Sediment Transport within Delft3D-FLOW*, Delft.

Ter Morshuizen, L.D., Whitfield, a. K. & Paterson, a. W., 1996. Influence of Freshwater Flow Regime on Fish Assemblages in the Great Fish River and Estuary. *Southern African Journal of Aquatic Sciences*, 22(1-2), pp.52–61. Available at: http://www.tandfonline.com/doi/abs/10.1080/10183469.1996.9631372 [Accessed October 6, 2014].

Msadala, V. et al., 2010. Sediment Yield Prediction for South Africa : 2010 Edition. , (1765).

Nichols, M. & Biggs, R., 1985. *Estuaries* R. Davis, ed., New York: Springer-Verlag.

NRIO, 1987. *Basic physical geography/hydro data for "estuaries" of the souther-eastern Cape*, Stellenbosch.

O'Keeffe, J.H. & De Moor, F.C., 1988. Changes in the physico-chemistry and benthic invertebrates of the Great Fish River, South Africa, following an interbasin transfer of water. *Regulated Rivers: Research and Management*, 2, pp.39–55.

Open University, 1999. *Waves, Tides and Shallow-Water Processes* 2nd ed., Butterworth Heineman.

Özsoy, E. & Ünlüata, Ü., 1982. Ebb - tidal Flow Characteristics near Inlets. *Estuarine, Coastal and Shelf Science*, 14, pp.251–263.

Ranasinghe, R., Pattiaratchi, C. & Masselink, G., 1999. A morphodynamic Model to Simulate the Seasonal Closure of Tidal Inlets. *Coastal Engineering*, 34, pp.1–36.

Reddering, J.S.. & Esterhuysen, K., 1982. Fluvial dominated sedimentation in the Great Fish estuary. *ROSIE Report 4*.

Reddering, J.S.. & Rust, I.C., 1990. Historical changes and sedimentary characteristics of souther African estuaries. *South African Journal of Science*, (86), pp.425–428.

Van Rijn, L.C., 1984. Part 1: Bed load transport & Part 2: Suspended load transport. *Jouranl of hydraulic engineering*, 110.

Rooseboom, A. et al., 2007. *Drainage Manual* 5th Editio. E. Kruger, ed., South African National Roads Agency.

SANHO, 2012. *South African Tide Tables 2012*, Simons Town: Office, South African Navy Hydrographic.

Savenije, H., 2005. *Salinity and Tides in Alluvial Estuaries*, Elsevier.

Savenije, H.H.G., 1993. Predictive model for salt intrusion in estuaries. *Journal of Hydrology*, 148(1-4), pp.203–218. Available at: http://linkinghub.elsevier.com/retrieve/pii/002216949390260G.

Savenije, H.H.G., 2012. Salinity and tides in alluvial estuaries.

Schumann, E., 2003. *Towards the management of marine sedimentation in South African estuaries with special reference to the Eastern Cape*,

Talmon, A.M., Struiksma, N. & van Mierlo, M.C.L.M., 1995. Laboratory measurements of the direction of sediment transport on transverse alluvial bed slopes. *J. Hyd.*, 33(no 4).

Tanser, F. & Palmer, A.R., 2000. Vegetation mapping of the Great Fish River basin , South Africa : Integrating spatial and multi-spectral remote sensing techniques. *Applied Vegetation Science*, 3, pp.197–203.

Tran, T.-T. et al., 2012. Cross-sectional stability of tidal inlets: A comparison between numerical and empirical approaches. *Coastal Engineering*, 60, pp.21–29. Available at: http://linkinghub.elsevier.com/retrieve/pii/S0378383911001554 [Accessed October 6, 2014].

USBR, 2006. *Erosion and Sedimentation Manual* Bureau of Reclamation, ed., Denver, Colorado: U.S. Department of the Interior.

Vorwerk, P.D., 2006. *A PRELIMINARY EXAMINATION OF SELECTED BIOLOGICAL LINKS BETWEEN FOUR EASTERN CAPE ESTUARIES AND THE INSHORE MARINE ENVIRONMENT*. Rhodes University.

Whitfield, A.K., 1992. A Characterization of South African Estuarine Systems. *Southern African Journal of Aquatic Sciences*, (18 (1/2)), pp.89–103.

Whitfield, A.K., 1995. *Available scientific information on individual South African estuarine systems*,

Yang, C.T., 1983. Rate of energy dissipation and River Sedimentation. *Procedings of the 2nd international Symposium on River Sedimentation*, pp.575–585.

**Appendix A: Hydrodynamic model simulation results (uncalibrated for fieldwork planning)**
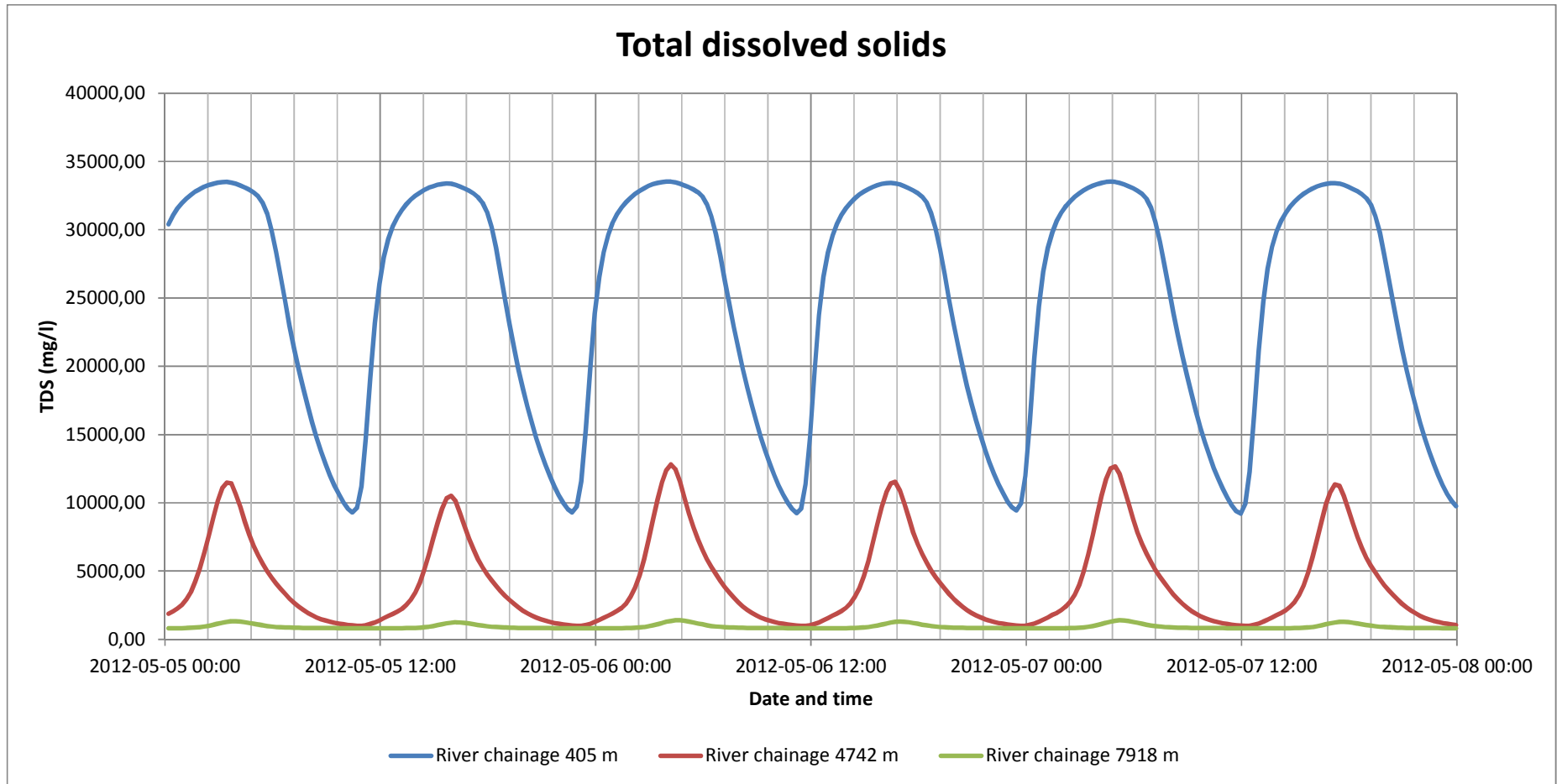
Figure A1: Simulated 1D model results (uncalibrated) of TDS concentration (mg/l) for chainages 405, 4742 and 7918 meters
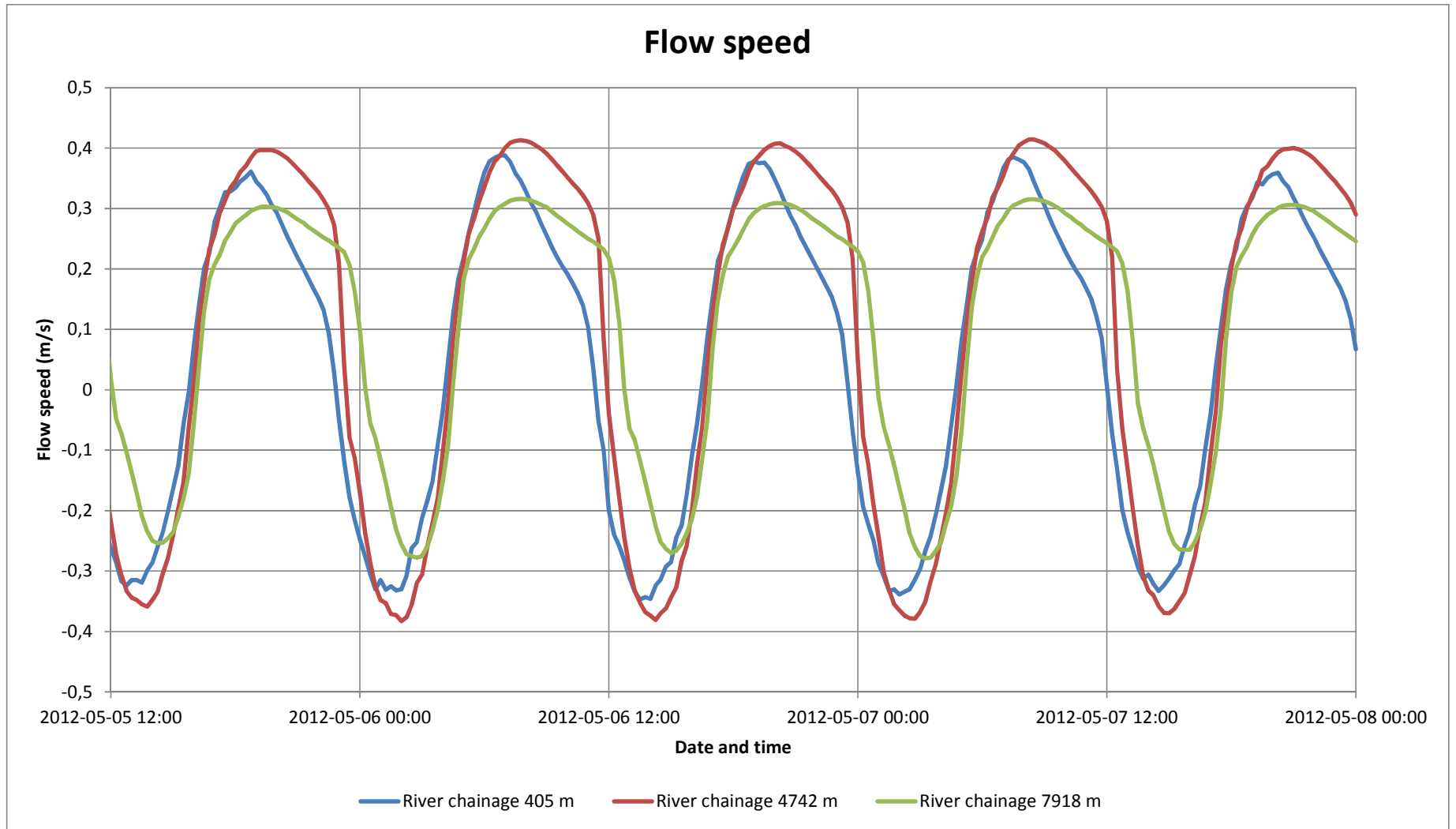
Figure A2: Simulated 1D model results (uncalibrated) of flow speed in meters per second for chainages 405, 4742 and 7918 meters

**Appendix B: Observed river discharge at gauging station Q9H018 (DWA website)**

| Date and time | Q9H018 Matomela Discharge (m³/s) |
|---|---|
| 2012/05/05 06:06 | 14.640 |
| 2012/05/05 06:12 | 14.400 |
| 2012/05/05 07:48 | 14.227 |
| 2012/05/05 07:54 | 13.963 |
| 2012/05/05 08:54 | 13.925 |
| 2012/05/05 09:00 | 13.888 |
| 2012/05/05 10:12 | 13.777 |
| 2012/05/05 10:18 | 13.720 |
| 2012/05/05 11:54 | 13.614 |
| 2012/05/05 12:00 | 13.515 |
| 2012/05/05 14:00 | 13.278 |
| 2012/05/05 14:06 | 13.072 |
| 2012/05/05 14:18 | 13.057 |
| 2012/05/05 14:24 | 13.042 |
| 2012/05/05 16:18 | 12.854 |
| 2012/05/05 16:24 | 12.775 |
| 2012/05/05 17:12 | 12.676 |
| 2012/05/05 17:18 | 12.621 |
| 2012/05/05 18:36 | 12.458 |
| 2012/05/05 18:42 | 12.284 |
| 2012/05/05 19:54 | 12.195 |
| 2012/05/05 20:00 | 12.058 |
| 2012/05/05 23:24 | 11.859 |
| 2012/05/05 23:30 | 11.670 |
| 2012/05/06 00:00 | 11.628 |
| 2012/05/06 00:06 | 11.523 |
| 2012/05/06 08:42 | 11.112 |
| 2012/05/06 08:48 | 10.693 |
| 2012/05/06 09:12 | 10.632 |
| 2012/05/06 09:18 | 10.594 |
| 2012/05/06 09:30 | 10.589 |
| 2012/05/06 09:36 | 10.583 |
| 2012/05/06 09:42 | 10.579 |
| 2012/05/06 09:48 | 10.576 |
| 2012/05/06 10:00 | 10.570 |
| 2012/05/06 10:06 | 10.565 |
| 2012/05/06 10:18 | 10.559 |
| 2012/05/06 10:24 | 10.554 |
| 2012/05/06 10:30 | 10.550 |
| 2012/05/06 10:36 | 10.546 |
| 2012/05/06 10:42 | 10.543 |
| 2012/05/06 10:48 | 10.539 |
| 2012/05/06 10:54 | 10.535 |

| Date and time | Q9H018 Matomela Discharge (m³/s) |
|---|---|
| 2012/05/06 11:00 | 10.532 |
| 2012/05/06 11:06 | 10.528 |
| 2012/05/06 11:12 | 10.488 |
| 2012/05/06 11:18 | 10.447 |
| 2012/05/06 11:24 | 10.442 |
| 2012/05/06 11:30 | 10.436 |
| 2012/05/06 11:36 | 10.431 |
| 2012/05/06 11:42 | 10.426 |
| 2012/05/06 11:48 | 10.421 |
| 2012/05/06 11:54 | 10.416 |
| 2012/05/06 12:00 | 10.411 |
| 2012/05/06 12:06 | 10.406 |
| 2012/05/06 12:12 | 10.401 |
| 2012/05/06 12:18 | 10.396 |
| 2012/05/06 12:24 | 10.391 |
| 2012/05/06 12:36 | 10.383 |
| 2012/05/06 12:42 | 10.375 |
| 2012/05/06 12:48 | 10.335 |
| 2012/05/06 12:54 | 10.295 |
| 2012/05/06 13:06 | 10.288 |
| 2012/05/06 13:12 | 10.281 |
| 2012/05/06 13:30 | 10.272 |
| 2012/05/06 13:36 | 10.263 |
| 2012/05/06 13:54 | 10.255 |
| 2012/05/06 14:00 | 10.246 |
| 2012/05/06 14:24 | 10.235 |
| 2012/05/06 14:30 | 10.224 |
| 2012/05/06 15:42 | 10.122 |
| 2012/05/06 15:48 | 10.085 |
| 2012/05/06 16:24 | 10.018 |
| 2012/05/06 16:30 | 9.940 |
| 2012/05/06 17:48 | 9.817 |
| 2012/05/06 17:54 | 9.751 |
| 2012/05/06 19:36 | 9.705 |
| 2012/05/06 19:42 | 9.618 |
| 2012/05/06 21:54 | 9.549 |
| 2012/05/06 22:00 | 9.457 |
| 2012/05/07 00:00 | 9.389 |
| 2012/05/07 00:06 | 9.312 |
| 2012/05/07 01:36 | 9.260 |
| 2012/05/07 01:42 | 9.243 |
| 2012/05/07 12:06 | 9.125 |
| 2012/05/07 12:12 | 9.074 |

| Date and time | Q9H018 Matomela Discharge (m³/s) |
|---|---|
| 2012/05/07 15:54 | 8.978 |
| 2012/05/07 16:00 | 8.903 |
| 2012/05/07 17:30 | 8.893 |
| 2012/05/07 17:36 | 8.882 |
| 2012/05/07 18:54 | 8.873 |
| 2012/05/07 19:00 | 8.864 |
| 2012/05/07 20:06 | 8.790 |
| 2012/05/07 20:12 | 8.775 |
| 2012/05/07 21:48 | 8.758 |
| 2012/05/07 21:54 | 8.742 |
| 2012/05/08 00:00 | 8.684 |

**Appendix C: Measured water levels at bridge (height from bridge deck)**

Note: *Height below bridge deck

| Date | Time | Water level *(mm) | Date | Time | Water Level *(mm) |
|------|------|-------------------|------|------|-------------------|
| 5 May 2012 | 10:15 | -7600 | 5 May 2012 | 14:00 | -6650 |
| 5 May 2012 | 10:30 | -7600 | 5 May 2012 | 14:15 | -6500 |
| 5 May 2012 | 10:45 | -7600 | 5 May 2012 | 14:30 | -6370 |
| 5 May 2012 | 11:00 | -7500 | 5 May 2012 | 14:45 | -6300 |
| 5 May 2012 | 11:15 | -7460 | 5 May 2012 | 15:00 | -6230 |
| 5 May 2012 | 11:30 | -7400 | 5 May 2012 | 15:15 | -6200 |
| 5 May 2012 | 11:45 | -7340 | 5 May 2012 | 15:30 | -6000 |
| 5 May 2012 | 12:00 | -7260 | 5 May 2012 | 15:45 | -5800 |
| 5 May 2012 | 12:15 | -7200 | 5 May 2012 | 16:00 | -5930 |
| 5 May 2012 | 12:30 | -7160 | 5 May 2012 | 16:15 | -5970 |
| 5 May 2012 | 12:45 | -7120 | 5 May 2012 | 16:30 | -6060 |
| 5 May 2012 | 13:00 | n/a | 5 May 2012 | 16:45 | -6120 |
| 5 May 2012 | 13:15 | -6900 | 5 May 2012 | 17:00 | -6150 |
| 5 May 2012 | 13:30 | -6800 | 5 May 2012 | 17:15 | n/a |
| 5 May 2012 | 13:45 | n/a | 5 May 2012 | 17:30 | -6400 |

| Date | Time | Water level * (mm) | Date | Time | Water Level *(mm) |
|------|------|--------------------|------|------|-------------------|
| 6 May 2012 | 07:30 | -6800 | 6 May 2012 | 13:00 | n/a |
| 6 May 2012 | 07:45 | -6920 | 6 May 2012 | 13:15 | n/a |
| 6 May 2012 | 08:00 | -7050 | 6 May 2012 | 13:30 | -6790 |
| 6 May 2012 | 08:15 | -7090 | 6 May 2012 | 13:45 | -6600 |
| 6 May 2012 | 08:30 | -7170 | 6 May 2012 | 14:00 | -6500 |
| 6 May 2012 | 08:45 | -7230 | 6 May 2012 | 14:15 | -6320 |
| 6 May 2012 | 09:00 | -7240 | 6 May 2012 | 14:30 | -6210 |
| 6 May 2012 | 09:15 | -7280 | 6 May 2012 | 14:45 | -6030 |
| 6 May 2012 | 09:30 | -7380 | 6 May 2012 | 15:00 | -6030 |
| 6 May 2012 | 09:45 | -7380 | 6 May 2012 | 15:15 | -6010 |
| 6 May 2012 | 10:00 | -7400 | 6 May 2012 | 15:30 | -5940 |
| 6 May 2012 | 10:15 | -7440 | 6 May 2012 | 15:45 | n/a |
| 6 May 2012 | 10:30 | n/a | 6 May 2012 | 16:04 | -6000 |
| 6 May 2012 | 10:45 | -7520 | 6 May 2012 | 16:15 | -6000 |
| 6 May 2012 | 11:00 | n/a | 6 May 2012 | 16:30 | -6000 |
| 6 May 2012 | 11:17 | -7480 | 6 May 2012 | 16:45 | -6030 |
| 6 May 2012 | 11:30 | n/a | 6 May 2012 | 17:00 | -6000 |
| 6 May 2012 | 11:47 | -7420 | 6 May 2012 | 17:15 | -6200 |
| 6 May 2012 | 12:00 | n/a | 6 May 2012 | 17:30 | -6250 |
| 6 May 2012 | 12:15 | n/a | 6 May 2012 | 17:45 | n/a |
| 6 May 2012 | 12:21 | -7230 | 6 May 2012 | 18:00 | -6380 |
| 6 May 2012 | 12:45 | n/a | | | |

| Date | Time | Water level *(mm) |
|------|------|-------------------|
| 7 May 2012 | 07:30 | -6750 |
| 7 May 2012 | 07:45 | -6800 |
| 7 May 2012 | 08:00 | -6900 |
| 7 May 2012 | 08:15 | -7030 |
| 7 May 2012 | 08:30 | -7070 |
| 7 May 2012 | 08:45 | -7140 |
| 7 May 2012 | 09:00 | -7240 |
| 7 May 2012 | 09:15 | -7270 |
| 7 May 2012 | 09:30 | -7320 |
| 7 May 2012 | 09:45 | -7380 |
| 7 May 2012 | 10:00 | -7400 |
| 7 May 2012 | 10:15 | -7470 |
| 7 May 2012 | 10:30 | -7550 |
| 7 May 2012 | 10:45 | -7550 |
| 7 May 2012 | 11:00 | -7590 |

X

**Appendix D: Sea water levels generated by WXTide32 software**

| Date | Time | Water Level (MSL) |
| --- | --- | --- |
| 05-May-12 | 00:00 | 0.439 |
| 05-May-12 | 01:00 | 0.854 |
| 05-May-12 | 02:00 | 1.139 |
| 05-May-12 | 03:00 | 1.229 |
| 05-May-12 | 04:00 | 1.089 |
| 05-May-12 | 05:00 | 0.759 |
| 05-May-12 | 06:00 | 0.314 |
| 05-May-12 | 07:00 | -0.131 |
| 05-May-12 | 08:00 | -0.466 |
| 05-May-12 | 09:00 | -0.601 |
| 05-May-12 | 10:00 | -0.516 |
| 05-May-12 | 11:00 | -0.216 |
| 05-May-12 | 12:00 | 0.204 |
| 05-May-12 | 13:00 | 0.649 |
| 05-May-12 | 14:00 | 0.999 |
| 05-May-12 | 15:00 | 1.174 |
| 05-May-12 | 16:00 | 1.119 |
| 05-May-12 | 17:00 | 0.849 |
| 05-May-12 | 18:00 | 0.429 |
| 05-May-12 | 19:00 | -0.026 |
| 05-May-12 | 20:00 | -0.401 |
| 05-May-12 | 21:00 | -0.596 |
| 05-May-12 | 22:00 | -0.561 |
| 05-May-12 | 23:00 | -0.306 |
| 06-May-12 | 00:00 | 0.114 |
| 06-May-12 | 01:00 | 0.589 |
| 06-May-12 | 02:00 | 0.999 |
| 06-May-12 | 03:00 | 1.244 |
| 06-May-12 | 04:00 | 1.264 |
| 06-May-12 | 05:00 | 1.039 |
| 06-May-12 | 06:00 | 0.639 |
| 06-May-12 | 07:00 | 0.149 |
| 06-May-12 | 08:00 | -0.296 |
| 06-May-12 | 09:00 | -0.586 |
| 06-May-12 | 10:00 | -0.656 |
| 06-May-12 | 11:00 | -0.486 |
| 06-May-12 | 12:00 | -0.116 |
| 06-May-12 | 13:00 | 0.349 |
| 06-May-12 | 14:00 | 0.804 |
| 06-May-12 | 15:00 | 1.119 |
| 06-May-12 | 16:00 | 1.224 |
| 06-May-12 | 17:00 | 1.099 |
| 06-May-12 | 18:00 | 0.759 |

| 06-May-12 | 19:00 | 0.299 |
| 06-May-12 | 20:00 | -0.156 |
| 06-May-12 | 21:00 | -0.496 |
| 06-May-12 | 22:00 | -0.626 |
| 06-May-12 | 23:00 | -0.516 |
| 07-May-12 | 00:00 | -0.196 |
| 07-May-12 | 01:00 | 0.259 |
| 07-May-12 | 02:00 | 0.729 |
| 07-May-12 | 03:00 | 1.099 |
| 07-May-12 | 04:00 | 1.274 |
| 07-May-12 | 05:00 | 1.209 |
| 07-May-12 | 06:00 | 0.919 |
| 07-May-12 | 07:00 | 0.479 |
| 07-May-12 | 08:00 | -0.011 |
| 07-May-12 | 09:00 | -0.421 |
| 07-May-12 | 10:00 | -0.636 |
| 07-May-12 | 11:00 | -0.626 |
| 07-May-12 | 12:00 | -0.376 |
| 07-May-12 | 13:00 | 0.029 |
| 07-May-12 | 14:00 | 0.499 |
| 07-May-12 | 15:00 | 0.914 |
| 07-May-12 | 16:00 | 1.169 |
| 07-May-12 | 17:00 | 1.204 |
| 07-May-12 | 18:00 | 0.999 |
| 07-May-12 | 19:00 | 0.629 |
| 07-May-12 | 20:00 | 0.169 |
| 07-May-12 | 21:00 | -0.251 |
| 07-May-12 | 22:00 | -0.521 |
| 07-May-12 | 23:00 | -0.576 |

**Appendix E: Observed salinity, electro conductivity and temperature data**

| 5 May 2012 | | | CSIR (lab) | | | Castaway (field) | | | |
|---|---|---|---|---|---|---|---|---|---|
| Time | Site | Description | Depth below surface (m) | EC (mS/m) | TDS (mg/l) | Depth below surface (m) | Temp (Celsius) | EC (mS/m) | TDS (mg/l) |
| 10:40 | 1A | Min | 0 | 600 | 3576 | 0.15 | 17.46 | 664 | 4699 |
| | | TDS | 0.5 | 640 | 3860 | 0.46 | 17.42 | 683 | 4844 |
| | | | 1 | 650 | 3952 | 0.76 | 17.41 | 689 | 4887 |
| | | | 1.5 | 590 | 4052 | 1.07 | 17.41 | 693 | 4917 |
| | | | 2 | 680 | 4166 | 1.38 | 17.41 | 705 | 5009 |
| | | | | | | 1.68 | 17.41 | 716 | 5094 |
| | | | | | | 1.99 | 17.41 | 719 | 5117 |
| | | | | | | 2.22 | 17.46 | 716 | 5093 |
| | | | | | | | | | |
| 11:24 | 1B | Min | 0 | 180 | 1068 | 0.15 | 17.83 | 165 | 950 |
| | | TDS | 0.5 | 500 | 2992 | 0.46 | 17.85 | 164 | 945 |
| | | | | | | 0.64 | 18.01 | 165 | 948 |
| | | | | | | | | | |
| 11:45 | 1C | Min | 0 | 120 | 760 | 0.15 | 17.87 | 120 | 611 |
| | | TDS | 0.5 | 120 | 736 | 0.46 | 17.88 | 120 | 611 |
| | | | 1 | 120 | 726 | 0.77 | 17.86 | 120 | 609 |
| | | | 1.5 | 122 | 762 | 1.07 | 17.78 | 120 | 610 |
| | | | | | | 1.38 | 17.81 | 120 | 613 |
| | | | | | | 1.57 | 17.83 | 121 | 621 |

XV

| 5 May 2012 | | | CSIR (lab) | | | Castaway (field) | | | |
|---|---|---|---|---|---|---|---|---|---|
| Time | Site | Description | Depth below surface (m) | EC (mS/m) | TDS (mg/l) | Depth below surface (m) | Temp (Celsius) | EC (mS/m) | TDS (mg/l) |
| 12:04 | 1D | Min | 0 | 108 | 682 | 0.15 | 17.66 | 110 | 532 |
| | | TDS | 0.5 | 108 | 686 | 0.46 | 17.58 | 110 | 533 |
| | | | 1 | 108 | 686 | 0.77 | 17.54 | 109 | 529 |
| | | | 1.5 | 108 | 670 | 1.07 | 17.50 | 108 | 522 |
| | | | 2 | 108 | 688 | 1.38 | 17.51 | 108 | 523 |
| | | | | | | 1.69 | 17.51 | 108 | 523 |
| | | | | | | 2.07 | 17.65 | 105 | 502 |
| | | | | | | | | | |
| 12:19 | 1E | Min | 0 | 108 | 682 | 0.15 | 17.50 | 109 | 529 |
| | | TDS | 0.5 | 108 | 664 | 0.46 | 17.49 | 109 | 530 |
| | | | 1 | 108 | 672 | 0.77 | 17.44 | 109 | 530 |
| | | | 1.5 | 107 | 680 | 1.07 | 17.40 | 109 | 530 |
| | | | 2 | 108 | 708 | 1.38 | 17.36 | 109 | 530 |
| | | | | | | 1.69 | 17.38 | 109 | 531 |
| | | | | | | 2.07 | 17.38 | 109 | 530 |
| | | | | | | | | | |
| 15:40 | 3A | Max | 0 | 5200 | 39386 | 0.15 | 17.48 | 5477 | 40883 |
| | | TDS | 0.5 | 5000 | 38574 | 0.45 | 17.49 | 5472 | 40844 |
| | | | 1 | 5200 | 39740 | 0.75 | 17.49 | 5473 | 40850 |
| | | | 1.5 | 5200 | 40312 | 1.04 | 17.49 | 5468 | 40817 |
| | | | 2 | 5200 | 38818 | 1.34 | 17.49 | 5464 | 40789 |
| | | | 3 | 5200 | 40208 | 1.64 | 17.49 | 5453 | 40700 |
| | | | | | | | | | |
| | | | | | | | | | |
| | | | | | | | | | |
| | | | | | | | | | |

| 5 May 2012 | | | CSIR (lab) | | | Castaway (field) | | | |
|---|---|---|---|---|---|---|---|---|---|
| Time | Site | Description | Depth below surface (m) | EC (mS/m) | TDS (mg/l) | Depth below surface (m) | Temperature (Celsius) | EC (mS/m) | TDS (mg/l) |
| 15:40 | 3A | Max | 4 | 5200 | 39292 | 1.94 | 17.49 | 5441 | 40615 |
| | | TDS | | | | 2.24 | 17.49 | 5433 | 40556 |
| | | | | | | 2.54 | 17.49 | 5433 | 40555 |
| | | | | | | 2.84 | 17.48 | 5435 | 40571 |
| | | | | | | 3.13 | 17.49 | 5429 | 40521 |
| | | | | | | 3.43 | 17.50 | 5432 | 40543 |
| | | | | | | 3.69 | 17.49 | 5398 | 40289 |
| | | | | | | | | | |
| 16:00 | 3B | Max | 0 | 5200 | 39046 | 0.15 | 17.58 | 5371 | 40090 |
| | | TDS | 0.5 | 5200 | 37332 | 0.45 | 17.58 | 5374 | 40111 |
| | | | 1 | 5200 | 38630 | 0.75 | 17.59 | 5377 | 40129 |
| | | | 1.5 | 5200 | 39386 | 1.05 | 17.59 | 5378 | 40140 |
| | | | 2 | 5200 | 38756 | 1.34 | 17.59 | 5380 | 40157 |
| | | | | | | 1.64 | 17.59 | 5385 | 40192 |
| | | | | | | 2.02 | 17.59 | 5433 | 40557 |
| | | | | | | | | | |
| 16:14 | 3C | Max | 0 | 850 | 5220 | 0.15 | 18.55 | 1230 | 8953 |
| | | TDS | 0.5 | 1550 | 9898 | 0.46 | 18.46 | 2198 | 16236 |
| | | | 1 | 4600 | 33562 | 0.76 | 18.06 | 4113 | 30630 |
| | | | 1.5 | 4800 | 34212 | 1.06 | 17.82 | 4922 | 36713 |
| | | | 2 | 4800 | 35268 | 1.36 | 17.76 | 5006 | 37339 |
| | | | | | | 1.66 | 17.75 | 4978 | 37134 |
| | | | | | | 1.96 | 17.76 | 4917 | 36671 |
| | | | | | | 2.23 | 17.77 | 4915 | 36660 |
| | | | | | | | | | |
| | | | | | | | | | |

| 5 May 2012 | | | CSIR (lab) | | | Castaway (field) | | | |
|---|---|---|---|---|---|---|---|---|---|
| Time | Site | Description | Depth below surface(m) | EC (mS/m) | TDS (mg/l) | Depth below surface (m) | Temperature (Celsius) | EC (mS/m) | TDS (mg/l) |
| 16:31 | 3D | Max | 0 | 185 | 1124 | 0.15 | 18.58 | 197 | 1192 |
| | | TDS | 0.5 | 200 | 1174 | 0.46 | 18.57 | 196 | 1181 |
| | | | 1 | 190 | 1094 | 0.77 | 18.57 | 194 | 1170 |
| | | | 1.5 | 190 | 1096 | 1.07 | 18.57 | 194 | 1166 |
| | | | 2 | 195 | 1116 | 1.38 | 18.58 | 196 | 1181 |
| | | | 3 | 200 | 1162 | 1.69 | 18.59 | 202 | 1225 |
| | | | | | | 1.99 | 18.60 | 201 | 1222 |
| | | | | | | 2.30 | 18.60 | 201 | 1218 |
| | | | | | | 2.60 | 18.60 | 201 | 1218 |
| | | | | | | 2.85 | 18.61 | 201 | 1223 |
| | | | | | | | | | |
| | | | | | | | | | |
| 16:48 | 3E | Max | 0 | 110 | 690 | 0.15 | 17.93 | 110 | 539 |
| | | TDS | 0.5 | 109 | 672 | 0.46 | 17.94 | 110 | 538 |
| | | | 1 | 110 | 670 | 0.77 | 17.94 | 110 | 539 |
| | | | 1.5 | 110 | 658 | 1.07 | 17.96 | 110 | 539 |
| | | | 2 | 110 | 652 | 1.38 | 17.97 | 110 | 539 |
| | | | 3 | 110 | 639 | 1.69 | 17.97 | 110 | 539 |
| | | | | | | 1.99 | 17.97 | 110 | 539 |
| | | | | | | 2.30 | 17.98 | 110 | 539 |
| | | | | | | 2.61 | 17.97 | 110 | 539 |
| | | | | | | 2.91 | 17.97 | 110 | 539 |
| | | | | | | 3.31 | 17.98 | 110 | 538 |

XVIII

| 6 May 2012 | | | CSIR (lab) | | | Castaway (field) | | | |
|---|---|---|---|---|---|---|---|---|---|
| Time | Site | Description | Depth below surface(m) | EC (mS/m) | TDS (mg/l) | Depth below surface (m) | Temperature (Celsius) | EC (mS/m) | TDS (mg/l) |
| 09:18 | 4F | Max | 0 | 102 | 591 | 0.15 | 16.57 | 104 | 493 |
| | | TDS | 0.5 | 103 | 566 | 0.46 | 16.56 | 104 | 493 |
| | | | 1 | 103 | 351 | 0.77 | 16.56 | 104 | 493 |
| | | | 1.5 | 103 | 617 | 1.07 | 16.56 | 104 | 493 |
| | | | 2 | 103 | 596 | 1.38 | 16.55 | 104 | 493 |
| | | | 3 | 104 | 652 | 1.69 | 16.55 | 104 | 492 |
| | | | 4 | 103 | 648 | 1.99 | 16.55 | 104 | 493 |
| | | | | | | 2.30 | 16.55 | 104 | 493 |
| | | | | | | 2.61 | 16.55 | 104 | 493 |
| | | | | | | 2.91 | 16.55 | 104 | 493 |
| | | | | | | 3.22 | 16.55 | 104 | 493 |
| | | | | | | 3.52 | 16.55 | 104 | 493 |
| | | | | | | 3.88 | 16.55 | 104 | 493 |
| | | | | | | | | | |
| 15:53 | 7A | Max | 0 | 5200 | 41548 | n/a | n/a | n/a | n/a |
| | | TDS | 0.5 | 5000 | 36652 | n/a | n/a | n/a | n/a |
| | | | 1 | 5200 | 34286 | n/a | n/a | n/a | n/a |
| | | | 1.5 | 5200 | 38642 | n/a | n/a | n/a | n/a |
| | | | 2 | 5200 | 37354 | n/a | n/a | n/a | n/a |
| | | | 3 | 5200 | 38724 | n/a | n/a | n/a | n/a |
| | | | | | | | | | |
| | | | | | | | | | |
| 16:11 | 7B | Max | 0 | 5200 | 39734 | 0.15 | 18.25 | 5435.80 | 40574.11 |
| | | TDS | 0.5 | 5200 | 40504 | 0.45 | 18.24 | 5436.62 | 40580.24 |
| | | | 1 | 5200 | 38650 | 0.75 | 18.24 | 5437.54 | 40587.18 |
| | | | | | | | | | |
| | | | | | | | | | |

XIX

| 6 May 2012 | | | CSIR (lab) | | | Castaway (field) | | | |
|---|---|---|---|---|---|---|---|---|---|
| Time | Site | Description | Depth below surface(m) | EC (mS/m) | TDS (mg/l) | Depth below surface(m) | Temperature (Celsius) | EC (mS/m) | TDS (mg/l) |
| | 7B | Max | 1.5 | 5200 | 38556 | 1.04 | 18.24 | 5437.67 | 40588.13 |
| | | TDS | 2 | 5200 | 38002 | 1.34 | 18.24 | 5438.16 | 40591.80 |
| | | | | | | 1.64 | 18.24 | 5438.17 | 40591.88 |
| | | | | | | 2.08 | 18.31 | 5432.83 | 40551.80 |
| 16:23 | 7C | Max | 0 | 2000 | 12776 | 0.15 | 18.78 | 4443.63 | 33115.13 |
| | | TDS | 0.5 | 4650 | 36330 | 0.45 | 18.61 | 4761.23 | 35502.83 |
| | | | 1 | 4850 | 35664 | 0.75 | 18.53 | 5014.47 | 37406.60 |
| | | | 1.5 | 4900 | 36660 | 1.05 | 18.52 | 5092.99 | 37996.91 |
| | | | 2 | 4850 | 36646 | 1.35 | 18.51 | 5124.82 | 38236.22 |
| | | | | | | 1.65 | 18.51 | 5127.61 | 38257.18 |
| | | | | | | 1.95 | 18.51 | 5123.89 | 38229.23 |
| | | | | | | 2.24 | 18.51 | 5120.13 | 38200.96 |
| | | | | | | 2.63 | 18.52 | 5112.96 | 38147.08 |
| 16:35 | 7D | Max | 0 | 200 | 1240 | 0.15 | 18.58 | 197.28 | 1191.93 |
| | | TDS | 0.5 | 250 | 1456 | 0.46 | 18.57 | 195.77 | 1180.60 |
| | | | 1 | 200 | 1196 | 0.77 | 18.57 | 194.41 | 1170.36 |
| | | | 1.5 | 200 | 1192 | 1.07 | 18.57 | 193.81 | 1165.87 |
| | | | 2 | 205 | 1188 | 1.38 | 18.58 | 195.83 | 1181.07 |
| | | | 3 | 205 | 1076 | 1.69 | 18.59 | 201.73 | 1225.41 |
| | | | | | | 1.99 | 18.60 | 201.29 | 1222.08 |
| | | | | | | 2.30 | 18.60 | 200.70 | 1217.65 |
| | | | | | | 2.60 | 18.60 | 200.71 | 1217.76 |
| | | | | | | 2.85 | 18.61 | 201.36 | 1222.59 |
| 6 May 2012 | | | CSIR (lab) | | | Castaway (field) | | | |
| Time | Site | Description | Depth below | EC | TDS | Depth below surface(m) | Temperature | EC | TDS (mg/l) |

XX

| Time | Site | Description | surface(m) | (mS/m) | (mg/l) | | (Celsius) | (mS/m) | |
|---|---|---|---|---|---|---|---|---|---|
| 16:49 | 7E | Max | 0 | 109 | 662 | 0.15 | 18.16 | 108.47 | 524.27 |
| | | TDS | 0.5 | 109 | 680 | 0.46 | 18.16 | 108.25 | 522.64 |
| | | | 1 | 108 | 674 | 0.77 | 18.16 | 108.36 | 523.49 |
| | | | 1.5 | 108 | 916 | 1.07 | 18.16 | 108.34 | 523.31 |
| | | | 2 | 108 | 666 | 1.38 | 18.16 | 108.34 | 523.34 |
| | | | 3 | 108 | 644 | 1.69 | 18.16 | 108.13 | 521.71 |
| | | | | | | 1.99 | 18.17 | 107.77 | 519.04 |
| | | | | | | 2.30 | 18.17 | 107.74 | 518.84 |
| | | | | | | 2.61 | 18.17 | 107.84 | 519.54 |
| | | | | | | 2.96 | 18.18 | 107.19 | 514.67 |
| 17:04 | 7F | Max | 0 | 104 | 662 | 0.15 | 17.70 | 104.21 | 492.28 |
| | | TDS | 0.5 | 105 | 656 | 0.46 | 17.71 | 104.04 | 490.99 |
| | | | 1 | 104 | 664 | 0.77 | 17.70 | 104.20 | 492.18 |
| | | | 1.5 | 104 | 626 | 1.07 | 17.70 | 104.21 | 492.24 |
| | | | 2 | 104 | 648 | 1.38 | 17.70 | 104.17 | 491.95 |
| | | | 3 | 104 | 662 | 1.69 | 17.69 | 104.10 | 491.43 |
| | | | 4 | 104 | 662 | 1.99 | 17.71 | 104.02 | 490.81 |
| | | | | | | 2.30 | 17.71 | 103.99 | 490.63 |
| | | | | | | 2.61 | 17.70 | 104.03 | 490.90 |
| | | | | | | 2.91 | 17.69 | 103.97 | 490.49 |
| | | | | | | 3.22 | 17.68 | 103.99 | 490.62 |
| | | | | | | 3.53 | 17.68 | 103.97 | 490.46 |
| | | | | | | 3.83 | 17.69 | 103.87 | 489.72 |
| | | | | | | 4.04 | 17.69 | 103.82 | 489.31 |

| 7 May 2012 | | | CSIR (lab) | | | Castaway (field) | | | |
|---|---|---|---|---|---|---|---|---|---|
| Time | Site | Description | Depth below surface (m) | EC (mS/m) | TDS (mg/l) | Depth below surface(m) | Temperature (Celsius) | EC (mS/m) | TDS (mg/l) |

XXI

| 09:14 | 8F | | 0 | | | 0.15 | 17.32 | 108.40 | 523.75 |
|---|---|---|---|---|---|---|---|---|---|
| | | | 0.5 | 109 | 648 | 0.46 | 17.32 | 108.22 | 522.43 |
| | | | 1 | 109 | 706 | 0.77 | 17.32 | 108.35 | 523.37 |
| | | | 1.5 | 109 | 658 | 1.07 | 17.32 | 108.40 | 523.76 |
| | | | 2 | 108 | 924 | 1.38 | 17.31 | 108.40 | 523.75 |
| | | | 3 | 109 | 696 | 1.69 | 17.31 | 108.40 | 523.77 |
| | | | 4 | 110 | 724 | 1.99 | 17.31 | 108.33 | 523.23 |
| | | | | | | 2.30 | 17.31 | 108.36 | 523.44 |
| | | | | | | 2.61 | 17.31 | 108.38 | 523.61 |
| | | | | | | 2.91 | 17.32 | 108.37 | 523.52 |
| | | | | | | 3.22 | 17.31 | 108.40 | 523.76 |
| | | | | | | 3.52 | 17.31 | 108.42 | 523.89 |
| | | | | | | 3.71 | 17.31 | 108.41 | 523.82 |

XXII

| Comparison between Castaway and CSIR laboratory results of total dissolved solids at specified site | Comparison between Castaway and CSIR laboratory results of electro conductivity at specified site |
|---|---|



Figure E1: TDS - site A



Figure E2: EC - site A



Figure E3: TDS - site B



Figure E4: EC - site B

Figure E5: TDS - site C

Figure E6: EC - site C

Figure E7: TDS - site D

Figure E8: EC - site D

Figure E9: TDS - site E

Figure E10: EC - site E

Figure E11: TDS - site F

Figure E12: EC - site F
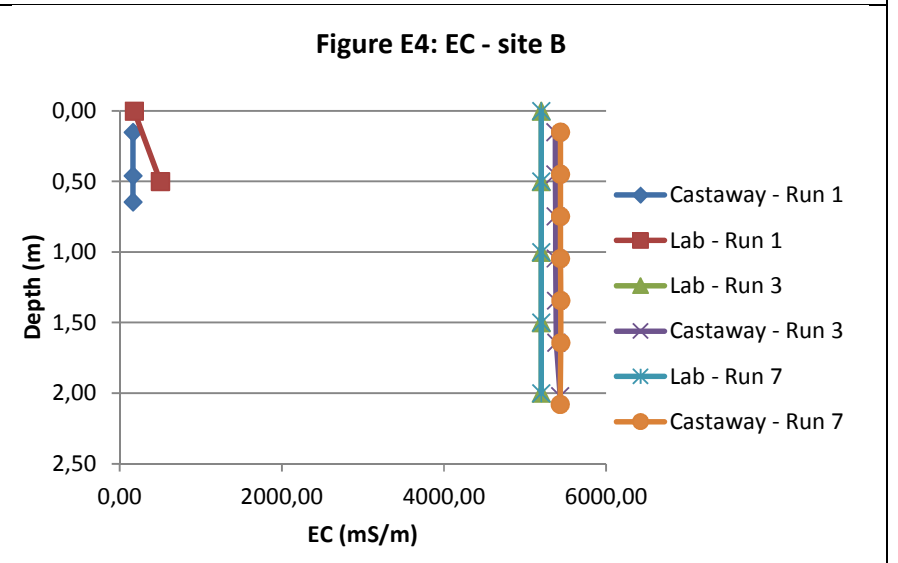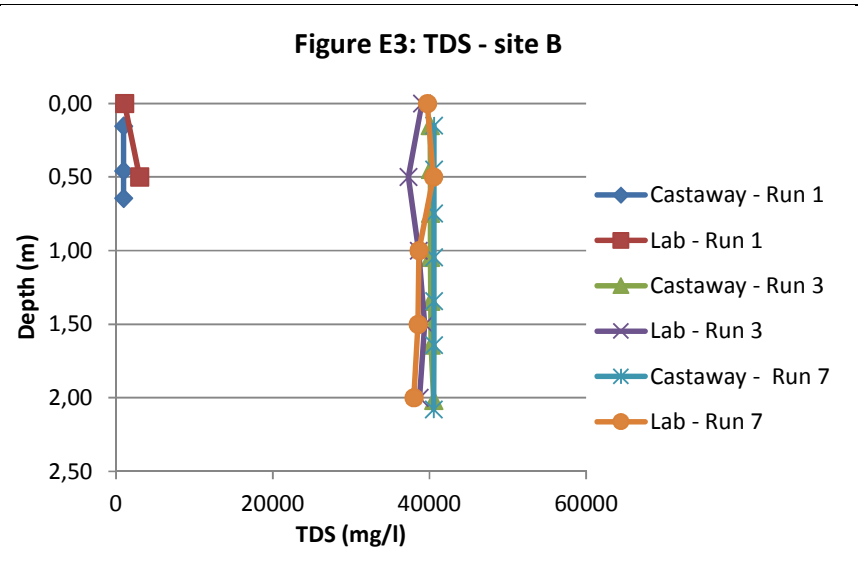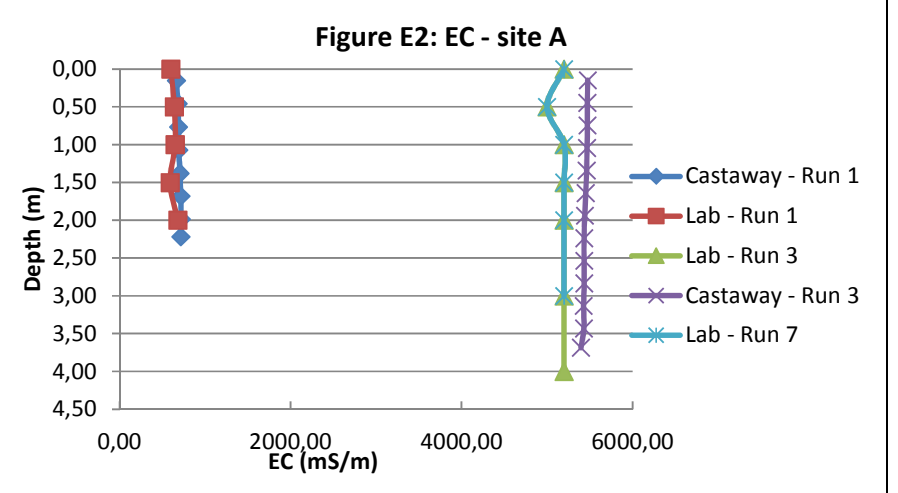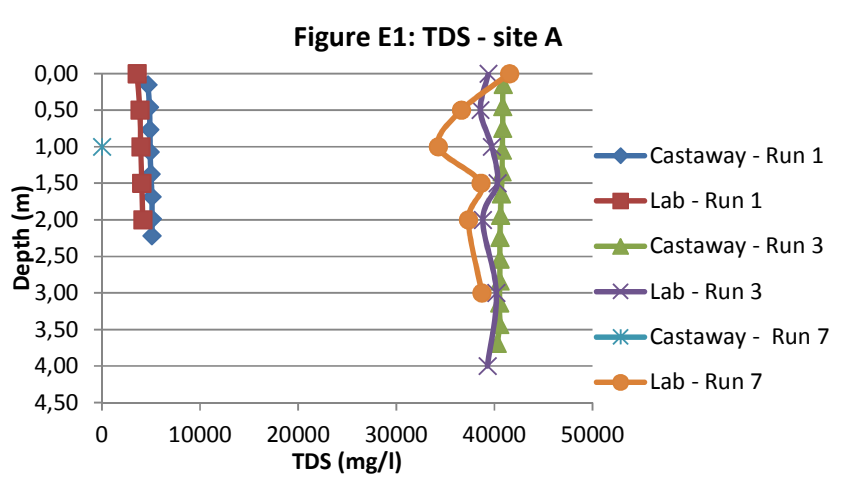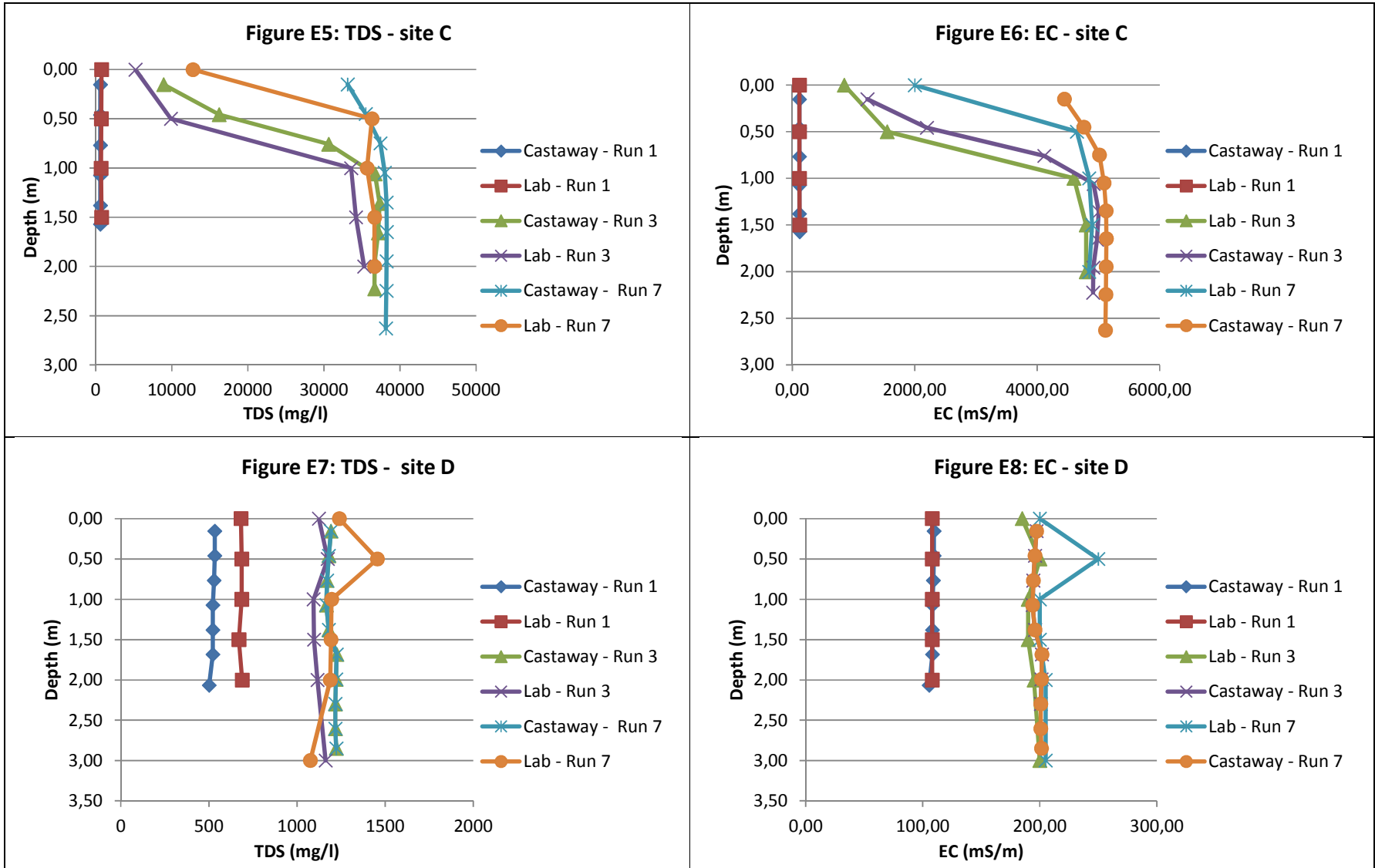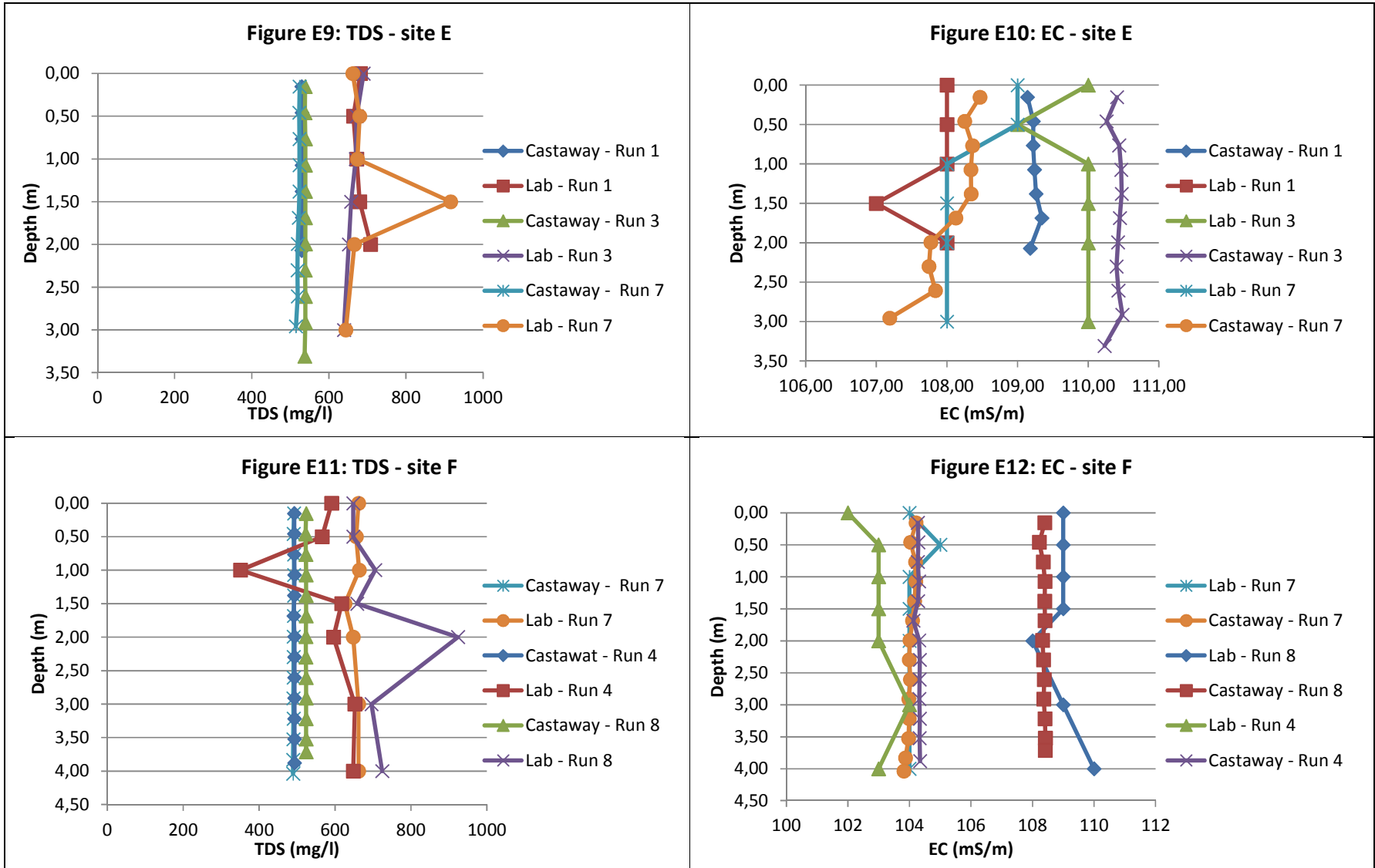
**Appendix F: Recorded flow velocities (ADCP)**

| Site | Run | Site location Lat | Site location Long | Measurement location Lat | Measurement location Long | Direction deg | Velocity V (m/s) | Flow depth (m) | Bed load (dry mass kg) | Time (s) | Bed load (kg/s.m) | Bedload sample d50* (mm) | Susp. Sediment Concentration (mg/l) | Susp. Sed Load =Cxq (kg/s.m) | Total load = Suspended + Bed load (kg/s.m) |
|---|---|---|---|---|---|---|---|---|---|---|---|---|---|---|---|
| A | 2 | -33.4936 | 27.1347 | -33.4935 | 27.1345 | -76.42 | 1.180 | 3.68 | 0.281 | 180 | 0.0156 | 0.2703 | 234 | 1.016 | 1.032 |
|  | 4 |  |  |  | 26.8656 | 91.23 | 0.873 | 3.14 | 0.339 | 120 | 0.0283 | 0.5710 | 91 | 0.249 | 0.278 |
|  | 6 |  |  | -33.4935 | 26.8656 | -58.41 | 1.135 | 3.27 | 0.398 | 90 | 0.0442 | 0.2067 | 104 | 0.385 | 0.430 |
|  | 8 |  |  | -33.4935 | 26.8653 | 103.13 | 1.307 | 3.03 | 0.755 | 74 | 0.1020 | 0.2387 | 210 | 0.831 | 0.933 |
| B | 2 | 33.4819 | 27.1106 | -33.4816 | 27.1099 | -64.29 | 0.428 | 1.81 | 0.343 | 360 | 0.0095 | 0.1436 | 104 | 0.081 | 0.090 |
|  | 4 |  |  |  | 26.8898 | 121.36 | 0.586 | 1.32 | 0.425 | 155 | 0.0274 | 0.0046 | 592 | 0.458 | 0.486 |
|  | 6 |  |  | -33.4817 | 26.8905 | -62.14 | 0.637 | 1.64 | 0.185 | 240 | 0.0077 | 0.0053 | 413 | 0.430 | 0.438 |
|  | 8 |  |  | -33.4819 | 26.8899 | 123.47 | 0.524 | 1.35 | 0.599 | 180 | 0.0333 | 0.0892 | 380 | 0.268 | 0.301 |
| C | 2 | 33.4725 | 27.0856 | -33.4722 | 27.0857 | -40.47 | 0.488 | 2.37 | 0.521 | 360 | 0.0145 | 0.1869 | 556 | 0.644 | 0.658 |
|  | 4 |  |  | -33.4725 | 26.9143 | 125.16 | 0.494 | 1.18 | 0.663 | 150 | 0.0442 | 0.1878 | 535 | 0.312 | 0.356 |
|  | 6 |  |  | -33.4719 | 26.9145 | -55.99 | 0.490 | 2.22 | 0.245 | 300 | 0.0082 | 0.2084 | 587 | 0.638 | 0.646 |
|  | 8 |  |  | -33.4722 | 26.9141 | 127.68 | 0.637 | 1.80 | 0.646 | 120 | 0.0538 | 0.1876 | 709 | 0.813 | 0.866 |
| D | 2 | 33.4547 | 27.0700 | -33.4547 | 27.0698 | 15.43 | 0.338 | 3.10 | 0.109 | 360 | 0.0030 | 0.2416 | 1038 | 1.088 | 1.091 |
|  | 4 |  |  | -33.4548 | 26.9303 | 194.48 | 0.428 | 2.09 | 0.360 | 120 | 0.0300 | 0.2029 | 284 | 0.255 | 0.285 |
|  | 6 |  |  | -33.4546 | 26.9301 | 13.59 | 0.476 | 2.82 | 0.196 | 360 | 0.0054 | 0.1747 | 424 | 0.569 | 0.575 |
|  | 8 |  |  | -33.4547 | 26.9300 | 193.25 | 0.395 | 2.35 | 0.051 | 360 | 0.0014 | 0.2056 | 3564 | 3.303 | 3.305 |
| E | 4 | 33.4375 | 27.0561 | -33.1542 | 27.0851 | 148.68 | 0.386 | 2.46 | 0.222 | 240 | 0.0093 | 0.2359 | 252 | 0.239 | 0.249 |
|  | 6 |  |  | -33.4371 | 27.0556 | -26.37 | 0.329 | 3.12 | 0.041 | 360 | 0.0011 | 0.2327 | 270 | 0.277 | 0.279 |
|  | 8 |  |  | -33.4373 | 26.9442 | 153.74 | 0.361 | 2.41 | 0.113 | 360 | 0.0031 | 0.2523 | 222 | 0.193 | 0.196 |
| F | 4 | 33.4032 | 27.0357 | -33.4025 | 26.9647 | 133.35 | 0.407 | 1.76 | n/a | n/a | n/a | n/a | n/a | n/a | n/a |
|  | 8 |  |  | -33.4033 | 26.9642 | 170.33 | 0.319 | 4.07 | 0.053 | 360 | 0.0015 | 0.4028 | 200 | 0.260 | 0.261 |

Note: * Median sediment diameter

XXVII

**Appendix G: Observed bedload sediment gradings**

Samples listed chronologically:

| Sample | 006 |
|---|---|
| Site | 2A |
| Coordinates | 33° 29' 37" S; 27° 08' 05" E |
| Chainage | 405 m |
| Tide | Ebb |
| Date | 05/05/2012 |
| Time | 13:38 |
| d50 | 0.270 mm |

| Units | % Concentration | Diameter (D) |
|---|---|---|
| mm | 100.00 | 75 |
| mm | 100.00 | 50 |
| mm | 100.00 | 37.5 |
| mm | 100.00 | 19 |
| mm | 100.00 | 9.5 |
| mm | 100.00 | 4.75 |
| mm | 100.00 | 2.36 |
| mm | 100.00 | 1.18 |
| mm | 100.00 | 0.6 |
| mm | 57.96 | 0.3 |
| mm | 5.02 | 0.15 |
| mm | 3.47 | 0.075 |
| mm | 3.11 | 0.0386 |
| mm | 3.11 | 0.0244 |
| mm | 3.11 | 0.0141 |
| mm | 3.11 | 0.0100 |
| mm | 3.11 | 0.0070 |
| mm | 3.11 | 0.0034 |
| mm | 3.11 | 0.0014 |

| Sample | | 007 |
|---|---|---|
| Site | | 2B |
| Coordinates | | 33° 28' 55" S; 27° 06' 38" E |
| Chainage | | 3026 m |
| Tide | | Ebb |
| Date | | 05/05/2012 |
| Time | | 14:21 |
| d50 | | 0.144 mm |

| Units | % Concentration | Diameter (D) |
|---|---|---|
| mm | 100.00 | 75 |
| mm | 100.00 | 50 |
| mm | 100.00 | 37.5 |
| mm | 100.00 | 19 |
| mm | 100.00 | 9.5 |
| mm | 100.00 | 4.75 |
| mm | 100.00 | 2.36 |
| mm | 100.00 | 1.18 |
| mm | 100.00 | 0.6 |
| mm | 90.77 | 0.3 |
| mm | 50.77 | 0.15 |
| mm | 38.46 | 0.075 |
| mm | 35.38 | 0.0338 |
| mm | 33.85 | 0.0216 |
| mm | 33.85 | 0.0125 |
| mm | 33.85 | 0.0088 |
| mm | 32.31 | 0.0063 |
| mm | 29.23 | 0.0031 |
| mm | 23.08 | 0.0013 |
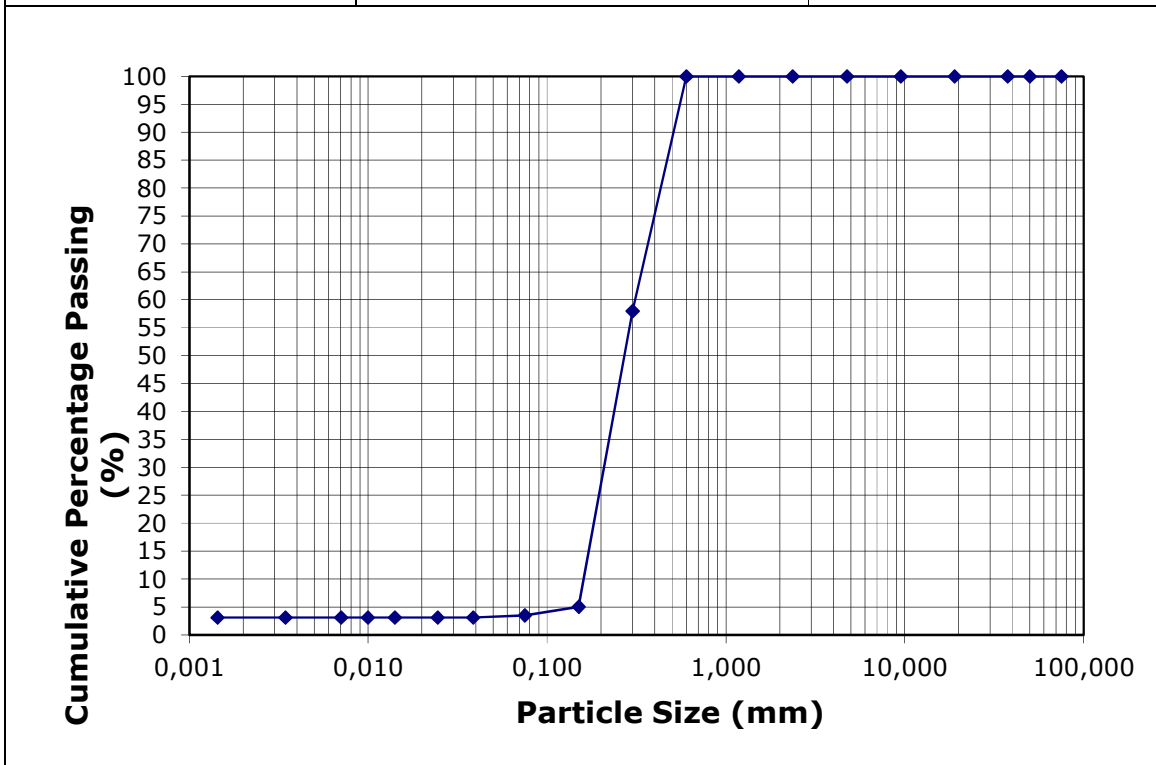


XXX
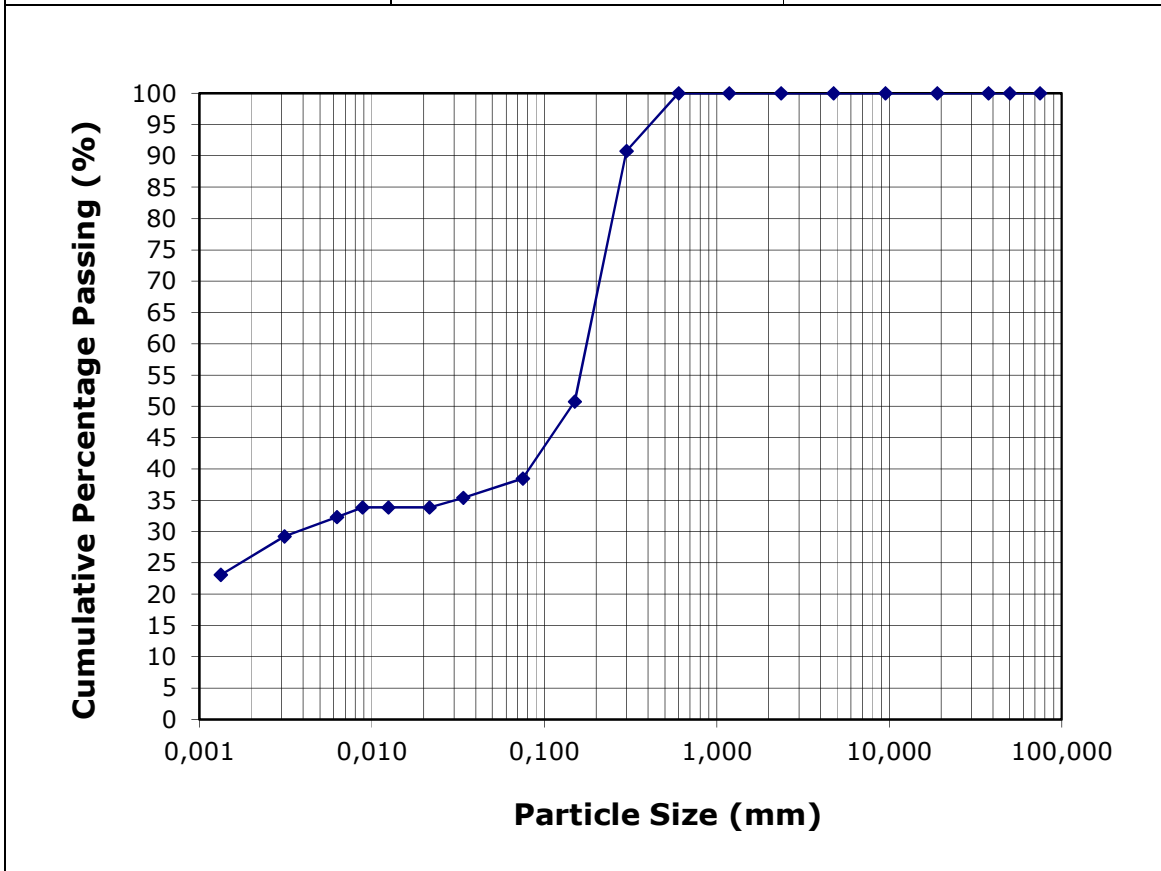
| Sample | 008 |
|---|---|
| Site | 2C |
| Coordinates | 33° 28' 21" S; 27° 05' 08" E |
| Chainage | 5645 m |
| Tide | Ebb |
| Date | 05/05/2012 |
| Time | 14:34 |
| d50 | 0.187 mm |

| Units | % Concentration | Diameter (D) |
|---|---|---|
| mm | 100.00 | 75 |
| mm | 100.00 | 50 |
| mm | 100.00 | 37.5 |
| mm | 100.00 | 19 |
| mm | 100.00 | 9.5 |
| mm | 100.00 | 4.75 |
| mm | 100.00 | 2.36 |
| mm | 100.00 | 1.18 |
| mm | 100.00 | 0.6 |
| mm | 96.67 | 0.3 |
| mm | 28.33 | 0.15 |
| mm | 16.67 | 0.075 |
| mm | 16.67 | 0.0367 |
| mm | 16.67 | 0.0232 |
| mm | 15.00 | 0.0135 |
| mm | 15.00 | 0.0096 |
| mm | 15.00 | 0.0068 |
| mm | 15.00 | 0.0033 |
| mm | 11.67 | 0.0014 |

| Sample | 009 |
|---|---|
| Site | 2D |
| Coordinates | 33° 27' 17" S; 27° 04' 12" E |
| Chainage | 8270 m |
| Tide | Ebb |
| Date | 05/05/2012 |
| Time | 14:55 |
| d50 | 0.242 mm |

| Units | % Concentration | Diameter (D) |
|---|---|---|
| mm | 100.00 | 75 |
| mm | 100.00 | 50 |
| mm | 100.00 | 37.5 |
| mm | 100.00 | 19 |
| mm | 100.00 | 9.5 |
| mm | 100.00 | 4.75 |
| mm | 100.00 | 2.36 |
| mm | 100.00 | 1.18 |
| mm | 100.00 | 0.6 |
| mm | 69.23 | 0.3 |
| mm | 7.69 | 0.15 |
| mm | 7.69 | 0.075 |
| mm | 7.69 | 0.0379 |
| mm | 7.69 | 0.0240 |
| mm | 7.69 | 0.0138 |
| mm | 7.69 | 0.0098 |
| mm | 7.69 | 0.0069 |
| mm | 7.69 | 0.0034 |
| mm | 7.69 | 0.0014 |
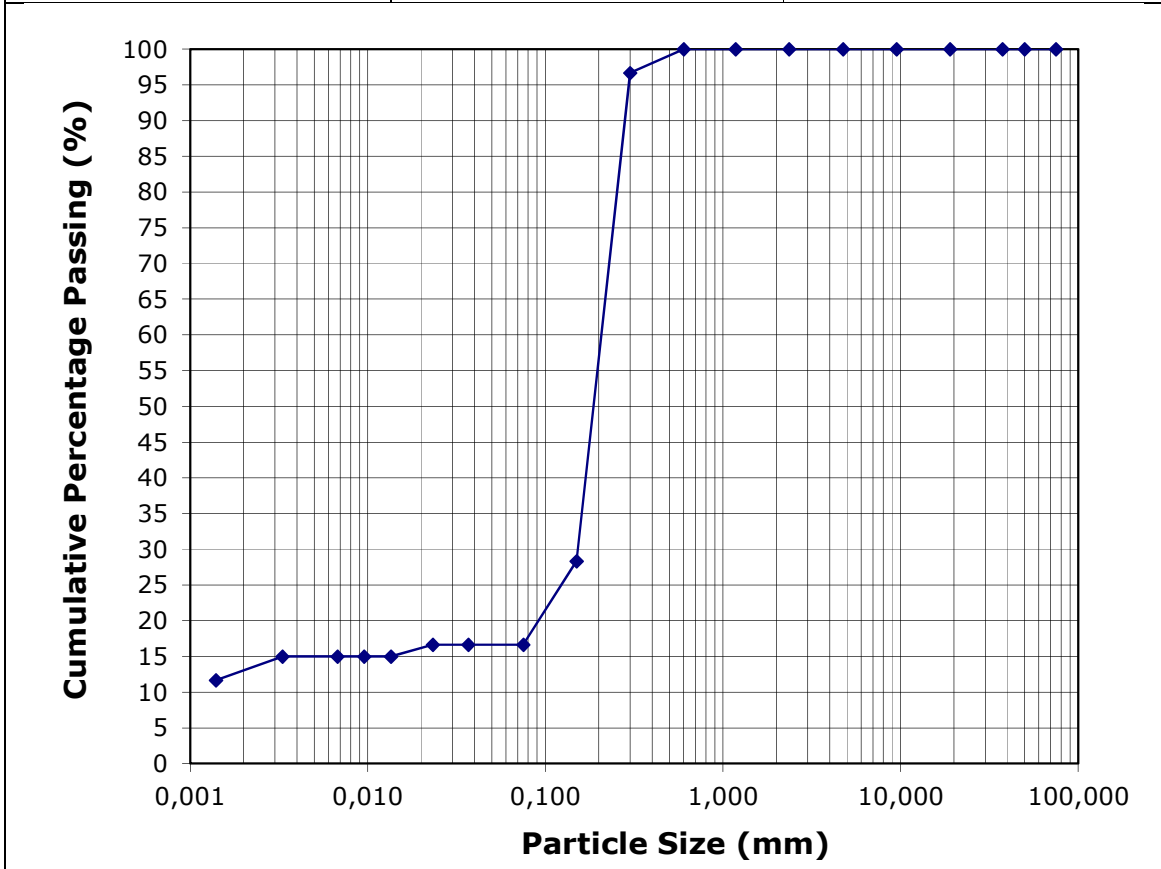


XXXII
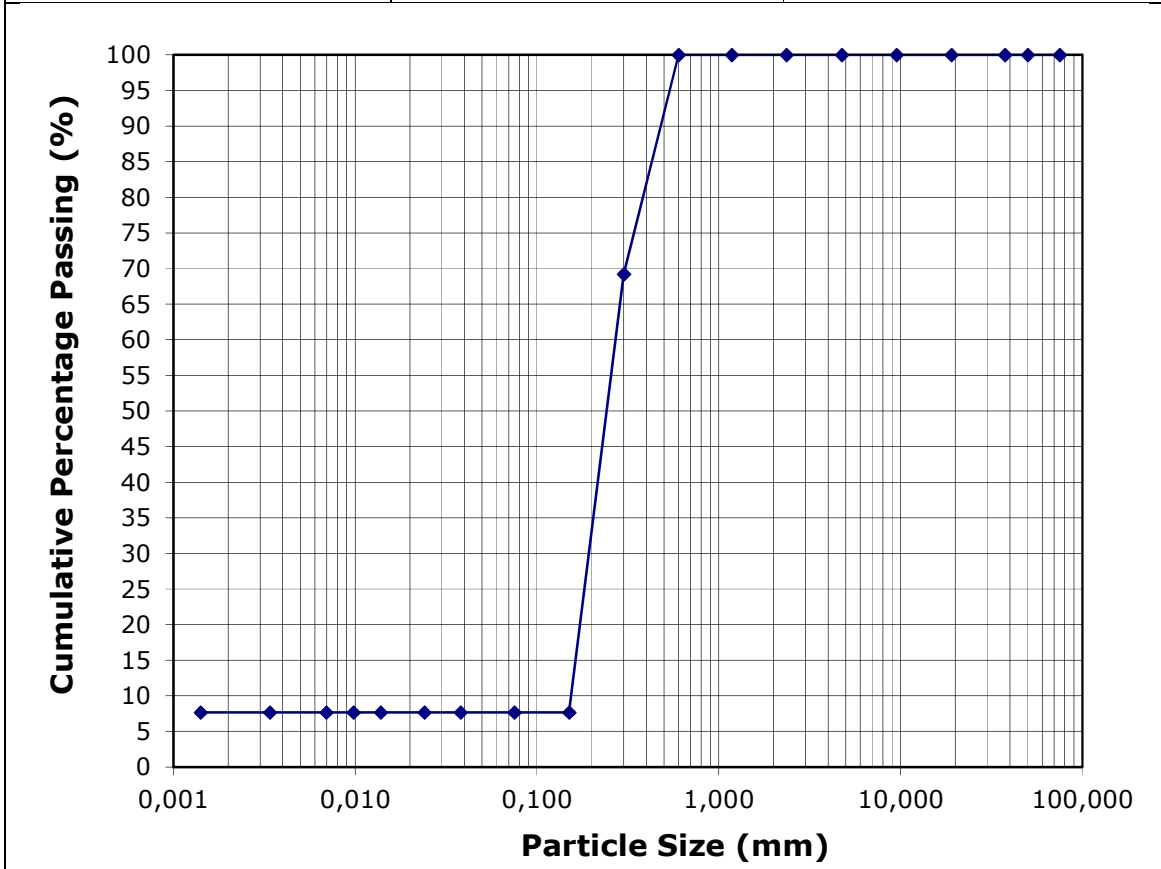
| Sample | 010 |
|---|---|
| Site | 4A |
| Coordinates | 33° 29' 37" S; 27° 08' 05" E |
| Chainage | 405 m |
| Tide | Flood |
| Date | 06/05/2012 |
| Time | 07:28 |
| d50 | 0.571 mm |

| Units | % Concentration | Diameter (D) |
|---|---|---|
| mm | 100.00 | 75 |
| mm | 100.00 | 50 |
| mm | 100.00 | 37.5 |
| mm | 100.00 | 19 |
| mm | 100.00 | 9.5 |
| mm | 100.00 | 4.75 |
| mm | 100.00 | 2.36 |
| mm | 100.00 | 1.18 |
| mm | 100.00 | 0.6 |
| mm | 53.85 | 0.3 |
| mm | 0.00 | 0.15 |
| mm | 0.00 | 0.075 |
| mm | 0.00 | 0.0389 |
| mm | 0.00 | 0.0246 |
| mm | 0.00 | 0.0142 |
| mm | 0.00 | 0.0101 |
| mm | 0.00 | 0.0071 |
| mm | 0.00 | 0.0035 |
| mm | 0.00 | 0.0015 |



XXXIII
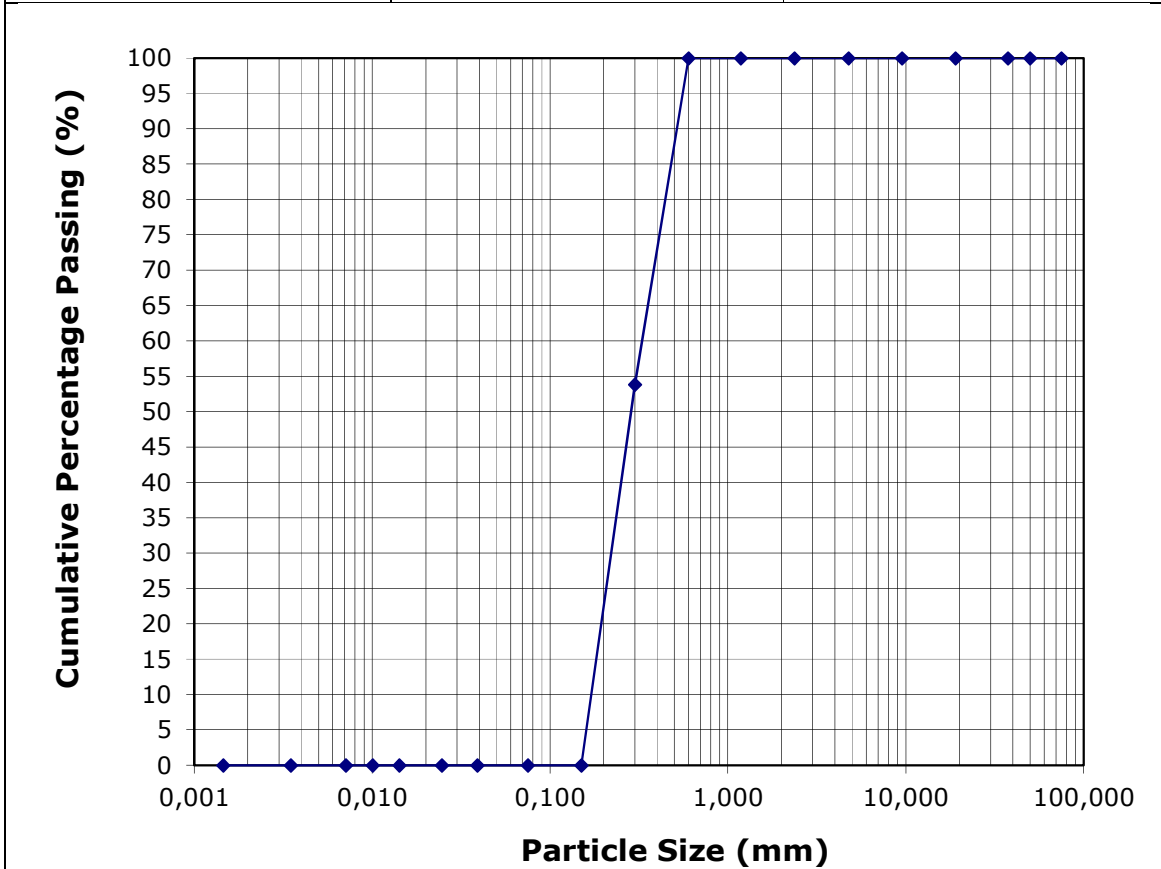
| Sample | | 011 |
|---|---|---|
| Site | | 4B |
| Coordinates | | 33° 28' 55" S; 27° 06' 38" E |
| Chainage | | 3026 m |
| Tide | | Flood |
| Date | | 06/05/2012 |
| Time | | 07:46 |
| d50 | | 0.005 mm |
| **Units** | **% Concentration** | **Diameter (D)** |
| mm | 100.00 | 75 |
| mm | 100.00 | 50 |
| mm | 100.00 | 37.5 |
| mm | 100.00 | 19 |
| mm | 100.00 | 9.5 |
| mm | 100.00 | 4.75 |
| mm | 100.00 | 2.36 |
| mm | 100.00 | 1.18 |
| mm | 100.00 | 0.6 |
| mm | 100.00 | 0.3 |
| mm | 90.00 | 0.15 |
| mm | 83.33 | 0.075 |
| mm | 68.33 | 0.0293 |
| mm | 65.00 | 0.0189 |
| mm | 60.00 | 0.0112 |
| mm | 58.33 | 0.0080 |
| mm | 53.33 | 0.0058 |
| mm | 43.33 | 0.0030 |
| mm | 31.67 | 0.0013 |



XXXIV
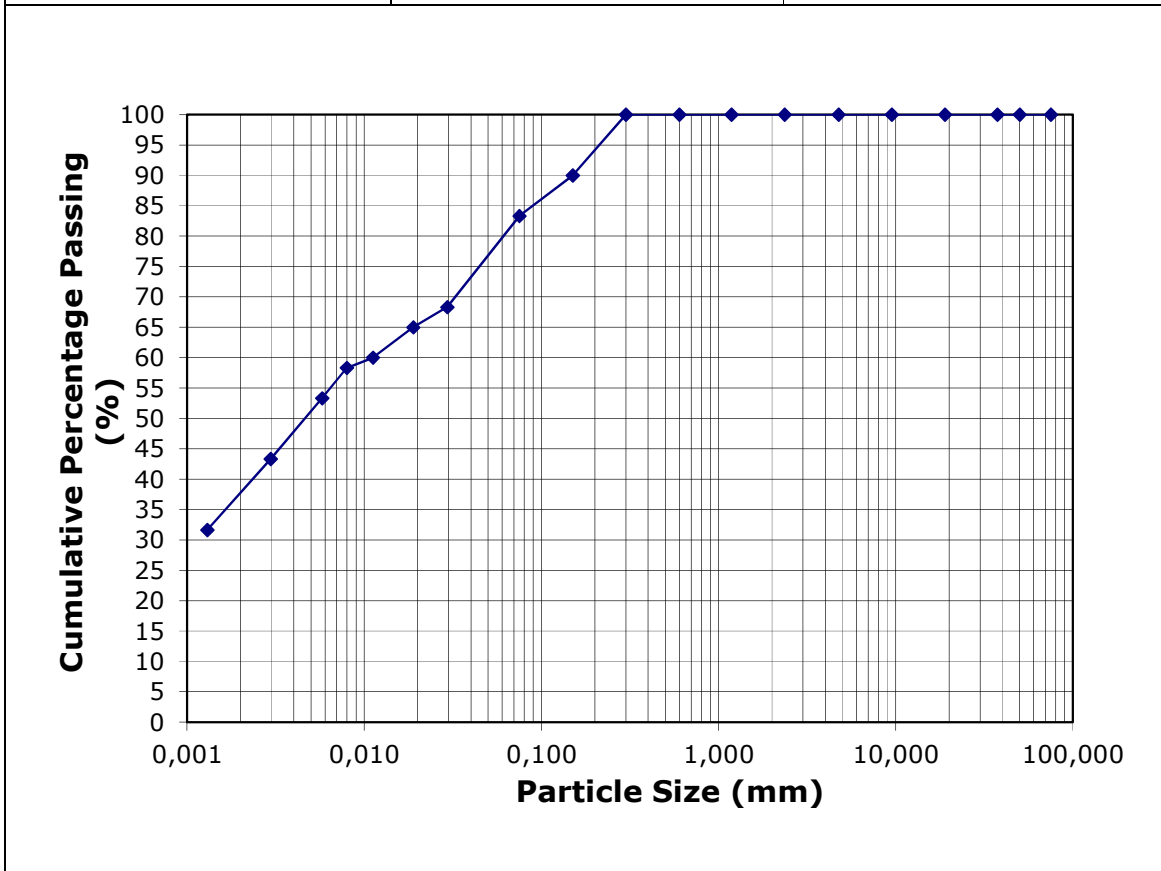
| Sample | 012 |
|---|---|
| Site | 4C |
| Coordinates | 33° 28' 21" S; 27° 05' 08" E |
| Chainage | 5645 m |
| Tide | Flood |
| Date | 06/05/2012 |
| Time | 08:01 |
| d50 | 0.189 mm |

| Units | % Concentration | Diameter (D) |
|---|---|---|
| mm | 100.00 | 75 |
| mm | 100.00 | 50 |
| mm | 100.00 | 37.5 |
| mm | 100.00 | 19 |
| mm | 100.00 | 9.5 |
| mm | 100.00 | 4.75 |
| mm | 100.00 | 2.36 |
| mm | 100.00 | 1.18 |
| mm | 100.00 | 0.6 |
| mm | 91.67 | 0.3 |
| mm | 30.00 | 0.15 |
| mm | 18.33 | 0.075 |
| mm | 18.33 | 0.0366 |
| mm | 18.33 | 0.0232 |
| mm | 18.33 | 0.0134 |
| mm | 18.33 | 0.0095 |
| mm | 16.67 | 0.0067 |
| mm | 15.00 | 0.0033 |
| mm | 13.33 | 0.0014 |



XXXV
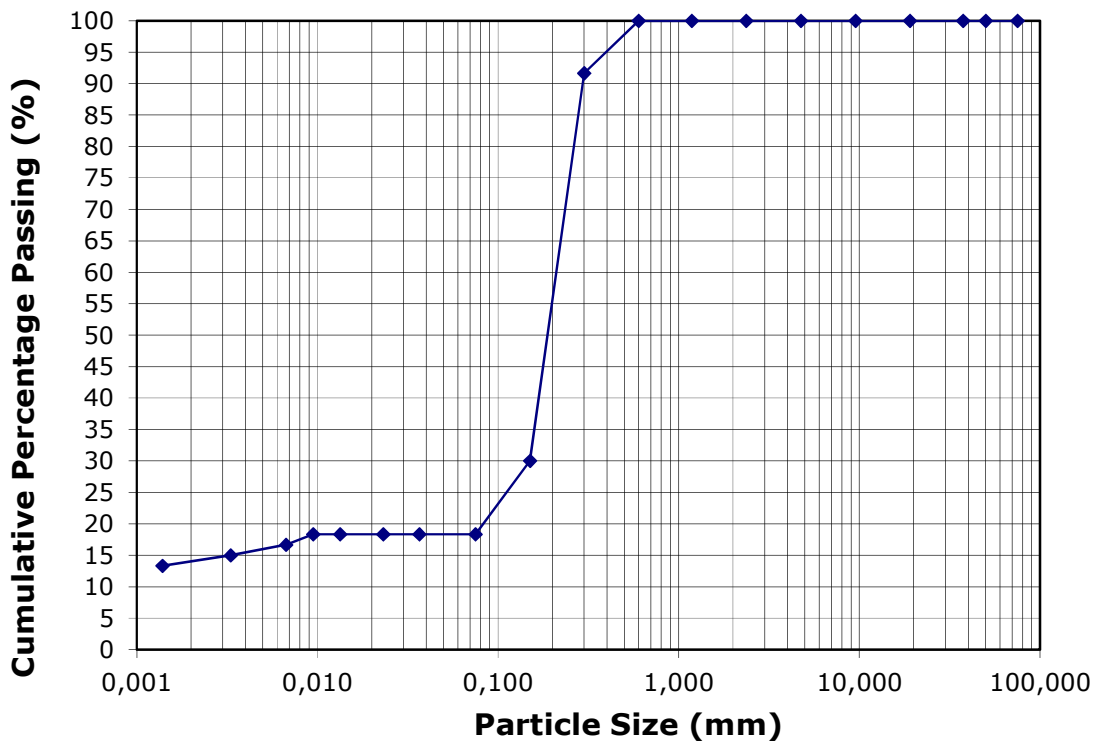
| Sample | 013 |
|---|---|
| Site | 4D |
| Coordinates | 33° 27' 17" S; 27° 04' 12" E |
| Chainage | 8270 m |
| Tide | Flood |
| Date | 06/05/2012 |
| Time | 08:17 |
| d50 | 0.203 mm |

| Units | % Concentration | Diameter (D) |
|---|---|---|
| mm | 100.00 | 75 |
| mm | 100.00 | 50 |
| mm | 100.00 | 37.5 |
| mm | 100.00 | 19 |
| mm | 100.00 | 9.5 |
| mm | 100.00 | 4.75 |
| mm | 100.00 | 2.36 |
| mm | 100.00 | 1.18 |
| mm | 100.00 | 0.6 |
| mm | 76.92 | 0.3 |
| mm | 29.23 | 0.15 |
| mm | 24.62 | 0.075 |
| mm | 24.62 | 0.0355 |
| mm | 23.08 | 0.0226 |
| mm | 21.54 | 0.0131 |
| mm | 21.54 | 0.0093 |
| mm | 21.54 | 0.0066 |
| mm | 20.00 | 0.0032 |
| mm | 15.38 | 0.0014 |



XXXVI
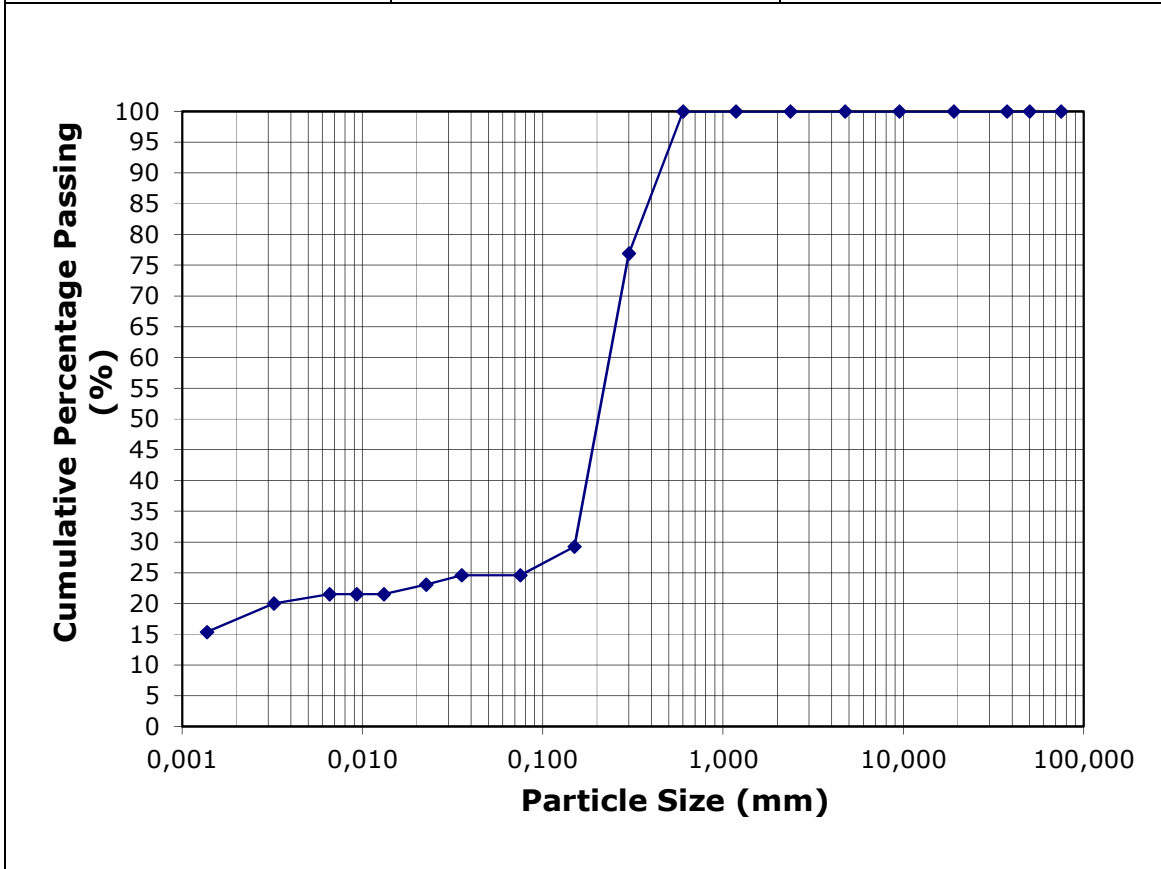
| Sample | 014 |
|---|---|
| Site | 4E |
| Coordinates | 33° 26' 15" S; 27° 03' 22" E |
| Chainage | 10888 m |
| Tide | Flood |
| Date | 06/05/2012 |
| Time | 08:29 |
| d50 | 0.236 mm |

| Units | % Concentration | Diameter (D) |
|---|---|---|
| mm | 100.00 | 75 |
| mm | 100.00 | 50 |
| mm | 100.00 | 37.5 |
| mm | 100.00 | 19 |
| mm | 100.00 | 9.5 |
| mm | 100.00 | 4.75 |
| mm | 100.00 | 2.36 |
| mm | 100.00 | 1.18 |
| mm | 100.00 | 0.6 |
| mm | 74.29 | 0.3 |
| mm | 4.29 | 0.15 |
| mm | 1.43 | 0.075 |
| mm | 1.43 | 0.0387 |
| mm | 1.43 | 0.0245 |
| mm | 1.43 | 0.0141 |
| mm | 1.43 | 0.0100 |
| mm | 1.43 | 0.0071 |
| mm | 1.43 | 0.0035 |
| mm | 1.43 | 0.0014 |



XXXVII
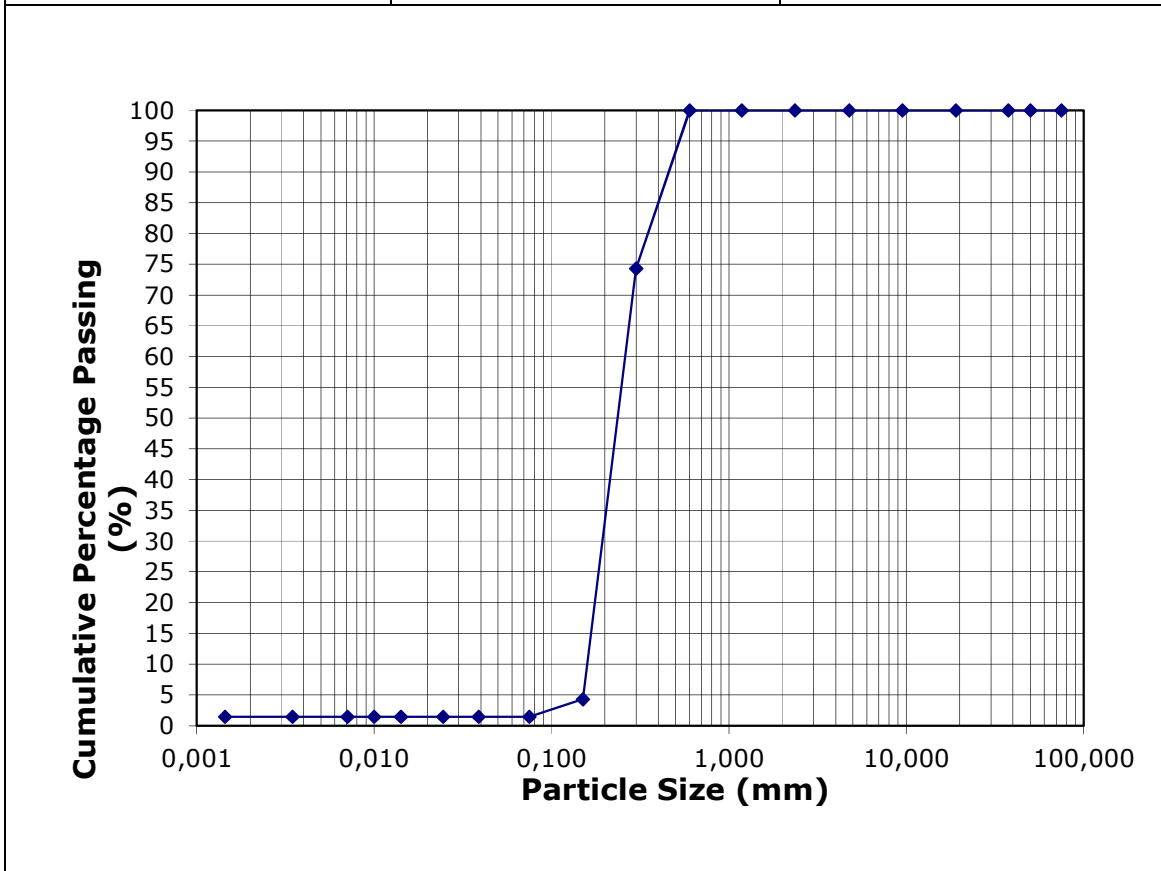
| Sample | 015 |
| --- | --- |
| Site | 6A |
| Coordinates | 33° 29' 37" S; 27° 08' 05" E |
| Chainage | 405 m |
| Tide | Ebb |
| Date | 06/05/2012 |
| Time | 13:40 |
| d50 | 0.207 mm |

| Units | % Concentration | Diameter (D) |
| --- | --- | --- |
| mm | 100.00 | 75 |
| mm | 100.00 | 50 |
| mm | 100.00 | 37.5 |
| mm | 100.00 | 19 |
| mm | 100.00 | 9.5 |
| mm | 100.00 | 4.75 |
| mm | 100.00 | 2.36 |
| mm | 100.00 | 1.18 |
| mm | 100.00 | 0.6 |
| mm | 93.85 | 0.3 |
| mm | 12.31 | 0.15 |
| mm | 3.08 | 0.075 |
| mm | 3.08 | 0.0386 |
| mm | 3.08 | 0.0244 |
| mm | 3.08 | 0.0141 |
| mm | 3.08 | 0.0100 |
| mm | 3.08 | 0.0070 |
| mm | 3.08 | 0.0034 |
| mm | 3.08 | 0.0014 |



XXXVIII
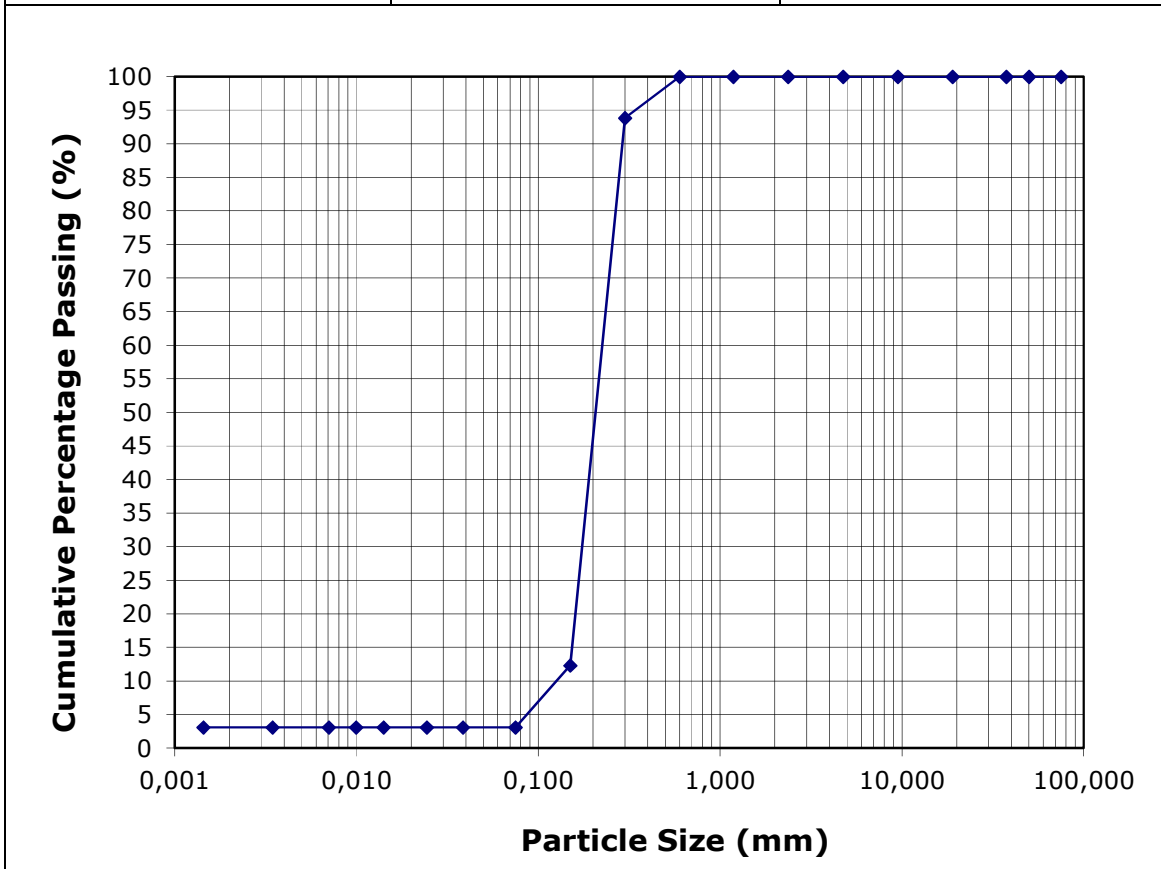
| Sample | 018 |
|---|---|
| Site | 6B |
| Coordinates | 33° 28' 55" S; 27° 06' 38" E |
| Chainage | 3026 m |
| Tide | Ebb |
| Date | 06/05/2012 |
| Time | 13:55 |
| d50 | 0.005 mm |

| Units | % Concentration | Diameter (D) |
|---|---|---|
| mm | 100.00 | 75 |
| mm | 100.00 | 50 |
| mm | 100.00 | 37.5 |
| mm | 100.00 | 19 |
| mm | 100.00 | 9.5 |
| mm | 100.00 | 4.75 |
| mm | 100.00 | 2.36 |
| mm | 100.00 | 1.18 |
| mm | 100.00 | 0.6 |
| mm | 95.38 | 0.3 |
| mm | 69.23 | 0.15 |
| mm | 64.62 | 0.075 |
| mm | 61.54 | 0.0295 |
| mm | 60.00 | 0.0189 |
| mm | 56.92 | 0.0111 |
| mm | 55.38 | 0.0079 |
| mm | 50.77 | 0.0057 |
| mm | 44.62 | 0.0029 |
| mm | 32.31 | 0.0013 |



XXXIX
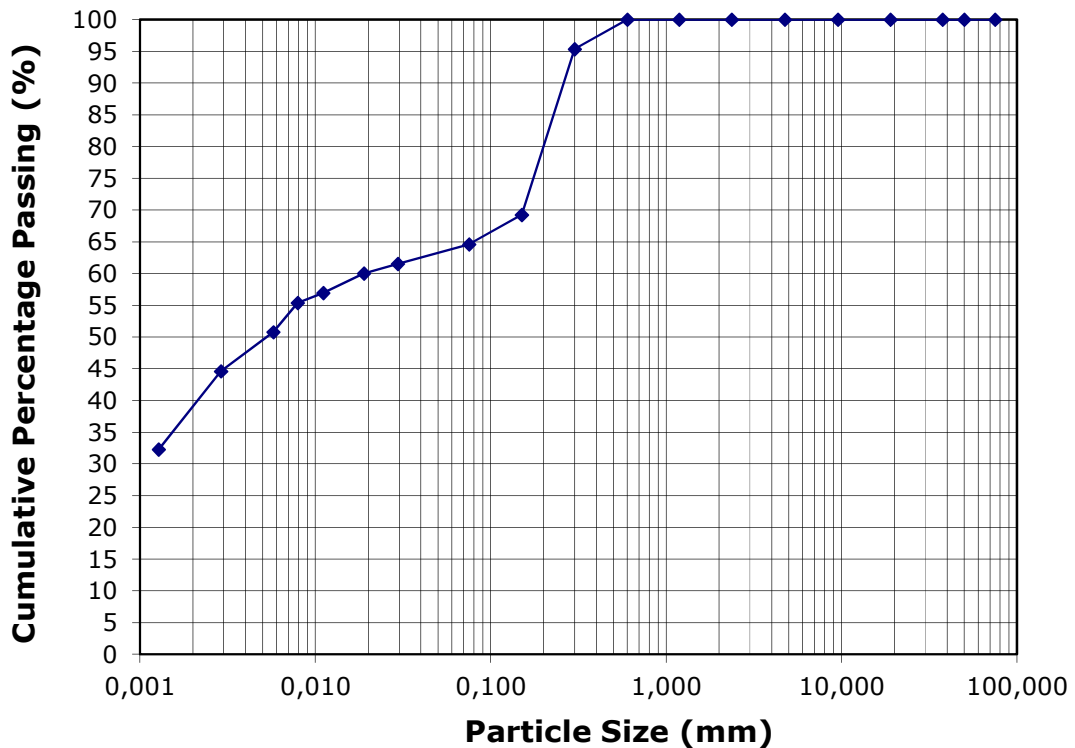
| Sample | | 019 |
|---|---|---|
| Site | | 6C |
| Coordinates | | 33° 28' 21" S; 27° 05' 08" E |
| Chainage | | 5645 m |
| Tide | | Ebb |
| Date | | 06/05/2012 |
| Time | | 14:20 |
| d50 | | 0.208 mm |

| Units | % Concentration | Diameter (D) |
|---|---|---|
| mm | 100.00 | 75 |
| mm | 100.00 | 50 |
| mm | 100.00 | 37.5 |
| mm | 100.00 | 19 |
| mm | 100.00 | 9.5 |
| mm | 100.00 | 4.75 |
| mm | 100.00 | 2.36 |
| mm | 100.00 | 1.18 |
| mm | 100.00 | 0.6 |
| mm | 96.92 | 0.3 |
| mm | 7.69 | 0.15 |
| mm | 1.54 | 0.075 |
| mm | 1.54 | 0.0387 |
| mm | 1.54 | 0.0245 |
| mm | 1.54 | 0.0141 |
| mm | 1.54 | 0.0100 |
| mm | 1.54 | 0.0071 |
| mm | 1.54 | 0.0035 |
| mm | 1.54 | 0.0014 |



XL
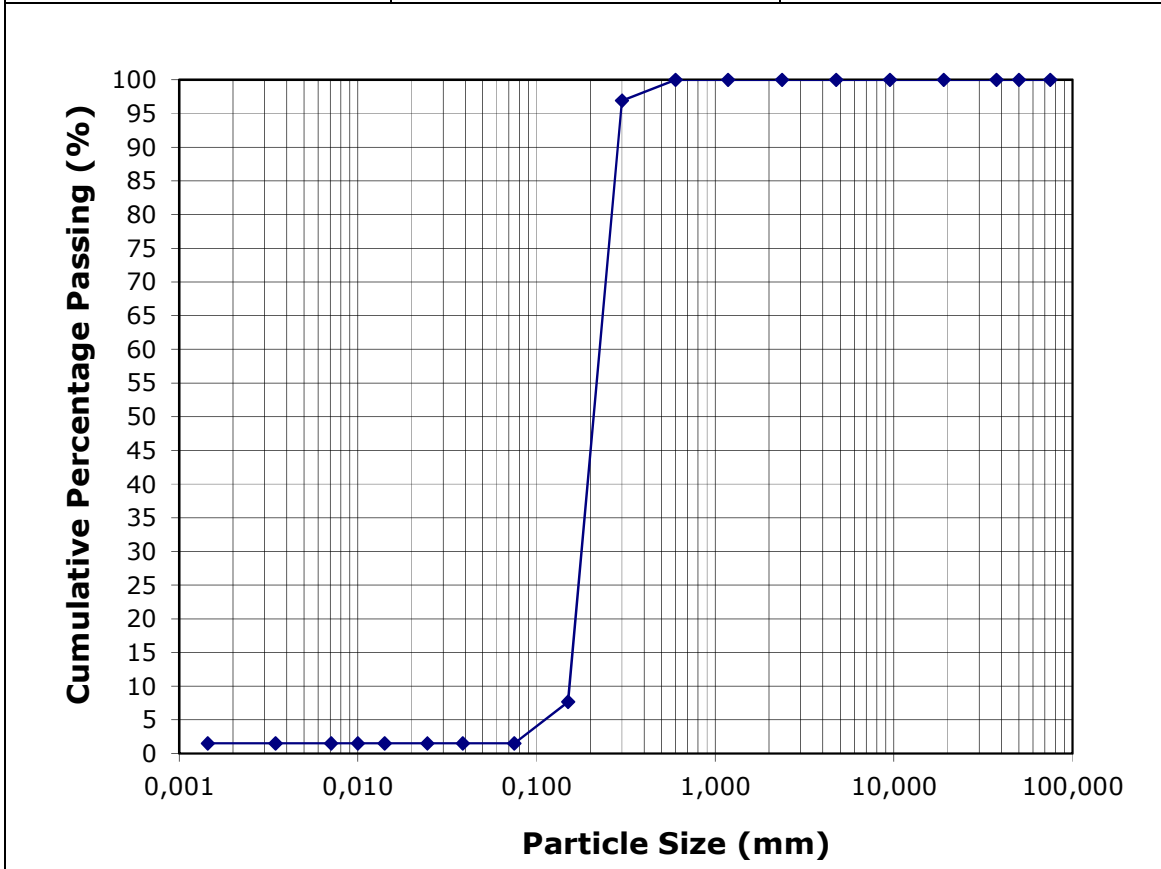
| Sample | 020 |
|---|---|
| Site | 6D |
| Coordinates | 33° 27' 17" S; 27° 04' 12" E |
| Chainage | 8270 m |
| Tide | Ebb |
| Date | 06/05/2012 |
| Time | 14:44 |
| d50 | 0.175 mm |

| Units | % Concentration | Diameter (D) |
|---|---|---|
| mm | 100.00 | 75 |
| mm | 100.00 | 50 |
| mm | 100.00 | 37.5 |
| mm | 100.00 | 19 |
| mm | 100.00 | 9.5 |
| mm | 100.00 | 4.75 |
| mm | 100.00 | 2.36 |
| mm | 100.00 | 1.18 |
| mm | 100.00 | 0.6 |
| mm | 80.00 | 0.3 |
| mm | 41.54 | 0.15 |
| mm | 38.46 | 0.075 |
| mm | 36.92 | 0.0335 |
| mm | 36.92 | 0.0212 |
| mm | 36.92 | 0.0122 |
| mm | 36.92 | 0.0087 |
| mm | 35.38 | 0.0062 |
| mm | 32.31 | 0.0031 |
| mm | 24.62 | 0.0013 |

| Sample | 021 |
|---|---|
| Site | 6E |
| Coordinates | 33° 26' 15" S; 27° 03' 22" E |
| Chainage | 10888 m |
| Tide | Ebb |
| Date | 06/05/2012 |
| Time | 15:10 |
| d50 | 0.233 mm |

| Units | % Concentration | Diameter (D) |
|---|---|---|
| mm | 100.00 | 75 |
| mm | 100.00 | 50 |
| mm | 100.00 | 37.5 |
| mm | 100.00 | 19 |
| mm | 100.00 | 9.5 |
| mm | 100.00 | 4.75 |
| mm | 100.00 | 2.36 |
| mm | 100.00 | 1.18 |
| mm | 100.00 | 0.6 |
| mm | 77.50 | 0.3 |
| mm | 2.50 | 0.15 |
| mm | 2.50 | 0.075 |
| mm | 2.50 | 0.0387 |
| mm | 2.50 | 0.0245 |
| mm | 2.50 | 0.0141 |
| mm | 2.50 | 0.0100 |
| mm | 2.50 | 0.0071 |
| mm | 2.50 | 0.0035 |
| mm | 2.50 | 0.0014 |

| Sample | 023 |
|---|---|
| Site | 8A |
| Coordinates | 33° 29' 37" S; 27° 08' 05" E |
| Chainage | 405 m |
| Tide | Flood |
| Date | 07/05/2012 |
| Time | 07:27 |
| d50 | 0.239 mm |

| Units | % Concentration | Diameter (D) |
|---|---|---|
| mm | 100.00 | 75 |
| mm | 100.00 | 50 |
| mm | 100.00 | 37.5 |
| mm | 100.00 | 19 |
| mm | 100.00 | 9.5 |
| mm | 100.00 | 4.75 |
| mm | 100.00 | 2.36 |
| mm | 100.00 | 1.18 |
| mm | 100.00 | 0.6 |
| mm | 72.31 | 0.3 |
| mm | 4.62 | 0.15 |
| mm | 1.54 | 0.075 |
| mm | 1.54 | 0.0387 |
| mm | 1.54 | 0.0245 |
| mm | 1.54 | 0.0141 |
| mm | 1.54 | 0.0100 |
| mm | 1.54 | 0.0071 |
| mm | 1.54 | 0.0035 |
| mm | 1.54 | 0.0014 |
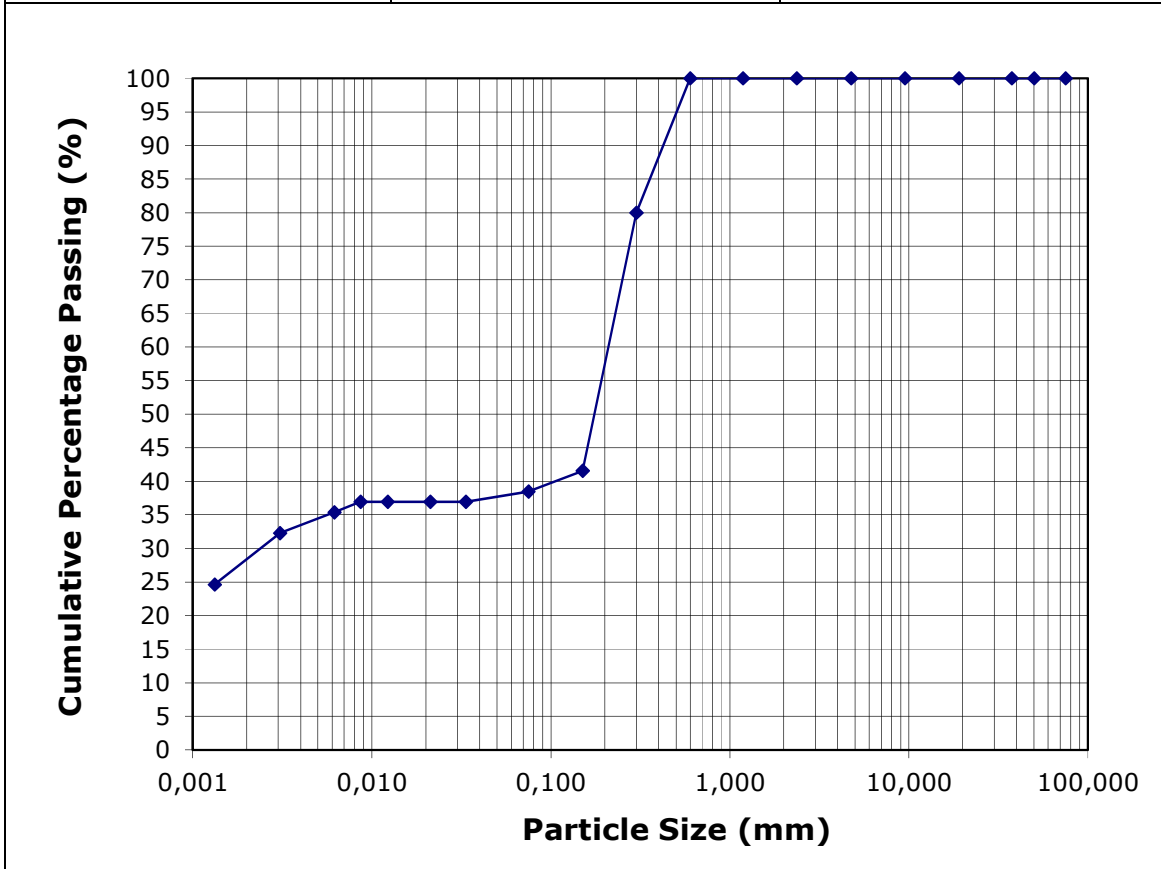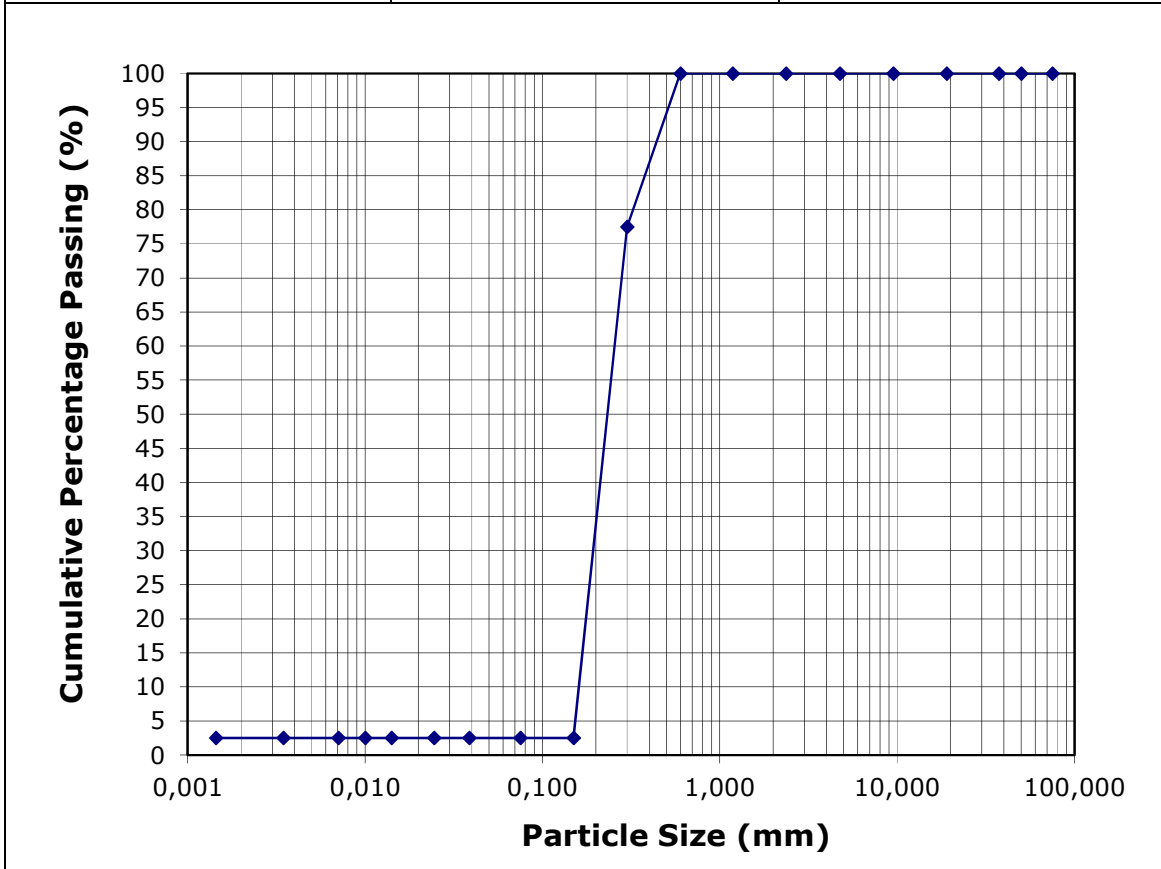


XLIII
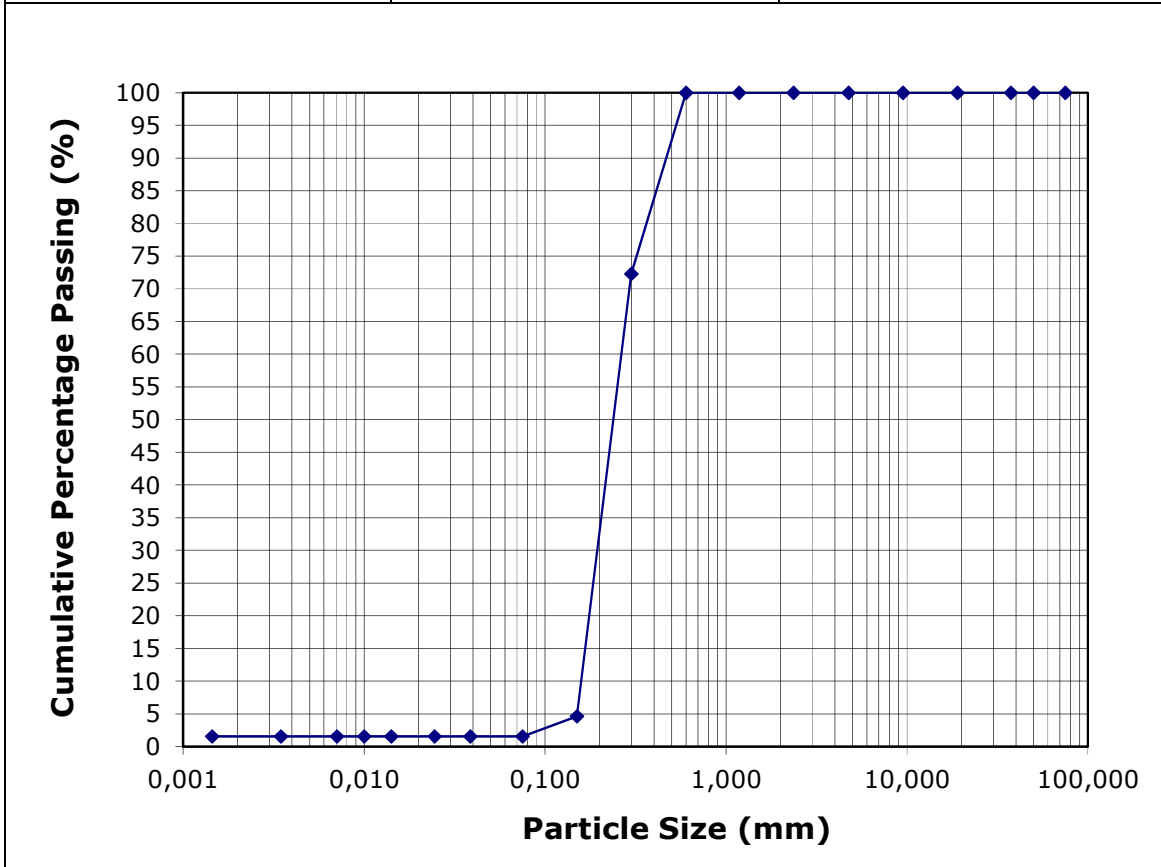
| Sample | 024 |
|---|---|
| Site | 8B |
| Coordinates | 33° 28' 55" S; 27° 06' 38" E |
| Chainage | 3026 m |
| Tide | Flood |
| Date | 07/05/2012 |
| Time | 07:53 |
| d50 | 0.089 mm |

| Units | % Concentration | Diameter (D) |
|---|---|---|
| mm | 100.00 | 75 |
| mm | 100.00 | 50 |
| mm | 100.00 | 37.5 |
| mm | 100.00 | 19 |
| mm | 100.00 | 9.5 |
| mm | 100.00 | 4.75 |
| mm | 100.00 | 2.36 |
| mm | 100.00 | 1.18 |
| mm | 100.00 | 0.6 |
| mm | 93.85 | 0.3 |
| mm | 56.92 | 0.15 |
| mm | 47.69 | 0.075 |
| mm | 44.62 | 0.0324 |
| mm | 44.62 | 0.0205 |
| mm | 44.62 | 0.0118 |
| mm | 43.08 | 0.0084 |
| mm | 41.54 | 0.0060 |
| mm | 38.46 | 0.0030 |
| mm | 29.23 | 0.0013 |



XLIV
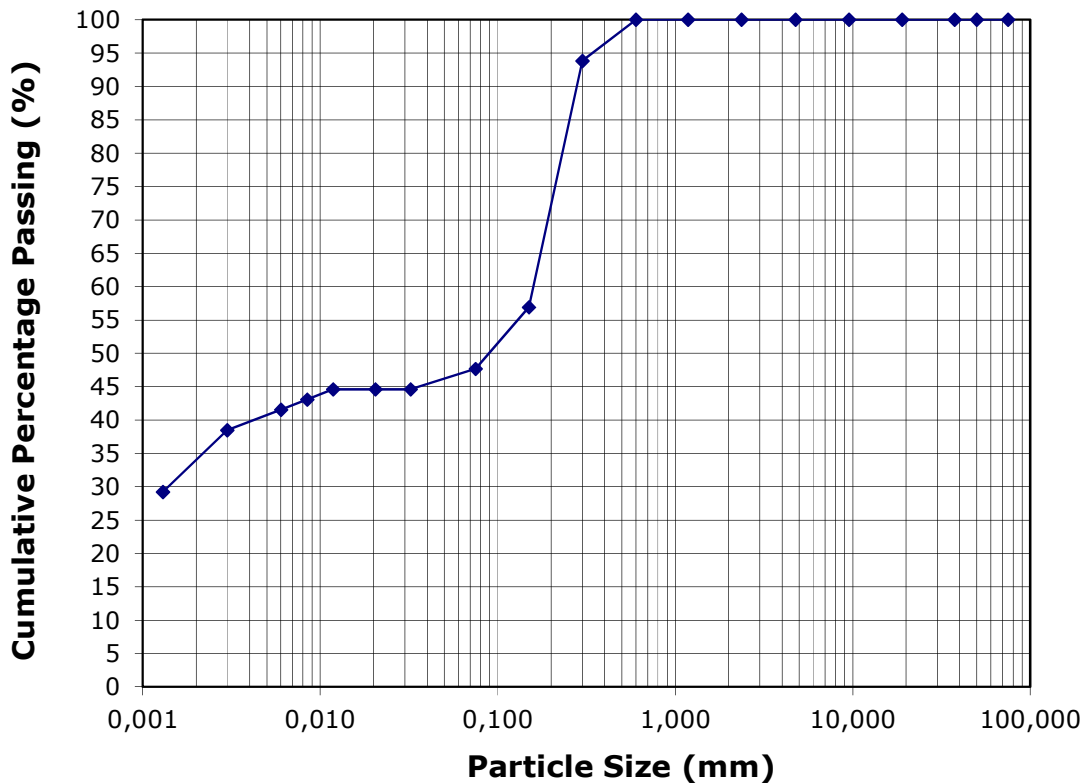
| Sample | 028 |
|---|---|
| Site | 8C |
| Coordinates | 33° 28' 21" S; 27° 05' 08" E |
| Chainage | 5645 m |
| Tide | Flood |
| Date | 07/05/2012 |
| Time | 08:20 |
| d50 | 0.188 mm |

| Units | % Concentration | Diameter (D) |
|---|---|---|
| mm | 100.00 | 75 |
| mm | 100.00 | 50 |
| mm | 100.00 | 37.5 |
| mm | 100.00 | 19 |
| mm | 100.00 | 9.5 |
| mm | 100.00 | 4.75 |
| mm | 100.00 | 2.36 |
| mm | 100.00 | 1.18 |
| mm | 100.00 | 0.6 |
| mm | 100.00 | 0.3 |
| mm | 26.15 | 0.15 |
| mm | 13.85 | 0.075 |
| mm | 13.85 | 0.0370 |
| mm | 13.85 | 0.0234 |
| mm | 13.85 | 0.0135 |
| mm | 13.85 | 0.0096 |
| mm | 13.85 | 0.0068 |
| mm | 13.85 | 0.0033 |
| mm | 10.77 | 0.0014 |

| Sample | 029 |
|---|---|
| Site | 8D |
| Coordinates | 33° 27' 17" S; 27° 04' 12" E |
| Chainage | 8270 m |
| Tide | Flood |
| Date | 07/05/2012 |
| Time | 08:36 |
| d50 | 0.206 mm |

| Units | % Concentration | Diameter (D) |
|---|---|---|
| mm | 100.00 | 75 |
| mm | 100.00 | 50 |
| mm | 100.00 | 37.5 |
| mm | 100.00 | 19 |
| mm | 100.00 | 9.5 |
| mm | 100.00 | 4.75 |
| mm | 100.00 | 2.36 |
| mm | 100.00 | 1.18 |
| mm | 100.00 | 0.6 |
| mm | 86.00 | 0.3 |
| mm | 20.00 | 0.15 |
| mm | 20.00 | 0.075 |
| mm | 18.00 | 0.0370 |
| mm | 18.00 | 0.0234 |
| mm | 18.00 | 0.0135 |
| mm | 16.00 | 0.0096 |
| mm | 16.00 | 0.0068 |
| mm | 16.00 | 0.0033 |
| mm | 14.00 | 0.0014 |
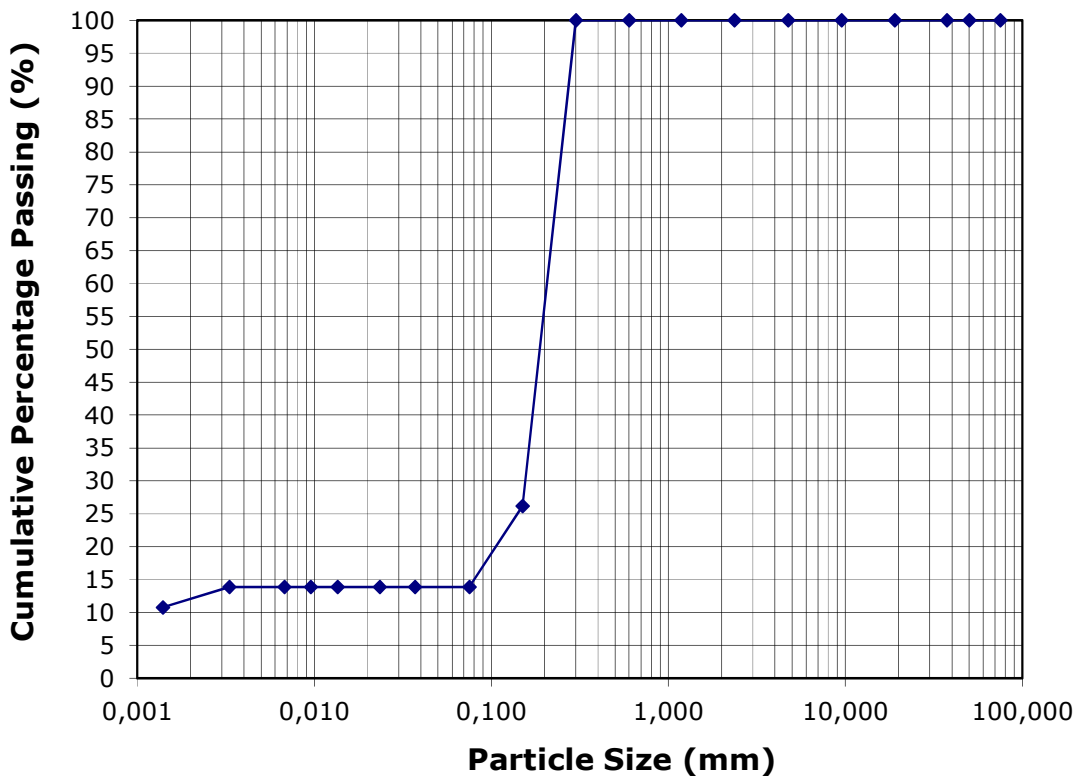


XLVI
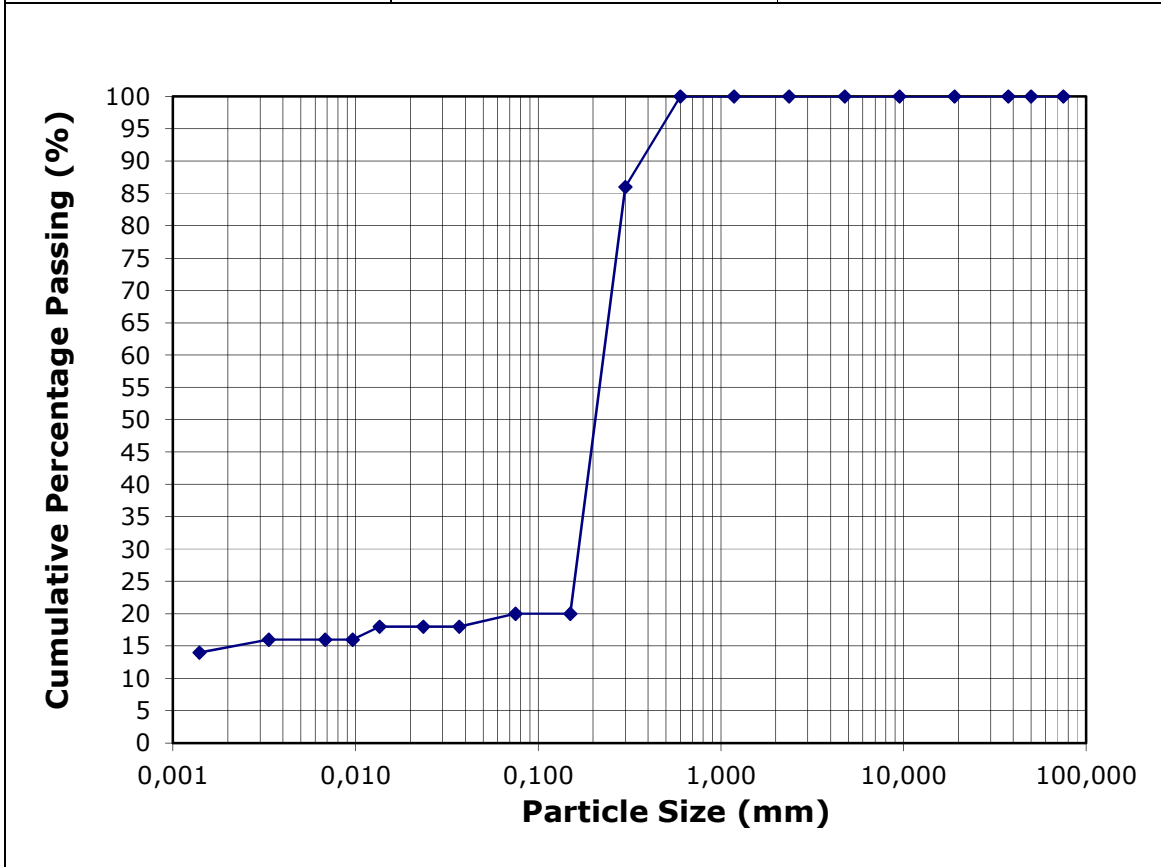
| Sample | 030 |
|---|---|
| Site | 8E |
| Coordinates | 33° 26' 15" S; 27° 03' 22" E |
| Chainage | 10888 m |
| Tide | Flood |
| Date | 07/05/2012 |
| Time | 08:52 |
| d50 | 0.252 mm |

| Units | % Concentration | Diameter (D) |
|---|---|---|
| mm | 100.00 | 75 |
| mm | 100.00 | 50 |
| mm | 100.00 | 37.5 |
| mm | 100.00 | 19 |
| mm | 100.00 | 9.5 |
| mm | 100.00 | 4.75 |
| mm | 100.00 | 2.36 |
| mm | 100.00 | 1.18 |
| mm | 100.00 | 0.6 |
| mm | 65.71 | 0.3 |
| mm | 2.86 | 0.15 |
| mm | 0.00 | 0.075 |
| mm | 0.00 | 0.0389 |
| mm | 0.00 | 0.0246 |
| mm | 0.00 | 0.0142 |
| mm | 0.00 | 0.0101 |
| mm | 0.00 | 0.0071 |
| mm | 0.00 | 0.0035 |
| mm | 0.00 | 0.0015 |



XLVII
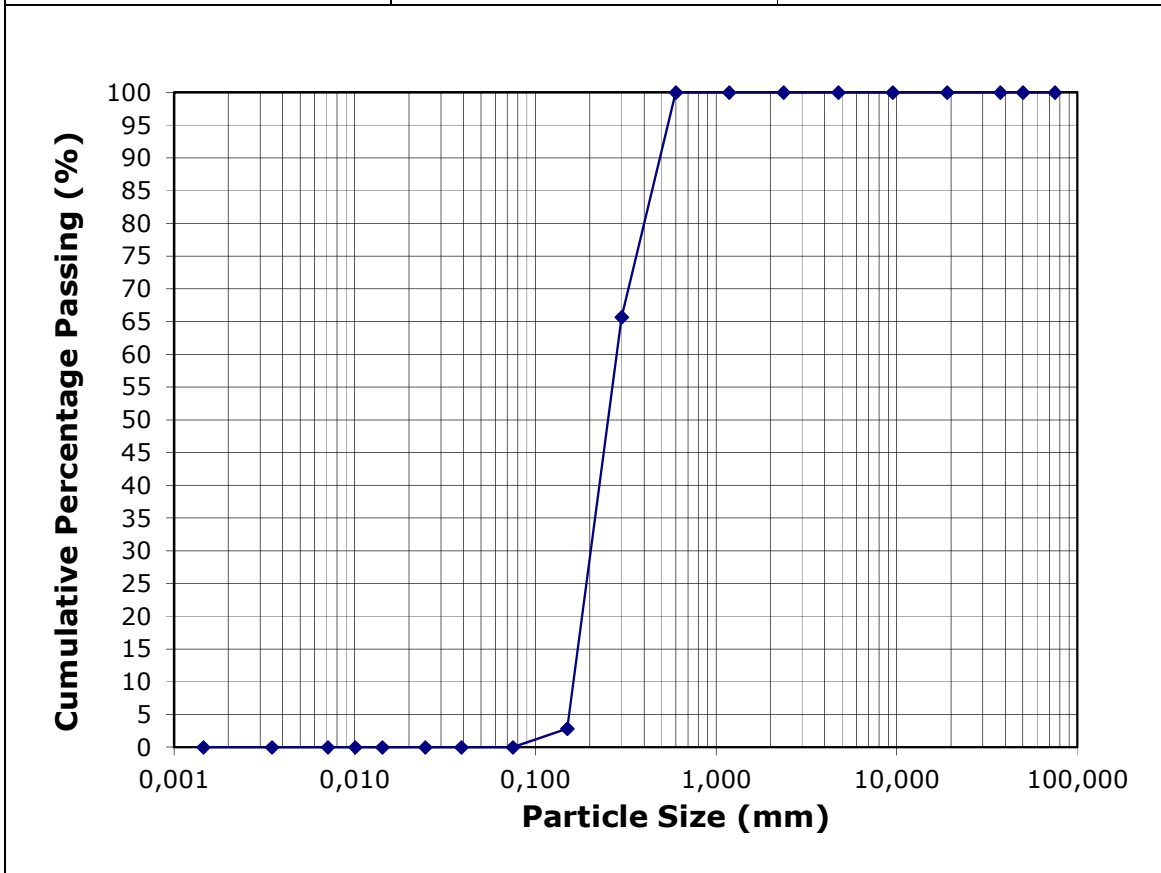
| Sample | 031 |
|---|---|
| Site | 8F |
| Coordinates | 33° 24' 12" S; 27° 02' 09" E |
| Chainage | 15200 m |
| Tide | Flood |
| Date | 07/05/2012 |
| Time | 09:14 |
| d50 | 0.403 mm |

| Units | % Concentration | Diameter (D) |
|---|---|---|
| mm | 100.00 | 75 |
| mm | 100.00 | 50 |
| mm | 100.00 | 37.5 |
| mm | 100.00 | 19 |
| mm | 100.00 | 9.5 |
| mm | 100.00 | 4.75 |
| mm | 100.00 | 2.36 |
| mm | 100.00 | 1.18 |
| mm | 96.00 | 0.6 |
| mm | 16.00 | 0.3 |
| mm | 2.00 | 0.15 |
| mm | 2.00 | 0.075 |
| mm | 0.00 | 0.0389 |
| mm | 0.00 | 0.0246 |
| mm | 0.00 | 0.0142 |
| mm | 0.00 | 0.0101 |
| mm | 0.00 | 0.0071 |
| mm | 0.00 | 0.0035 |
| mm | 0.00 | 0.0015 |



XLVIII

# Appendix H: Observed suspended sediment concentrations
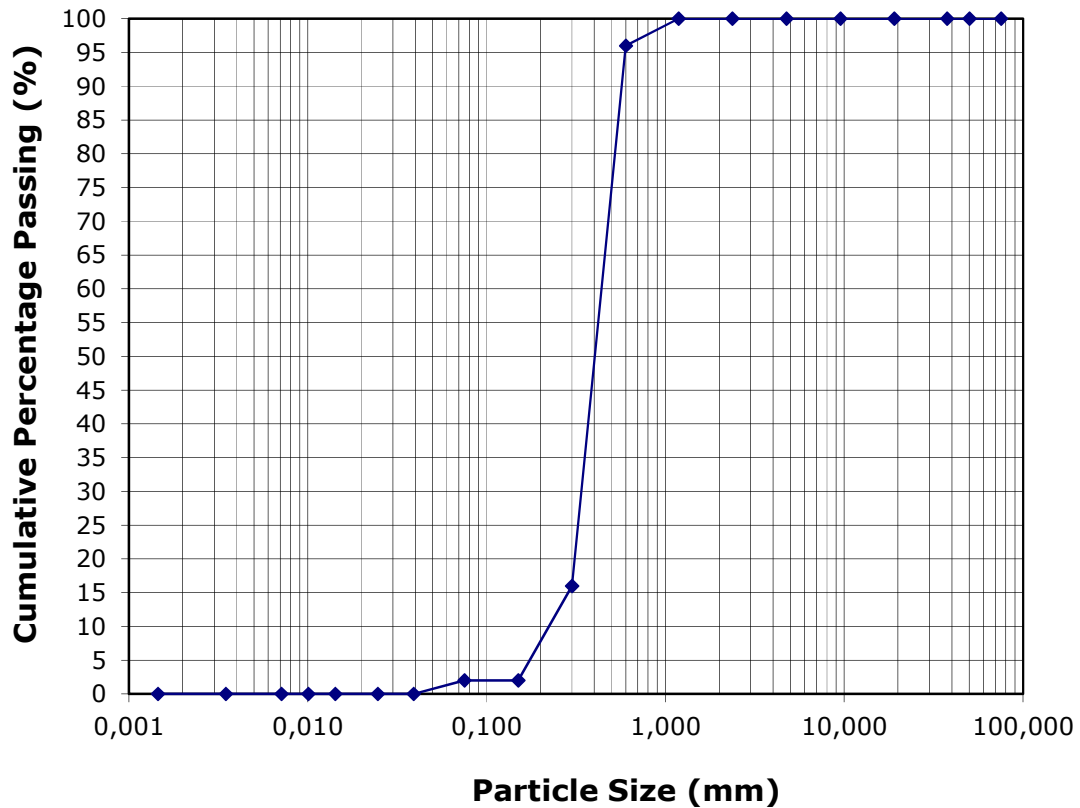
| Site | Distance upstream of mouth (m) | Date | Time | Sample nr. | Suspended sediment concentration (mg/l) | Tide |
|------|--------|------|------|------|------|------|
| Observed Great Fish River suspended sediment concentrations May 2012 |||||| |
| 2A | 405 | 05-May-12 | 13:38 | 006 | 234 | Ebb |
| 2B | 3026 | | 14:21 | 007 | 104 | Ebb |
| 2C | 5645 | | 14:34 | 008 | 556 | Ebb |
| 2D | 8270 | | 14:55 | 009 | 1038 | Ebb |
| | | | | | | |
| 4A | 405 | 06-May-12 | 07:28 | 010 | 91 | Flood |
| 4B | 3026 | | 07:46 | 011 | 592 | Flood |
| 4C | 5645 | | 08:01 | 012 | 535 | Flood |
| 4D | 8270 | | 08:17 | 013 | 284 | Flood |
| 4E | 10888 | | 08:29 | 014 | 252 | Flood |
| | | | | | | |
| 6A | 405 | 06-May-12 | 13:40 | 017 | 104 | Ebb |
| 6B | 3026 | | 13:55 | 018 | 413 | Ebb |
| 6C | 5645 | | 14:20 | 019 | 587 | Ebb |
| 6D | 8270 | | 14:44 | 020 | 424 | Ebb |
| 6E | 10888 | | 15:10 | 021 | 270 | Ebb |
| | | | | | | |
| 8A | 405 | 07-May-12 | 07:27 | 023 | 74 | Flood |
| 8B | 3026 | | 07:53 | 024 | 380 | Flood |
| 8C | 5645 | | 08:20 | 028 | 709 | Flood |
| 8D | 8270 | | 08:36 | 029 | 3564 | Flood |
| 8E | 10888 | | 08:52 | 030 | 222 | Flood |
| 8F | 15200 | | 09:14 | 031 | 200 | Flood |

L

**Appendix I: ADCP observed velocity and cross-section plots**

| | |
|---|---|
| **Date** | 6 May 2012 |
| **Time** | 09:07 |
| **Site** | E |
| **Run** | 4 |
| **Section number** | 1 |
| **River Width** | 20.5 m |
| **Average Depth** | 1.79 m |
| **Total Discharge** | 16.0 m³/s |
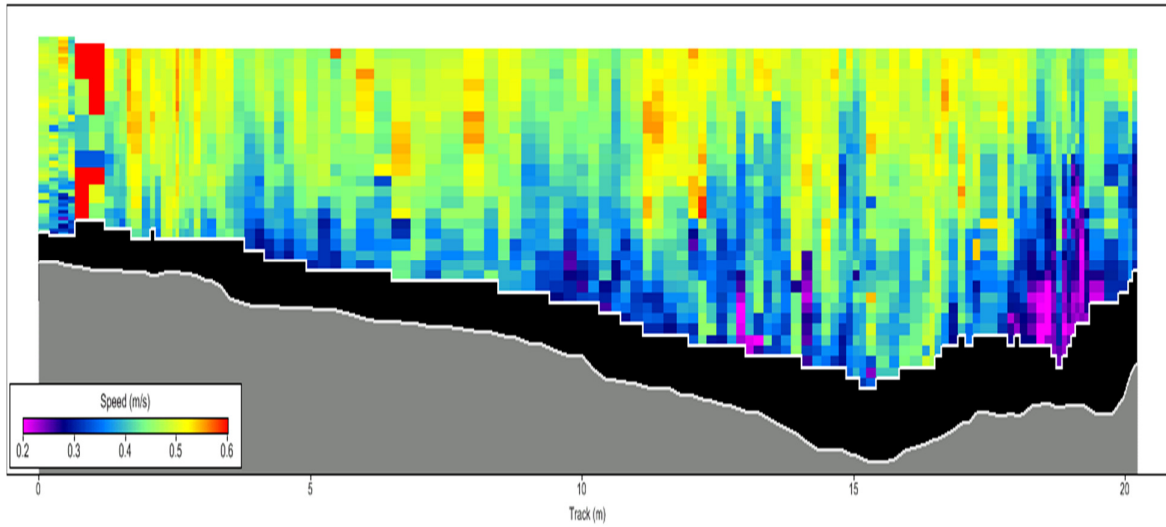


Figure I1: Cross-sectional velocity profile at Site E during run 4 (viewed looking downstream)

| Date | 6 May 2012 |
|---|---|
| Time | 09:12 |
| Site | E |
| Run | 4 |
| Section number | 2 |
| River Width | 26.72 m |
| Average Depth | 1.488 |
| Total Discharge | 21.2 m$^3$/s |
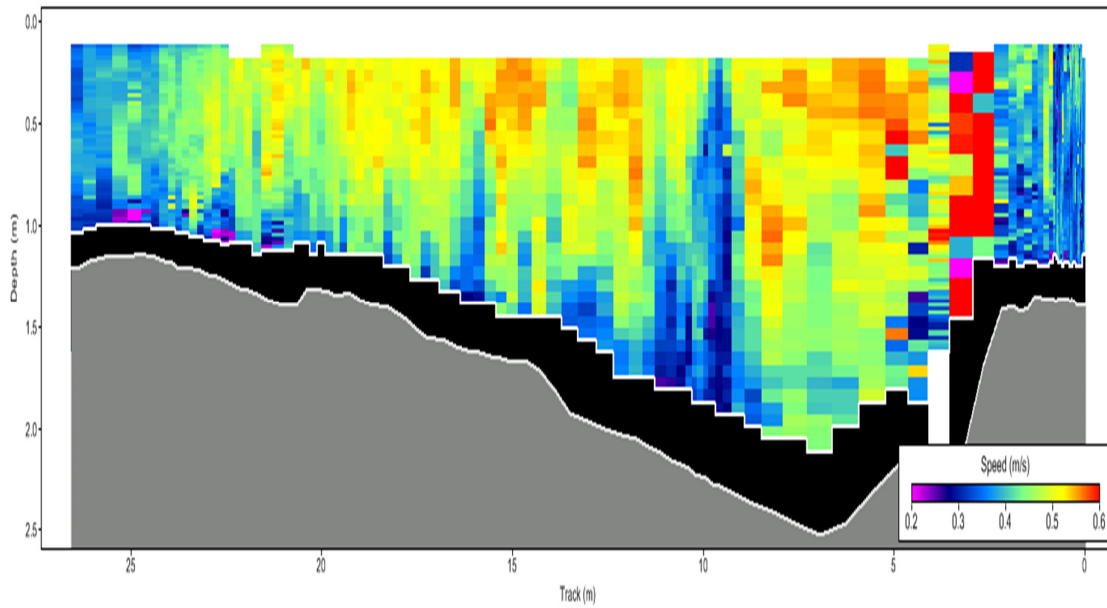


Figure I2: Cross-sectional velocity profile at Site E during run 4 (viewed looking downstream)

| Date | 7 May 2012 |
|---|---|
| Time | 07:53 |
| Site | B |
| Run | 8 |
| Section number | 1 |
| River Width | 158.8 m |
| Average Depth | 1.1 m |
| Total Discharge | 71.3 m³/s |
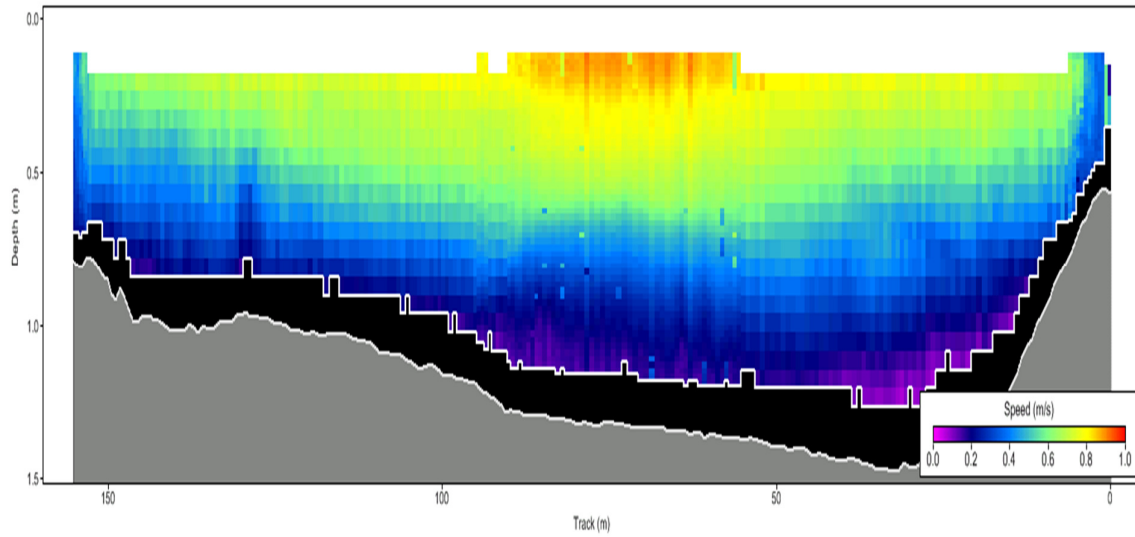


Figure I3: Cross-sectional velocity profile at Site B during run 8a (viewed looking downstream)

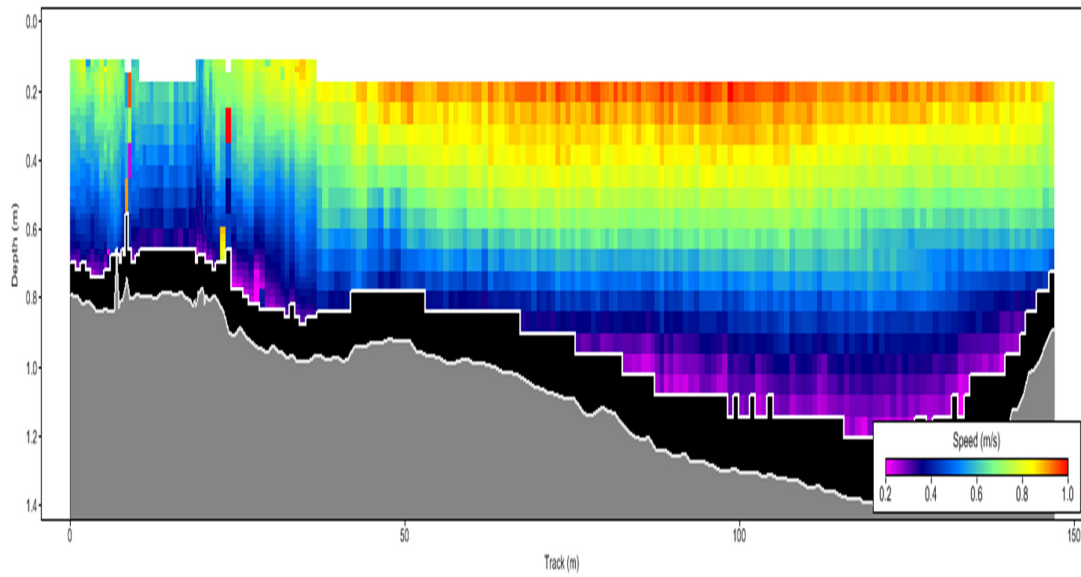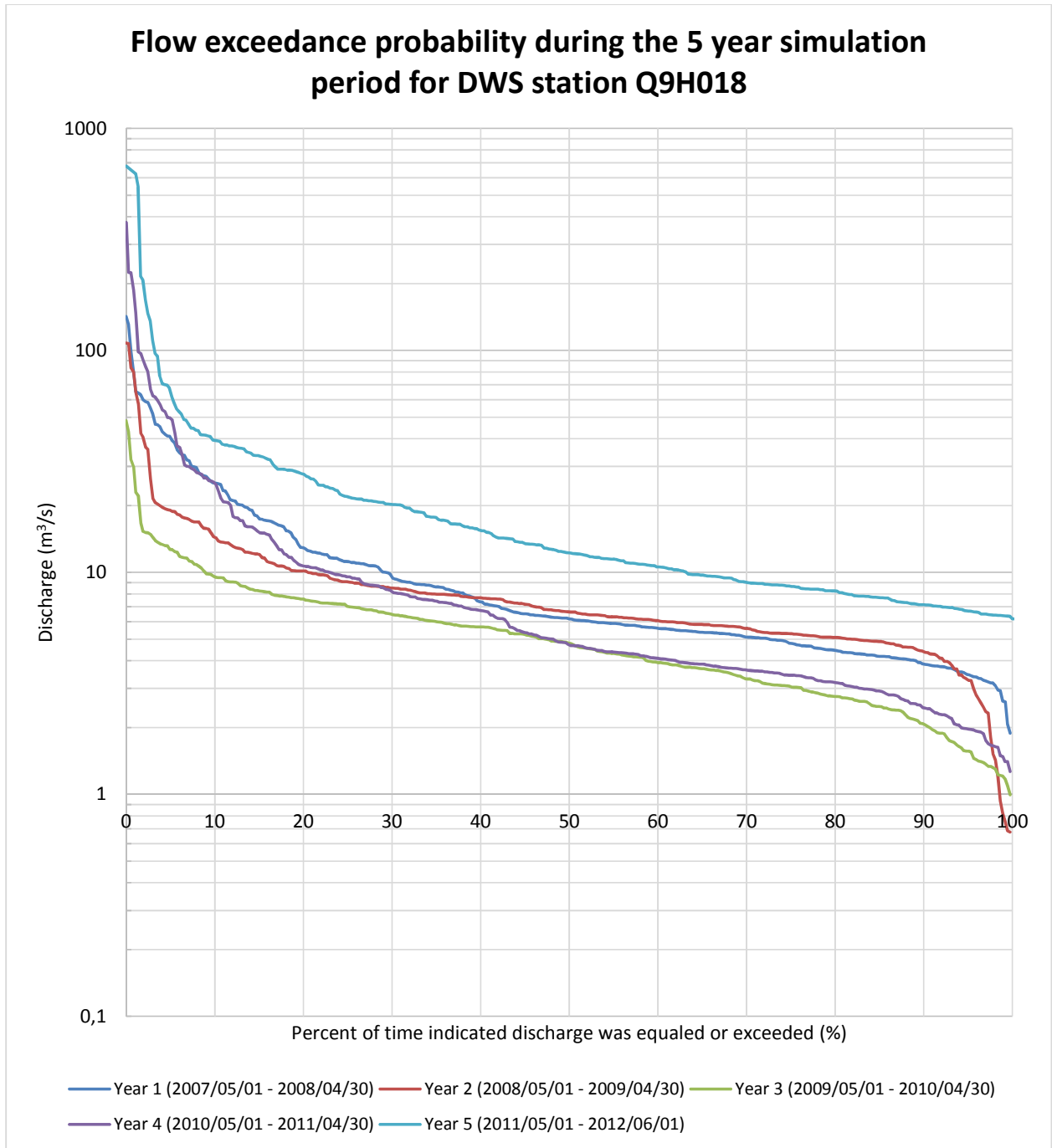| Date | 7 May 2012 |
|---|---|
| Time | 07:57 |
| Site | B |
| Run | 8 |
| Section number | 2 |
| River Width | 147 m |
| Average Depth | 1.1 m |
| Total Discharge | 87.2 m$^3$/s |



Figure I4: Cross-sectional velocity profile at Site B during run 8b (viewed looking downstream)

LV

**Appendix J: Great Fish River statistics at station Q9H018**



Flow exceedance probability during the 5 year simulation period for DWS station Q9H018

| Year - Month | Min of Q (m³/s) | Average of Q (m³/s)2 | Max of Q (m³/s)3 |
|---|---|---|---|
| **2007** | **1.89** | **11.12** | **254.99** |
| 1 | 3.28 | 7.94 | 17.28 |
| 2 | 3.09 | 4.88 | 8.24 |
| 3 | 6.07 | 39.60 | 254.99 |
| 4 | 5.17 | 8.12 | 15.97 |
| 5 | 3.71 | 5.10 | 10.01 |
| 6 | 3.60 | 8.13 | 16.51 |
| 7 | 3.39 | 7.90 | 17.37 |
| 8 | 3.87 | 5.50 | 6.60 |
| 9 | 3.32 | 7.35 | 19.16 |
| 10 | 3.27 | 5.28 | 9.29 |
| 11 | 1.89 | 4.10 | 11.32 |
| 12 | 4.37 | 28.39 | 141.87 |
| **2008** | **0.68** | **10.91** | **65.14** |
| 1 | 6.85 | 30.29 | 65.14 |
| 2 | 3.17 | 10.67 | 35.64 |
| 3 | 7.05 | 20.45 | 63.24 |
| 4 | 5.08 | 6.87 | 11.07 |
| 5 | 4.61 | 7.42 | 20.65 |
| 6 | 5.09 | 8.01 | 21.52 |
| 7 | 4.11 | 6.66 | 15.04 |
| 8 | 5.84 | 9.39 | 17.74 |
| 9 | 4.79 | 8.06 | 13.84 |
| 10 | 4.22 | 6.75 | 9.89 |
| 11 | 0.68 | 8.71 | 19.95 |
| 12 | 3.00 | 7.27 | 18.15 |
| **2009** | **1.10** | **7.94** | **107.87** |
| 1 | 2.32 | 5.01 | 8.07 |
| 2 | 2.47 | 16.22 | 80.01 |
| 3 | 4.29 | 22.21 | 107.87 |
| 4 | 3.97 | 6.04 | 10.47 |
| 5 | 4.58 | 7.39 | 15.10 |
| 6 | 3.69 | 7.70 | 16.71 |
| 7 | 3.92 | 6.87 | 13.16 |
| 8 | 4.91 | 8.42 | 13.45 |
| 9 | 2.49 | 5.18 | 9.83 |
| 10 | 1.10 | 4.92 | 15.09 |
| 11 | 1.56 | 3.14 | 6.96 |
| 12 | 1.21 | 2.64 | 5.25 |
| **2010** | **1.00** | **4.82** | **48.11** |
| 1 | 1.00 | 8.04 | 48.11 |
| 2 | 2.20 | 6.43 | 22.96 |
| 3 | 1.39 | 4.27 | 13.90 |
| 4 | 2.38 | 4.08 | 6.09 |
| 5 | 2.79 | 4.10 | 7.12 |
| 6 | 1.88 | 5.56 | 10.63 |
| 7 | 3.42 | 5.63 | 16.02 |
| 8 | 1.27 | 3.31 | 5.67 |
| 9 | 1.48 | 2.82 | 4.21 |
| 10 | 1.91 | 3.91 | 10.52 |
| 11 | 2.98 | 4.36 | 7.74 |
| 12 | 1.40 | 5.37 | 11.33 |
| **2011** | **2.83** | **29.26** | **676.09** |
| 1 | 6.21 | 28.03 | 96.64 |
| 2 | 9.42 | 53.90 | 376.93 |
| 3 | 4.07 | 31.65 | 186.78 |
| 4 | 6.42 | 8.11 | 14.71 |
| 5 | 5.02 | 19.97 | 48.81 |
| 6 | 8.65 | 105.50 | 676.09 |
| 7 | 11.00 | 36.73 | 168.48 |

| | | | |
|---|---|---|---|
| 8 | 11.70 | 23.90 | 46.48 |
| 9 | 5.80 | 8.91 | 16.57 |
| 10 | 4.00 | 12.25 | 43.52 |
| 11 | 2.83 | 6.56 | 12.28 |
| 12 | 5.43 | 18.38 | 51.54 |
| **2012** | **4.39** | **16.89** | **126.88** |
| 1 | 4.97 | 12.12 | 37.13 |
| 2 | 5.86 | 17.75 | 67.86 |
| 3 | 4.39 | 9.31 | 23.95 |
| 4 | 7.31 | 18.91 | 76.70 |
| 5 | 5.86 | 8.49 | 13.46 |
| 6 | 7.32 | 10.33 | 14.29 |
| 7 | 9.58 | 25.61 | 81.33 |
| 8 | 8.83 | 26.71 | 93.42 |
| 9 | 6.40 | 8.04 | 12.16 |
| 10 | 5.15 | 28.71 | 126.88 |
| 11 | 5.35 | 19.49 | 95.61 |
| **Grand Total** | **0.68** | **13.44** | **676.09** |

## Appendix K: Final bathymetry